RADIOLABELLED CARBOHYDRATE CONJUGATES: STUDIES OF ALZHEIMER'S DISEASE THERAPEUTICS AND TUMOR IMAGING

by

MERYN LOUISA BOWEN

B.Sc.(Hons.), The University of Canterbury (New Zealand), 2002

A THESIS SUBMITTED IN PARTIAL FULFILLMENT OF
THE REQUIREMENTS FOR THE DEGREE OF

DOCTOR OF PHILOSOPHY

in

THE FACULTY OF GRADUATE STUDIES

(Chemistry)

THE UNIVERSITY OF BRITISH COLUMBA
(Vancouver)

March 2009

ABSTRACT

This thesis is split into two distinct parts, with the common theme being the radiolabeling of carbohydrate-conjugates. Chapter 2 discusses radioiodinating 3-hydroxy-4-pyridinones, of interest in treating Alzheimer's disease. Chapters 3 - 5 describe glucosamine conjugates of ^{99m}Tc investigated as potential carbohydrate-based SPECT imaging agents.

Alzheimer's disease (AD) sufferers develop characteristic beta-amyloid plaques in their brains, made up of beta-amyloid protein with high concentrations of zinc and copper. The redox active copper ion can form reactive oxygen species (ROS) which damage surrounding tissue and lead to cell death. 3-Hydroxy-4-pyridinones are of interest in the treatment of AD because they are antioxidants and metal chelators, targeting both the plaques and ROS. Functionalisation of these pyridinones with a glucose moiety masks the chelating portion of the molecule, and may facilitate blood brain barrier (BBB) crossing via the GLUT glucose transporters. To determine this BBB permeability, two compounds were labelled with ^{125}I and then assessed using a rat brain perfusion procedure. They were observed to cross the BBB, a crucial finding in the decision to pursue this line of research for AD therapy.

A ^{99m}Tc-based SPECT tumor imaging agent would increase worldwide access to the important diagnostic tools of nuclear medicine. Chapters 3 – 5 discuss the synthesis, characterization and assay results of several monoanionic glucosamine-appended tridentate ligands and their complexes with the ^{99m}Tc and Re tricarbonyl cores. The length of the linker between the glucosamine and the metal binding portion of the molecule range between two and eleven carbons. The binding moiety was also varied to give a library of molecules with different binding groups and linker lengths; useful for structure-activity relationship determination in a range of assays. The interaction of the compounds with hexokinase was assessed, and none of the compounds were found to be substrates for hexokinase. Transport of the compounds into cells by the GLUT transporters was also assayed, and found to be insignificant for all compounds tested. Valuable information on the tolerances of these proteins was discovered and Chapter 6 includes ideas for improvements in future compounds.

TABLE OF CONTENTS

LIST OF TABLES

LIST OF FIGURES

LIST OF SCHEMES

ABBREVIATIONS

~	approximate
2D	two dimensional
3D	three dimensional
α	alpha or alpha particle
Å	angstrom, 1 x 10^{-10} metre
β	beta
β^-	beta particle
β^+	positron
γ	gamma ray
δ	chemical shift in parts per million (ppm)
ε	extinction coefficient ($L.mol^{-1}.cm^{-1}$) (UV-visible)
λ	wavelength
μ	micro (10^{-6})
ν	stretching frequency (IR)
Aβ	β-amyloid
Ac	acetyl
ACN	acetonitrile
AcOH	acetic acid
AD	Alzheimer's disease
ADEPT	antibody directed enzyme prodrug therapy
ADP	adenosine diphosphate
ALS	amytrophic lateral sclerosis

APOE	apolipoprotein E
APP	amyloid precursor protein
APT	attached proton test (NMR)
atm	atmosphere
ATP	adenosine triphosphate
BBB	blood brain barrier
Bn	benzyl
BNCT	boron neutron capture therapy
br	broad (IR signal)
Bq	Becquerel
°C	degrees celsius
Calc.	calculated
Ci	Curie
CIS	coordination induced shift
cm^{-1}	wavenumber(s), reciprocal centimetre
CNS	central nervous system
COSY	correlation spectroscopy (NMR)
Cp	cyclopentadienyl
CQ	clioquinol
CSF	cerebrospinal fluid
CT	computed tomography
d	day(s) OR doublet (NMR)
DA	Diels-Alder reaction
DCC	dicyclohexylcarbodiimide
DCM	dichloromethane

DFO	desferrioxamine
DFT	density functional theory
DLT	double ligand transfer
DMAP	4-dimethylaminopyridine
DMF	dimethylformamide
DMSO	dimethylsulfoxide
DTPA	diethylenetriaminepentaacetic acid
EA	elemental analysis
EC	electron capture
EDC	1-ethyl-3-(3-dimethylaminopropyl)carbodiimide hydrochloride
EIMS	electron impact mass spectrometry
ESIMS	electrospray ionization mass spectrometry
EtOH	ethanol
EtOAc	ethyl acetate
eq	equivalents (of a reagent)
fac	facial (ligand arrangement in O_h complexes)
FAD	familial Alzheimer's disease
Fc	ferrocene
FDA	Food and Drug Administration (USA)
FDG	[^{18}F]2-deoxy-2-flouro-D-glucose
g	gram
G6P	glucose-6-phosphate
G6PDH	glucose-6-phosphate dehydrogenase
GLUT	glucose transporter
hr	hour(s)

HK	hexokinase
HMBC	heteronuclear multiple bond coherence (NMR)
HMQC	heteronuclear multiple quantum coherence (NMR)
HPLC	high performance liquid chromatography
HR-MS	high resolution mass spectrometry
HSAB	hard soft acid base
Hz	hertz (s^{-1})
IC_{50}	compound concentration which kills 50 % of the cells present
%ID/g	the percentage of the total injected dose (of radioactivity into an animal) that ends up in one gram of a particular tissue type
IR	infrared
J	coupling constant (NMR)
k	kilo (10^3)
K	Kelvin
K_a	acidity constant
K_i	inhibition constant
L	litre OR ligand
m	metre OR milli- (10^{-3}) OR medium (IR) OR multiplet (NMR)
M	molar (moles/litre) OR metal OR mega (10^6)
MAG_3	mercaptoacetyltriglycine
MeOH	methanol
min	minute(s)
mol	mole(s)
MRI	magnetic resonance imaging
MS	mass spectrometry

MTT	3(4,5-dimethylthiazol-2-yl)-2,5-diphenyltetrazolium bromide
m/z	mass per charge (MS)
n	nano- (10^{-9}) OR number of samples
NADH	nicotinamide adenine dinucleotide, reduced form
NFT	neurofibrillary tangles
NMR	nuclear magnetic resonance
NSAID	non-steroidal anti-inflammatory drug
ORTEP	Oak Ridge Thermal Ellipsoid Program
PBS	phosphate buffered saline
Pd/C	palladium on carbon (10 % by weight)
PET	positron emission tomography
PEG	polyethyleneglycol
pH	$-\log[H_3O^+]$
ppm	parts per million
psi	pounds per square inch
q	quartet (NMR)
RBF	round bottom flask
R_f	retention factor (TLC)
ROS	reactive oxygen species
RPM	revolutions per minute
rt	retention time (HPLC)
s	strong (IR) OR singlet (NMR)
SD	standard deviation
sec	second(s)
SLT	single ligand transfer

SPECT	single photon emission computed tomography
t	triplet (NMR)
T	temperature
$t_{1/2}$	half-life
TEOA	triethanolamine
TFA	trifluoroacetic acid
Tg	transgenic
TLC	thin layer chromatography
™	trademark
TMEDA	tetramethylethylenediamine
TOCSY	total correlation spectroscopy
UBC	University of British Columbia
UV	ultraviolet
w	weak (IR)

ACKNOWLEDGMENTS

Thanks to Dr. Chris Orvig for taking me into his group, always being positive and encouraging, and allowing me the freedom to carry my research in the direction I wanted. Dr. Mike Adam has made an excellent second boss, he has always been cheerful, happy to talk over ideas, and very helpful. Thanks to all the Orvig group members who have made for a great workplace over the years: particularly Tim, Neil, Cara, Eszter, Dr. Chen, Adrienne, and Michael who either worked with me, taught me various aspects of chemistry or have been the source of useful discussions.

The PET group at TRIUMF have been very accommodating, and I would especially like to thank Wade English and Ken Buckley for continuously having to fix the HPLC, and Dr. Jianming Lu for the use of his lab and isotopes. MDS Nordion generously supplied ^{123}I, and the UBC Hospital Department of Nuclear Medicine the ^{99m}Tc.

Thanks to our collaborators at Texas Tech University who carried out the *in vivo* Alzheimer's work: Fancy Thomas with Dr. David Allen and Dr. Paul Lockman. I am very grateful to Dr. Urs Häfeli and Ripen Misri in the Faculty of Pharmaceutical Sciences at UBC, who have been very generous with their time and expertise in setting up the cell uptake studies.

UBC NMR, MS and Biological Services staff as well as members of the mechanical and electrical shops have been nothing but helpful in my interactions with them.

Finally I would like to thank my family – my parents encouraged me into chemistry when I may not have chosen that path myself, as they could see that was where my interests lay. And they have been nothing but supportive since. My brothers who have never understood why anyone would do chemistry when it obviously meant getting a job mixing paints in a factory, have made me think, and always made me laugh. And Michael, who still has no idea about chemistry but never ceases to ask questions anyway. He is always encouraging and challenging, and able to make me laugh, with chemistry as with all aspects of life. It certainly wouldn't have been as enjoyable a ride without him.

CO-AUTHORSHIP STATEMENT

Everything in this thesis was designed, researched, performed, analysed and written by myself except the following:

Chapter 2

- The non-radioactive form of **pyrB** was made by Dr. Michael Merkel. Dr. Merkel and I developed the radiolabeling for **pyrB** together, based on work I had already done with **pyrA**.
- The rat brain perfusion experiments were carried out by collaborators: Dr. David Allen, Dr. Paul Lockman and Fancy Thomas at the Texas Tech University Health Sciences Centre, Armadillo, TX.

Chapter 3

- Compounds $\mathbf{HL^3}$, $\mathbf{HL^4}$ were first made by Chuck Ewart and Dr. Neil Lim, respectively. Compound $\mathbf{L^5}$ was made by Dr. Tim Storr.

Chapter 4

- The C6, C8 and C11 ligands and their rhenium complexes were first made by Dr. Zhen-Feng Chen under my guidance. I designed and carried out some research into these compounds, and Dr. Chen did further research and was responsible for performing the synthesis.
- Adrienne Roos was a summer student under my supervision who performed the MTT and hexokinase phosphorylation assays. I was responsible for the design and research of these assays. Adrienne performed the experiments and manipulated the data with guidance and some assistance from me.

Chapters 2- 5

- The GLUT-1 cell uptake assay was designed by myself with assistance from Dr. Urs Häfeli, Faculty of Pharmaceutical Sciences, UBC. Cell maintenance and counting was done by Ripen Misri. The experiments were all carried out by myself.

CHAPTER 1

Introduction*

1.1 Medicinal Inorganic Chemistry

Medicinal inorganic chemistry is the application of inorganic chemistry to the therapy or diagnosis of disease. As shown in Figure 1.1, this can involve either addition or removal of an inorganic substance to or from a biological system in a controlled manner. The purpose of these actions is either diagnostic or therapeutic, to determine the nature and severity of a problem, or to treat a determined disease state.

As seen in Figure 1.1, therapy can take the form of removing excess metals from biological systems by administration of an organic metal chelator. Desferrioxamine is used to treat patients with an excess of iron in their bodies, by binding tightly to Fe^{3+} and solubilizing it so it can be excreted from the body.[3] Before a species like this is introduced to a living system, the interaction of the chelator with the metal ion(s) of interest will have been thoroughly investigated. Therapy in medicinal inorganic chemistry may alternatively involve administration of a metal complex where the properties of the metal impart a therapeutic effect to the drug. Cisplatin kills cancer cells because the weakly bound chloride ligands on the platinum are replaced by guanine *N*-7 donors in DNA. This causes cross linking of DNA strands, affecting the cells' ability to replicate and eventually killing the cells.[1] In terms of diagnostics, various properties of metals can be exploited to impart functionalities not available from purely organic compounds. An excellent example of this is the gadolinium based MRI contrast agents, where the large paramagnetic field of the metal ions (7 unpaired electrons on each Gd^{3+}) leads to an improved signal from nearby water molecules.[2] The examples given here illustrate some of the advantages that can be garnered by using a metal ion to impart certain properties that may not be available in a purely organic molecule. However, adding a metal to a potential drug also increases the need for caution, as the complex needs to be shown to stay intact under biological conditions. For example, in the case of the Gd^{3+} contrast agents, the metal ion itself is toxic and must stay bound to its chelate *in vivo* to prevent detrimental side effects. A large battery of

---

* A portion of this chapter has been published: Bowen, M. L. and Orvig, C. ^{99m}Technetium carbohydrate conjugates as potential agents in molecular imaging. *Chem. Commun.* **2008**, 5077 – 5091.

References begin on Pg 34

toxicological and stability studies are required for any compound that may be used in humans, regardless of the type of compound being investigated. The wide range of properties available when utilising most of the Periodic Table, as inorganic chemists do, have potential benefits that make these many elements worth exploring.

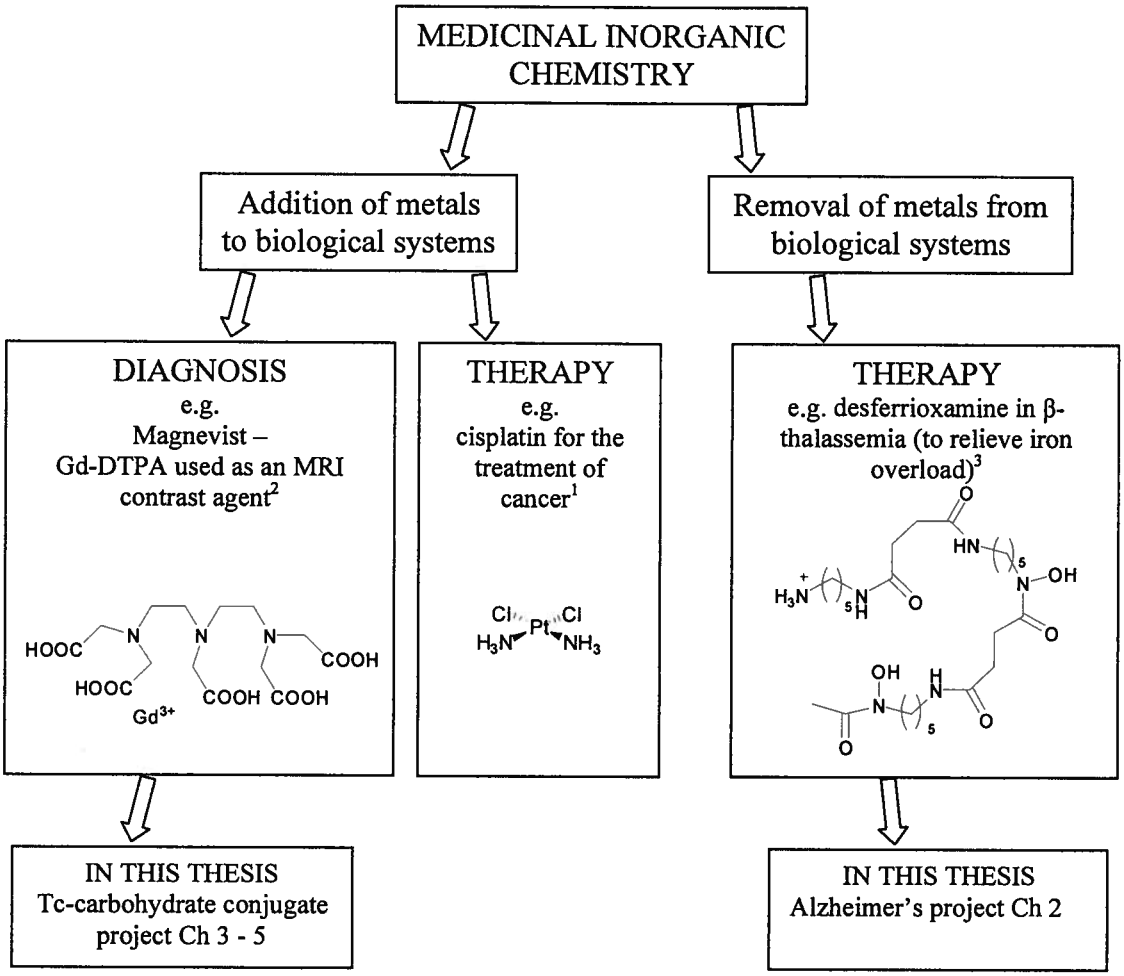

Figure 1.1 Medicinal inorganic chemistry is the application of inorganic chemistry to diagnosing and treating disease states.

1.2 Nuclear Medicine

Nuclear medicine is the use of radioactive isotopes incorporated into diagnostic or therapeutic agents. The compounds used in nuclear medicine are often referred to as radiopharmaceuticals, pharmaceuticals containing radioactivity. Therapeutic effects are achieved by damaging and killing diseased tissue, normally cancer cells, with the radiation

References begin on Pg 34

given off by the radioisotope. Diagnosis is achieved by using special cameras to image the radioactivity given off by decay events.

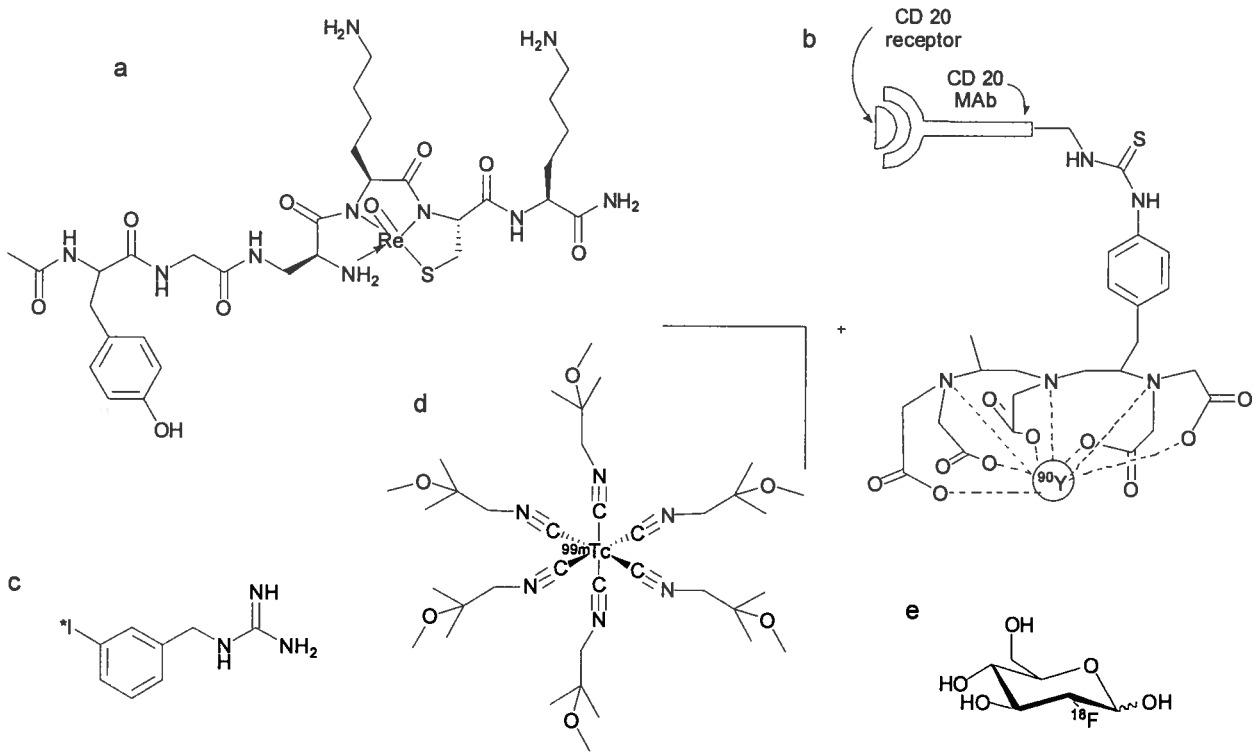

Figure 1.2 Some examples of therapeutic (a, b and c) and diagnostic (c, d and e) compounds used in nuclear medicine: a) ^{188}Re-P2045 is undergoing clinical trials as a treatment of non-small cell lung carcinoma[4] b) Zevalin – an antibody that targets non-Hodgkin's lymphoma cells, and kills them with the β radiation given off by the ^{90}Y[5] c) MIBG – metaiodobenzylguanidine used for imaging (^{123}I) and therapy (^{131}I) of adrenal cancers[6] d) Cardiolite – ^{99m}Tc sestamibi, used for imaging heart function with SPECT[7, 8] e) FDG, 2-^{18}F-fluoro-2-deoxyglucose, used to image areas of increased (e.g. cancer)[9] and decreased (e.g. dementia or heart ventricle dysfunction)[10] glucose metabolizm using PET.

1.2.1 Types of Radioactivity

Nuclear decay can be divided into three categories; α, β and γ. Table 1.1 shows some properties of these types of radiation as well as some commonly used isotopes of each kind.

Radioactive particles in nuclear medicine come from nuclear decay, but it is important to note that they are simply high energy particles; for example, α radiation is a He^{2+} nucleus with a certain amount of kinetic energy. Radiation interacts with, and sometimes damages

References begin on Pg 34

different materials by transferring some of its energy. Many forms of radioactivity contain large amounts of kinetic energy gained from the nuclear decay event, and depending on the mass and the speed of the particle will distribute that energy to surrounding matter over a certain time and area. The smaller the space over which the energy is transfered, the more damaging the interaction will be to the receiving tissue.

Table 1.1 Some important properties and uses in nuclear medicine of the three major types of radiation.

Radiation Type	Particle or Type	Shielding	Range in Air	Range in Tissue[11]	Ionising?	Use
α	2 protons and 2 neutrons (He^{2+})	a sheet of paper	1 - 10 cm	2 – 10 cells	strongly	therapy
β	electron (β^-) or positron (β^+)	perspex or aluminum	1 - 10 m	10 – 500 cells	medium	therapy, imaging (PET)
γ	photon	lead or thick concrete	100 - 1000 m	whole bodies	low	imaging (SPECT)

Alpha particles are relatively heavy, travel quite slowly and only have a small amount of kinetic energy to lose before coming to rest. They are not hazardous unless ingested, as the outer layers of skin are capable of stopping their progress. Beta particles have masses about 1/2000 the size of alpha particles, so for a set energy input will have more velocity than an alpha, and are able to travel moderate distances through air. In tissue they will only travel short distances, and so are more of a hazard if internalised than if exposure is from an external source. Gamma rays are a form of electromagnetic radiation, with no mass and high energy. They travel very quickly (at the speed of light) and with a short wavelength, so will travel a long way if not attenuated by a dense material such as concrete or lead. These pose as much risk of tissue damage whether the exposure is internal or external to the body, as they can easily penetrate living tissue (it is not dense enough to attenuate them). This also

References begin on Pg 34

means that the amount of energy transfer to the tissue is small compared to other radiation types, so long exposure is required for enough energy to accumulate in a given area for damage to be observed.

These properties are what make each type of radiation useful for a certain task. As shown in Table 1.1, alpha and beta radiation do not travel very far in tissue, so energy from the radiation they emit will all be deposited in nearby tissue. This makes them useful for damaging tissue in a certain area if they can be made to accumulate in that area. Gamma rays on the other hand are not particularly damaging and travel a long way through tissue without their path being significantly perturbed, making them ideal for use in imaging. Again the isotope needs to accumulate in the tissue to be imaged and then, using cameras sensitive to gamma rays, the position of the radiation source can be determined. This type of decay can be imaged using Single Photon Emission Computed Tomography – SPECT.

Positrons are the antiparticles to electrons and are denoted β^+. These have similar properties to β^- radiation, but behave quite differently. Because they are antiparticles of electrons, whenever they come into contact with an electron the two annihilate with each other and are transformed into energy. Conservation of both mass and energy means that this interaction produces two gamma rays at 180 ° to each other with energies of 511 keV. These gamma rays can then be imaged in a similar manner to the gamma rays produced by simple gamma decay, although in this case the two parallel rays travelling at the same speed in opposite directions give additional spatial information. This type of radiation can be imaged using a technique known as Positron Emission Tomography – PET.

1.2.2 Therapy in Nuclear Medicine

Therapy in nuclear medicine is generally aimed towards killing cells rather than healing them. Nuclear medicine therapeutics are therefore mainly used in cancer, although there are other applications too, such as overactive thyroid (hyperthyroidosis), and bone pain palliation. Hyperthyroidosis is treated with an oral dose of ^{131}I, where the β emission damages the surrounding tissue to reduce the activity of the thyroid.[12] As ^{131}I also has some γ emission, it can also be used for imaging of the thyroid. ^{89}Sr strontium chloride – Metastron - is administered intraveneously for the reduction of bone pain in bone cancer

patients.[13] It works because Sr^{2+}, behaving similarly to Ca^{2+}, accumulates in bone, and the β emission in the bone reduces pain, though the exact mechanism of this pain reduction is not well understood. ^{89}Sr has a half life of 50 days, so pain is alleviated for months at a time with a single injection.

Zevalin (Figure 1.2b) was approved by the Food and Drug Administration in the USA in 2002 as an anti-cancer agent. It contains an antibody that targets non-Hodgkin's lymphoma cells by binding to the CD20 antigen expressed on their surface.[14] ^{90}Y is bound to the antibody, and the β radiation given off by its decay kills nearby cells. An advantage of antibody therapy is that antibodies bind specifically to their antigens, allowing for more specific delivery of the radioisotope to the desired site than most small molecules can attain.[14] More specific targetting leads to reduced damage to healthy tissue, and therefore to less side effects. An example of a small molecule radiotherapeutic is MIBG, metaiodobenzylguanidine, which is used for both therapy and imaging (^{131}I and ^{123}I respectively).[6] MIBG is specific for cells that produce adrenalin, and as such is used mainly for cancer of the adrenal gland and certain kinds of brain cancer. It is more commonly used for imaging.[15]

There are currently no commercially available alpha emitter therapeutics.[16] There are however several that have been, or are currently, in advanced stage clinical trials.[16] Progress in this area has been quite slow, likely for several reasons. Alpha emitters are all heavy isotopes, often of toxic elements, and most do not have a large depth of research into their coordination chemistry. This means there has to be a substantial amount of work done on the coordination chemistry of these species to ensure containment of the radioisotope once the molecule is introduced to a biological system. Alpha emitters do have the advantage of being much easier to shield and transport than other types of radiation as their emissions are not able to penetrate even standard laboratory containers. They generally have quite long half lives, meaning they can be transported considerable distances without a significant loss of activity.

The alpha emitters that have undergone the most research include ^{211}At, ^{213}Bi and ^{223}Ra. Alpharadin ($^{223}RaCl_2$, $t_{1/2}$ = 11 days) is currently in Phase III clinical trials for the treatment of skeletal metastases in prostate cancer patients. It successfully completed phase II clinical

References begin on Pg 34

trials, where it was found to improve disease state markers and extend patient survival time compared to placebo treated controls.[17] $^{223}Ra^{2+}$ is thought to target bone because of its similarity to Ca^{2+}, and because of this mechanism of action the authors propose it will be useful for treating bone cancer and metastases from other cancer types as well. As ^{223}Ra is administered as an ionic compound, strength of chelation is not a concern, as is often the case with other alpha emitters.

^{213}Bi has been conjugated to antibodies and investigated as a treatment for prostate cancer. It is chelated via a DTPA moiety attached to the J591 antibody which is targeted to the prostate specific membrane antigen expressed in high concentrations on the surfaces of prostate cancers and their metastases.[18] It has been investigated for treating lung cancer, also by conjugation to an antibody,[19] but no commercial product has yet come out of these studies.

^{211}At is being investigated by several groups.[20] Astatine is a large element, and as a halogen requires different types of binding to the other large elements used in radiochemistry, which are normally metals. The Wilbur group at the University of Washington works with astatine bound to carboranes, and they find the resulting compounds to be very stable, and relatively easy to conjugate to a wide range of antibodies and other targeting molecules.[21, 22] Other approaches to astatine conjugation include binding it via a single covalent bond to an aryl group, which has been found to be of adequate *in vivo* stability depending on the substitution pattern of the aryl ring.[23, 24]

1.2.3 Imaging in Nuclear Medicine

Imaging in nuclear medicine is achieved using either a γ (gamma) emitting nucleus which can be imaged with single photon emission computed tomography (SPECT), or a β^+ (positron) emitting isotope, via positron emission tomography (PET). In SPECT a single γ ray is emitted by each decay event, and three dimensional (3D) data can be recorded on cameras and reconstructed to give a meaningful image of the area of interest. In PET an emitted positron travels until it meets an electron (its anti-particle), at which time the two annihilate, resulting in two opposing γ rays which can be recorded on 3D cameras and used to reconstruct an image. The most commonly used PET diagnostic in nuclear medicine, is 2-^{18}F-fluoro-2-deoxyglucose (FDG) (Figure 1.2d). In this compound, the 2- position of

References begin on Pg 34

glucose contains an ^{18}F atom instead of the native hydroxyl group.[25] ^{18}F is a β^+ emitting isotope, $t_{1/2}$ = 110 min. Because FDG is very similar to glucose, it is used as a measure of glucose metabolizm.[25] The most commonly used SPECT compound, in nuclear medicine is Cardiolite – ^{99m}Tc-Sestamibi (shown in Figure 1.2d). This works as a blood perfusion agent for imaging heart function as its charge (+1) and lipophilicity (which comes from the branched organic chains on each of the six ligands) lead to a favourable accumulation in this tissue. The important properties of the two imaging modalities, PET and SPECT, are recorded in Table 1.2.

Table 1.2 Properties and comparison of PET *vs.* SPECT for imaging in nuclear medicine.

PET	SPECT
Positron Emission Tomography	Single Photon Emission Computed Tomography
Positron (β^+ particle) emitters	Gamma (γ photon) emitters
Short lived isotopes	Range of half lives
e.g. ^{11}C, ^{13}N, ^{15}O, ^{18}F	e.g. ^{99m}Tc, ^{111}In, ^{123}I
Annihilates with $e^- \rightarrow 2\ \gamma$ rays 180° apart	Imaged with a 3D camera
Scanners less widely available	Scanners available at all major hospitals

Part of this thesis is concerned with the design of new SPECT based imaging agents. The reasons for this interest can be seen in comparing the two imaging modalities in Table 1.2. SPECT isotopes are generally longer lived than PET isotopes, and many do not need to be produced in a cyclotron. One major effect of this is that SPECT isotopes are generally cheaper than PET isotopes.[26] SPECT isotopes are generally more widely available too, because they can be produced in more locations and transported further without excess decay. In addition, there are many more SPECT than PET cameras available - as of December 2006 there were 616 SPECT scanners (including 3 SPECT/CT instruments) and 27 PET scannera (including PET/CT instruments) in use in Canada.[27] It can be seen that these properties combined make SPECT much more widely available than PET in terms of both geography and cost.

References begin on Pg 34

For these PET or SPECT images to be useful for diagnosis,[28] the radionuclide must accumulate in tissue of a certain type. This is often achieved by adding a radioactive isotope to a compound known to accumulate in the target tissue. These targeting compounds are often biomolecules, like peptides,[28] antibodies,[14] lipids,[29] carbohydrates,[25] nucleic acids[30] or small molecules such as biotin,[31] as naturally occuring substrates have high affinities for their receptors. In this approach the radionuclide must be added in a way that minimizes its effect on the biodistribution of the parent biomolecule.

In this regard, PET has the advantage that its nuclei such as ^{18}F and ^{11}C can be covalently incorporated into a molecule. They can often be used to replace a non-radioactive, naturally occuring isotope such that no chemical change is seen in forming the radioactive species. As most of the commonly used SPECT isotopes are metallic (e.g. ^{99m}Tc, ^{111}In, ^{67}Ga), and do not occur naturally *in vivo*, an important part of the design of SPECT radiopharmaceuticals is the chelation of the radionuclide. The chelation needs to be strong such that the radioisotope stays bound to the rest of the molecule. The free radioisotope will probably not accumulate in the tissue of interest as well as the complex does, so its biodistribution will become unpredictable, leading to increased background noise which decreases image quality and therefore diagnostic capability, as well as raising the dose to the patient as the unbound isotope may not clear well from the body. Most biomolecules or small molecules that target certain tissue types do not bind strongly to metals, so a chelating portion needs to be added to the target molecule. The compounds made to address these issues are a class of bioconjugates. These are illustrated in Figure 1.3, where it can be seen that there are several functionalities designed into molecules of this type. The metal binding portion must attach strongly to the radionuclide. The biomolecule will hopefully be responsible for the biological activity and distribution of the resulting complex. The linker needs to be robust, so the complex does not fall apart, and may also be used to impart other properties to the complex such as sufficient separation of the two functional parts of the molecule or adjustment of the overall lipophilicity.

In the carbohydrate-based imaging that is the focus of this thesis, these bioconjugates are formed by conjugation of a radioactive atom via a metal binding moiety and a linker to a sugar, in the hopes that the biodistribution of that sugar is essentially maintained. In this work, the tether, the linker and the metal binding portions have all been varied and the

References begin on Pg 34

effects of these on the activity of the compounds with the relevant enzymes investigated. Given the focus of this thesis on carbohydrate derivatives, the compounds examined here will have the ultimate aim of being used to image areas of unusual sugar metabolism; either raised, as in cancer, or diminished, as in stroke, heart attack, or Alzheimer's disease. The SPECT analogues we are attempting to produce have the potential to make a very useful diagnostic technique available to a much larger number of patients, due to the wider availability of SPECT compared with PET.

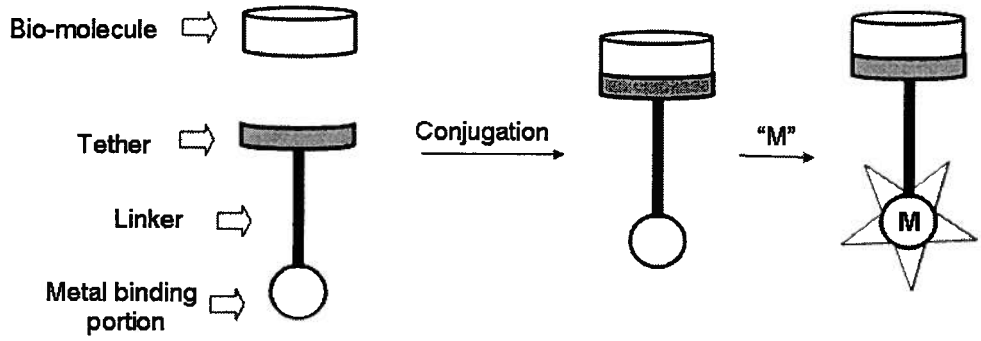

Figure 1.3 A generic model of a bioconjugate used to bind to a radioactive metal such as technetium, resulting in a bioconjugated radiotracer.

1.3 Carbohydrates – Some Relevant *In Vivo* Considerations

Carbohydrates are the main source of fuel for the body. As well as providing energy they are intimately involved in many vital processes, such as cell signaling, molecular recognition, surface adhesion, providing structure, the inflammation response, and in the fertilization and development of the fetus.[32] Because carbohydrates are such important biological molecules, life forms have many enzymatic systems in place to monitor their levels as well as to transport, chemically modify, and metabolize them.

The major use of glucose is in metabolizm, through the complex, tightly regulated processes of glycolysis, the citric acid cycle and oxidative phosphorylation. Because of this, life has developed very efficient and particular processes for the transport of glucose into and out of cells, and for the processing and breakdown of the glucose once inside cells. Glycolysis is one way cells make ATP – the biological energy currency. Cells also use oxidative phosphorylation for this purpose; this is a much more efficient process, producing around 32

References begin on Pg 34

ATP per glucose, compared to two ATP per glucose for glycolysis.[33] One of the most pronounced and well studied differences between cancerous and normal tissue is the increase in glycolysis and decrease in oxidative phosphorylation in cancerous *vs.* normal cells. This results in inefficiency in the metabolizm of cancer cells, so their glucose intake requirements are much higher than those of normal cells to achieve the same energy production level, a fundamental difference known as the Warburg effect.[34] The consequent enzymatic enhancements of tumor cells over many other cell types can be exploited by using glucose as a targeting vector for diagnostic or therapeutic compounds.

A key carbohydrate processing enzyme that is notably overexpressed in cancer cells is hexokinase (HK).[35] As HK is the first enzyme in the glycolysis pathway, changes in its activity have a large affect on overall energy production of a cell. HK has many isoforms, but most found in humans are membrane bound and are about 100 kDa in size. Each enzyme is comprised of two similar domains, with the active site residing in a cleft between the two.[36] When a substrate, such as glucose, is bound in the active site, the two portions of the enzyme rotate together by 12° to narrow the cleft and allow for the transfer of a phosphate group from an ATP (also present at the active site) to the hydroxyl group at the *C*-6 position of the sugar.[36] The products of this reaction (as shown in Scheme 1.1) are ADP and glucose-6-phosphate, which is negatively charged at physiological pH, and therefore not able to permeate the cell membrane.

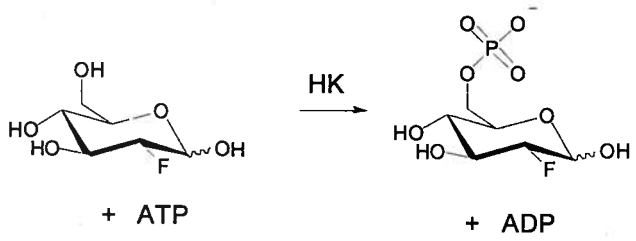

Scheme 1.1 Phosphorylation of FDG by hexokinase (HK) leads to a negatively charged product which is trapped in cells, in the process ATP is converted to ADP.

This means that for a given amount of glucose transported into a cell, the more hexokinase activity the cell exhibits, the higher its concentration of trapped carbohydrate metabolites will be. In cancer cells, HK activity in often high due to either overexpression of the protein, or incorporation of a larger proportion of HK into a membrane, which is known to increase its activity.[37] Compounds that are known inhibitors of hexokinase are being investigated as

References begin on Pg 34

potential chemotherapies for various types of cancer.[38] 3-Bromopyruvate (Figure 1.4a) is an inhibitor of HK that has been shown to deplete ATP in cancer cells.[38] *N*-appended glucosamine derivatives were tested by Bertoni and Weintraub,[39] who found several compounds that exhibited competitive inhibition of hexokinase. *N*-Benzoylglucosamine (Figure 1.4b) exhibited the highest inhibition of human brain hexokinase of the compounds tested, with K_i values of 8.6 - 22 nM depending on the isoform of hexokinase used.[39] The fluorescent dye 2-NBDG (Figure 1.4c), was found to be phosphorylated by hexokinase in *E. coli* cells.[40]

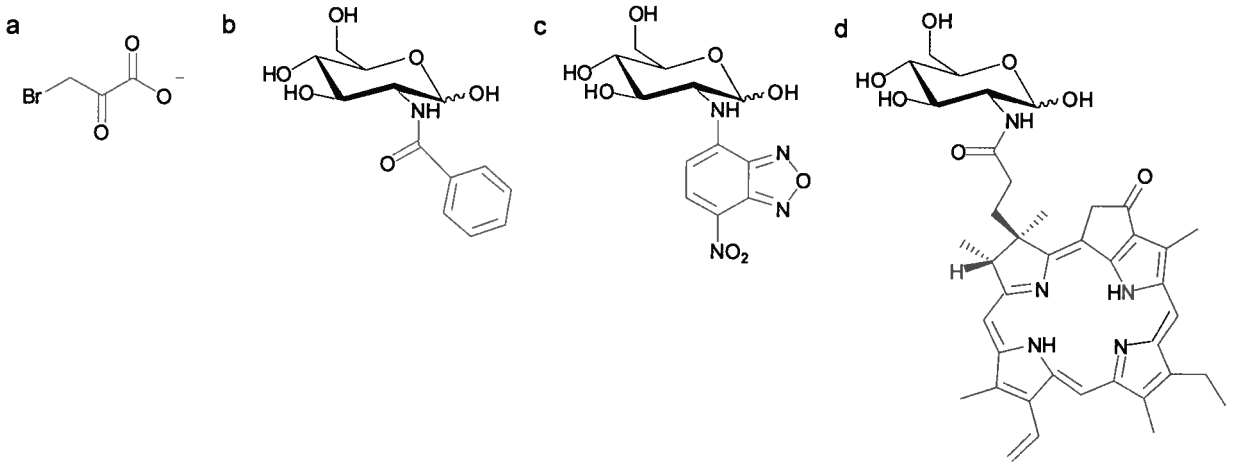

Figure 1.4 Compounds found to interact with key carbohydrate metabolizing proteins *in vivo*. Competitive inhibitors of hexokinase: a) 3-bromopyruvate[38] b) N-benzoylglucosamine[39] c) 2-NBDG.[41] Functionalized glucose and glucosamine analogues that exhibit GLUT glucose transporter activity: c) 2-NBDG[41] d) a near-IR dye appended to glucosamine.[43]

Carbohydrates are very polar molecules, and as such have very poor membrane (lipid) permeability. The GLUTs are a class of transmembrane proteins used to facilitate transport of glucose and other sugars, in an energy independent manner, across key membranes. They are ubiquitous in mammalian cells, although cells express varying amounts of different isoforms, depending on their energy requirements. In humans there are thirteen known isoforms of the GLUT family; they range from 45 - 60 kDa in size, and all contain twelve membrane spanning domains with high sequence homology.[44] GLUT transporters are found in high concentrations in the membranes of cells with high energy requirements, and at the blood brain barrier (BBB).

The BBB is a series of tight endothelial junctions between the cells that line the interior walls of the blood vessels in the brain. The purpose of these tight junctions is to stop the

References begin on Pg 34

influx, to the very important and sensitive organ that is the brain, of any unwanted and potentially harmful components that are circulating in the blood stream. As glucose is the primary source of energy for the brain, which is responsible for the consumption of 25 % of the body's glucose despite making up only 2 % of its mass, it is crucial that there be mechanisms in place to ensure an adequate supply of carbohydrates to the brain. Thus there is a high concentration of GLUTs, particularly GLUT-1, found at the BBB. This is utilised in our approach to Alzheimer's disease therapeutics, as addressed in Chapter 2 of this thesis.

As tumors grow rapidly and have altered metabolizm, they have correspondingly high energy requirements.[45, 46] This leads to a higher demand for carbohydrates, which means that their uptake into cells must be increased, necessitating an increased expression of GLUTs compared to normal cells. This fact was used in the design of the ^{99m}Tc based carbohydrate conjugates explored as potential imaging agents in Chapters 3 – 5.

Although many of the GLUT proteins are known to exhibit high substrate specificity (e.g. GLUT-1 transports D-glucose, but not its enantiomer L-glucose), the transport of non-natural substrates across otherwise impermeable membranes has been observed. Appending a carbohydrate moiety to a compound to enhance either BBB or cell permeability has proved useful with a number of different molecules.[42] However, *C*-2-functionalised glucosamine analogues have perhaps shown the most promising GLUT substrate scope. Zheng and coworkers appended a large porphyrin that acts as a near-infrared dye to the nitrogen of glucosamine (Figure 1.4e) and found that the compound was transported into cells.[43] 2-NBDG (Figure 1.4c) has a fluorescent probe attached to the nitrogen of glucosamine, and was found to be transported into human erythrocytes. This cellular uptake was competitively inhibited by D-glucose, meaning the transport could be attributed to GLUT-1 rather than passive diffusion, as this would not be affected by the presence of glucose.[41] As mentioned above 2-NBDG is also phosphorylated by hexokinase.

An example of a molecule that has biological activity with both the GLUT transporters and hexokinase is FDG (seen above in Figure 1.2e and Scheme 1.1). FDG is taken up into cells by the GLUT transporters due to its similarity to glucose.[47] Once inside a cell, glucose is phosphorylated at the 6 position by HK, then dehydrated across the *C*-1 – *C*-2 bond by glucose-6-phosphatedehydrogenase (G6PDH). FDG is phosphorylated at *C*-6 by HK, but the

References begin on Pg 34

resulting FDG-6-phosphate is not active under G6PDH because it has a fluorine in the 2-position, not the requisite hydroxyl (see Scheme 1.1). FDG-6-phosphate is not a major substrate for any other enzymes; and because it is negatively charged and cannot diffuse through membranes, it simply accumulates in the cells with the greatest GLUT and hexokinase activities; normally cancer cells.[48] These properties explain why FDG is such a good imaging agent for glucose metabolizm, and these are the properties we aim to mimic in designing new SPECT carbohydrate analogues.

1.4 Technetium and its Use in Nuclear Medicine

^{99m}Tc is the most commonly used isotope in nuclear medicine, accounting for about 90 % of all diagnostic nuclear medicine scans worldwide.[49] This is due to the near ideal physical properties of the ^{99m}Tc isotope; it has a six hour half life and emits γ rays with an energy of 141 keV. This means there is sufficient time to chemically manipulate the isotope before injection into a patient, and allow for its accumulation in target tissue while still having a significant amount of the original activity left to image. This emission energy is fairly low; meaning the radiation dose to the patient is minimized, comparable to that from a conventional medical X-ray. The other appealing practicality of ^{99m}Tc is that it is produced in a generator from ^{99}Mo, $t_{1/2}$ = 66 hr. The technetium is eluted as required in the form of $[^{99m}TcO_4]^-$ taking advantage of the charge difference between $[MoO_4]^{2-}$ and $[TcO_4]^-$ to elute ^{99m}Tc selectively. This means that technetium is inexpensive and easily transportable, making a useful SPECT isotope available wherever there is a SPECT scanner.

There is also interest in the third row congener of technetium, rhenium, which has two potentially useful radioactive isotopes – ^{186}Re and ^{188}Re. ^{186}Re, $t_{1/2}$ = 3.7 days, decays via emission of both β (E_{max} = 1.07 MeV, maximum distance in tissue = 5 mm) and γ (9 %, 137 keV) radiation. ^{188}Re, $t_{1/2}$ = 17 hr, also emits both β (E_{max} = 2.12 MeV, maximum distance in tissue = 11 mm) and γ (15 %, 155 keV) radiation. β emission is capable of killing cells, and if the isotope can be targeted to a tumor then the short tissue range of the radiation allows for selective cell death, resulting in reduced side effects compared to less specific radio- or chemotherapies. The γ emission of these compounds may allow for concomitant imaging, to

References begin on Pg 34

help tailor dosage, and to monitor accumulation of the compound in the areas of concern.

Technetium, whose name comes from *technetos*, greek for artificial, does not have any non-radioactive isotopes. Thus it is standard practice when working with technetium to use non-radioactive (or cold) rhenium, to perform larger scale chemistry and characterization. In the past, a β emitter, ^{99}Tc, $t_{1/2} = 2.13x10^5$ years, was used, but as radioactive licensing becomes stricter and our understanding of the similarities between technetium and rhenium chemistry increases, this is becoming less common. Rhenium exhibits very similar chemistry to technetium. Rhenium is slightly larger, and because of this is a little softer, so may have slightly different affinities for different ligating atoms. Rhenium has a slightly lower reduction potential than technetium, meaning that it is harder to reduce from the +7 oxidation state in which these metals are commonly supplied as the $[MO_4]^-$ anion. Given that these limitations are fairly well understood, and that all other aspects of the chemistry of these two elements are comparable, similarity can be assumed. For those not very well acquainted with radiochemistry, a note on the characterization of radioactive compounds: due to the minute concentration ranges being dealt with, as well as the hazards involved with the use of radioactivity, radioactive compounds cannot be characterized via the same methods as are non-radioactive "cold" compounds. HPLC retention time comparison with the analogous, thoroughly characterized rhenium compound is used as the primary method of identification of technetium complexes. If coinjection of the rhenium complex and the technetium reaction mixture give peaks at the same retention time, this is considered proof that the equivalent technetium complex has been formed. The retention times of starting materials are also known, and these must be different to those of the complexes for the results to be meaningful.

The radiochemistry of rhenium is less developed than that of technetium, so many of the compounds made in this area of research are made for cold rhenium and for technetium but not for radioactive rhenium.

1.4.1 Oxidation States of Technetium

Although all oxidation states from -1 to +7 are known for technetium, the vast majority of the chemistry to date has focused on two of them, +5 and +1.[50] There has been a lot of work,

over a long period of time, on the use of ^{99m}Tc(V)-based imaging agents.[51, 52] A commonly studied species in this oxidation state is the technetium oxo species, $[^{99m}TcO]^{3+}$. The coordination chemistry of this system has been well studied, and it is known to form stable distorted square pyramidal compounds with tetradentate ligands. Although a wide range of donor atoms have been investigated with this core, much of the work directed towards radiopharmaceutical application has involved N_xS_{4-x} coordination spheres, first reported by Davison, Orvig and coworkers.[53] A derivative of this complex type that has found significant use is the N_3S mercaptoacetyltriglycine or MAG_3 core, which is often appended with various groups, as shown in Figure 1.5. There are many ^{99m}Tc(V) compounds in clinical use today,[51] most of which owe their favourable biodistribution and tissue accumulation to their overall size, charge and lipophilicity, rather that the presence of a directing group such as a biomolecule. The major problems associated with these species are the lack of control over the isomers formed[54] (the *syn* and *anti* isomers are illustrated in Figure 1.5), and difficulties in characterizing the protonation states of the complexes at physiologically relevant pH.[55] The resulting diastereoisomers display different physiological properties.

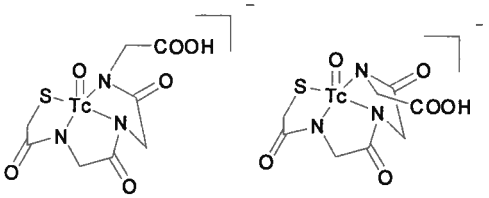

Figure 1.5 MAG_3 isomers – *syn* and *anti* (named for the relative orientation of the Tc=O bond and the pendant carboxylic acid).

As an example, ^{99m}Tc-Depreotide is a cyclic oligopeptide that acts as a somatostatin receptor (overexpressed by certain types of cancer cells) ligand and has been FDA approved for use in imaging lung cancer since 1999. It was only in 2007 that the *syn* and *anti* diastereomers of this compound were separated, thoroughly chemically identified, and their individual receptor affinities and biodistributions examined.[56, 57] The *syn* diastereomer makes up about 90 % of the complex when it is synthesized via the kit preparation used in making the radiopharmaceutical. This isomer has an IC_{50} of 0.15 nM, and a tumor uptake in mice of 6.58 % ID/g (the percentage of total injected dose that ends up in one gram of a particular

References begin on Pg 34

tissue) compared to the lower affinity *anti* isomer which exhibits an IC_{50} of 0.89 nM and a tumor uptake of 3.38 % ID/g. Given that both isomers have favourable imaging characteristics, the small percentage of the lower affinity *anti* isomer does not prove problematic, however a gap of eight years between the introduction of ^{99m}Tc-Depreotide onto the market and the full characterization and understanding of its components is quite surprising.

The other technetium core that has historically been the subject of much research also sees technetium in the (proposed) +5 oxidation state,[58] here combined with a hydrazinonicotinamide (HYNIC) ligand system (see Figure 1.6). These compounds are synthesized from the $[^{99m}TcO]^{3+}$ core by reaction with a functionalised hydrazine which replaces the oxo group. As the HYNIC ligand does not fill the coordination sphere, there tend to be multiple products formed as other ligand types and denticities bind to the metal, and although stable (no free pertechnetate is detected *in vivo*), the lack of thorough chemical characterisation of these compounds is problematic. The choice of co-ligand is crucial to the stability and biodistribution of these complexes, and work in this area is ongoing.[58-60]

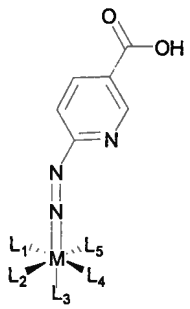

Figure 1.6 A generic HYNIC ligand system – the pyridyl nitrogen may bind to the metal in one of the L sites. The acid can be used for conjugation to a biomolecule such as a protein.

A simple and elegant synthesis of the very useful $[^{99m}Tc(CO)_3(H_2O)_3]^+$ core (Figure 1.7) by Alberto *et al.*[61] has sparked great interest in researching new SPECT radiotracers of this radionuclide. The core is attractive for several reasons; it is small, kinetically inert, stable to oxidation, and is amenable to chelation by several types of ligating atoms. Given this exciting combination of properties, Mallinckrodt Inc. (now called Covidien) has developed a kit preparation of this core by boranocarbonate reduction from the pertechnetate anion: Isolink™. This has prompted an explosion of research interest, and has lead to the discovery

References begin on Pg 34

of many new and potentially interesting coordination compounds. Using this tricarbonyl core, the formation of well defined and thoroughly characterized rhenium and technetium complexes is now possible.

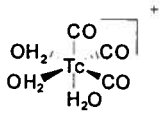

Figure 1.7 The technetium(I) tricarbonyl core pioneered by Alberto and coworkers;[61] the aqua ligands can be readily replaced, creating a useful platform for radiopharmaceutical development.

1.4.2 Technetium (I) Bioconjugates

Jaouen and coworkers were pioneers in the field of protein labeling with the organometallic tricarbonyl core. In 1993 they reported the labeling of proteins with $[CpRe(CO)_3]$ (where Cp is cyclopentadiene).[62] An *N*-hydroxysuccinimide ester bound to the Cp was reacted with free amines on the protein of interest, and the monoclonal antibody JOSS2-2 was found to retain satisfactory receptor recognition upon being labeled on 15 % of its available sites in this fashion.[62] After the development of the aqueous precursor for the tricarbonyl core,[61] a lot more research began to focus on these M(I) labelled bioconjugates. The first synthesis of an organometallic bioconjugate starting from the $[^{99m}Tc(H_2O)_3(CO)_3]^+$ core was by Alberto, Schibli and Schubiger,[63] who successfully labeled a 5-HT_{1A} serotonergic receptor ligand (Figure 1.8a), and found it to retain its receptor affinity once labeled. Since then, the major classes of biomolecules (nucleic acids, lipids, peptides and carbohydrates) plus examples of other small molecule receptor ligands have all been labelled with the tricarbonyl core.

Two examples of small molecule labelling with ^{99m}Tc are shown in Figure 1.8. 1-(2-Methoxyphenyl)-piperazine has been bound to the tricarbonyl core via a bidentate chelate (Figure 1.8a), as well as by way of a cyclopentadieneyl (Cp) moiety (see Chapter 5 for more information). The rhenium complex of this Cp ligand has a very high affinity (IC_{50} = 6 nM) for the 5-HT_{1A} serotonergic receptor.[64] Another example of small molecule bioconjugate formation came from Zubieta and coworkers;[65] biotin was linked via a five carbon alkyl chain to a fluorescent tridentate binding site (Figure 1.8b). This ligand forms stable complexes with both the rhenium and technetium tricarbonyl cores, and these complexes retain very high binding affinity for the biotin receptor avidin.[65]

References begin on Pg 34

Single nucleotide bases have been bound to the tricarbonyl cores. Guanine binds in a monodentate fashion through its *N*-7 atom, and two guanine molecules may be bound to each metal (Figure 1.8c).[66] In the solid state these two guanines are found in a head to tail arrangement. An in depth NMR study of the solution isomers and conformations resulting from the binding of nucleoside monophosphates (NMPs) to the rhenium tricarbonyl core showed that many binding modes were possible with NMPs – with monodentate binding being the most common.[67] There is particular interest in these species as it has been proposed that $[Re(CO)_3(H_2O)_3]^+$ may exhibit anticancer properties in cell studies, possibly by crosslinking DNA bases, in a way mechanistically similar to cisplatin.[67] Recently, chelating moieties have been appended to a structural mimic of DNA, in the hope of using this as an antisense oligodeoxynucleotide that is recognized by mRNA and incorporated into areas with upregulated gene expression of a targeted gene. No biological data is yet available, but this technology would be an important development in cancer diagnostics, as changes in patterns of gene expression may point to disease states before symptoms appear.[68]

Fatty acid type labeling has been achieved using C_{18} alkyl chains as Lipiodol surrogates – Lipiodol is a mixture of iodinated (with ^{131}I for therapy in liver cancer) fatty acid esters from poppy seed oil found to accumulate in and be retained by the liver. Coordination via both bidentate and tridentate ligand sets with pendant C_{18} chains to the Re, ^{99m}Tc and ^{186}Re tricarbonyl cores was reported by Alberto and coworkers.[29] The resulting complexes (Figure 1.8d) were stable for 24 hr in Lipiodol and 48 hr in an ethanol/water mixture, and are being investigated as potential diagnostic (^{99m}Tc) and radiotherapeutic ($^{186/188}Re$) pairs for the treatment of liver cancer.

Most work on bioconjugates of technetium has focused on the functionalisation of peptides. Santos and coworkers have used pyrazole-based tripodal ligands to attach a fragment of the peptide bombesin to the tricarbonyl core, and found that the resulting complexes were stable and retained affinity for cells that contained the receptor for bombesin.[28] Zubieta, Valliant and coworkers developed the single amino acid chelate (SAAC) technology, which incorporates a non-natural amino acid containing a tridentate metal binding group in its sidechain, which can then be added into a peptide chain.[71] An elegant extension of this work involved the incorporation of the non-natural, chelating amino acid, either alone or with the rhenium tricarbonyl core bound, into the automated synthesis of a peptide, with the resulting

compounds having similar affinity for the receptor as the parent (Figure 1.8e).[69] The same group has reported a method for the direct labeling of proteins by reaction with maleimide linked to one end of their bifunctional chelate. The maleimide reacts selectively with sulfhydryl groups to produce a stable thioether linkage between the metal chelate and the side chain of cysteine residues.[72] Recently Alberto and coworkers reported the synthesis of a single amino acid labeled with $[^{99m}Tc(CO)_3]^+$ (Figure 1.8f).[70] Its rhenium analog is taken up into cells via the LAT-1 amino acid transporter. This is an important discovery, as it shows that adding significant bulk (a linker, binding group and a metal ion) to a relatively small amino acid, does not always mean sacrificing the enzymatic recognition and activity of the parent molecule.

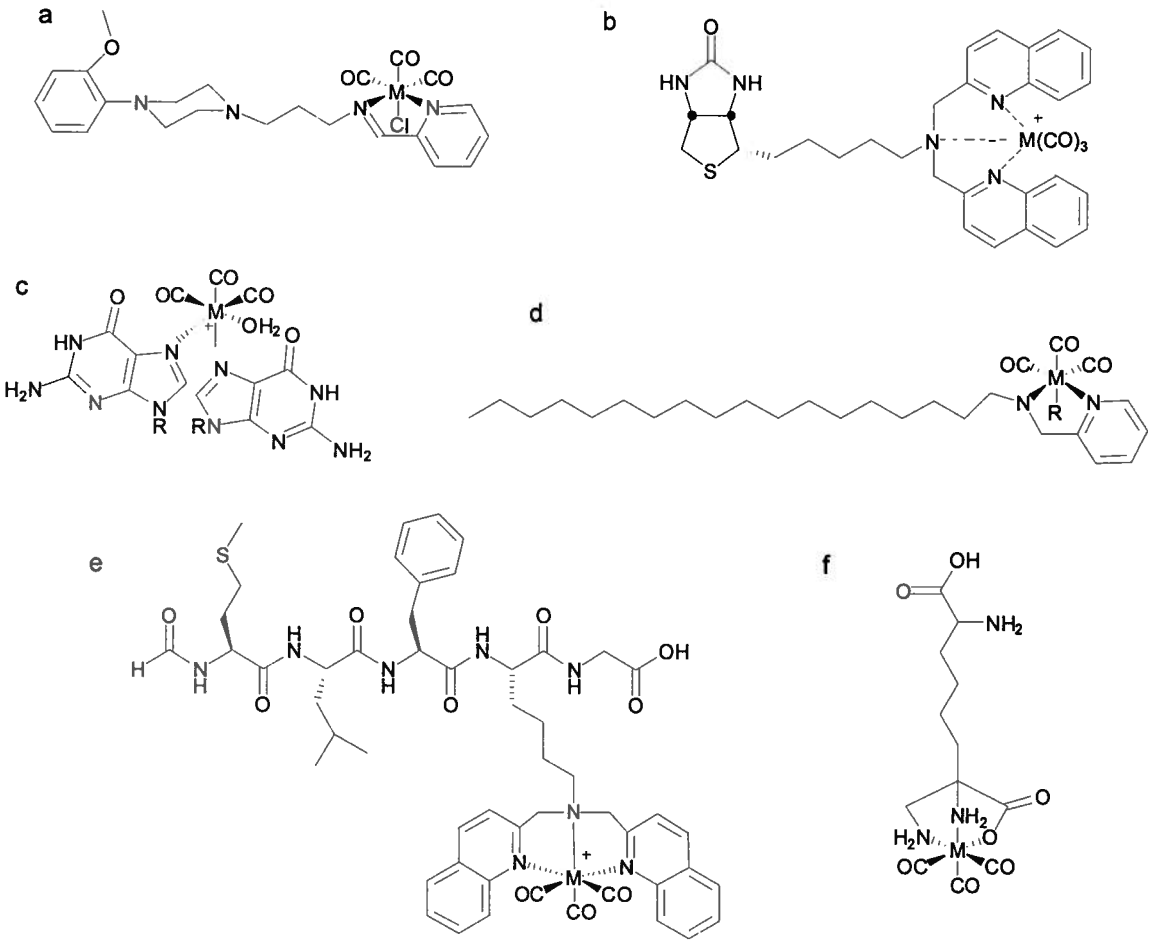

Figure 1.8 Some examples of small biologically active molecules labeled with the tricarbonyl core: a) a 5-HT_{1A} serotonergic receptor ligand with a bidentate chelate, M = ^{99m}Tc[63] b) a fluorescent biotin-conjugated compound, M = Re, ^{99m}Tc[65] c) the binding of guanine to the tricarbonyl core[66] d) a long Lipiodol-like alkyl chain labeled with the tricarbonyl core,[29] M = Re, ^{99m}Tc, ^{186}Re e) a peptide incorporating a single amino acid chelate[69] f) a non-natural amino acid that retains LAT-1 amino acid transporter activity.[70]

References begin on Pg 34

Carbohydrates have also been conjugated to the technetium tricarbonyl core, but as this area is the topic of a large part of this thesis, it is covered in more detail in the introduction sections of the relevant chapters.

1.5 Alzheimer's Disease

Alzheimer's Disease (AD) is a debilitating condition that is the fourth leading cause of death in the Western world.[73] Although AD was first discovered by Alois Alzheimer in 1906,[74] over a century later we still rely on the same primitive post mortem analysis to definitively diagnose AD. This is done by looking for two histological features in a brain biopsy; neurofibrillary tangles and β-amyloid plaques. The tangles are made of hyperphosphorylated τ-protein, while the plaques consist mainly of the β-amyloid protein.

AD affected 26.6 million people worldwide in 2006,[75] with incidence predicted to triple by 2050.[73] The Canadian health care system is estimated to have spent $1.7 billion in 2001 on the treatment and care of people with AD,[76] and that amount will continue to increase as incidence grows.[77] The symptoms of AD are a loss of memory and cognitive function, which lead to a gradual loss of overall function, and an inability to live an independent life. There is no known cure, so this decline in function and abilities, after a variable length of time, culminates in death. As the populations in developed countries continue to age, AD will place an increasing burden on society, both socially and financially.

1.5.1 The Amyloid Cascade Hypothesis

While 95 % of AD cases are late-onset, where age is the only firmly verified risk factor, there is a small percentage of the affected population that develops the disease at a young age (below 60). These people are said to have early onset AD. Genetic testing has shown mutation in four key genes to be a risk factor for developing AD: amyloid precursor protein (APP), presenilin 1 (PS1), and presenilin 2 (PS2) mutants have been linked with early onset AD. A certain allele (E4) of apolipoprotein, ApoE4, has been shown to be a risk factor for late onset AD, with those having two copies of E4 having increased risk over those with one copy. Amyloid Precursor Protein (APP) is a membrane bound protein that is cleaved to produce smaller Aβ fragments. Depending on the enzymes that control the cleavage, $A\beta_{1\text{-}40}$ or $A\beta_{1\text{-}42}$ will be produced.

References begin on Pg 34

Although both these fragments are found ubiquitously and are normal in undiseased individuals, they are found in high concentrations in the brains of people with AD, and the $A\beta_{1-42}$ that is normally the minor component is seen in higher relative concentrations. Although the exact role of PS1 and 2 are not known, they are known to be involved in the processing of APP, so may be involved with an overproduction of Aβ and/or the alteration in the $A\beta_{1-40}/A\beta_{1-42}$ ratio seen in AD. ApoE is a protein found in many organs of the body and with several functions involved in the binding and transporting of lipids. There are two main ways in which it has been implicated in AD; one is in the proteolytic degradation of Aβ, leading to a decrease in brain concentration of soluble Aβ,[78] and the other is in the binding and cross linking of the Aβ fragments.[79] Work in this area is ongoing, and there is still contention as to how these functions fit together to increase the risk of AD.

These genetic studies have helped to elucidate the key proteins in the cause and progression of AD, and aid our current understanding of the disease. As these mutations account for only a very small proportion of people who develop AD, work into these genetic causal and predictive factors is continuing.[80] Although apoE4 was identified as a risk factor for old age AD in 1993,[81] and the usefulness of such genetic markers is widely recognized, it remains the only reliable genetic determinant of late onset AD.[82]

The amyloid cascade hypothesis was first postulated by Hardy and Higgins in 1992.[83] It proposed that the deposition of β-amyloid was the cause and first step in the progression of AD, and that all other histologies and symptoms are downstream effects. In the years following this proposal, a great deal of research has verified and expanded upon this idea, and it is now accepted by many working on AD that the errant behavior of the amyloid protein is a key causal factor in the development of AD. The key evolution to this theory is that it is not simply the presence of the characteristic amyloid deposits themselves that are the toxic, problematic species, but it is now thought to be soluble forms of amyloid in close proximity with metal ions that are the key toxic species.[84]

β-Amyloid (amyloid, or Aβ) is a protein found ubiquitously in human cells, but its natural function is not yet well understood. It is formed by the precise cutting of a amyloid precursor protein (APP), and there are several enzymes involved in this cleavage; α, β, and γ-secretases. β-secretase cleaves to form the N-terminal end of the Aβ, while the position the γ-secretase cuts

References begin on Pg 34

determines the exact position of the C-terminus, and therefore the length of the resulting peptide. Normally γ-secretase cleaves to give a 40 amino acid peptide called $A\beta_{1-40}$, but in AD, for reasons not fully understood, APP is more frequently cleaved between residue 42 and 43 to give a larger proportion of $A\beta_{1-42}$. Residues 41 and 42 are alanine and isoleucine respectively, both quite hydrophobic amino acids, which gives $A\beta_{1-42}$ a much higher propensity for aggregating with itself, meaning it is more prone to forming oligomers and plaques in the aqueous environment of our bodies.

β-Amyloid contains some very high affinity copper binding sites,[85] reminiscent of those found on prion proteins that are known to bind copper *in vivo*. It is thought that the natural role of β-amyloid may somehow involve the transport and/or storage of copper. There has been much speculation as to why a protein that naturally occurs throughout our bodies can lead to such toxicity in this disease state. One well documented answer is that it is the position of the amyloid within the cell that is problematic. Under normal circumstances the vast majority of amyloid is membrane-associated. When binding metals, amyloid forms a hexamer, which is embedded in a membrane, and is not redox active. The propensity of the amyloid to be inserted into the membrane is affected by several factors such as the pH, lipid composition and the presence of metal ions, and as such is very delicately balanced.[86] If the amyloid becomes oxidized, it is proposed that it becomes redox active, and less strongly associated with the membrane. This initial oxidation is likely caused by the increased concentrations of freely releasable redox active copper in the aging brain. As the brain becomes aged and worn, the many enzymes required for the tightly regulated homeostasis of potentially reactive metal ions may not do their job so well, and the concentrations of free metal ions may increase.

There are high levels of iron, copper and zinc found in the neuropil of the brains of AD sufferers.[87] The levels of these metals found are three to five times those occurring in the brains of non-AD sufferers of the same age.[87] There is evidence that the normal enzyme-assisted homeostasis of these metal ions is drastically altered in AD brains.[88] The mechanisms that control the homeostasis of these ions become worn and less efficient with age, which may help explain why age is the main causal factor in developing AD. Also, as the blood brain barrier becomes worn with age it may not do such a good job of regulating the brain's uptake and regulation, so this may lead to altered metal concentrations.

References begin on Pg 34

Free copper may be taken up by the high affinity binding sites on amyloid, but if the system becomes overwhelmed with copper, it is possible that other, redox active sites on the Aβ become occupied, or that the copper is not bound, so will react when it comes into contact with a suitable oxidation partner. Cu^{2+} can be reduced to Cu^{+} quite readily in the presence of an easily oxidized substrate such as a methionine or tyrosine residue.[89] Aβ oxidized at Met^{35}, a very common site of oxidation, has been shown to emerge from within the membrane, and at this point the solubilised peptide, bound to, or in close proximity to free metal ions, becomes capable of redox activity to produce peroxide. Once peroxide is produced in the vicinity of the metal ions copper and iron, Fenton type chemistry can lead to the production of reactive oxygen species (ROS) such as $OH^{\bullet}$, a highly reactive radical. The reactivity of ROS means that they are unselective in their activity, and will react with and damage whatever molecules they first come into contact with. *In vivo* they are commonly in close proximity and therefore react with peptides, lipids, or DNA. Damage to such important molecules leads to a loss of function, may stimulate the inflammatory response with all the complications that invokes, and particularly in the case of DNA damage can lead to cell death.

In 1999 it was proposed that soluble forms of amyloid were responsible for the problems associated with AD.[90] Although amyloid plaque loading could be used to categorize patients as AD and non-AD, it did not vary reliably with disease severity, and was in fact found to be inversely correlated to oxidative damage.[91] On the other hand, soluble amyloid was shown to vary in line with stage and severity of disease. If the species that produce ROS are soluble, they are not confined to one specific area within the brain. They can diffuse into and around the interstitial spaces where they continue to catalytically produce ROS and damage cells and under certain circumstances they can also run into high concentrations of zinc ions. Zinc is released from synapses upon activation by electrical pulse. This is the method *via* which signals are transmitted and information is passed through the nervous system. Under normal conditions, as soon as the nerve impulse has passed, the synapse reabsorbs the zinc. But if amyloid oligomers are nearby, they will compete for the zinc by binding it in one of their many possible metal binding sites. It has been shown that some of the binding sites on Aβ have a high enough affinity for Zn^{2+} that they can compete for the zinc on the time scale of reabsorption by the synapses.[92] The metal ions can catalyse the cross-linking of nearby peptides, so these zinc bound species can get quite large, and become insoluble fibrils with all kinds of oxidative cross-linking taking place to cement the aggregate together. The binding of zinc to the oligomers

References begin on Pg 34

quenches some of the redox activity, possibly through the replacement of the copper by the redox silent zinc.

It has been proposed that the amyloid plaques are actually protective, and that their formation leads to the trapping and redox-silencing of potentially dangerous metal ions.[91] Despite the idea that it is likely the soluble oligomers of amyloid that cause the most damage, the presence of plaques is also detrimental. Plaques are still found to be able to produce peroxide and ROS, and cause secondary effects such as the inflammatory response and microglial activation.[93] It is also possible that the plaques act as reservoirs which are in equilibrium with the soluble amyloid, and release oligomers over time to keep the levels of soluble species at a constant concentration.[94]

1.5.2 Current Treatments for Alzheimer's Disease

There is no cure for Alzheimer's disease. Symptoms develop due to extensive cell damage and death, and these effects are not reversible. Current treatments are administered with the hope of slowing the progression of the disease. There is significant research going on into both treatments and early diagnostic tools for AD.

It is possible to predict and diagnose the development of AD with currently existing methods. For example, FDG (shown in Scheme 1.1) has been used in many clinical studies, and provides reliable differentiation between AD patients and age matched controls.[95] Several studies have found that glucose metabolizm is lowered in certain brain regions in patients who will go on to develop dementia compared to those who will not.[96] However, it is not yet accurate enough to be used in routine screening, and does not do a reliable job of predicting AD compared to other types of dementia. Practically this type of diagnosis is not viable, as the whole population would need to be scanned before any symptoms were visible, but it is important to help understand the development of the disease.

There are four compounds currently approved for the treatment of AD in Canada; these are shown in Figure 1.9. Galantamine, rivastigimine and donepezil (Figure 1.9a-c) are approved for use in mild to moderate disease states, and all work as acetylcholinesterase inhibitors. The main function of these compounds in treating AD is in inhibiting the action of the protein that breaks down acetylcholine – a neurotransmitter that has reduced levels in AD.[97] By preventing this

References begin on Pg 34

breakdown, the brain has more of this important neurotransmitter. This is now agreed to be a very downstream affect in AD; given the efficacy of these treatments it has been proposed that they may act on some other, upstream, targets as well, and that this may lead to the observed therapeutic effect.

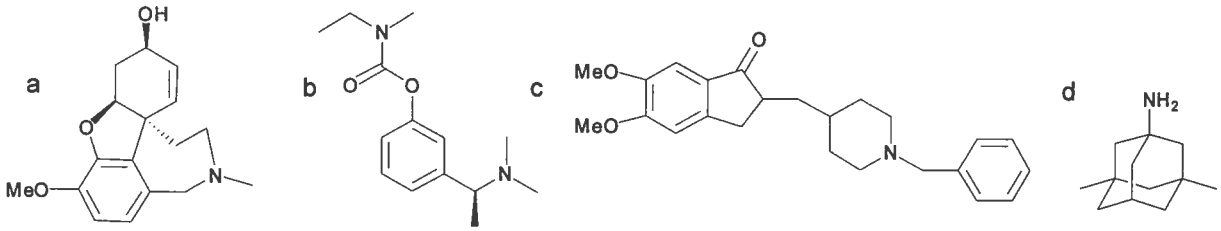

Figure 1.9 Drugs currently on the market in Canada for the treatment of AD: a) galantamine b) rivastigimine c) donepezil d) memantine.

Memantine (Figure 1.9d) is used in moderate to advanced disease states, and works as an NMDAR antagonist.[98] NMDA is N-methyl-D-aspartic acid, and its receptor NMDAR is an ion channel (especially important for Ca^{2+} transmission) that is open when bound to its natural substrate glutamate. In AD, glutamate, an excitatory neurotransmitter, is often overproduced, and this can lead to overstimulation of the NMDA receptor and cell death. Memantine binds to the NMDA receptor in the brain and inhibits the natural substrate glutamate from stimulating the receptor. Memantine is of low enough affinity that it can be displaced by high concentrations of glutamate, allowing for normal neurotransmission to take place.

Antioxidants are currently used in the treatment of AD. These react with free radicals in the brain to prevent them reacting with other biologically important molecules, and thus to prevent the furthering of oxidative damage. As the oxidative damage is only one facet of a complicated disease, this treatment appears to be somewhat symptomatic, and does not fully prevent the advancement of AD, only slows it down.[99] A clinical trial of α-tocopherol (vitamin E), a known antioxidant, administered to AD patients showed that this strategy has merit.[100] The patients who were given vitamin E lived on average 230 days longer, and had delayed admission to an institution compared to the non-treated control group.[100] However, there was no significant improvement in the cognitive test scores of the treated vs. the non-treated patients.[100] This suggests that while antioxidants have a role to play in reducing the downstream effects of AD, alone they are not powerful enough to stop or reverse the disease's progress.

References begin on Pg 34

Non-steroidal anti-inflammatory drugs (NSAIDs) have been postulated to help in AD for quite some time.[101] They are expected to help relieve the symptoms of AD by reducing inflammation that occurs as part of the natural inflammatory response. Alzheimer's patients exhibit a significant inflammatory response as a result of the biochemical trauma that occurs in their brains. A study of transgenic mice who were given large daily doses of ibuprofen for six months from the time their AD symptoms first started developing showed a significant reduction in the number and size of Aβ plaques compared to non-treated controls.[102] There have been conflicting reports on the effectiveness of such treatments in humans. One of the most comprehensive studies was published recently, where seven different doses of 21 NSAIDs were given to over 49,000 patients over a five year time period.[103] Four of the NSAIDs were also known to have anti-$A\beta_{1-42}$ effects, and decrease serum levels of the peptide as seen in transgenic mice. Overall there were some protective effects seen, and these were more noticeable in the cases of known anti-Aβ NSAIDs, and the longer the subject was given the drug.

Beta (β) and gamma (γ) secretases are responsible for cleaving the ends of Aβ from APP.[104] Inhibition of these enzymes as a method to control the amount of amyloid produced have been the subject substantial research over the past decade or so, including at big pharmaceutical companies. Gamma secretase cleaves the C-terminus of Aβ, and can do so in several positions to form a peptide between 39 - 42 residues long.[104] Gamma secretase is a complex structure made up of several proteins embedded in the membrane,[105] and known to contain PS1 and 2, genetic mutations of which are linked with early onset AD (see above). Beta secretase or BACE-1 (beta site of APP cleaving enzyme 1) is responsible for the first step in the formation of Aβ - the cleavage of the N terminus.[104] This area of the APP can alternatively be cleaved by alpha secretase, and when this occurs a different fragment is produced that does not go on to produce any of the effects of AD. BACE has not been genetically linked to AD, but it is found in high levels in the brains of people with late onset AD.

Inhibition of either of these secretases reduces the amount of Aβ in the brain, so inhibitors of both have been under investigation as AD therapeutics. A gamma secretase inhibitor was tested in a trial of 51 AD patients by Eli Lilly for 12 weeks.[106] They found a significant reduction in the $A\beta_{1-40}$ in the plasma (~ 60 %) of treated patients, and could not measure the $A\beta_{1-42}$. There was no significant change in the levels of $A\beta_{1-40}$ or $A\beta_{1-42}$ in the CSF (cerebrospinal fluid) of treated patients, as was expected. This may be due to the lag time of Aβ levels equilibrating

References begin on Pg 34

between the serum and the CSF. There were no changes in the behavioural testing of the treated group, but the authors state that given the relatively short time frame of the study and the slow rate of disease progression, this may be affected if treatment was sustained over a longer time period.[106]

β-secretase (BACE) inhibitors are a little behind the γ-secretases in development, but a lot of research is now being done in this area. Many research groups and companies have come up with potent inhibitors of β-secretase,[107] including some that show reduction of Aβ in animal models.[108] But it is yet to be seen how these perform in large scale human trials.

Another strategy for the potential treatment of AD has been the development of an anti-amyloid vaccine.[109] The way a vaccine would work is by the immunised body raising antigens to the peptide, allowing it to develop increased clearance mechanisms for Aβ. Problems occurred in clinical trials when a small but significant percentage of the population developed meningoencephalitis due to reaction of the $A\beta_{1-42}$.[110] This problem is being circumvented by using shorter chain Aβ analogs, which are showing promise in mouse and monkey models.[111]

A slightly less orthodox suggestion is that the restriction of calories may help to treat AD.[112] This is proposed to work because a significant lack of calories may trigger a mild stress response which is known to increase the production of proteins that promote the growth and survival of neurons.

As AD is such a complex condition that is still not thoroughly understood, there are several other avenues of possible treatment being investigated. Those outlined here are either currently used drugs or those with a large amount of research interest that have shown promise as potential therapeutics.

1.5.3 Metal Chelators to Treat Alzheimer's Disease

Desferrioxamine (DFO) (Figure 1.1, right hand box), a well known metal chelator, with a particularly high affinity for trivalent metal ions, was investigated as a treatment for AD.[113] At the time it was thought that aluminum was involved in AD, so the hypothesis behind these tests was that the DFO would chelate the Al^{3+} ions and thereby slow the progression of dementia.

References begin on Pg 34

After two years of twice daily intramuscular DFO injections, it was found that the DFO had had a significant effect, with the non-treated group intellectually deteriorating twice as fast as the treated group. There were no improvements, just a slowing of decline observed in the treated patients. The authors note that the DFO would chelate Fe^{3+} even more readily than Al^{3+}, though when iron levels were low a threefold increase in aluminum levels in the urine was induced by the DFO. However, it is mentioned in this initial paper, and research since this publication has added much weight to the argument, that it may be the chelation of the iron that was responsible for a significant amount or even the majority of the observed effect. It is noted in the paper that the formation of radicals is promoted by free iron, so the removal of this would have the capacity to reduce the oxidative stress of the patient, slowing oxidative damage and therefore neurological decline.

There was a large time lapse between the DFO studies and the next investigations of metal chelators as a treatment option for AD. Clioquinol (CQ) (Figure 1.10a) is a bidentate chelator, with an *N,O* binding sphere, known to bind to a range of metals.[114, 115] It was used as an off-the-shelf, proof of concept therapeutic, as it had FDA approval as an anti-infective,[116] meaning it could relatively easily be used in human trials. *In vitro* studies had established that CQ could dissolve Aβ aggregates and inhibit the toxicity of Aβ to neuronal cells.[117] Preclinical trials were carried out in Tg2576 mice that were genetically engineered to overexpress $A\beta_{1\text{-}42}$ and thus develop the histologies and symptoms of AD.[117] These mice were dosed with CQ at 30 mg/kg/day for 9 weeks and at the end of this time they showed improved cognitive abilities, as measured in a water maze, compared with their control treated transgenic peers.[117] The treated mice were also found to have a 49 % reduction in Aβ deposition over this time period. By the end of the nine weeks, the treated animals were more healthy than the non-treated controls in terms of weight and various toxicology measures.[117] Interestingly triethylaminetetraamine (TETA) (Figure 1.10b) was used as a control for general metal chelation throughout the body being responsible for the observed effects, and it was found not to have a significant effect on these mice. This is proposed to be because unlike CQ, TETA does not cross the BBB, so cannot access the brain and therefore cannot chelate the metals in the crucial places.[117] This finding shows the lack of utility in the approach to systemic metal chelation as a treatment for AD – the potential therapeutic must have brain access to be effective, at least in the area of metal chelation.

References begin on Pg 34

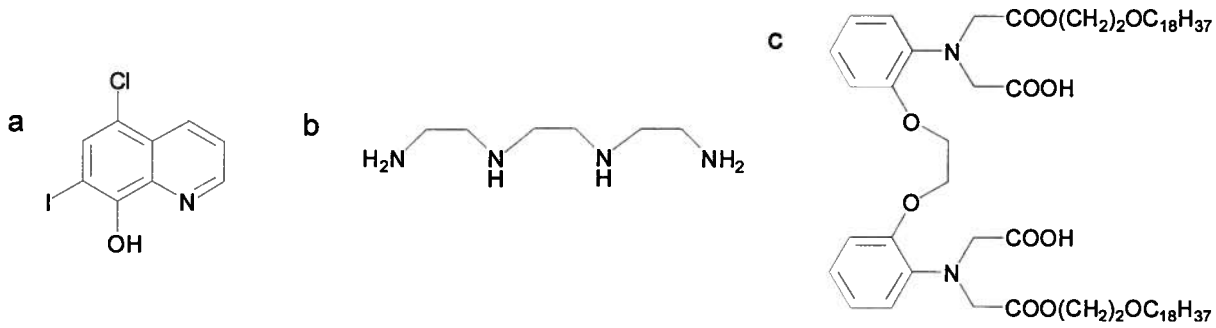

Figure 1.10 a) Clioquinol (CQ) and b) triethylenetetraamine (TETA)[117] c) DP-109,[118] chelators used in mouse model studies of AD.

These results from the CQ mouse study were promising, so a phase II clinical trial was carried out in humans (phase I was not required as CQ had prior FDA approval for human use, and the major side effects are known).[116] Here the results were mildly encouraging. Thirty six patients with varying stages of AD were given oral doses of CQ twice daily for 36 weeks with all doses increasing over time.[116] Benefit was most obvious in the patients with more advanced AD, but it was not found to be statistically significant over those given placebo after 36 weeks as measured by cognitive testing results. After four weeks there was a small improvement seen in the severe cases, and the authors propose this is due to the ability of CQ to neutralize the pool of soluble Aβ.[116] Plasma levels of $A\beta_{1\text{-}42}$ were measured and were found to decrease in the treated patients, and to maintain a lower level over the course of the trials.[116] This finding was more pronounced in the more severe cases of AD. Plasma metal levels were also monitored, and the amount of zinc in the plasma increased upon treatment with CQ, whereas the copper plasma levels were not affected.[116] Zinc levels prior to beginning the study were lower than age matched controls, so an increase in zinc may indicate some kind of restorative effect. A study of two patients with early onset AD showed similar results.[119] The nature of this study means that no hard conclusions can be drawn, but one patient was observed to be stable over the fourteen months of treatment, while the other showed a slight improvement followed by stabilization over the nine months of CQ administration.

The authors propose CQ as a prototypical metal-protein attenuating compound (MPAC).[116] CQ is a moderate affinity chelator, but is not strong enough to, for example, remove copper from the highest affinity binding site on Aβ – with approx 8 aM affinity.[85] CQ could effectively treat AD despite having a lower affinity for key metal ions than some of the protein sites with which it was competing. This led the authors to suggest that the metal did not have to be fully removed

References begin on Pg 34

from the M – Aβ interaction, but rather that interaction just needed to be perturbed so that the brain's homeostatic mechanisms could have a chance to catch up and reinstate its normal state of being.[120] Thus the attenuation of the disease state was all that was required, and the brain would help itself once some of the plaques and oligomers were broken up, and the rate of ROS production was slowed.

A compound very similar to CQ, PBT2 whose structure has never been disclosed, was designed to overcome some of the weaknesses in CQ.[121] It is also an 8-hydroxyquinoline, but without an iodine attached, and is easier to synthesize and has improved solubility and increased BBB permeability as compared to CQ.[122] In vitro PBT2 displayed the same traits as CQ in its ability to inhibit the formation of crosslinked Aβ oligomers, to redissolve Zn-aggregated species and to prevent the redox activity that leads to the formation of H_2O_2.[121] In AD models in mice it was able to improve the learning and memory in a matter of hours after administration.[122] This is proposed to be due to the rapid clearance and redistribution of soluble Aβ in the interstitial fluid, which the authors claim is maybe what causes the symptoms of AD. The compounds were tested in two different strains of mice and this theory is the only one consistent with the results seen in the two varieties of mice.[122] The authors suggest that this interstitial Aβ affects the neurons ability to transmit signals, and that this may be an underappreciated facet of the human disease as well. PBT2 is proposed to chaperone Cu and Zn ions away from Aβ and into cells where the normal homeostatic mechanisms can take over. As discussed above, the complicated relationship between metal ion levels and Aβ can be easily perturbed, and this helping hand may be all that is needed to let the body heal itself by utilizing its normal feedback cycles of protein expression and regulation. PBT2 treatment of transgenic mice did not affect the levels of metal ions seen in either the brain or the body, suggesting to the authors that it acts as an ionophore, chaperoning metal ions for a time only.

PBT2 has recently finished a phase IIa clinical trial with good results.[123] It was administered to 49 AD patients in two different doses in a once daily oral dose for three months. There were no significant adverse effects seen. The higher dose of PBT2 elicited a significant reduction in the concentration of $A\beta_{1-42}$ in the CSF, but not in the plasma. This shows that PBT2 is somehow affecting central Aβ clearance *in vivo*. Serum metal concentrations were not affected, again supporting the fact that this compound helps redistribute metals rather than strongly binding them. Most notably, there was a statistically significant improvement in executive function seen

References begin on Pg 34

in the patients receiving the higher dose of PBT2. Although the authors note that these findings need to be verified in a larger sample size over a longer period of time, these results are very exciting for the future of the MPAC approach to the treatment of AD.

Other chelators have since been investigated in what others believe could be a useful methodology for treating this debilitating disease. DP-109 is a lipophilic chelator,[118] the structure of which is given in Figure 1.10c. It was found to reduce the number of amyloid plaques while increasing levels of dissolved Aβ when administered daily for three months in Tg2576 mice.[118] The authors claim DP-109 shows some selectivity for copper and zinc over other metal ions and that it likely crosses the BBB due to its lipophilicity and efficacy.[118]

Our approach is to incorporate these metal binding characteristics that show such promising results with more biologically relevant features (*vide infra*). This involves the addition of antioxidant capability into the molecules to passivate ROS, as well as glycosylation to improve water solubility, mask the chelating part of the molecule and target the resulting prodrugs to cross the blood brain barrier.

1.6 Thesis Overview

This thesis focuses on the use of carbohydrate conjugation as a method for controlling the biodistribution of compounds for use in medicinal inorganic chemistry. The thesis covers two distinct projects. This work fits into the categories of medicinal inorganic chemistry as outlined in Figure 1.1.

The first focuses on Alzheimer's disease therapeutics developed in the Orvig group. The role of this work in that project was to use radiochemistry as a tool to determine the *in vivo* distribution of the compounds. As Alzheimer's disease is a disease of the brain, the radiolabelled compounds that were synthesized in this work were tested to see if they crossed the blood brain barrier into the brain. This was a crucial step in the progress of this project, and as the outcome was positive for the compounds crossing into the brain, work on this project has progressed with increased hope of finding a multifunctional way to treat Alzheimer's disease. This work is discussed in Chapter 2.

References begin on Pg 34

The second part of this thesis focuses on the development of carbohydrate conjugates for molecular imaging with ^{99m}Tc. This work includes a study of different tridentate, monoanionic, glucosamine based ligands and their binding to the $[M(CO)_3]^+$ core (M = Re, ^{99m}Tc). It also examines the effects of varying the length of the linker between the carbohydrate and the metal binding portion of the molecule. The variation in linker length is applied to both the tridentate ligand sets and Cp (cyclopentadienyl) based compounds. These compounds are synthesized (both cold and radioactive analogs), characterised, and tested for stability under biologically relevant conditions. They are then subjected to assays with the key enzymes in carbohydrate biodistribution; GLUT-1 and hexokinase. This work is outlined in Chapters 3, 4 and 5.

References begin on Pg 34

1.7 References

1. Alderden, R. A.; Hall, M. D.; Hambley, T. W., *J. Chem. Ed.* **2006,** *83*, 728 - 734.

2. Chan, K. W.-Y.; Wong, W.-T., *Coord. Chem. Rev.* **2007,** *251*, 2428 - 2451.

3. Singh, S.; Khodr, H.; Taylor, M. I.; Hider, R. C., Therapeutic Iron Chelators and Their Potential Side-effects. In *Free Radicals and Oxidative Stress: Environment, Drugs and Food Additives*, Rice-Evans, C.; Halliwell, B.; Lunt, G. G., Eds. Portland Press: London, 1995; pp 127-137.

4. Cyr, J. E.; Pearson, D. E.; Wilson, D. W.; Nelson, C. E.; Guaraldi, M.; Azure, M. T.; Lister-James, J.; Dinkelborg, L. M.; Dean, R. T., *J. Med. Chem.* **2007,** *50*, 1354 - 1364.

5. Sharkey, R. M.; Goldenberg, D. M., *J. Nucl. Med.* **2005,** *46*, S115 - S127.

6. Rose, B.; Matthay, K. K.; Price, D.; Huberty, J.; Klencke, B.; Norton, J. A.; Fitzgerald, P. A., *Cancer* **2003,** *98*, 239 - 248.

7. Abrams, M. J.; Davison, A.; Jones, A. G.; Costello, C. E.; Pang, H., *Inorg. Chem.* **1983,** *22*, 2798 - 2800.

8. Boucher, C. A.; Wackers, F. J.; Zaret, B. L.; Mena, I. G., *Am. J. Cardiol.* **1992,** *69*, 22 - 27.

9. Delbeke, D., *J. Nucl. Med.* **1999,** *40*, 591 - 603.

10. Foster, N. L., *Exp. Neurol.* **2003,** *184*, 2 - 8.

11. Grossband, M. L., *Monoclonal Antibody-Based Therapy of Cancer*. Marcel Dekker: New York, 1998.

12. Gittoes, N. J.; Franklyn, J. A., *Drugs* **1998,** *55*, 543 - 553.

13. Lee, C. K.; Aeppli, D. M.; Unger, J.; Boudreau, R. J.; Levitt, S. H., *Am. J. Clin. Oncol.* **1996,** *19*, 102 - 107.

14. Davies, A. J., *Oncogene* **2007,** *26*, 3614 - 3628.

15. Rufini, V.; Fisher, G. A.; Shulkin, B. L.; Sission, J. C.; Shapiro, B., *J. Nucl. Med.* **1996,** *37*, 1464 - 1468.

16. Sgouros, G., *Adv. Drug. Deliver. Rev.* **2008,** *60*, 1402 - 1406.

17. Nilsson, S.; Franzen, L.; Parker, C.; Tyrrell, C.; Blom, R.; Tennvall, J.; Lennernas, B.; Petersson, U.; Johannessen, D. C.; Sokal, M.; Pigott, K.; Yachnin, J.; Garkavij, M.; Strang, P.; Harmenberg, J.; Bolstad, B.; Bruland, O. S., *Lancet Oncol.* **2007,** *8*, 587 - 594.

18. Li, Y.; Tian, Z.; Rizvi, S. M. A.; Bander, N. H.; Allen, B. J., *Prostate Cancer P. D.* **2002,** *5*, 36 - 46.

19. Allen, T. M., *Nat. Rev. Cancer* **2002,** *2*, 750 - 763.

20. Zalutsky, M. R.; Vaidyanathan, G., *Curr. Pharm. Design* **2000,** *6*, 1433 - 1455.

21. Wilbur, D. S.; Hamlin, D. K.; Chyan, M.-K.; Brechbiel, M. W., *Bioconjugate Chem.* **2008,** *19*, 158 - 170.

22. Steffen, A. C.; Almqvist, Y.; Chyan, M.-K.; Lundqvist, H.; Tolmachev, V.; Wilbur, D. S.; Carlsson, J., *Oncol. Rep.* **2007,** *17*, 1141 - 1147.

23. Talanov, V. S.; Yordanov, A. T.; Garmestani, K.; Milenic, D. E.; Arora, H. C.; Plascjak, P. S.; Eckelman, W. C.; Waldmann, T. A.; Brechbiel, M. W., *Nucl. Med. Biol.* **2004,** *31*, 1061 - 1071.

24. Robinson, M. K.; Shaller, C.; Garmestani, K.; Plascjak, P. S.; Hodge, K. M.; Yuan, Q.-A.; Marks, J. D.; Waldmann, T. A.; Brechbiel, M. W.; Adams, G. P., *Clin. Cancer Res.* **2008,** *14*, 875 - 882.

25. Adam, M. J., *J. Labelled Compd. Radiopharm.* **2002,** *45*, 167 - 180.

26. Knesaurek, K.; Machac, J., *BMC. Nucl. Med.* **2006,** *6*, 5.

27. Canadian, I. f. H. I., *Medical Imaging Technologies in Canada, 2006 - Supply, Utilization and Sources of Operating Funds* **2006.**

28. Alves, S.; Paulo, A.; Correia, J. D. G.; Gano, L.; Smith, C. J.; Hoffman, T. J.; Santos, I., *Bioconjugate Chem.* **2005,** *16*, 438 - 449.

29. Saw, M. M.; Kurz, P.; Agorastos, N.; Hor, T. S. A.; Sundram, F. X.; Yan, Y. K.; Alberto, R., *Inorg. Chim. Acta* **2006,** *359*, 4087 - 4094.

30. Lawrentschuk, N.; Poon, A. M. T.; Scott, A. M., *Clin. Nucl. Med.* **2006,** *31*, 788 - 789.

31. Lazzeri, E.; Manca, M.; Molea, N.; Marchetti, S.; Consoli, V.; Bodei, L.; Bianchi, R.; Chinol, M.; Paganelli, G.; Mariani, G., *Eur. J. Nucl. Med.* **1999,** *26*, 606 - 614.

32. Stick, R. V., *Carbohydrates: The Sweet Molecules of Life*. Academic Press: London, 2001.

33. Garrett, R. H.; Grisham, C. M., *Biochemistry*. 2 ed.; Saunders College Publishing: Orlando, 1999; p 705.

34. Warburg, O., *Science* **1956,** *123*, 309 - 314.

35. Brown, R. S.; Goodman, T. M.; Zasadny, K. R.; Greenson, J. K.; Wahl, R. L., *Nucl. Med. Biol.* **2002,** *29*, 443 - 453.

36. Bennett, W. S. J.; Steitz, T. A., *Proc. Natl. Acad. Sci.* **1978,** *75*, 4848 - 4852.

37. Rempel, A.; Mathupala, S. P.; Pedersen, P. L., Glucose Catabolism in Cancer Cells: Role and Regulation of Hexokinase Overexpression. In *Cell Growth and Oncogenesis*, Bannasch, P.; Kanduc, D.; Papa, S.; Tager, J. M., Eds. Birkhauser: Basel, 1998; pp 3 - 14.

38. Pelicano, H.; Martin, D. S.; Xu, R.-H.; Huang, P., *Oncogene* **2006,** *25*, 4633 - 4646.

39. Bertoni, J. M.; Weintraub, S. T., *J. Neurochem.* **1984,** *42*, 513 - 518.

40. Yoshioka, K.; Saito, M.; Oh, K.-B.; Nemoto, Y.; Matsuoka, H.; Natsume, M.; Abe, H., *Biosci. Biotech. Biochem.* **1996,** *60*, 1899 - 1901.

41. Speizer, L.; Richard, H.; Howard, K., *Biochim. Biophys. Acta* **1985,** *815*, 75 - 84.

42. Battaglia, G.; La Russa, M.; Bruno, V.; Arenare, L.; Ippolito, R.; Copani, A.; Bonina, F.; Nicoletti, F., *Brain Res.* **2000,** *860*, 149 - 156.

43. Zhang, M.; Zhang, Z.; Blessington, D.; Li, H.; Busch, T. M.; Madrak, V.; Miles, J.; Chance, B.; Glickson, J. D.; Zheng, G., *Bioconjugate Chem.* **2003,** *14*, 709 - 714.

44. Joost, H.-G.; Thorens, B., *Mol. Membr. Biol.* **2001,** *18*, 247 - 256.

45. Medina, R. A.; Owen, G. I., *Biol. Res.* **2002,** *35*, 9 - 26.

46. Rudlowski, C.; Moser, M.; Becker, A. J.; Rath, W.; Buttner, R.; Schroder, W.; Schurmann, A., *Oncology* **2004,** *66*, 404 - 410.

47. Maschauer, S.; Prante, O.; Hoffmann, M.; Deichen, J. T.; Kuwert, T., *J. Nucl. Med.* **2004,** *45*, 455 - 460.

48. Smith, T. A. D., *Nuc. Med. Biol.* **2001,** *28*, 1 - 4.

49. Dilworth, J. R.; Parrott, S. J., *Chem. Soc. Rev.* **1998,** *27*, 43 - 55.

50. Banerjee, S. R.; Maresca, K. P.; Francesconi, L. C.; Valliant, J. F.; Babich, J. W.; Zubieta, J., *Nuc. Med. Biol.* **2005,** *32*, 1 - 20.

51. Mahmood, A.; Jones, A. G., Technetium Radiopharmaceuticals. In *Handbook of Radiopharmaceuticals*, 1 ed.; Welch, M. J.; Redvanly, C. S., Eds. John Wiley & Sons Ltd.: Chichester, England, 2003; pp 323 - 362.

52. Liu, S., *Chem. Soc. Rev.* **2004,** *33*, 445 - 461.

53. Davison, A.; Jones, A. G.; Orvig, C.; Sohn, M., *Inorg. Chem.* **1981,** *20*, 1629 - 1632.

54. O'Neil, J. P.; Wilson, S. R.; Katzenellenbogen, J. A., *Inorg. Chem.* **1994,** *33*, 319 - 323.

55. Marzilli, L. G.; Banaszczyk, M. G.; Hansen, L.; Kuklenyik, Z.; Cini, R.; Taylor, A. J., *Inorg. Chem.* **1994,** *33*, 4850 - 4860.

56. Cantorias, M. V.; Howell, R. C.; Todaro, L.; Cyr, J. E.; Berndorff, D.; Rogers, R. D.; Francesconi, L. C., *Inorg. Chem.* **2007,** *46*, 7326 - 7340.

57. Cyr, J. E.; Pearson, D. E.; Nelson, C. A.; Lyons, B. A.; Zheng, Y.; Bartis, J.; He, J.; Cantorias, M. V.; Howell, R. C.; Francesconi, L. C., *J. Med. Chem.* **2007,** *50*, 4295 - 4303.

58. King, R. C.; Surfraz, M., B.-U.; Biagini, S. C. G.; Blower, P. J.; Mather, S. J., *Dalton Trans.* **2007**, 4998 - 5007.

59. Babich, J. W.; Coco, W. G.; Barrow, S.; Fischman, A. J.; Femia, F. J.; Zubieta, J., *Inorg. Chim. Acta* **2000,** *309*, 123 - 136.

60. Kovacs, M. S.; Hein, P.; Sattarzadeh, S.; Patrick, B. O.; Orvig, C., *J. Chem. Soc., Dalton Trans.* **2001**, 3015 - 3024.

61. Alberto, R.; Schibli, R.; Elgi, A.; Schubiger, P. A., *J. Am. Chem. Soc.* **1998,** *120*, 7987 - 7988.

62. Salmain, M.; Gunn, M.; Gorfti, A.; Top, S.; Jaouen, G., *Bioconjugate Chem.* **1993,** *4*, 425 - 433.

63. Alberto, R.; Schibli, R.; Schubiger, P. A.; Abram, U.; Pietzsch, H.-J.; Johannsen, B., *J. Am. Chem. Soc.* **1999,** *121*, 6076 - 6077.

64. Bernard, J.; Ortner, K.; Spingler, B.; Pietzsch, H.-J.; Alberto, R., *Inorg. Chem.* **2003,** *42*, 1014 - 1022.

65. James, S.; Maresca, K. P.; Babich, J. W.; Valliant, J. F.; Doering, L.; Zubieta, J., *Bioconjugate Chem.* **2006,** *17*, 590 - 596.

66. Zobi, F.; Springler, B.; Fox, T.; Alberto, R., *Inorg. Chem.* **2003,** *42*, 2818 - 2820.

67. Adams, K. M.; Marzilli, L. G., *Inorg. Chem.* **2007,** *46*, 4926 - 4936.

68. Xavier, C.; Pak, J. K.; Santos, I.; Alberto, R., *J. Organomet. Chem.* **2007,** *692*, 1332 - 1339.

69. Stephenson, K. A.; Banerjee, S. R.; Besanger, T.; Sogbein, O. O.; Levadala, M. K.; McFarlane, N.; Lemon, J. A.; Boreham, D. R.; Maresca, K. P.; Brennan, J. D.; Babich, J. W.; Zubieta, J.; Valliant, J. F., *J. Am. Chem. Soc.* **2004,** *126*, 8598 - 8599.

70. Liu, Y.; Pak, J. K.; Schmutz, P.; Bauwens, M.; Mertens, J.; Knight, H.; Alberto, R., *J. Am. Chem. Soc.* **2006,** *128*, 15996 - 15997.

71. Banerjee, S. R.; Levadala, M. K.; Lazarova, N.; Wei, L.; Valliant, J. F.; Stephenson, K. A.; Babich, J. W.; Maresca, K. P.; Zubieta, J., *Inorg. Chem.* **2002,** *41*, 6417 - 6425.

72. Banerjee, S. R.; Schaffer, P.; Babich, J. W.; Valliant, J. F.; Zubieta, J., *Dalton Trans.* **2005**, 3886 - 3897.

73. Cavalli, A.; Bolognesi, M. L.; Minarini, A.; Rosini, M.; Tumiatti, V.; Recanatini, M.; Melchiorre, C., *J. Med. Chem.* **2008,** *51*, 347 - 372.

74. Alzheimer, A., *Allg. Zschr. f Psychiatr. Psychisch-Gerichtl. Mediz.* **1907,** *64*, 146-148.

75. Brookmeyer, R.; Johnson, E.; Ziegler-Graham, K.; Arrighi, H. M., *Alz. Dement.* **2007,** *3*, 186 - 191.

76. Tator, C.; Bray, G.; Morin, D., *Can. J. Neurol. Sci.* **2007,** *34*, 268 - 269.

77. Ostbye, T.; Crosse, E., *Can. Med. Assoc. J.* **1994,** *151*, 1457 - 1464.

78. Jiang, Q.; Lee, C. Y. D.; S., M.; Wilkinson, B.; Cramer, P.; Zelcer, N.; Mann, K.; Lamb, B.; Willson, T. M.; Collins, J. L.; Richardson, J. C.; Smith, J. D.; Comery, T. A.; Riddell, D.; Holtzman, D. M.; Tontonoz, P.; Landreth, G. E., *Neuron* **2008,** *58*, 681 - 693.

79. Gunzburg, M. J.; Perugini, M. A.; Howlett, G. J., *J. Biol. Chem.* **2007,** *282*, 35831 - 35841.

80. Bertram, L.; Hiltunen, M.; Parkinson, M.; Ingelsson, M.; Lange, C.; Ramasamy, K.; Mullin, K.; Menon, R.; Sampson, A. J.; Hsiao, M. Y.; Elliott, K. J.; Velicelebi, G.; Moscarillo, T. J.; Hyman, B. T.; Wagner, S. L.; Becker, K. D.; Blacker, D.; Tanzi, R., *N. Engl. J. Med.* **2005,** *352*, 884 - 894.

81. Strittmatter, W.; Saunders, A. J.; Schmechel, D.; Pericak, V.; Enghild, J.; Salvesen, G. S.; Roses, A. D., *Proc. Natl. Acad. Sci.* **1993,** *90*, 1977 - 1981.

82. Lambert, J.-C.; Amouyer, P., *Psychoneuroendocrinol.* **2007,** *32*, S62 - S70.

83. Hardy, J. A.; Higgins, G. A., *Science* **1992,** *256*, 184-5.

84. Gong, Y. S.; Chang, L.; Viola, K. L.; Lacor, P. N.; Lambert, M. P.; Finch, C. E.; Krafft, G. A.; Klein, W. L., *Proc. Natl. Acad. Sci.* **2003,** *100*, 10417 - 10422.

85. Atwood, C. S.; Scarpa, R. C.; Huang, X.; Moir, R. D.; Jones, W. D.; Fairlie, D. P.; Tanzi, R. E.; Bush, A. I., *J. Neurochem.* **2000,** *75*, 1219 - 1233.

86. Curtain, C. C.; Ali, F. E.; Smith, D. G.; Bush, A. I.; Masters, C. L.; Barnham, K. J., *J. Biol. Chem.* **2003,** *278*, 2977-2982.

87. Lovell, M. A.; Robertson, J. D.; Teesdale, W. J.; Campbell, J. L.; Markesbery, W. R., *J. Neurol. Sci.* **1998,** *158*, 47-52.

88. Atwood, C. S.; Huang, X.; Moir, R. D.; Tanzi, R. E.; Bush, A. I., *Met. Ions Biol. Syst.* **1999,** *36*, 309 - 364.

89. Atwood, C. S.; Perry, G.; Zeng, H.; Kato, Y.; Jones, W. D.; Ling, K. Q.; Huang, X. D.; Moir, R. D.; Wang, D. D.; Sayre, L. M.; Smith, M. A.; Chen, S. G.; Bush, A. I., *Biochemistry* **2004,** *43*, 560 - 568.

90. McLean, C. A.; Cherny, R. A.; Fraser, F. W.; Fuller, S. J.; Smith, M. J.; Beyreuther, K.; Bush, A. I.; Masters, C. L., *Ann. Neurol.* **1999,** *46*, 860-866.

91. Cuajungco, M. P.; Goldstein, L. E.; Nunomura, A.; Smith, M. A.; Lim, J. T.; Atwood, C. S.; Huang, X.; Farrag, Y. W.; Perry, G.; Bush, A. I., *J. Biol. Chem.* **2000,** *275*, 19439 - 19442.

92. Noy, D.; Solomonov, I.; Sinkevich, O.; Arad, T.; Kjaer, K.; Sagi, I., *J. Am. Chem. Soc.* **2008,** *130*, 1376 - 1383.

93. Giulian, D.; Haverkamp, L. J.; Yu, J. H.; Karshin, W.; Tom, D.; Li, J. H.; Kirkpatrick, J.; Kuo, Y.-M.; Roher, A. E., *J. Neurosci.* **1996,** *16*, 6021 - 6037.

94. Barnham, K. J.; Masters, C. L.; Bush, A. I., *Nat. Rev. Drug Discov.* **2004,** *3*, 205-214.

95. Herholz, K.; Salmon, E.; Perani, D.; Baron, J.-C.; Holthoff, V.; Frolich, L.; Schonknecht, P.; Ito, K.; Mielke, R.; Kalbe, E.; Zundorf, G.; Delbeuck, X.; Pelati, O.; Anchisi, D.; Fazio, F.; Kerrouche, N.; Desgranges, B.; Eustache, F.; Beuthien-Baumann, B.; Menzel, C.; Schroder, J.; Kato, T.; Arahata, Y.; Henze, M.; Heiss, W.-D., *NeuroImage* **2002,** *17*, 302 - 316.

96. de Leon, M. J.; Mosconi, L.; Blennow, K.; DeSanti, S.; Zinkowski, R.; Mehta, P. D.; Practico, D.; Tsui, W.; Saint Louis, L. A.; Sobanska, L.; Brys, M.; Li, Y.; Rich, K.; Rinne, J.; Rusinek, H., *Ann. N.Y. Acad. Sci.* **2007,** *1097*, 114 - 145.

97. Kasa, P.; Rakonczay, Z.; Gulya, K., *Prog. Neurobiol.* **1997,** *52*, 511 - 535.

98. Robinson, D. M.; Keating, G. M., *Drugs* **2006,** *66*, 1515 - 1534.

99. Gilgun-Sherki, Y.; Melamed, E.; Offen, D., *J. Mol. Neurosci.* **2003,** *21*, 1 - 11.

100. Sano, M.; Ernesto, C.; Thomas, R. G.; Klauber, M. R.; Schafer, K.; Grundman, M.; Woodbury, P.; Growdon, J.; Cotman, D. W.; Pfeiffer, E.; Schneider, L. S.; Thal, L. J., *N. Engl. J. Med.* **1997,** *336*, 1216-1222.

101. Breitner, J. C. S., *Annu. Rev. Med.* **1996,** *47*, 401 - 411.

102. Lim, G. P.; Yang, F.; Chu, T.; Chen, P.; Beech, W.; Teter, B.; Tran, T.; Ubeda, O.; Ashe, K. H.; Frautschy, S. A.; Cole, G. M., *J. Neurosci.* **2000,** *20*, 5709 - 5714.

103. Vlad, S. C.; Miller, D. R.; Kowall, N. W.; Felson, D. T., *Neurology* **2008,** *70*, 1672 - 1677.

104. Selkoe, D. J., *Nature* **1999,** *399*, A23 - A31.

105. Ogura, T.; Mio, K.; Hiyashi, I.; Miyashita, H.; Fukuda, R.; Kopan, R.; Kodama, T.; Hamakubo, T.; Iwatsubo, T.; Tomita, T.; Sato, C., *Biochem. Biophys. Res. Commun.* **2006,** *343*, 525 - 534.

106. Fleisher, A. S.; Raman, R.; Siemers, E. R.; Becerra, L.; Clark, C. M.; Dean, R. A.; Farlow, M. R.; Galvin, J. E.; Peskind, E. R.; Quinn, J. F.; Sherzai, A.; Sowell, B. B.; Aisen, P. S.; Thal, L. J., *Arch. Neurol.* **2008,** *65*, 1031 - 1038.

107. Baxter, E. W.; Conway, K. A.; Kennis, L.; Bischoff, F.; Mercken, M. H.; De Winter, H. L.; Reynolds, C. H.; Tounge, B. A.; Luo, C.; Scott, M. K.; Huang, Y.; Braeken, M.; Pieters, S. M. A.; Berthelot, D. J. C.; NMasure, S.; Bruinzeel, W. D.; Jordan, A. D.; Parker, M. H.; Boyd, R. E.; Qu, J.; Alexander, R. S.; Brenneman, D. E.; Reitz, A. B., *J. Med. Chem.* **2007,** *50*, 4261 - 4264.

108. Hussain, I.; Hawkins, J.; Harrison, D.; Hille, C.; Wayne, G.; Cutler, L.; Buck, T.; Walter, D.; Demont, E.; Howes, C.; Naylor, A.; Jeffrey, P.; Gonzalez, M. I.; Dingwall, C.; Michel, A.; Redshaw, S.; Davis, J. B., *J. Neurochem.* **2007,** *100*, 802 - 809.

109. Imbimbo, B. P., *Drug Dev. Res.* **2002,** *56*, 150-162.

110. Orgogozo, J.-M.; Gilman, S.; Dartigues, J.-F.; Laurent, B.; Puel, M.; Kirby, L. C.; Jouanny, P.; Dubois, B.; Eisner, L.; Flitman, S.; Michel, B. F.; Boada, M.; Frank, A.; Hock, C., *Neurology* **2003,** *61*, 46 - 54.

111. Maier, M.; Seabrook, T. J.; Lazo, N. D.; Jiang, L.; Das, P.; Janus, C.; Lemere, C. A., *J. Neurosci.* **2006,** *26*, 4717 - 4728.

112. Mattson, M. P., *Neurology* **2003,** *60*, 690 - 695.

113. McLachlan, D. R. C.; Dalton, A. J.; Kruck, T. P.; Bell, M. Y.; Smith, W. L.; Kalow, W.; Andrews, D. F., *Lancet* **1991,** *337*, 1304 - 1308.

114. Tamura, Z.; Yoshioka, M.; Imanari, T.; Fukaya, J.; Kusaka, J.; Samejima, K., *Clin. Chim. Acta* **1973,** *47*, 13 - 20.

115. Arbiser, J. L.; Kraeft, S. K.; van Leeuwen, R.; Hurwitz, S. J.; Selig, M.; Dickersin, G. R.; Flint, A.; Byers, H. R.; Chen, L. B., *Mol. Med.* **1998,** *4*, 665-670.

116. Ritchie, C. W.; Bush, A. I.; Mackinnon, A.; Macfarlane, S.; Mastwyk, M.; MacGregor, L.; Kiers, L.; Cherny, R.; Li, Q. X.; Tammer, A.; Carrington, D.; Mavros, C.; Volitakis, I.; Xilinas, M.; Ames, D.; Davis, S.; Beyreuther, K.; Tanzi, R. E.; Masters, C. L., *Arch. Neurol.* **2003,** *60*, 1685-1691.

117. Cherny, R. A.; Atwood, C. S.; Xilinas, M. E.; Gray, D. N.; Jones, W. D.; McLean, C. A.; Barnham, K. J.; Volitakis, I.; Fraser, F. W.; Kim, Y. S.; Huang, X. D.; Goldstein, L. E.;

Moir, R. D.; Lim, J. T.; Beyreuther, K.; Zheng, H.; Tanzi, R. E.; Masters, C. L.; Bush, A. I., *Neuron* **2001,** *30*, 665-676.

118. Lee, J.-Y.; Friedman, J. E.; Angel, I.; Kozak, A.; Koh, J. Y., *Neurobiol. Aging* **2004,** *25*, 1315 - 1321.

119. Ibach, B.; Haen, E.; Marienhagen, J.; Hajak, G., *Pharmacopsychiatry* **2005,** *28*, 178 - 179.

120. Bush, A. I., *Trends Neurosci.* **2003,** *26*, 207-214.

121. Cherny, R. A.; Barnham, K. J.; Bush, A. I.; Cappai, R.; Gautier, E. C. L.; Masters, C. L.; Carrington, D.; Kocak, G.; Volitakis, I.; Kok, G. B., *Alz. Dement.* **2006,** *2*, S646.

122. Adlard, P. A.; Cherny, R. A.; Finkelstein, D. I.; Gautier, E.; Robb, E.; Cortes, M.; Volitakis, I.; Liu, X.; Smith, J. P.; Perez, K.; Laughton, K.; Li, Q.-X.; Charman, S. A.; Nicolazzo, J. A.; Wilkins, S.; Deleva, K.; Lynch, T.; Kok, G.; Ritchie, C. W.; Tanzi, R. E.; Cappai, R.; Masters, C. L.; Barnham, K. J.; Bush, A. I., *Neuron* **2008,** *59*, 43 - 55.

123. Lannfelt, L.; Blennow, K.; Zetterberg, H.; Batsman, S.; Ames, D.; Harrison, J.; Masters, C.; Targum, S.; Bush, A.; Murdoch, R.; Wilson, J. E.; Ritchie, C. W., *Lancet Neurol.* **2008,** *7*, 779 - 786.

CHAPTER 2

Radioiodination of Glycosylated Pyridinones as Potential Therapeutics for Alzheimer's Disease*

2.1 Introduction

2.1.1 Metals in Alzheimer's Disease

Aβ (β-amyloid) plaques found in Alzheimer's brains contain elevated levels of the metal ions copper, zinc and iron; up to 400 μM for copper, 1 mM for zinc, and 1 mM for iron.[1, 2] It has been found that iron does not actually bind to the amyloid, or induce fibril formation, but is associated with the plaques *in vivo*.[3] This is not the case for Cu and Zn, however, and the ions of these metals are thought to play key roles in binding to the Aβ protein and in causing some of the subsequent aggregation, redox activity and downstream problems. There are many metal binding sites provided by the residues present in the Aβ proteins, particularly the histidine and tyrosine side chains. It has been postulated that the natural role of endogenous Aβ is as a copper binding and regulating protein. This is a very complicated cycle, the full details of which have not yet been conclusively determined, but it is proposed to involve free copper triggering the production of more APP and Aβ.[4] In healthy brains this system works because Aβ binds free copper, but in Alzheimer's disease (AD), both the copper and the Aβ are required for the observed toxicity, so one increasing the other only serves to increase progression of the disease.

Copper is found *in vivo* in both the monocationic and dicationic states. These two states are both readily accessible under biological conditions, making copper ions potential producers of free radicals. For this reason the body has many control mechanisms for copper, and in a normally functioning organism nearly all the copper present is protein bound so it is either being utilized or stabilized in one oxidation state. As these control mechanisms become worn with age and work less efficiently, small amounts of copper ions are left free *in vivo*, where they will react to

---

* Parts of this chapter have been published: Schugar, H. J.; Green, D. E.; Bowen, M. L.; Scott, L. E.; Storr, T.; Böhmerle, K.; Thomas, F.; Allen, D. D.; Lockman, P. R.; Merkel, M.; Thompson, K. H.; Orvig, C. Combating Alzheimer's Disease With Multifunctional Molecules Designed for Metal Passivation. *Angew. Chem. Int. Ed.* **2007**, *46*, 1716 - 1718.

References begin on Pg 61

give or take electrons from whatever source they find themselves near. This is proposed to be a mechanism at play early on in the aberrant metal binding and oxidative damage seen in AD.[5]

Oxidative damage is caused by radicals, very reactive species that react non-selectively with whatever is in their proximity. In this way essential molecules such as proteins, cell membranes and DNA are damaged, which leads to the inflammatory response being triggered, and eventually to cell death. Reactive oxygen species (ROS) do not form without the presence of metal ions. Amyloid is found not to be toxic to cells without the associated copper or iron.[6] It is not yet known if amyloid oligomerises *in vivo* in the absence of metal ions. Thus an intervention that has received a considerable amount of attention recently is the use of metal chelators.

Proponents of the MPAC (metal protein attenuating compound) approach to treating AD have previously used an FDA-approved agent clioquinol (CQ) as a proof of principle drug.[7] CQ, and a similar compound, known as PBT2, are 8-hydroxyquinolines, and bind in a bidentate fashion with high affinity to a range of metal ions.[8] These compounds are able to slow the progression of dementia in Tg2576, AD type transgenic mice.[7, 9] They are also able to affect the levels of Aβ found in the plasma of human subjects with AD,[10, 11] though it is not yet known if they will be effective at alleviating symptoms in people over the long term. As compounds of these types only treat one specific point in the complex cascade that leads to the effects of AD, current research often tries to build on the basic promise seen in approaches like this by adding multiple functionalities into one molecule to better treat the many factors occurring simultaneously in AD.

2.1.2 The Multifunctional Approach to Treating Alzheimer's Disease

As AD is such a multi-faceted and overall poorly understood disease, it is widely acknowledged that a combination of two or more types of therapy is much more likely to form a successful treatment than any one could alone, as has been found to be the case with other complex diseases like cancer and HIV.[12, 13] The investigation of multifunctional compounds to treat AD has been reviewed recently,[14] in a dense 26 page article, indicating the recent enthusiasm for therapies of this nature. Some examples of proposed multifunctional compounds are shown in Figure 2.1. The benefits of combining different functionalities into one molecule include alleviating the need

References begin on Pg 61

for multiple pills and the increased complications that come from drugs interacting with each other *in vivo*.[14] Cavalli *et al.* encourage the use of the term multi-target-directed ligands (MTDLs) for compounds that are designed to interact with multiple targets, and they stress the importance of this approach in complex multi-faceted diseases like AD.[14] It is interesting to note that the number of patents for multiple compound medications has overtaken those for single molecular entities for the treatment of AD.[14]

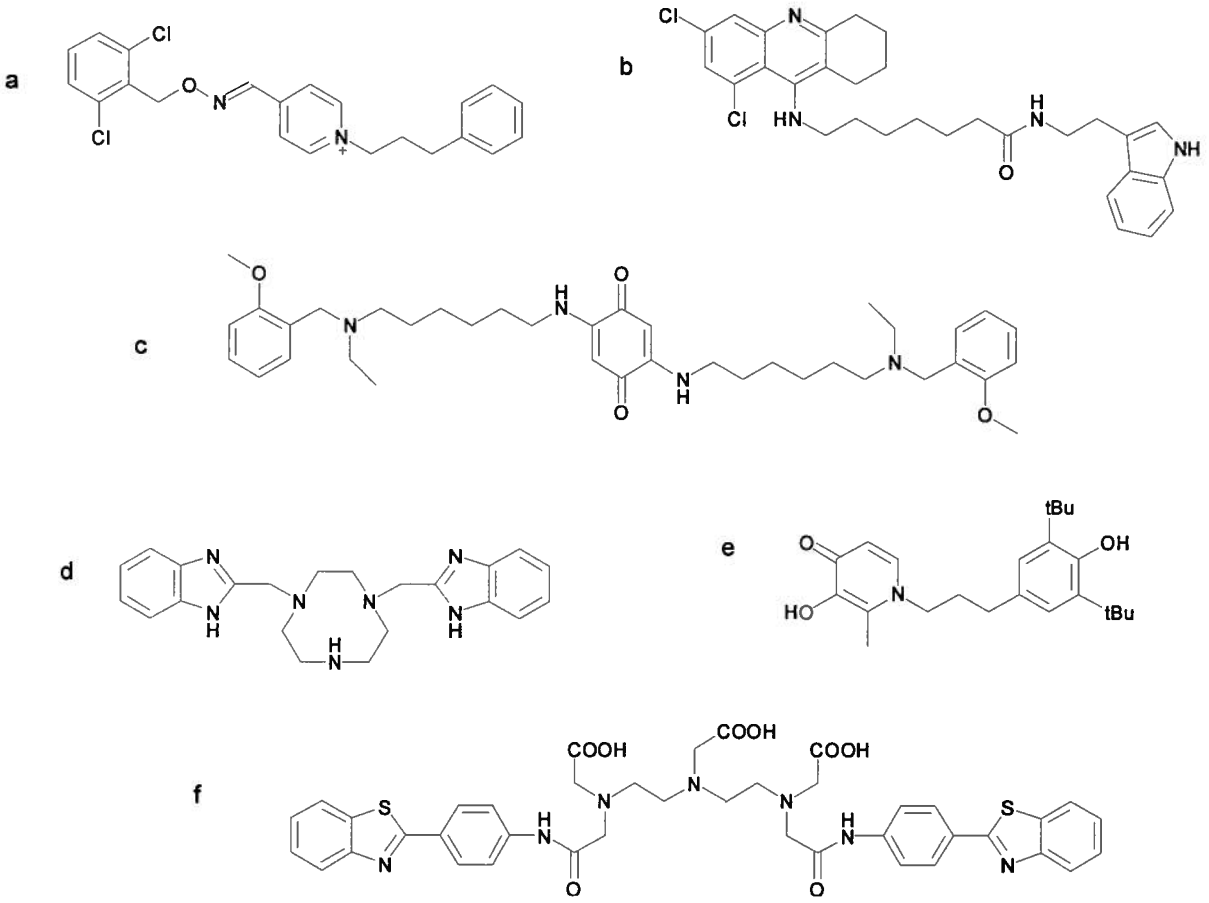

Figure 2.1 Multi-target-directed-ligands under research as AD therapeutics: a) an AChEI that also stops Aβ aggregation b) an AChEI with antioxidant potential c) Memoquin has four different anti-AD functionalities d) and e) combine metal chelating abilities with antioxidant capacity f) a metal chelator that also targets Aβ aggregates.

As three of the four AD therapeutics currently on the market in Canada are acetylcholinesterase inhibitors (AChEI) (see Chapter 1), most of the work towards multifunctional compounds incorporates this functionality. Two examples of molecules of this kind are shown in Figure 2.1a and b. Figure 2.1a shows a molecule that was designed to be an AChEI that can also inhibit

References begin on Pg 61

the self-aggregation of Aβ.[15] Although it was found to be successful in these two functions with an IC_{50} of 0.18 μM against AChE and the ability to prevent 60 % of the Aβ self aggregation at a concentration of 100 μM, the charge on the compound will likely limit its BBB permeability and therefore its therapeutic potential. It is still a contentious issue as to whether the self aggregation of Aβ is problematic in the absence of metal ions; if this is determined not to be the case it would limit the use of this kind of a therapeutic agent. Figure 2.1b shows a compound that combines AChEI activity with antioxidant potential.[16] The compound has a very high affinity for AChE with an IC_{50} of 8 pM, and also shows good antioxidant capacity with a TEAC (Trolox Equivalent Antioxidant Capacity) value of 2.5, where Trolox is a water soluble vitamin E analogue normalized to a TEAC value of one. The authors predict it will cross the BBB, although no experimental evidence of this was presented.

Figure 2.1c shows Memoquin, a molecule with four different AD functionalities built in.[17] It is a nM inhibitor of AChE, shows antioxidant properties, and can inhibit the aggregation of Aβ, either when left to self-aggregate or when induced to do so by AChE. Finally, Memoquin can act as a BACE-1 (β secretase – see Chapter 1.5) inhibitor to reduce the amount of Aβ produced. These properties were tested *in vitro*, and then *in vivo* in mouse AD models, with very promising, and multi-faceted results. Memoquin prevented neurodegeneration, and reversed or prevented (depending on the advancement of the disease state) choline deficit, τ hyperphosphorylation and behavioral / memory problems. This is a very promising strategy, and shows the potential benefits of the MTDL approach to AD.

Other groups, including our own, have been interested in the potential of combining metal chelating ability with other relevant functionalities. Figure 2.1d shows a compound proposed to be useful for AD as it combines metal chelation and antioxidant capabilities.[18] Interestingly, this compound was proposed by theoretical chemists, though it has not been practically tested as of this writing. The reasons they chose this type of compound is because of its high affinity for copper, and ability to still act as an antioxidant (electron acceptor) once bound to a copper ion. They also note that these compounds should be easy to modify to add further functionality such as Aβ aggregation inhibitors, and that they are expected to be BBB permeable and non-toxic, according to their calculations.

References begin on Pg 61

There has long been interest in pyridinones as potential therapeutics for a range of conditions.[19-21] Bebbington *et al.* made a series of *N*-substituted pyridinones and tested them as antioxidants with an interest in AD among other applications.[22] The most promising candidate of this study is shown in Figure 2.1e.[22] This compound showed synergistic properties in that the antioxidant capacity observed was greater than that for the administration of the two parts of the compound separately: the pyridinone and the radical scavenger substituted phenol. This is very encouraging for the line of compounds our group has been functionalizing.

XH1 (Figure 2.1f) contains both a metal chelating and an amyloid binding portion in one molecule.[23] It was found to decrease Aβ aggregation *in vitro*, and to reduce APP expression in human neuronal cells. XH1 was found to reduce $A\beta_{1\text{-}40}$ concentrations and plaque formation in AD expressing transgenic mice after four weeks of oral treatment.[23] From these results it was proposed that the compound crosses the BBB, though no experiments were done to determine this.

2.1.3 Our Approach to Multi-Target-Directed-Ligands for Alzheimer's Disease

In the Orvig group, we are interested in designing MTDLs based on the bidentate chelating pyridinones shown in Figure 2.2. We have chosen to funstionalize them in several ways to improve their usefulness as AD therapeutics. The pyridinone nitrogen can be substituted relatively easily, and the two functionalities we have successfully employed in this position are antioxidant[24] and Aβ plaque targeting moieties.[25] We have also chosen to form the glycosylated prodrugs of the metal chelators, which we propose will confer several benefits.[24] The glucose moiety increases the water solubility of the compounds. While the glucose is in place, the compounds will not chelate metal ions. This is important because the 3-hydroxy-4-pyridinones are fairly high affinity chelators, especially for iron, so by adding a glucose molecule to mask this chelating functionality, we hope to prevent systemic chelation of essential elements in the body. We have shown that the glycosyl bond can be cleaved enzymatically to reveal the active chelator,[24] and we propose this may occur *in vivo*. Finally, the glucose moiety may increase BBB permeability of our compounds, an advantageous property perhaps available via facilitated transport into the brain on the GLUT-1 glucose transporters. These transporters are found in

References begin on Pg 61

high concentration at the BBB, and as such may increase the amount of our compounds that get into the brain as compared to entering by passive diffusion in the non-glycosylated form.

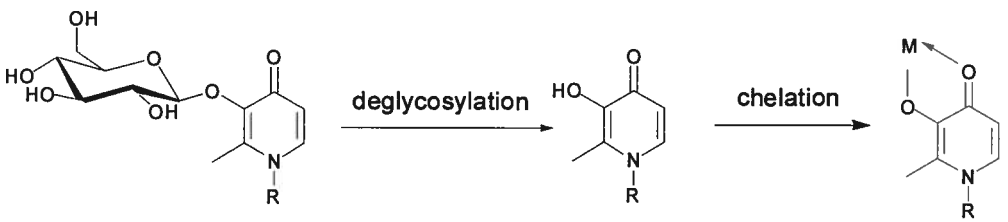

R = H, Me, Et, phenyl, 4-hydroxyphenyl etc.

Figure 2.2 3-Hydroxy-4-pyridinones synthesized in the Orvig group.[24] A representative range of R groups are shown, but many more have been made. It can be seen that once deglycosylated the free pyridinone is able to act as a bidentate ligand.

The aim of the work in this thesis chapter was to create a radiolabelled pyridinone for use in assessing the blood brain barrier permeability of these glycosylated prodrugs *in vivo*. The two iodinated compounds prepared in this work are shown in Figure 2.3.

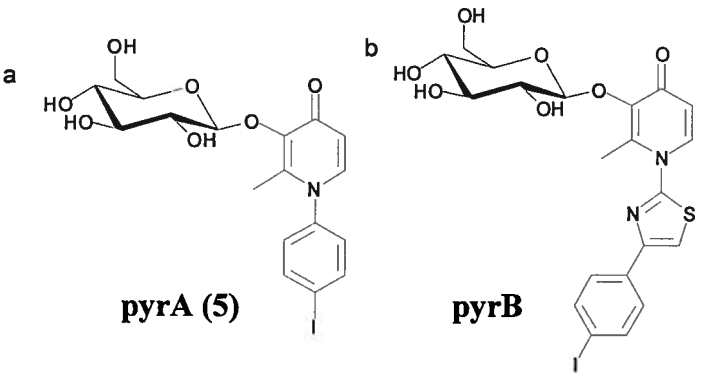

Figure 2.3 The two iodinated compounds in this chapter: a) **pyrA (5)** , made by myself b) **pyrB**, first made by myself and Dr. Michael Merkel; the non-radioactive I, ^{123}I and ^{125}I analogues were prepared for each.

References begin on Pg 61

2.2 Experimental

2.2.1 Instruments and Materials

All solvents and reagents were used as received. Reagents were purchased from Sigma-Aldrich unless otherwise stated. Maltol (3-hydroxy-2-methyl-4-pyrone) was purchased from Cultor Food Sciences, New York. Solvents were HPLC grade, and were purchased from Fisher Scientific. Toluene was dried over activated 4Å molecular sieves for at least 48 hr prior to use. Na[^{123}I] was generously supplied by MDS Nordion. Na[^{125}I] was a gift from Dr. Jianming Lu of TRIUMF, Vancouver.

The tributylstannyl derivative of compound **pyrB** shown in Figure 2.3b (2-methyl-3-(2,3,4,6-tetra-O-acetyl-β-D-glucopyranosyloxy)-1-[4-(4-tributylstannylphenyl)-2-thiazolyl]-4pyridinone) was made by Dr. Michael Merkel. The radiolabelling of this compound was carried out by myself and Dr. Merkel in a manner similar to that used for the radioiodination of compound **pyrA**.

The analytical TLC plates, which were aluminum backed ultra pure silica gel 60, 250 μm, and the flash column silica gel (standard grade, 60 Å, 32-63 mm) used were provided by Silicycle. Sep-paks were provided by Supelco. ^{1}H and ^{13}C NMR, ^{13}C NMR APT, 2D ^{1}H-^{1}H COSY and ^{1}H-^{13}C HMQC spectra were recorded at ambient temperature on Bruker AV300, AV400 or DRX400 instruments. The NMR spectra are expressed on the δ scale and were referenced to the residual solvent peaks. Infrared spectra were recorded on a Nicolet 6700 FT-IR spectrophotometer in transmission mode between 400 and 4000 cm^{-1} at a resolution of ± 0.09 cm^{-1}. ESI mass spectra were recorded on a Micromass LCT instrument. High resolution mass spectra (Micromass LCT TOFMS) and elemental analysis (Carlo Erba EA 1108 Elemental Analyzer) were provided by the Analytical Services Facility, Department of Chemistry, University of British Columbia. Radioactive TLC analysis was done using a Bioscan System 200 Imaging Scanner fitted with a Bioscan 1000 Autochanger.

References begin on Pg 61

In vivo rat brain perfusion experiments were carried out by Dr. David Allen, Dr. Paul Lockman and Fancy Thomas at Texas Tech University Health Sciences Centre, using the procedure detailed in Appendix 1.

2.2.2 Chemical Synthesis

1-(4-Bromophenyl)-3-hydroxy-2-methyl-4-pyridinone (1)

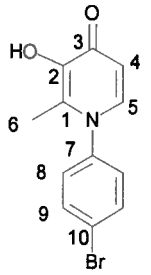

Maltol (2-methyl-3-hydroxy-4-pyrone) (10.75 g, 85.25 mmol) and 4-bromoaniline (29.21 g, 170.0 mmol) were placed in a round bottom flask with 80 mL methanol and 200 mL dilute hydrochloric acid (5 mL 12 M HCl in water). The resulting mixture was heated, dissolving to give an orange solution, and refluxed for 48 hr. The contents of the flask were filtered to give a dark pink precipitate which was recrystallised from hot methanol to give a pale pink product (12.56 g, 53 % yield). ^{1}H NMR (300 MHz, DMSO–d_6, δ): 7.75 (d, $^3J_{8,9}$ = 8.1 Hz, 2H; *H*8), 7.54 (d, $^3J_{4,5}$ = 7.1 Hz, 1H; *H*4), 7.43 (d, $^3J_{9,8}$ = 8.1 Hz, 2H; *H*9), 6.20 (d, $^3J_{5,4}$ = 7.1 Hz, 1H; *H*5), 1.95 (s, 3H; *H*6). HR-MS (ES+ of MNa^+): m/z calcd for $C_{12}H_{10}{}^{79}BrNO_2Na$: 301.9793, found: 301.9784. Anal. Calcd. (found) for $C_{12}H_{10Br}NO_2$: C, 51.45 (51.82); H, 3.57 (3.81); N, 5.00 (5.29).

1-(4-Bromophenyl)- 2-methyl -3-(2,3,4,6-tetra-O-acetyl-β-D-glucopyranosyloxy)-4-pyridinone (2)

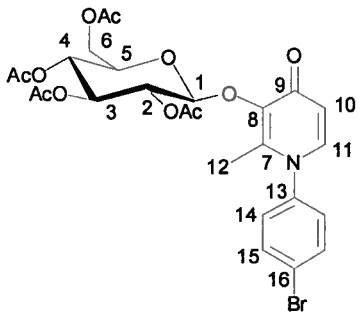

1 (6.25 g, 22.3 mmol), acetobromo-α-D-glucose (3.35 g, 8.15 mmol) and tetrabutylammonium bromide (2.66 g, 8.24 mmol) were suspended in 35 mL CH_2Cl_2 and heated to 35 °C. NaOH (35 mL, 1 M) was added and the resulting heterogeneous mixture stirred vigorously for 3 hr, during which time it turned dark red. The reaction was cooled to room temperature, and EtOAc (50 mL) added. The organic layer was separated and washed with 3 x 50 mL 1M NaOH, 50 mL water then 50 mL saturated brine. The organic layer was then dried over $MgSO_4$, the drying agent filtered off, and the resulting liquid evacuated on a rotary evaporator. Column chromatography on silica gel using EtOAc:MeOH (9:1) gave a white solid (1.12 g, 23 % yield). ^{1}H NMR (400 MHz, MeOH-d_4, δ): 7.76 (d, $^3J_{15,14}$ = 8.8 Hz, 2H, *H*15), 7.67 (d, $^3J_{11,10}$ =

7.5 Hz, 1H, *H*11), 7.37 (d, $^3J_{14,15}$ = 8.5 Hz, 2H, *H*14), 6.49 (d, $^3J_{10,11}$ = 7.5 Hz, 1H, *H*10), 5.57 (d, $^3J_{1,2}$ = 7.9 Hz, 1H, *H*1), 5.34 (dd, $^3J_{4,3}$ = 9.6 Hz, $^3J_{4,5}$ = 9.6 Hz, 1H, *H*4), 5.10 (m, 2H, *H*2, *H*3), 4.26 (dd, $^3J_{6a,5}$ = 4.6 Hz, $^3J_{6a,6b}$ = 12.3 Hz, 1H, *H*6a) 4.14 (dd, $^3J_{6b,5}$ = 2.4 Hz, $^3J_{6b,6a}$ = 12.5 Hz, 1H, *H*6b), 3.81 (ddd, $^3J_{5,4}$ = 9.6 Hz, $^3J_{5,6a}$ = 4.5 Hz, $^3J_{5,6b}$ = 2.4 Hz, 1H, *H*5), 2.12 (s, 3H, *H*12), 2.10 (s, 3H, COCH_3), 2.01 (s, 3H, COCH_3), 2.00 (s, 3H, COCH_3), 1.98 (s, 3H, COCH_3). HR-MS (ES+ of MNa^+): m/z calcd for $C_{26}H_{28}{}^{79}BrNO_{11}Na$: 632.0743, found: 632.0736. Anal. Calcd. (found) for $C_{26}H_{28}BrNO_{11}$: C, 51.16 (51.49); H, 4.62 (4.75); N, 2.29 (2.66).

2-Methyl-3-(2,3,4,6-tetra-O-acetyl-β-D-glucopyranosyloxy)-1-(4-tributylstannylphenyl) -4-pyridinone (3)

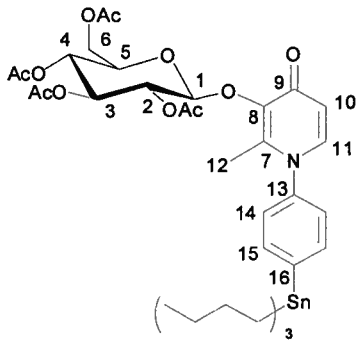

2 (0.52 g, 0.84 mmol) and tetrakis(triphenylphosphine)palladium(0) (0.10 g, 0.088 mmol) were weighed into a two necked RBF under an inert atmosphere. Dry toluene (15 mL) and hexabutylditin (2.1 mL, 4.2 mmol) were added via syringe, and the resulting solution brought to reflux under Ar. After 16 hr at reflux the solution was cooled to room temperature and filtered through Celite with thorough washing with CH_2Cl_2. The resulting solution was evaporated to dryness on a rotary evaporator, dissolved in 10 mL acetonitrile and washed three times with 30 mL hexanes to remove any remaining butyltin species. The acetonitrile layer was dried and then purified by silica gel column chromatography using 2 % MeOH in EtOAc as eluent. A colourless oil was produced that became a clear white glassy solid after vacuum drying (0.16 g, 38 % yield). ^{1}H NMR (400 MHz, DMSO–d_6, δ): 7.64 (d, $^3J_{11,10}$ = 7.5 Hz, 1H, *H*11), 7.62 (d, $^3J_{15,14}$ = 8.1 Hz, 2H, *H*15), 7.38 (d, $^3J_{14,15}$ = 8.2 Hz, 2H, *H*14), 6.22 (d, $^3J_{10,11}$ = 7.6 Hz, 1H, *H*10), 5.42 (d, $^3J_{1,2}$ = 7.9 Hz, 1H, *H*1), 5.37 (dd, $^3J_{4,3}$ = 9.7 Hz, $^3J_{4,5}$ = 9.6 Hz, 1H, *H*4), 4.96 (dd, $^3J_{2,1}$ = 7.9 Hz, $^3J_{2,3}$ = 9.9 Hz, 1H, *H*2), 4.93 (dd, $^3J_{3,2}$ = 9.8 Hz, $^3J_{3,4}$ = 9.6 Hz, 1H, *H*3), 4.13 (dd, $^3J_{6a,5}$ = 5.2 Hz, $^3J_{6a,6b}$ = 12.4 Hz, 1H, *H*6a), 4.02 (dd, $^3J_{6b,5}$ = 2.3 Hz, $^3J_{6b,6a}$ = 12.2 Hz, 1H, *H*6b), 3.96 (ddd, $^3J_{5,4}$ = 9.7 Hz, $^3J_{5,6a}$ = 4.9 Hz, $^3J_{5,6b}$ = 2.4 Hz, 1H, *H*5), 2.04 (s, 3H, *H*12), 1.99 (s, 3H, COCH_3) , 1.97 (s, 3H, COCH_3) , 1.93 (s, 6H, COCH_3), 1.52 (m, 6H, SnCH_2CH$_2$CH$_2$CH$_3$), 1.29 (m, 6H, SnCH$_2$CH_2CH$_2$CH$_3$), 1.09 (m, 6H, SnCH$_2$CH$_2$CH_2CH$_3$), 0.85 (m, 9H, SnC$_3$H$_6$CH_3). HR-MS (ES+ of MNa^+): m/z calcd for $C_{38}H_{55}NO_{11}{}^{118}SnNa$: 842.2689, found: 842.2680.

References begin on Pg 61

1-(4-Iodophenyl)-2-methyl-3-(2,3,4,6-tetra-O-acetyl-β-D-glucopyranosyloxy)-4-pyridinone (4)

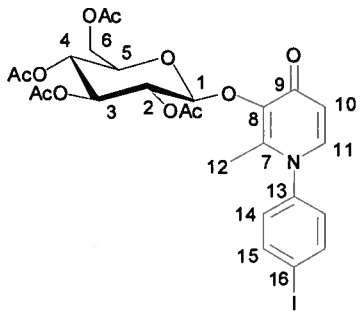

3 (0.060 g, 0.073 mmol) was dissolved in 5 mL of MeOH. Chloramine-T (8.3 mg, 0.037 mmol) was added, followed by NaI (5.6 mg, 0.037 mmol). The reaction mixture was stirred for 30 mins. It was then quenched with an aqueous solution of $NaHSO_3$ (0.1 M) until the yellow coloured reaction mixture became colourless (3.1 mg, 64 % yield). ^{1}H NMR (300 MHz, MeOH-d_4, δ): 7.95 (d, $^3J_{11,10}$ = 7.4 Hz, 1H, *H*11), 7.68 (d, $^3J_{15,14}$ = 8.5 Hz, 2H, *H*15), 7.34 (d, $^3J_{14,15}$ = 8.4 Hz, 2H, *H*14), 6.52 (d, $^3J_{10,11}$ = 7.4 Hz, 1H, *H*10), 5.56 (d, $^3J_{1,2}$ = 7.8 Hz, 1H, *H*1), 5.33 (dd, $^3J_{4,3}$ = 9.5 Hz, $^3J_{4,5}$ = 9.6 Hz, 1H, *H*4), 5.09 (m, 2H, *H2,3*), 4.27 (m, 1H, *H6a*), 4.14 (m, 1H, *H6b*), 3.80 (m, 1H, *H5*), 2.15 (s, 3H, *H12*) 2.12, 2.10, 2.01, 1.99 (s, 3H, $COCH_3$). ESI-MS (ES+ of MH^+): m/z calcd for $C_{26}H_{29}INO_{11}$: 658.0, found: 658.0.

3-(β-D-Glucopyranosyloxy)-1-(4-iodophenyl)-2-methyl-4-pyridinone (5, pyrA)

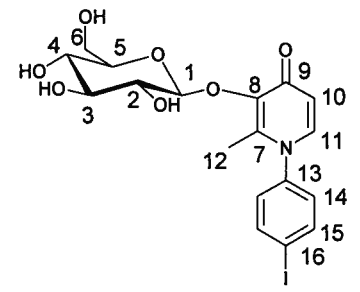

4 (3.1 mg, 0.047 mmol) was dissolved in MeOH, and an excess of NaOMe (5.4 mg, 0.1 mmol) added. The reaction mixture was stirred for 10 min, and then quenched with Amberlite. The solution was filtered and evacuated on a rotary evaporator to give crude product. This was purified by semipreparative HPLC (1 mg, 43 % yield). ^{1}H NMR (400 MHz, MeOH-d_4, δ) 7.95 (d, $^3J_{11,10}$ = 7.4 Hz, 1H, *H*11), 7.76 (d, $^3J_{15,14}$ = 8.5 Hz, 2H, *H*15), 7.34 (d, $^3J_{14,15}$ = 8.5 Hz, 2H, *H*14), 6.55 (d, $^3J_{10,11}$ = 7.4 Hz, 1H, *H*10), 4.73 (d, $^3J_{1,2}$ = 7.4 Hz, 1H, *H*1), 4.84 (m, 1H, *H4*), 3.65 (m, 2H, *H2,3*), 3.43 (m, 3H, *H5,6*), 2.26 (s, 3H, *H12*). ESI-MS (ES+ of MH^+): m/z calcd for $C_{18}H_{21}INO_7$: 490.0, found: 489.9.

3-(β-D-Glucopyranosyloxy)-1-(4-[$^{125/123}$I]iodophenyl)-2-methyl-4-pyridinone(^{125}I-pyrA or ^{123}I-pyrA)

To a sample of Na[^{125}I] (~ 0.5 mCi) or Na[^{123}I] (~ 2 mCi) was added 2.5 μL of 0.05 N H_3PO_4, and the resulting neutralised solution then added to an ethanolic solution of the tributylstannyl precursor **3** (1.3 mg) in 200 μL of ethanol. A freshly prepared aqueous solution of Chloramine-T (1 mg in 100 μL) was added to the reaction mixture that was then stirred at RT. After 20 min the

References begin on Pg 61

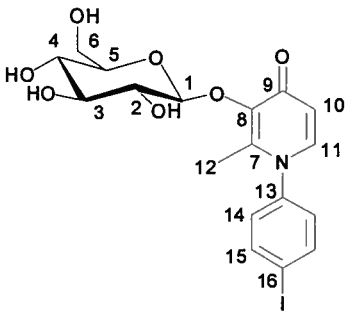

reaction was quenched by the addition of sodium chloride solution (100 μL; 20 % conc) and the radioiodination product (**4**) was extracted with ethyl acetate (x 2). The solvent was removed from the combined organic layers under a stream of air and the residue dissolved in 200 μL methanol for the subsequent deprotection of the glucose moiety. Sodium methoxide (1 mg in 50 μL of methanol/water (1:1)) was added and the reaction mixture stirred for 15 min. After addition of Amberlite resin (H^+-form) and stirring for another 7 min at RT, the solution was diluted with 5 mL of water and passed through a Sep-Pak cartridge (6 mL size, C-18 silica). The cartridge was washed with water (5 mL) and finally the product eluted with 2.5 mL of methanol. According to TLC analysis the radiolabelled product was obtained in a radiochemical purity of ~97 %. Its identity was confirmed by comparing the R_f-values (0.25; on silica using ethyl acetate/methanol 4:1) of the labelled and cold analogues of **5**.

2.2.3 GLUT-1 Cell Uptake Assay

These experiments were conducted by me using LCC6-HER2 cells – a human breast cancer cell line chosen for its overexpression of the glucose transporter GLUT-1.[26] LCC6-HER2 cells were plated with Dulbecco's Modified Eagle Medium (D-MEM) (1X), liquid (high glucose) supplemented with 10 % Fetal Bovine Serum and 1 % Penicillin/Streptomycin. The cells were allowed to adhere at 37 °C in a humidified atmosphere containing 5 % CO_2. The plating was carried out in 75 cm^2 tissue culture flasks with 0.2 μm vented caps. The cultures were maintained in a humidified 5 % CO_2 atmosphere, with medium changes every alternate day. Subculturing was carried out every 3-4 days using Trypsin-EDTA 1X (0.25 % Trypsin with Na_4EDTA), incubated for about 5 min at 37 °C for cell detachment. A hemacytometer was used for counting the cells to monitor cell proliferation.

On the experiment day, $1x10^6$ cells/mL concentration of cells was prepared in 1 % PBS (pH 7.4) and aliquoted into 1.5 mL Eppendorf vials to get a final volume of 0.5 mL in each vial ($5x10^5$ cells). The compound to be tested was then added to the cells and the vial gently inverted. The ^{123}I complex (15 μCi) and ^{18}F-FDG (30 μCi) were used in 500 μL PBS solution. Each compound was added to the cells in glucose-free conditions, and in a final concentration of 5

mM D-glucose. The resulting suspensions were incubated at 37 °C for 30 min with shaking at 400 RPM (revolutions per minute). Following incubation the vials were centrifuged at 1100 RPM for 5 min then 900 μL of the supernatant was removed. Cold PBS solution (900 μL) was added, and gentle mixing of the cells into the solution was achieved by gentle uptake and release of the solution from the pipette tip three times. This centrifuging and washing procedure was repeated four times in total to give the original supernatant and three washing supernatants. Finally the cells were vortexed in cold PBS (1 mL) to remove them from the vial wall and transferred to a tube for gamma counting.

The activity in each cell sample was divided by the sum of all the supernatants for that sample to give a percentage of the original amount of activity that ended up associated with the cells. All experiments were carried out in quadruplicate. FDG was used as a positive control, and was repeated each day that these experiments were carried out to ensure experimental integrity.

2.3 Results and Discussion

2.3.1 Synthesis

The synthetic route used to make the radioiodinated, glycosylated pyridinone **pyrA** is shown in Scheme 2.1. Synthesis of the *para*-bromophenyl pyridinone from maltol via an acid catalysed amine insertion and condensation proceeded in adequate yield. This is comparable to that observed for the insertion reaction of other aromatic amines to maltol.[27]

Many methods for the glycosylation of the hydroxyl group were investigated. Initially the glucose was installed as the tetrabenzyl protected species. This was made using the α-bromo tetrabenzylated sugar starting material with $BF_3.OEt_2$ as a Lewis acid catalyst for the S_N2 substitution; however, this benzylated substrate was not suitable for use in radiosynthesis, as the removal of the benzyl groups proved problematic. As radioactivity decays over time, to maximize the useful yield of a reaction sequence, reactions must proceed quickly. Removal of the four benzyl groups via hydrogenation does not proceed quickly under ambient pressures of hydrogen, and the use of high pressure equipment was not feasible in this case. Removal of the benzyl groups of the bromopyridinone with HBr resulted in loss of the bromine from the phenyl

References begin on Pg 61

ring. As the C-I bond is weaker than the C-Br bond, it was assumed that the iodine would also be lost under these reaction conditions.

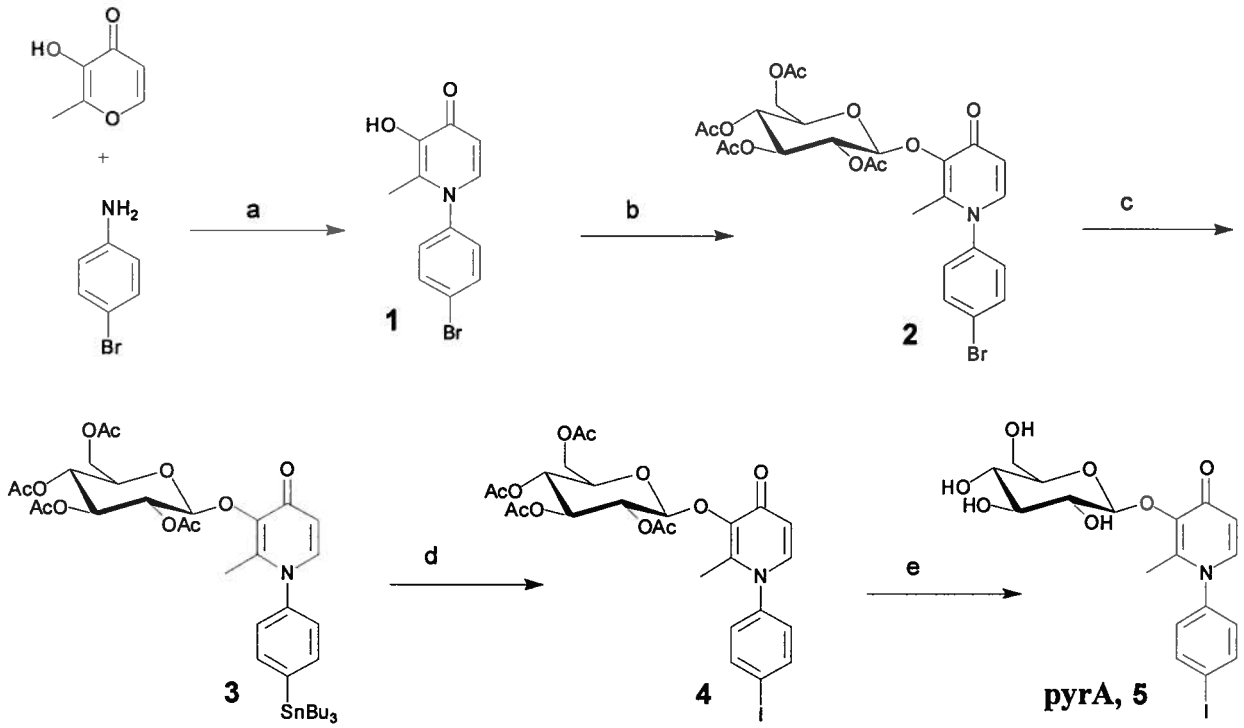

Scheme 2.1 Reaction scheme for synthesis described in this chapter: a) HCl, H_2O/MeOH, reflux, 48 hr b) acetobromo-α-D-glucose, NBu_4Br, CH_2Cl_2/1 M NaOH, 35 °C, 3 hr c) Sn_2Bu_6, $Pd(PPh_3)_4$, toluene, reflux, 16 hr d) NaI ($^{123/125/127}I$), Chloramine-T, MeOH, 30 min e) NaOMe, MeOH, 1 hr.

Acetyl protecting groups were used, as these can be quickly and reliably removed under conditions not expected to affect the C-I bond. Several methods were investigated for the addition of the tetraacetyl protected glucose. The Mitsunobu reaction and Koenigs-Knorr reaction were used (starting from the sugar with a free hydroxyl at *C*-1), as well as Lewis acid catalysis with $BF_3.OEt_2$ and Bronsted base catalysis with hydroxide (the latter two starting with the α-bromo sugar). Despite finding some success with each of these reactions, it was a phase transfer reaction that became the synthetic method of choice. This involves a biphasic reaction mixture consisting of methylene chloride and an aqueous solution of 1M NaOH. The two partners to be coupled were added to this mixture along with tetrabutylammonium bromide which behaves as a phase transfer catalyst; the reaction mixture was heated at 30 °C and stirred vigorously for three hours. After workup and column purification, only modest yields are

References begin on Pg 61

achieved, but this reaction is favourable in its short reaction time, and ease of product purification.

A Stille reaction was then performed to obtain a relatively weak C-Sn bond that is known to be readily cleaved by an I^+ electrophile.[28] The chemistry of this type of palladium cross-coupling reaction is fairly well understood,[29] and standard reaction conditions were used to obtain adequate yields of the tributyltin substituted pyridinone. As an excess of tin reagent was used, an acetonitrile:hexanes extraction was very helpful in removing some of the excess butyltin species prior to column chromatography, where they tended to streak. Substitution of the tin with iodine proceeded smoothly, regardless of iodine isotope used. This reaction is performed using NaI and an oxidant which oxidises the I^- to I^+, which is believed to be the active species. In this work the oxidant that gave the best results was Chloramine-T. Removal of the acetyl protecting groups proceeded in a straightforward manner using NaOMe in MeOH in an essentially quantitative yield.

When performing radioiodination the same chemical reagents were utilized, the only difference being the isotope of iodine used: ^{123}I for preliminary work and ^{125}I for the animal studies. ^{123}I has a half life of 13 hr, decaying quickly enough that it can be conveniently left in shielded storage in the radiochemistry lab. It is a very useful tool for optimization of chemistry, purification, analysis and storage conditions. Once these systems had been optimized, the chemistry was transferred to the longer lived ^{125}I isotope, $t_{1/2}$ = 60 days. As expected, the chemistry proceeded in an analogous manner. The final ^{125}I labelled product was shipped to our collaborators in Texas for the *in vivo* studies. A sample was retained and kept under the same conditions (in ethanolic solution at room temperature) and tested to ensure stability over the time frame required for animal studies. The sample did not degrade appreciably over the several days during which it was tested. A representative TLC trace is shown in Figure 2.4.

References begin on Pg 61

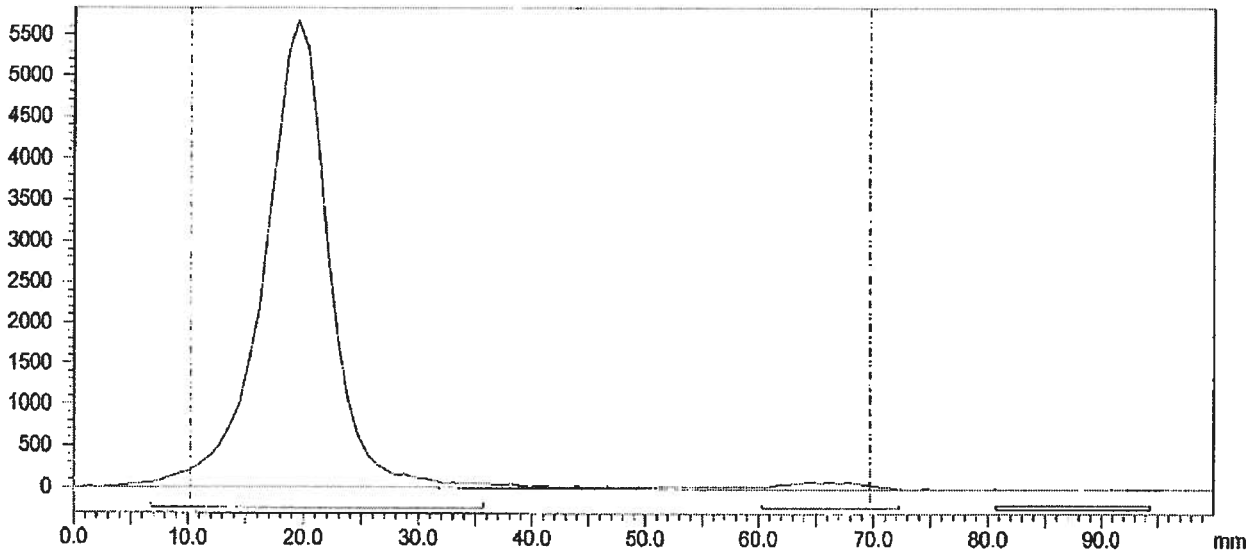

Figure 2.4 Radio-TLC trace of final iodinated pyridinone **pyrA**, R_f = 0.24 – 97.8% pure. The line at 10 mm represents the baseline, and that at 70 mm shows the solvent front. Units on the lefthand side are counts of activity.

2.3.2 *In Vivo* Studies

In vivo rat brain perfusion experiments were carried out by Dr. David Allen, Dr. Paul Lockman and Fancy Thomas at Texas Tech University Health Sciences Centre. The key finding from the perspective of the advancement of our Alzheimer's project is that these glycosylated prodrugs do indeed cross the blood brain barrier.

This type of brain perfusion experiment is very fast, with only 60 sec available for BBB penetration. The reason that such a short timeframe is used is to render any outflow from the brain negligible. It can then be assumed that the entire amount of compound taken into the brain in that 60 sec is still in there at the end of the measured period, greatly simplifying the interpretation of the results. Choline was used as a control in this experiment, as it is known to cross the BBB.[30]

References begin on Pg 61

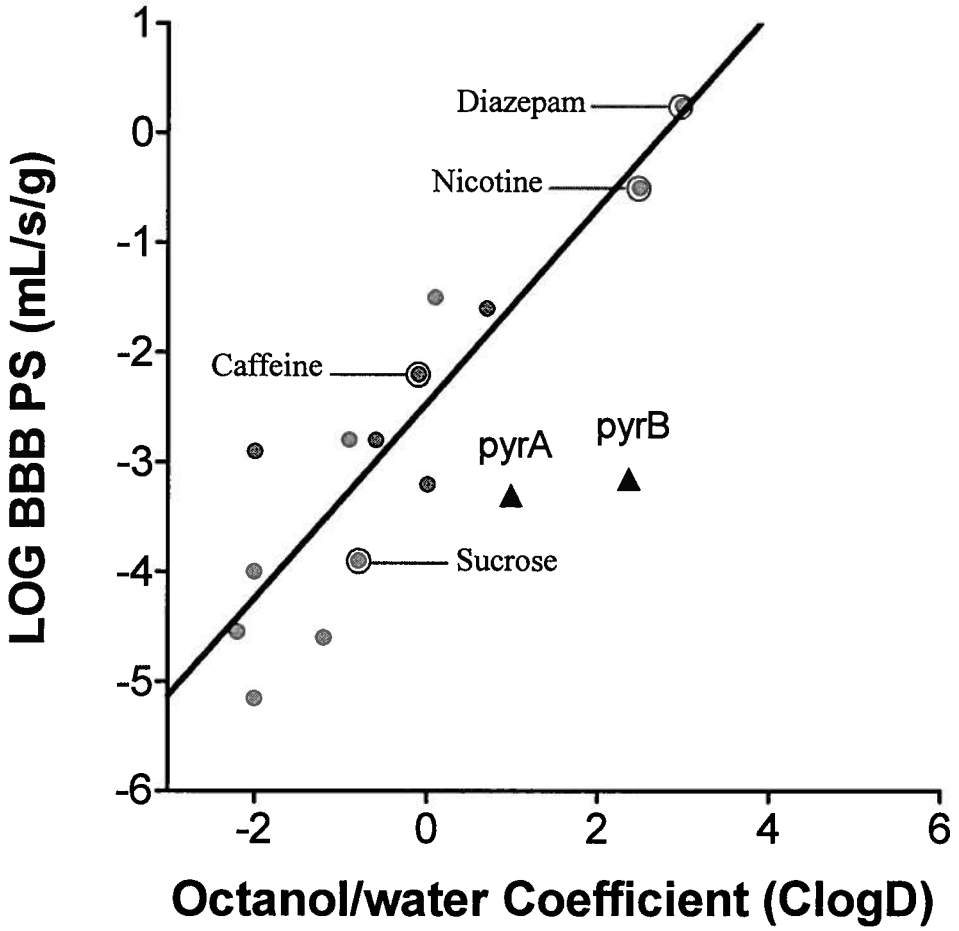

Figure 2.5 Representation of BBB permeability of **pyrA** and **pyrB** shown with various compounds of known permeability for context. ClogD is the calculated octanol/water partition coefficient, a measure of lipophilicity, and BBB PS is a measure of the brain permeability of each compound.

The results of this experiment are shown graphically in Figure 2.5, where they are contextualized with some compounds of known BBB permeability. The diagonal line running through the graph corresponds to the expected uptake from passive diffusion. Sucrose crosses the BBB very slowly, and is commonly used as a negative control in experiments of this type, where its presence inside the brain would show either a compromised BBB or poor experimental technique. Caffeine and nicotine are very commonly used drugs, with their rapid effects stemming from the ease with which they enter the brain. Nicotine is a very small molecule (MW 162 $g.mol^{-1}$) which crosses the BBB via passive diffusion and is therefore situated on the diagonal trend line in the graph above. Caffeine (MW 194 $g.mol^{-1}$), while also small, is a

References begin on Pg 61

structural analogue of the purine base adenosine, and as such cross the BBB via both passive diffusion and carrier mediated transport.[31] This is why caffeine sits above the trend line on the graph above – it is taken up into the brain faster than if it were transported by passive diffusion alone.

The BBB uptake of **pyrA** was found to be $6.4x10^{-4} \pm 4.2x10^{-4}$ mL/sec/g and that of **pyrB** was found to be $8.9x10^{-4} \pm 4.1x10^{-4}$ mL/sec/g. In Figure 2.5 both **pyrA** and **pyrB** are reasonably far away from the passive diffusion trend line. As they are below this line, the brain uptake rate that they experience is lower than that expected from passive diffusion. The timescale of the BBB perfusion experiment used in this study is very short (60 sec), meaning efflux is highly unlikely. This indicates that the compounds either undergo passive diffusion very slowly, or that there is another mechanism at play. However the compounds are getting into the brain, they are doing it relatively slowly.

Initially it was thought that the mechanism of the two compounds' entry into the brain was by transport on the glucose transporter GLUT-1. This is one of a family of GLUTs that facilitate transport of sugars through various membranes, as detailed in Chapter 1. The GLUT-1 isoform is known to be expressed in high concentrations at the blood brain barrier and in erythrocytes. Because of this, and the fact that that there are sugars present in these molecules, it is possible that the compounds entered the brain via the GLUT-1 transporters. It is unlikely that these compounds, with their deprotected sugars, would be lipophilic enough to cross into the brain via passive diffusion. As the compounds tested were quite different to glucose, it is plausible that any GLUT-mediated transport would occur at a considerably slower rate than that of native glucose.

2.3.3 *In Vitro* Studies

In vitro cell studies were done to help verify the *in vivo* results, and also to deduce a little more about the mechanism of the brain uptake observed in the rats.

The *in vitro* cell uptake studies were performed in LCC6-HER2 cells – a human breast cancer cell line chosen for its overexpression of the glucose transporter GLUT-1.[26] The cellular uptake

References begin on Pg 61

of an ^{123}I labelled compound - **pyrB** - was examined under both glucose free and high glucose (10 mM) conditions, and was found to be 0.10 ± 0.02 % and 0.12 ± 0.02 % of the total radiation respectively.

Any changes in amount of radioactive species seen in the cells under these two conditions were attributed to the presence of glucose, as all other conditions were kept constant. If the test compound was utilizing the same transport mechanism as the glucose, the large excess of glucose molecules present would occupy and be transported by GLUT-1 such that less transporters would be free to move the test compound. The presence of the glucose does not make a significant difference to the amount of test compound getting into the cells, implying that the compound tested does not enter the cells via the GLUT-1 transporters.

A limitation of this assay is that it does not distinguish between the radioactive compound being inside the cell or just being embedded in the membrane. However, the fact that these compounds get into the brain leads us to believe that they also getting into the cells, as the BBB is generally less permeable than are cell membranes. The mechanism for this brain entry is still not known. Possibilities are passive diffusion, though is seems unlikely as outlined above, or entry through another transporter such as the Na^+/K^+ pump, as has been observed with other compounds.[32]

The amount of activity associated with the cells after a 30 min incubation is very small. This is in keeping with the findings of the rat brain perfusion studies which found that the same compound was able to cross the blood brain barrier, though only in small amounts in the given time frame. Although the uptake observed in both these studies is not particularly fast, it is likely sufficient for the proposed purpose of compounds of this type as AD therapeutics. If glycosylated pyridinones of this type were found to be useful in the treatment of AD, this rate of BBB permeation would likely be adequate to elicit a therapeutic effect, as once the compounds were administered, they would have much longer than 60 sec in which to cross the BBB.

This raises the possibility of administering the non-glycosylated version of the compounds, as these may permeate key membranes more quickly. As mentioned above, there were several proposed benefits of appending the glucose, and the water solubility and protection of the chelating moiety are both important features that may be compromised if the glucose pro-drug

References begin on Pg 61

form of the molecule is not used. From the studies performed to date we cannot be sure that the glycosidic bond remained intact during either of these assays. A sample of iodinated compound was retained and tested for degradation after 3 days, and it was found to be intact. However, once inside an animal or interacting with cells, we cannot be sure that the glucose remained bound to the pyridinone. More work needs to be done in this area to ensure the integrity of this bond under more biologically relevant conditions, and to assess the BBB permeability of the glycosylated *vs.* non-glycosylated compounds.

2.4 Conclusion

This was a critical set of experiments in order to determine the potential utility of this approach in treating AD. In this work two glucose-protected 3-hydroxy-4-pyridinones were successfully radioiodinated. The radiolabelled compounds were assessed using an *in vivo* brain perfusion study in rats, and were found to cross the BBB. If these glycosylated pyridinones were not BBB permeable there would be little point in continuing this line of investigation and the current compounds would require significant modification to improve their *in vivo* properties. Although the brain uptakes observed were relatively low compared to those seen in native brain substrates, this approach does not necessarily require very fast brain uptake. As these glycosylated pyridinones have been found to be non-toxic to human cells,[24] it is possible that a larger dose could be administered and slow BBB permeation could lead to a constant supply of deprotected prodrug in the brain. It is not known exactly how these many factors will interplay, but more and more information is being gathered as work on this project is continuing in the Orvig group. The aim of this particular study was met with a successful determination of BBB permeation at what we deemed to be a great enough rate to continue this work.

References begin on Pg 61

2.5 References

1. Lovell, M. A.; Robertson, J. D.; Teesdale, W. J.; Campbell, J. L.; Markesbery, W. R., *J. Neurol. Sci.* **1998,** *158*, 47-52.

2. Smith, M. A.; Harris, P. L. R.; Sayre, L. M.; Perry, G., *Proc. Natl. Acad. Sci. U. S. A.* **1997,** *94*, 9866-9868.

3. Dong, J.; Atwood, C. S.; Anderson, V. E.; Siedlak, S. L.; Smith, M. A.; Perry, G.; Carey, P. R., *Biochemistry* **2003,** *42*, 2768-2773.

4. Armendariz, A. D.; Gonzalez, M.; Loguinov, A. V.; Vulpe, C. D., *Physiol. Genomics* **2004,** *20*, 45 - 54.

5. Bush, A. I., *Trends Neurosci.* **2003,** *26*, 207-214.

6. Rottkamp, C. A.; Raina, A. K.; Zhu, X.; Gaier, E.; Bush, A. I.; Atwood, C. S.; Chevion, M.; Perry, G.; Smith, M. A., *Free Radic. Biol. Med.* **2001,** *30*, 447-450.

7. Cherny, R. A.; Atwood, C. S.; Xilinas, M. E.; Gray, D. N.; Jones, W. D.; McLean, C. A.; Barnham, K. J.; Volitakis, I.; Fraser, F. W.; Kim, Y. S.; Huang, X. D.; Goldstein, L. E.; Moir, R. D.; Lim, J. T.; Beyreuther, K.; Zheng, H.; Tanzi, R. E.; Masters, C. L.; Bush, A. I., *Neuron* **2001,** *30*, 665-676.

8. Yurdakul, S.; Arici, K., *J. Mol. Struct.* **2004,** *691*, 45 - 49.

9. Adlard, P. A.; Cherny, R. A.; Finkelstein, D. I.; Gautier, E.; Robb, E.; Cortes, M.; Volitakis, I.; Liu, X.; Smith, J. P.; Perez, K.; Laughton, K.; Li, Q.-X.; Charman, S. A.; Nicolazzo, J. A.; Wilkins, S.; Deleva, K.; Lynch, T.; Kok, G.; Ritchie, C. W.; Tanzi, R. E.; Cappai, R.; Masters, C. L.; Barnham, K. J.; Bush, A. I., *Neuron* **2008,** *59*, 43 - 55.

10. Ritchie, C. W.; Bush, A. I.; Mackinnon, A.; Macfarlane, S.; Mastwyk, M.; MacGregor, L.; Kiers, L.; Cherny, R.; Li, Q. X.; Tammer, A.; Carrington, D.; Mavros, C.; Volitakis, I.; Xilinas, M.; Ames, D.; Davis, S.; Beyreuther, K.; Tanzi, R. E.; Masters, C. L., *Arch. Neurol.* **2003,** *60*, 1685-1691.

11. Lannfelt, L.; Blennow, K.; Zetterberg, H.; Batsman, S.; Ames, D.; Harrison, J.; Masters, C.; Targum, S.; Bush, A.; Murdoch, R.; Wilson, J. E.; Ritchie, C. W., *Lancet Neurol.* **2008,** *7*, 779 - 786.

12. McKelvey, E. M.; Gottlieb, J. A.; Wilson, H. E.; Haut, A.; Talley, R. W.; Stephens, R.; Lane, M.; Gamble, J. F.; Jones, S. E.; Grozea, P. N.; Gutterman, J.; Coltman, C.; Moon, T. E., *Cancer* **1976,** *38*, 1484 - 1493.

13. Egger, M.; Hirschel, B.; Francioli, P.; Sudre, P.; Wirz, M.; Flepp, M.; Rickenbach, M.; Malinverni, R.; Vernazza, P.; Battegay, M., *Brit. Med. J.* **1997,** *315*, 1194 - 1199.

14. Cavalli, A.; Bolognesi, M. L.; Minarini, A.; Rosini, M.; Tumiatti, V.; Recanatini, M.; Melchiorre, C., *J. Med. Chem.* **2008,** *51*, 347 - 372.

15. Kapkova, P.; Alptuzun, V.; Frey, P.; Erciyas, E.; Holzgrabe, U., *Bioorg. Med. Chem.* **2006,** *14*, 472 - 478.

16. Rodriguez-Franco, M. I.; Fernandez-Bachiller, M. I.; Perez, C.; Hernandez-Ledesma, B.; Bartolome, B., *J. Med. Chem.* **2006,** *49*, 459 - 462.

17. Cavalli, A.; Bolognesi, M. L.; Capsoni, S.; Andrisano, V.; Bartolini, M.; Margotti, E.; Cattaneo, A.; Recanatini, M.; Melchiorre, C., *Angew. Chem. Int. Ed.* **2007,** *46*, 3689 - 3692.

18. Ji, H. F.; Zhang, H. Y., *Bioorg. Med. Chem. Lett.* **2005,** *15*, 21-24.

19. Hider, R. C.; Liu, Z. D., *J. Pharm. Pharmacol.* **1997,** *49*, 59-64.

20. Hider, R. C., *Toxicol. Lett.* **1995,** *82-3*, 961-967.

21. Dobbin, P. S.; Hider, R. C.; Hall, A. D.; Taylor, P. D.; Sarpong, P.; Porter, J. B.; Xiao, G. Y.; Vanderhelm, D., *J. Med. Chem.* **1993,** *36*, 2448-2458.

22. Bebbington, D.; Monck, N. J. T.; Gaur, S.; Palmer, A. M.; Benwell, K.; Harvey, V.; Malcolm, C. S.; Porter, R. H. P., *J. Med. Chem.* **2000,** *43*, 2779-2782.

23. Dedeoglu, A.; Cormier, K.; Payton, S. M.; Tseitlin, K. A.; Kremsky, J. N.; Lai, L.; Li, X.; Moir, R. D.; Tanzi, R. E.; Bush, A. I.; Kowall, N. W.; Rogers, J. T.; Huang, X., *Exp. Gerontol.* **2004,** *39*, 1641 - 1649.

24. Schugar, H.; Green, D. E.; Bowen, M. L.; Scott, L. E.; Storr, T.; Bohmerle, K.; Thomas, F.; Allen, D. D.; Lockman, P. R.; Merkel, M.; Thompson, K.; Orvig, C., *Angew. Chem. Int. Ed.* **2007,** *46*, 1716 - 1718.

25. Scott, L. E.; Page, B. P.; Merkel, M.; Orvig, C., unpublished results.

26. Dragowska, W. H.; Ruth, T. J.; Adam, M. J.; Kozlowski, P.; Skov, K.; Bally, M. B.; Yapp, D. T. T. In *Studies of Tumor Microenvironment and Metabolic Activity in HER-2/neu Overexpressing Breast Cancer Xenografts by MicroPET and MRI*, American Association for Cancer Research, 2005; 2005; p 900.

27. Zhang, Z.; Rettig, S. J.; Orvig, C., *Can. J. Chem.* **1992,** *70*, 763 - 770.

28. Lindegren, S.; Skarnemark, G.; Jacobsson, L.; Karlsson, B., *Nucl. Med. Biol.* **1998,** *25*, 659 - 665.

29. Espinet, P.; Echavarren, A. M., *Angew. Chem. Int. Ed.* **2004,** *43*, 4704 - 4734.

30. Allen, D. D.; Smith, Q. R., *Journal of Neurochemistry* **2001,** *76*, 1032 - 1041.

31. Di, L.; Kerns, E. H.; Fan, K.; McConnell, O. J.; Carter, G. T., *Eur. J. Med. Chem.* **2003,** *38*, 223 - 232.

32. Kishimoto, S.; Kawazoe, Y.; Ikeno, M.; Saitoh, M.; Nakano, Y.; Nishi, Y.; Fukushima, S.; Takeuchi, Y., *Cancer Chemoth. Pharm.* **2006,** *57*, 84 - 90.

CHAPTER 3

Monoanionic Glucosamine-based Ligands for the Formation of Neutral Complexes with the $[M(CO)_3]^+$ Core (M = Re, ^{99m}Tc)*

3.1 Introduction

3.1.1 Designing a Carbohydrate-based Imaging Agent

The ability to image the location of carbohydrate metabolism is a very useful diagnostic tool. It can be used to derive information on cell function, with increased carbohydrate processing activity found in areas such as cancerous tissue,[1] and decreased activity indicating areas with a loss of metabolic function, such as atrophied brain areas in Alzheimer's disease.[2]

Although there is currently a very useful carbohydrate based imaging agent available in the form of FDG (2-^{18}F-fluoro-2-deoxyglucose, Figure 3.1b), its availability is somewhat limited. The mechanism of action of FDG is discussed in more detail in Chapters 1.2 and 1.3. In summary, the structural similarity between glucose and FDG (illustrated in Figure 3.1) means that FDG is transported and to some extent metabolised as if it were glucose. The difference between the two means that the metabolism of FDG can only proceed so far, and as such FDG does not get broken down, but instead gets trapped in cells, particularly those which overexpress certain proteins; GLUT and hexokinase.

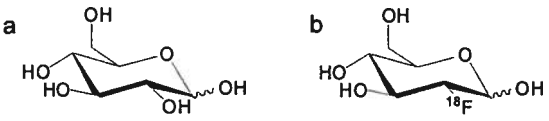

Figure 3.1 a) D-glucose b) 2-^{18}F-fluoro-2-deoxyglucose (FDG). The substitution of ^{18}F for -OH at *C*-2 is the only difference between the two molecules.

Access to the ^{18}F isotope used in FDG is not widespread as it has a short half life ($t_{1/2}$ – 110

---

* A portion of this chapter has been published: Bowen, M. L. and Orvig, C. ^{99m}Technetium carbohydrate conjugates as potential agents in molecular imaging. *Chem. Commun,* **2008**, 5077 – 5091. A version of this chapter will be submitted for publication: Bowen, M. L., Lim, N. A. C., Ewart, C. B., Adam, M. J. and Orvig, C. Glucosamine Conjugates Bearing *N,N,O*-donors: Potential Imaging Agents Utilizing $[M(CO)_3]^+$ Core (M = Re, Tc).

References begin on Pg 106

min) and is produced in a cyclotron.[3, 4] This means that the patient must be geographically close to a cyclotron in order for it to be feasible to use such a short lived isotope without too much loss of activity. Countries with no cyclotron, such as New Zealand, do not have regular access to this very versatile and useful diagnostic agent. This is one of the main reasons behind the interest in the nuclear medicine community in discovering a SPECT carbohydrate-based imaging agent.

In designing a carbohydrate based imaging agent, it is vital to retain a reasonable level of activity with both GLUTs (glucose transporters) and HK (hexokinase) compared to the parent carbohydrate. To produce useful images, an agent must accumulate in target tissue at a faster rate than it does in background tissue. For this to happen the radiolabelled compound needs to access cells (GLUT), and be trapped there (HK), so cells that have overactive GLUT and HK, as do most cancer cells, are the cells that are targeted by this approach. This was discussed in detail in Chapter 1.3.

3.1.2 Technetium Glycoconjugates

There have been many ^{99m}Tc glycoconjugates made over the years utilizing several different approaches to metal binding. Due to the high dilution involved in ^{99m}Tc chemistry, sugars were often modified by adding a binding moiety with a higher affinity for the metal ion than the native hydroxyl groups exhibit.[5] As with much early work on sugar coordination chemistry, the compounds were often not subjected to rigorous chemical characterization, so the exact structures were not known.[5, 6] *In vivo* studies of ^{99m}Tc labelled 5-thio-D-glucose showed that the compound did not behave like a glucose analogue, suggesting it contained too many modifications compared to glucose for it to be recognized and/or used by the native transport and metabolizing proteins.[7] Recent studies of ^{99m}Tc labelled 1-thio-β-D-glucose[8] result in very different HPLC traces depending on the pH of the solution and the concentration of the ligand. The complex formed is not particularly stable, given that at neutral pH the ^{99m}Tc complex is no longer intact after 2 hr.[8] From a coordination chemistry perspective, this also suggests that there may be more than one chemical species present under physiological conditions, which greatly complicates interpretation of any biodistribution data that may be obtained. The authors note they cannot form the rhenium analogues, which is unusual given that technetium and rhenium normally exhibit very similar

References begin on Pg 106

coordination chemistry.[8] Cellular uptake is not affected by the presence of glucose, suggesting that the compound is not transported by the GLUT transporters.[8]

Yang and coworkers have made and studied a species with ^{99m}Tc(V) bound to ethylenedicysteine-deoxyglucose (ECDG) (Figure 3.2a).[9] This is a tetradentate ligand with an N_2S_2 binding sphere and two appended glucosamines, bound to the chelate via amide bonds at their *C*-2 nitrogens. Radiolabelling proceeds from $[^{99m}TcO_4]^-$ in the presence of $SnCl_2$ in 94 % radiochemical yield.[9] The ECDG ligand was subjected to a hexokinase assay, and the authors claim that ECDG could be phosphorylated by hexokinase, though the experimental results presented in this paper do not seem to provide enough information to verify this claim.[9] An *in vitro* cell uptake study of ^{99m}Tc-ECDG was performed in human lung cancer cells, and it was found that cellular uptake was similar to that observed for FDG (0.5 vs. 0.6 % of total activity used).[9] It was also found that uptake of ^{99m}Tc-ECDG decreased in the presence of D-glucose, but not in the presence of L-glucose, suggesting that the uptake observed is due to the same transport mechanisms as those used for D-glucose i.e. GLUT transporters.[9]

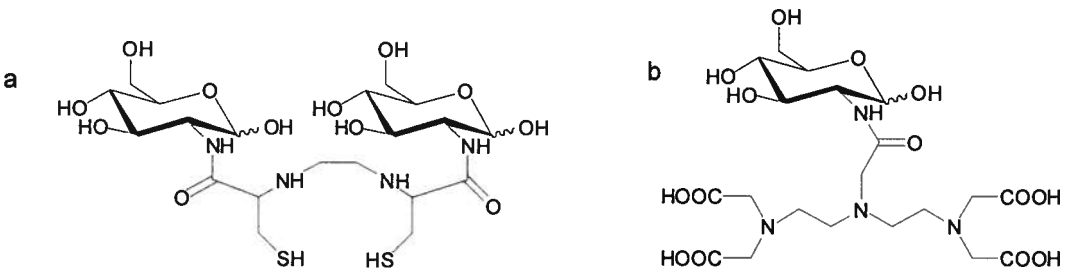

Figure 3.2 a) ECDG[9] b) DTPA-DG;[10] protonation states when complexed to metal ions are not discussed in the original papers.

In vivo it was found that rats which had been pretreated with insulin had increased tumor uptake of ^{99m}Tc-ECDG, again suggesting the cellular uptake is due to a glucose related mechanism.[11] The authors suggest the complex is stable as there is no accumulation of activity in the thyroid *in vivo*.[11] If technetium were to become uncomplexed, under physiological conditions it would be oxidised to pertechnetate, which is known to accumulate in the thyroid.[12] Biodistribution results show good tumor-to-muscle ratios 4 hr post injection, suggesting some potential utility as an imaging agent. The amount of activity in the blood is twice as much as in the tumor at all time points, and this ratio does not

References begin on Pg 106

increase over time, as it does for FDG.[11] It is therefore possible that ECDG is not phosphorylated by hexokinase as the authors suggest, and is therefore not trapped in cells, but reaches an equilibrium concentration due to constant influx and efflux rates. Nonetheless, images obtained from tumor-bearing rats with ^{99m}Tc-ECDG clearly show the tumor, while those from the nonglycosylated ^{99m}Tc-EC control complex only show activity in the excretory organs.[11] This demonstrates the utility of the sugar conjugation approach in molecular imaging. ^{99m}Tc-ECDG was also used to monitor treatment efficiency, by imaging tumor-bearing rats before and after treatment with the known anticancer agents Paclitaxel and Cisplatin.[11] Differences were seen in the images obtained before and after treatment, and the authors suggest ^{99m}Tc-ECDG may be useful in assessing the therapeutic response of cancer treatments.[11]

Another study on the use of carbohydrate-containing ligands for the $[^{99m}TcO]^{3+}$ core utilizes glucosamine bound to a diethylenetriaminepentaacetic acid (DTPA) chelate via an amide bond between the *C*-2 nitrogen of the sugar and the acetate moiety on the central nitrogen of the DTPA, giving diethylenetriaminepentaacetic acid deoxyglucose (DTPA-DG) (Figure 3.2b).[10] DTPA is known to be a strong metal chelator, and here the labelling with ^{99m}Tc proceeded in excellent radiochemical purity, although there is little characterization data provided for either the ligand or the technetium complex.[10] The ligand, as drawn in the original paper, has seven obvious chelating atoms, and no mention is made as to which of these atoms are believed to be bound to the technetium. The complex was found to be stable in solution for six hours, and is proposed to stay intact *in vivo* due to lack of activity in the thyroid,[10] a known site of accumulation for free pertechnetate. *In vitro* cellular uptake of ^{99m}Tc-DTPA-DG was found to be about the same as for ^{99m}Tc-ECDG - 0.5 % of administered activity compared to ~ 0.6 % for FDG. Similar to the findings for ^{99m}Tc-ECDG, the tumor-to-muscle ratios for the test compound were significantly higher than for FDG, while the tumor-to-blood ratios were lower. Both the tumor-to-blood and tumor-to-muscle ratios for the test compound increase over time to the two hour time point and then remain constant out to eight hours.[10] Images with ^{99m}Tc-DTPA-DG of tumor bearing rats enable visualization of the tumor, while control images with ^{99m}Tc-DTPA show only the liver and kidneys.[10] In a subsequent study, selectivity of ^{99m}Tc-DTPA-DG for cancerous rather than inflamed tissue was also demonstrated.[13] The ^{188}Re analogue of this compound was prepared and ~9 MBq was injected into the tail vein of tumor-bearing mice.[14] Planar

References begin on Pg 106

scintigraphy imaging clearly shows the tumor tissue.[14] Twenty one days after this treatment the tumors of the treated animals had reduced in size significantly (around 30 %) with respect to those of a control group.[14] This finding illustrates the potential of using ^{99m}Tc and ^{188}Re analogues of the same ligand system for imaging and therapy, respectively.

Liu and coworkers examined three deoxyglucose conjugates as ligands for the $[^{99m}TcO]^{3+}$ core (Figure 3.3).[15] The ligands were made by conjugation via an amide bond to the nitrogen at the *C*-2 position of glucosamine.[15] One of the ligands (Figure 3.3a) appears to be *NS*-bidentate (though there is no discussion ruling out the involvement of the proximal sugar hydroxyl groups in binding to the metal, or the formation of an ML_2 species) and the two others are tetradentate, one N_3S (Figure 3.3b), and the other N_2S_2 (Figure 3.3c). Radiolabelling via an exchange reaction with ^{99m}Tc-glucoheptonate provided the desired compounds in very good radiochemical yields.[15] Biodistribution studies in tumor-bearing mice show these compounds to all exhibit tumor-to-muscle ratios of 2 - 3 four hours post injection, and tumor-to-blood ratios of 0.5 - 1.[15] The compound based on a derivatized MAG_3 shows the most promise for further studies (Figure 3.3b),[15] though the tumor-to-blood ratio would ideally need to be increased to give improved image quality.

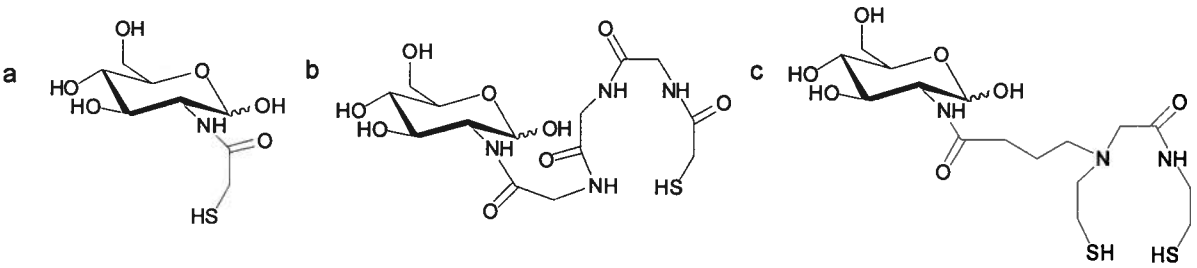

Figure 3.3 Three ligands used for binding to $[^{99m}TcO]^{3+}$.[15]

It seems that despite significant work in this area over several decades, there have not been any major breakthroughs made towards a useful glycosylated $[^{99m}TcO]^{3+}$-based compound for molecular imaging. As discussed in Chapter 1.4.1, with any ligand that is not C_2 symmetric, it is not possible to synthesize a single diastereomeric complex of this core, and the resulting isomers may exhibit different biological properties. The lack of thorough molecular characterization of these compounds is also problematic, in terms of understanding results and improving on design. A lack of stability studies may also cast

References begin on Pg 106

doubt on the exact nature of the ^{99m}Tc species that is being imaged in a given *in vivo* experiment.

3.1.3 $[^{99m}Tc(CO)_3]^+$ Glycoconjugates

The advent of the $[M(CO)_3]^+$ core has revolutionalized the field of ^{99m}Tc chemistry.[16] This core brings together many properties of importance in radiopharmaceutical chemistry to provide a very attractive base upon which to build SPECT tracers. $[M(CO)_3]^+$ is small, kinetically inert, of moderate lipophilicity, and easy to prepare, especially when made via a Mallinkcrodt (now Covidien) Isolink™ kit. These properties, combined with the favourable characteristics of ^{99m}Tc as a SPECT tracer ($t_{1/2}$ = 6 hr, γ = 140 keV, generator produced), give a very attractive starting point for radiopharmaceutical design.

As this is the core used in the work described in this thesis, the glycoconjugates previously made on this core are very relevant, so will be covered in some detail here.

3.1.3.1 Bidentate Ligand Systems

Given the promising results seen in the enzymatic activity retention of *N*-functionalized glucosamines, the Orvig group's first work in this field involved a glucosamine conjugated ligand.[17] This was designed to bind in a bidentate fashion via a phenolate oxygen and a secondary amine: the nitrogen of the glucosamine (Figure 3.4).[17] ^{1}H NMR spectroscopic studies of the rhenium complex of this ligand indicated binding of the *C*-3 hydroxyl group of the sugar in addition to the phenolate and amino donors, giving a tridentate facially coordinated ligand in solution.[17] As this ligand was not designed to have three atoms binding to the metal, the donor atoms were not optimised, and the NO_2 binding sphere did not show the desired stability when incubated with high concentrations of cysteine and histidine ligands for 24 hr.[17] This finding confirms the discussion in Chapter 1: that carbohydrates themselves do not make very good ligands. In this case the *C*-3 hydroxyl is held very close to the vacant coordination site on the metal, so this proximal geometry may encourage binding of a rather weak donor atom that may not bind under other conditions. This type of ligand system was not investigated further, as it was thought that if the carbohydrate is bound to a metal, it would not be recognized and metabolized *in vivo* as the

References begin on Pg 106

parent carbohydrate would, and thus the complex would likely not be useful as a carbohydrate based imaging agent.

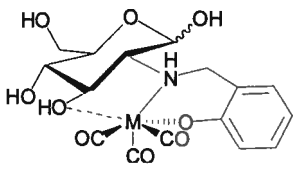

Figure 3.4 A ligand designed to be bidentate shows coordination of the *C*-3 hydroxyl group of the carbohydrate in solution, M = Re, ^{99m}Tc, ^{186}Re.[17]

The coordination of 3-hydroxy-4-pyridinone ligands with pendant carbohydrates to the $[M(CO)_3]^+$ core was then examined, as it was thought that a larger gap between the metal binding atoms and the carbohydrate would likely force the latter to remain pendant.[18] These ligands consist of two oxygen atoms *ortho* to one another on a six membered, aromatic ring (Figure 3.5). The hydroxyl group is deprotonated upon metal binding, giving a monoanionic ligand capable of neutralizing the positive charge on the tricarbonyl core to yield a neutral overall complex with a stable five-membered chelate ring. There was reason to believe that this kind of ligand system could be useful for the $[M(CO)_3]^+$ core as the pyridinone basicity is comparable to that of the aromatic amines that are known to be excellent donors for these metal centers. Five ligands were examined in this study, and they were composed of three different carbohydrate attachment methods: via an ether linkage to *C*-1 of glucose, an amide linkage at the *C*-6 of glucose, and to the nitrogen at *C*-2 of glucosamine, while also varying the distance between the carbohydrate and the chelating oxygen atoms.[18] These ligands were found to bind in a bidentate fashion, with the remaining coordination sites on the metal being occupied by the three carbonyl ligands, and a (predicted) water molecule in aqueous solution.[18] The labelling with both ^{99m}Tc and ^{186}Re proceeded in excellent yields, and the stability in excess cysteine and histidine was essentially quantitative after a 4 hr incubation, with some degradation seen in the histidine experiment after 24 hr.[18] The interaction of these compounds with the glucose metabolizing enzyme hexokinase (HK) was examined, but these compounds were found not to inhibit, or be phosphorylated by, HK under the conditions tested.[18] This means that the change in environment of the sugar disrupts the interactions between the carbohydrate and the enzyme to such an extent that the compound either is not recognized or cannot be phosphorylated.

References begin on Pg 106

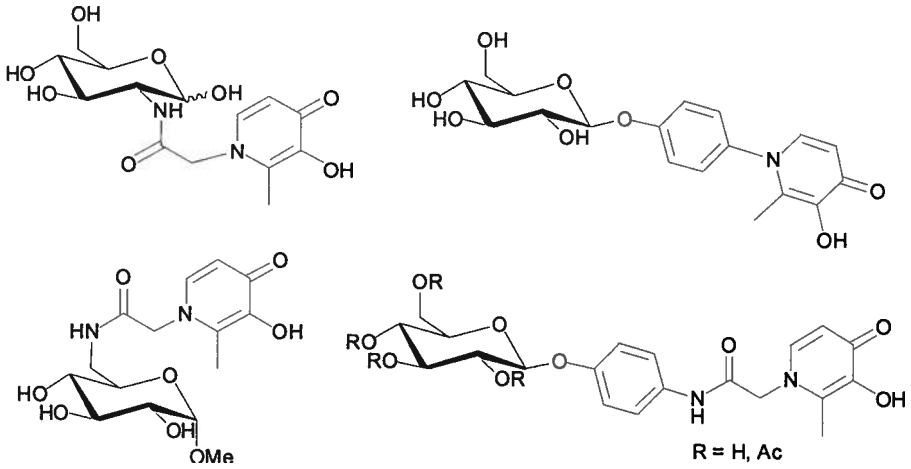

Figure 3.5 Five glucose appended ligands investigated as bidentate chelates for the $[M(CO)_3]^+$ core where M = Re, ^{99m}Tc, ^{186}Re.[18]

In collaboration with the Yano/Mikata group at Nara Women's University in Japan, the Orvig group has complexed the Re and ^{99m}Tc tricarbonyl cores to a range of small, well defined, N_2 bidentate, carbohydrate bearing ligands (Figure 3.6).[19] The sugars were all linked to a chelating 1,3-diaminopropyl group via an ether linkage at *C*-1.[20] The ligands were bound to the metal tricarbonyl core via two primary amine donors, and the remaining coordination sites on the metal ion were occupied by three carbonyls and one bromide ligand for the rhenium complexes, or a proposed aqua ligand under the more dilute tracer conditions used for technetium.[19] The desired pendant nature of the various carbohydrates was confirmed by a lack of coordination induced shift in the ^{1}H NMR spectroscopy solution studies, and by X-ray crystallographic analysis of two of the complexes in the solid state.[19] The ^{99m}Tc complexes of these ligands were formed very readily, and their stability when incubated with high concentrations of the biologically relevant, potential ligands cysteine and histidine for 24 hours were >90 % for cysteine and >68 % for histidine (which has been shown to have a high affinity for the $[M(CO)_3]^+$ core[21]).[19] It is interesting to note that the relative stability of the complexes is in line with the steric size of the ligands, suggesting that the larger ligands may not leave enough space for an adventitious amino acid to reach the vacant coordination site on the metal.

References begin on Pg 106

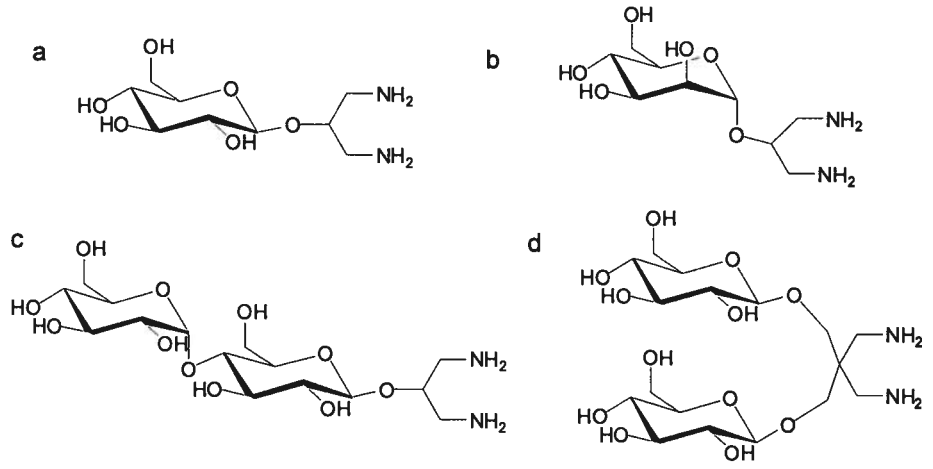

Figure 3.6 Diamino carbohydrate-based ligands:[20] a) the β anomer was synthesized for glucose (shown) as well as xylose and galactose b) the α anomers were synthesized for mannose (shown) and galactose, c) and d) ligands which showed higher stability *in vitro* perhaps due to their increased steric bulk.

Gottschaldt, Yano and coworkers have developed a set of ligands where the carbohydrate is linked to a metal chelate by a thioether moiety (Figure 3.7).[22] This is proposed to help circumvent the enzymatic cleavage that can occur with *O*-glycosidic bonds *in vivo*. The three ligands examined in this study consist of N_2, 2,2'-bipyridyl, bidentate chelates, appended with two identical sugars at the 4 and 4' positions of the bipyridine.[22] Glucose, galactose and mannose were attached to the chelate via thioether linkages at the *C*-1 positions. These ligands were bound to the rhenium tricarbonyl core in good yields, resulting in complexes where the metal is bound to the three carbonyl ligands, the two nitrogen atoms of the bipyridyl, and one anionic chloride to fill out the binding sphere and provide a neutral complex.[22] A solid state X-ray crystal structure of the acetyl protected glucose derivative was obtained and it verifies the above coordination sphere as well as confirming that the carbohydrates do indeed remain pendant, and outside the binding sphere of the metal, at least while acetyl protected.[22] The analogous ^{99m}Tc complexes were also formed in good yields (>95 % radiochemical purity), and were found to exhibit satisfactory stability when incubated with excess histidine for 4.5 hr.[22] After incubating for 24 hr significant degradation was observed, though the product of this process is not the [^{99m}Tc(His)(CO)$_3$] species that may be expected (as verified by HPLC comparison with the presynthesized histidine complex).[22] The authors speculate that the observed products are a result of the replacement of the one labile position (occupied by a water molecule or a halide) with a histidine, while the rest of the coordination sphere remains intact.[22]

References begin on Pg 106

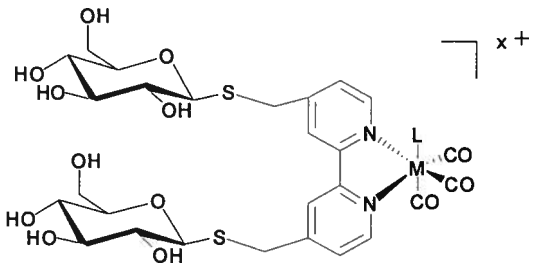

Figure 3.7 An example of a bipyridine complex made by Gottschaldt *et al.*[22] M = Re, L = Cl, x = 0 and M = ^{99m}Tc, L = H_2O, x = 1.

Other workers have also found the stability of bidentate complexes to be lower than required for successful *in vivo* application.[23, 24] This is thought to be due to the binding of some other competing endogenous ligand (such as a protein *in vivo*), to the vacant coordination site on the metal, and eventual replacement of the original ligand over time. Consequently, work on the tricarbonyl cores now mainly focuses on tridentate ligands. Initial work on ligand binding experiments,[23] and more recent verification in the form of DFT (density functional theory) calculations,[25, 26] has shown that the higher the nitrogen content of the binding sphere, the more stable the resulting complexes will be. This means that most work in this area now incorporates at least one nitrogen donor atom into a tridentate core. Work on basic coordination chemistry to optimize the metal binding portion of bioconjugates is ongoing in our labs and others.[27, 28]

3.1.3.2 Tridentate Ligand Systems

The first organometallic carbohydrate containing complexes of group 7 metals were reported in 2001 (Figure 3.8).[29] Two ligands were synthesized, one containing glucose and the other 2-deoxyglucose, both connected via a linker at *C*-1 to an NO_2 tridentate binding sphere made up of a tertiary amine and two carboxylates. These ligands were complexed to both the rhenium and technetium tricarbonyl cores, and were found to quickly form stable complexes, as evidenced by the small amount of decomposition seen after incubation of the complexes in serum for 24 hr.[29] Detailed NMR spectral studies support the coordination of the ligand via the three intended donor atoms with the carbohydrate remaining pendant.[29] This was further verified by failed attempts to coordinate the sugars alone, where the same reaction conditions did not produce any stable compounds.[29]

References begin on Pg 106

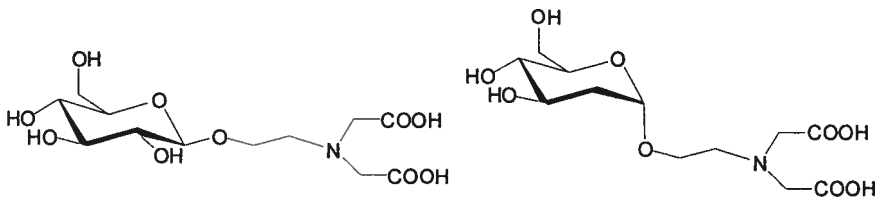

Figure 3.8 The two ligands used in the first organometallic carbohydrate containing complexes of group 7 metals.[29]

In 2005, Schibli and coworkers reported the synthesis of three tridentate ligands where the metal binding portion of the molecule was joined to the *C*-3 position of a glucose (Figure 3.9).[30] In each case there was a C_2 linker between the oxygen at the *C*-3 position and the metal binding sphere.[30] The donor atoms were made up of an alkyl amine in combination with aromatic nitrogens and/or carboxylic acids to give either an N_2O or an NO_2 binding sphere.[30] Interestingly, coordination to the rhenium tricarbonyl core proceeded extremely well for the NO_2, dianionic ligand (94 %), whereas only moderate yields were obtained with the two monoanionic ligands (54 – 57 %).[31] The opposite was observed on the tracer level, where reaction with ^{99m}Tc gave over 90 % for the monoanionic N_2O ligands and 78 % for the NO_2 ligand.[31]

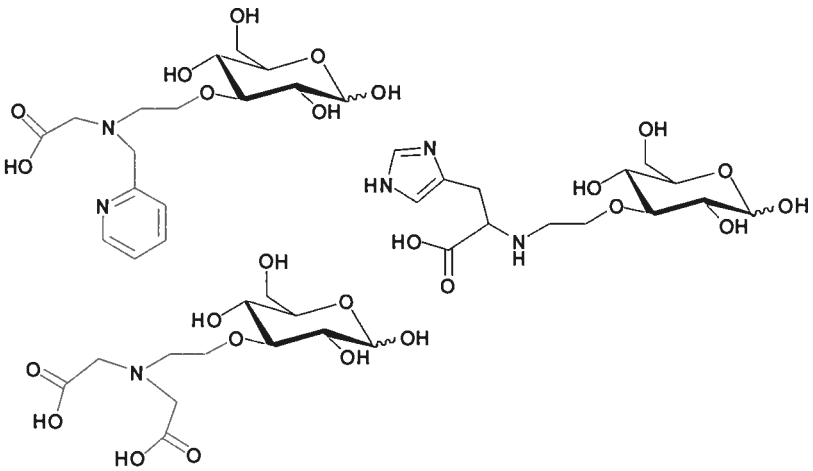

Figure 3.9 Glucose-based *C*-3 functionalized tridentate ligands for the technetium tricarbonyl core.[30]

A feasibility study of key *in vitro* tests of these *C*-1 and *C*-3 linked compounds (Figures 3.8 left and 3.9) with some previously synthesized *C*-2 and *C*-6 analogues[32] (see Figure 3.10)

References begin on Pg 106

was reported in 2005.[31] Labelling with ^{99m}Tc proceeded in good yields regardless of linker length or position of attachment to the glucose.[31] Complex stability was examined by incubation at 37 °C with excess cysteine or histidine.[31] A small amount of degradation (5–10 % after 24 hr) was observed with the aminodiacetate ligand sets, whereas the N_2O and N_3 binding groups showed no detectable exchange under the conditions tested.[31]

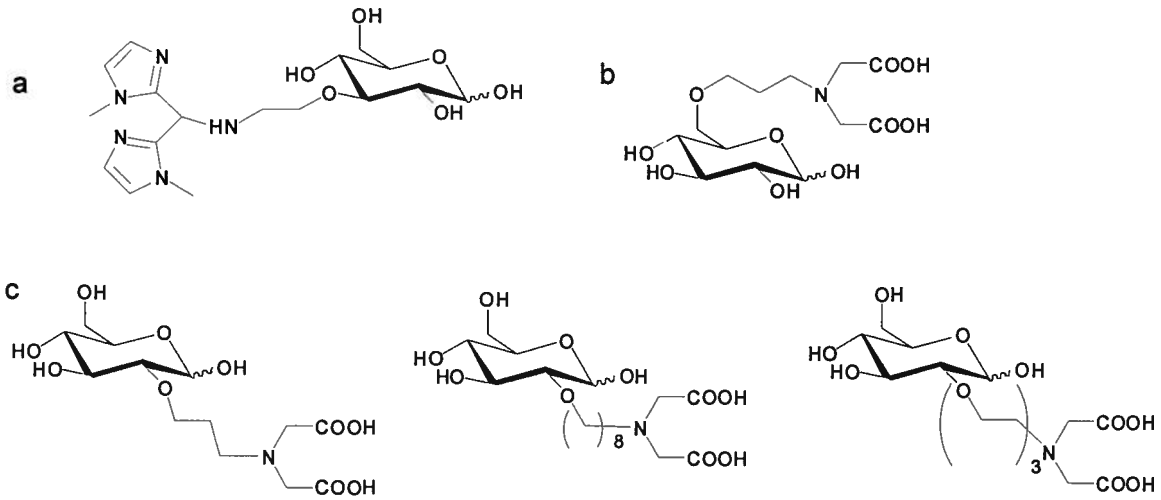

Figure 3.10 Some a) *C*-3 b) *C*-6 c) *C*-2 functionalized glucose-based tridentate ligands examined for binding to the $[^{99m}Tc(CO)_3]^+$ core and subjected to *in vitro* assays.[30, 31]

These nine ligands and their metal tricarbonyl complexes were subjected to a series of *in vitro* assays to examine their interactions with key enzymes in the uptake and metabolism of glucose[31] – vital interactions to maintain if these ^{99m}Tc compounds are to be useful as SPECT imaging agents. The ability of the compounds to inhibit the phosphorylation of glucose by hexokinase was examined, and two of the rhenium complexes were found to be millimolar inhibitors of this process (K_i = 0.25 – 5.8 mM).[31] Interestingly, the corresponding free ligands did not show any inhibitory character.[31] As was predicted by molecular docking studies where the size and shape of the active site cleft of hexokinase was modeled, the two species that showed HK activity were those with long alkyl chains linking the sugar and metal binding portions of the molecule (the latter two ligands shown in Figure 3.10c).[31] It is thought that this type of linker is thin enough to fit between the two domains of hexokinase while the bulky metal chelating portion is far enough removed that it can remain outside this cleft. Due to these promising results, the compounds were then examined to see if they were substrates for hexokinase, but none of them were - *i.e.* they were not themselves

References begin on Pg 106

phosphorylated.[31] Finally, the cellular uptake of the ^{99m}Tc complexes was examined in HT29 cells which are known to overexpress the GLUT-1 glucose transporter.[31] Small amounts of some complexes were found to get into the cells;[31] however, these amounts were low, and they were neither dose dependent nor affected by the addition of cytochalasin B, a known GLUT-1 inhibitor.[33] These observations, combined with the fact that the highest uptake was observed for the most lipophilic compound (using the ligand shown in Figure 3.10a), led to the conclusion that the uptake observed was from unspecific passive diffusion rather than GLUT facilitated transport.[31]

Meanwhile, the Orvig group had started working on a set of carbohydrate-pendant ligands where the metal binding portion was a dipicolylamine entity.[34] This provides an N_3 binding sphere consisting of one tertiary amine and two aromatic amines. Four compounds were investigated: a glucose (Figure 3.11a), xylose (Figure 3.11b) and mannose (Figure 3.11c) sugar linked via an ethylene spacer to the metal binding moiety at *C*-1,[35] and a glucosamine linked via a glycine to the nitrogen at the *C*-2 position (Figure 3.11d).[36]

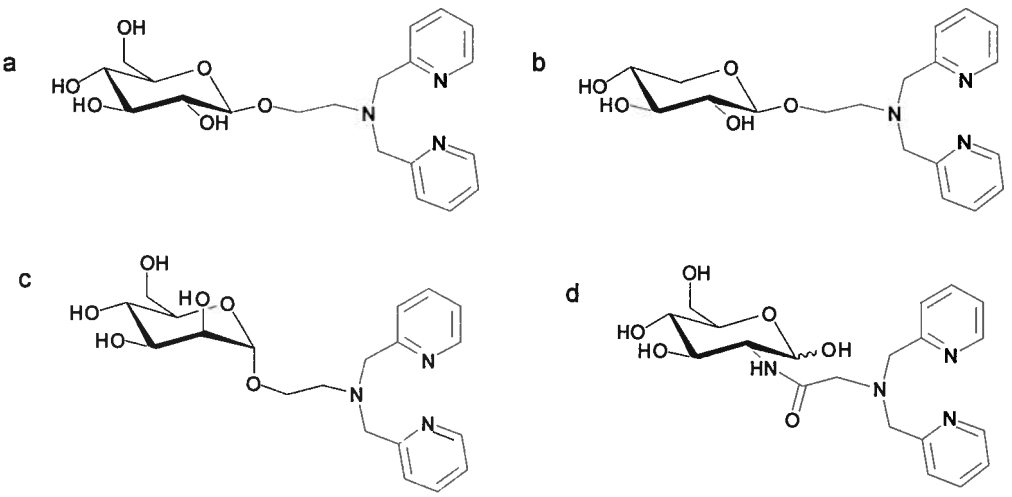

Figure 3.11 Dipicolylamine tridentate ligands for binding to the rhenium and technetium tricarbonyl cores:[34-36] carbohydrate = a) glucose b) xylose c) mannose d) glucosamine.

The expected pendant nature of the carbohydrate was confirmed in each case by ^{1}H NMR spectroscopy of the rhenium complexes in solution, and crystallographic analysis of the glucose rhenium complex in the solid state.[35] These ligands all reacted quantitatively with the $[^{99m}Tc(CO)_3]^+$ core, and the resulting complexes were at least 94 % stable in 100-fold

References begin on Pg 106

excess of cysteine or histidine after incubation for 24 hr.[35] Biodistribution of these and similar complexes in tumor-bearing mice suggest that they are not taken up into cells and/or not phosphorylated by hexokinase.[37] This is deduced by the fact that the washout rates of the tumors parallel those of blood; they decrease at similar rates over time. This suggests that the observed increase in activity of the tumors over the background tissue is perhaps due to increased vasculature that is known to occur in tumors.[37]

Recently, Zubieta and coworkers have reported carbohydrate conjugates that utilize fluorescent quinolinoyl moieties as metal binding agents for the tricarbonyl cores (Figure 3.12).[38] These ligands consist of glucosamine (with either free or acetyl protected hydroxyl groups) conjugated to *C*-2 via a linker (of varying length) leading to an N_3 tridentate binding core made up of one tertiary amine and two aromatic amines that are part of the fluorescent quinolinoyl groups.[38] The idea behind this ligand set is that it could be bound to $[^{99m}Tc(CO)_3]^+$ to form a complex suitable for SPECT imaging, and also bound to $[Re(CO)_3]^+$ to give a complex suitable for fluorescence imaging – useful for *in vitro* testing of cellular uptake and visualizing areas of localization within cells.[38] Although ^{99m}Tc binding was not reported,[38] the binding to rhenium proceeded in good yield, so it is likely the same will be observed on the tracer level.

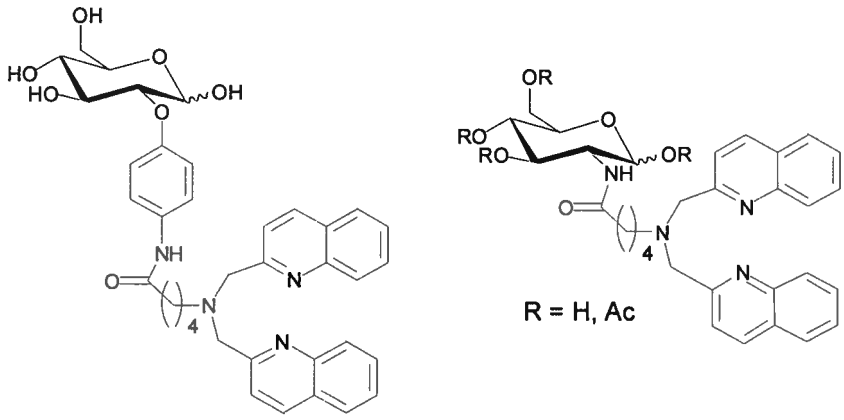

Figure 3.12 Fluorescent glucosamine conjugates for the tricarbonyl core.[38]

Schibli and coworkers recently developed an elegant method for forming tridentate chelates for the $[M(CO)_3]^+$ core using "click chemistry".[39] This approach was applied to a galactose analogue as well as to examples of the other major classes of biologically relevant molecules

References begin on Pg 106

as proof of principle.[39] 1-Azido-1-deoxy-β-D-galactopyranose was reacted with L-propargyl glycine in the presence of $Cu(OAc)_2$ and sodium ascorbate at 100 °C for 30 min to give a quantitative yield of the expected triazole (Scheme 3.1).[39] This reaction proceeds without the need for protecting groups, and forms an N_2O tridentate binding sphere comprised of a nitrogen from the newly formed triazole ring, and a primary amine and carboxylic acid that were part of the original glycine starting material.[39] This compound was found to bind to both the rhenium and technetium tricarbonyl cores in excellent yields.[39] Importantly, neither the glycine nor the carbohydrate precursors produced any kind of stable complex with ^{99m}Tc alone.[39] This allowed for the development of a one pot synthesis wherein the reagents necessary for the ligand formation via click chemistry were heated together for 30 min; the $[^{99m}Tc(CO)_3(H_2O)_3]^+$ precursor was then added into the reaction mixture and, following an additional 30 min of heating, the desired complex was determined to have been produced in very high radiochemical yield.[39] The bombesin analog – the bombesin oligopeptide replaces the galactose but the metal chelating portion of the molecule remains unchanged – was assessed for *in vivo* and *in vitro* stability, and both of these were found to be very high.[39] This is an exciting new development with a myriad of possibilities for future developments in radiopharmaceuticals, where fast and efficient synthesis is crucial.

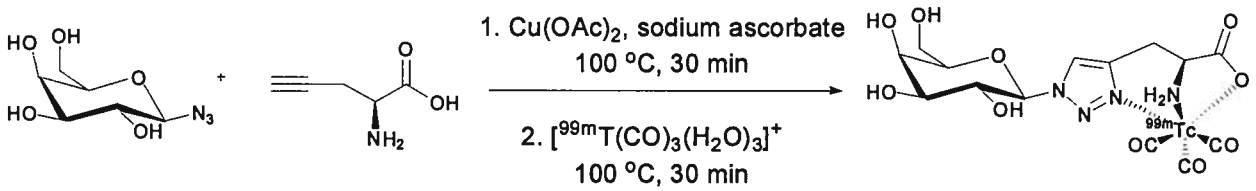

Scheme 3.1 "Click to chelate" – a fast and efficient synthesis of a galactose-appended tridentate ligand suitable for binding to the Re and ^{99m}Tc tricarbonyl cores.[39]

Although there has been significant work performed with the aim of making a ^{99m}Tc carbohydrate-based imaging agent, to date none of these efforts have been successful. The above work has pointed out the neccessity of a tridentate binding group and nitrogenous donors for complex stability. From previous work in the Orvig group it is known that monocationic compounds of this type give biodistributions characteristic of charged rather than sugar-type species,[37] so this work focuses on monoanionic ligands to provide neutral metal complexes. Other studies in the Orvig group have shown the utility of using a phenolate as an anionic donor group for the tricarbonyl core, as this results in stable

References begin on Pg 106

complexes, while increasing the lipophilicty compared to the commonly used acid group.[27] The work in this chapter aims to combine these factors by examining various combinations of binding groups that result in monoanionic, tridentate ligands. The resulting rhenium and technetium-99m tricarbonyl complexes are tested in appropriate assays to assess their potential as molecular imaging agents.

3.2 Experimental

3.2.1 Instruments and Materials

All solvents and chemicals were reagent grade and used as received unless specified otherwise. Reagents were purchased from Acros unless otherwise stated. Salicylaldehyde was purchased from Alfa Aesar. Sodium borohydride was purchased from Fisher Scientific. $Pd(OH)_2$ (20 % on carbon), 1-methyl-2-imidazolecarboxaldehyde and 2-pyridinecarboxaldehyde were purchased from Aldrich. Glucose (hexokinase) assay kits, glucose standard solution and hexokinase were obtained from Aldrich. $Re(CO)_5Br$ is commercially available (STREM). $[Re(CO)_3(H_2O)_3]Br$,[40] *N,N*-dibenzylglycine,[41] and 1,3,4,6-tetra-*O*-acetyl-β-D-glucosamine.HCl[42] were prepared as previously described. Solvents were HPLC grade, and were purchased from Fisher Scientific. Ethanol was dried over activated 4Å molecular sieves for at least 48 hours prior to use. Hydrogen and argon were purchased from Praxair. Isolink™ kits were provided by Mallinckrodt Inc. (now Covidien). $Na^{99m}TcO_4$ was provided by the Nuclear Medicine Department at the University of British Columbia Hospital. **HL^3** and **ReL^3** were first made by Mr. Chuck Ewart,[43] **HL^4** and **ReL^4** were made by Dr. Neil Lim.[44] Compound numbers refer to Figure 3.13 on page 89.

The analytical TLC plates, which were aluminum backed ultra pure silica gel 60, 250 μm, and the flash column silica gel (standard grade, 60 Å, 32-63 mm) used were provided by Silicycle. ^1H and ^{13}C NMR, ^{13}C NMR APT, 2D ^1H-^1H COSY and ^1H-^{13}C HMQC spectra were recorded on Bruker AV400 or DRX400 instruments at ambient temperature. The NMR spectra are expressed on the δ scale and were referenced to the residual peaks of the deuterated solvent. Infrared spectra were recorded on a Nicolet 6700 FT-IR (Fourier transform infrared) spectrophotometer in transmission mode between 400 and 4000 cm^{-1} at a resolution of ± 0.09 cm^{-1}. ESI mass spectra were recorded on a Micromass LCT instrument.

References begin on Pg 106

High resolution mass spectra (Micromass LCT TOF-MS) and elemental analysis (Carlo Erba EA 1108 Elemental Analyzer) were provided by the Analytical Services Facility, Department of Chemistry, University of British Columbia. HPLC analysis of non-radioactive compounds was done on a Phenomenex Synergi 4 μm Hydro-RP 80Å column (250 x 4.6 mm) in a Waters WE 600 HPLC system equipped with a 2478 dual wavelength absorbance UV detector run using the Empower software package. HPLC analyses of radiolabelled complexes were performed on a Knauer Wellchrom K-1001 HPLC equipped with a K-2501 absorption detector and a Capintec radiometric well counter. A Phenomenex Hydro-Synergi 4 μm C18 RP analytical column with dimensions of 250 x 4.6 mm was used.

3.2.2 Synthesis

2-((*N, N*-Dibenzylamino)acetamido)-2-deoxy-*D*-glucopyranose (2)

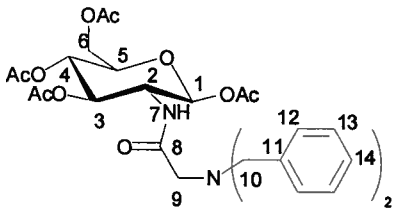

The synthesis of this compound was improved from that reported previously.[43] *N, N*-dibenzylglycine (10.7 g, 0.0421 mol) was dissolved in hot dimethylformamide (150 mL), and the resulting solution cooled on ice. 1-Ethyl-3-(3-dimethylaminopropyl) carbodiimide hydrochloride (EDC) (8.07 g, 0.0421 mol) and 4-dimethylaminopyridine (DMAP) (0.514 g, 4.21 mmol) were added; the solution was purged with argon, and stirred for one hour. Meanwhile, 1,3,4,6-tetra-*O*-acetyl-β-D-glucosamine.HCl (**1**) (18.0 g, 0.0468 mol) was stirred vigorously with 1 M Na_2CO_3 solution (250 mL) and dichloromethane (200 mL) for 30 min. The organic layer was separated and the aqueous layer washed with two further portions of dichloromethane (100 mL). The organic extracts were combined, dried over $MgSO_4$, filtered and reduced on a rotary evaporator to give the free amine which was added to the dimethylformamide solution and the reaction mixture was stirred under inert atmosphere at room temperature for 16 hr. The dimethylformamide was removed on a rotary evaporator to give a very thick off-white oil which was taken up in dichloromethane and washed sequentially with saturated Na_2CO_3 solution, 1 M HCl solution, water, and then brine. It was then dried over $MgSO_4$, filtered and reduced on a rotary evaporator to an off white solid. This solid was dissolved in a minimum amount of warm dichloromethane, and precipitated by addition of ethyl acetate (200 mL). Filtration and washing with cold ethyl acetate gave a pure white solid (14.3 g, 52 % yield). ^{1}H NMR (DMSO-d_6, 400 MHz, δ): 7.53 (m, 4H, *H12*), 7.43 (m, 6H, *H13,14*), 5.85

References begin on Pg 106

(s, 1H, *H1*), 5.33 (s, 1H, *H3*), 4.90 (dd, $^3J_{4,3}$ = 10.0 Hz, $^3J_{4,5}$ = 9.6 Hz, 1H, *H4*), 4.19 (dd, $^3J_{6a,5}$ = 4.8 Hz, $^3J_{6a,6b}$ = 7.8 Hz, 1H, *H6a*), 4.08 (m, 1H, *H5*), 4.00 (m, 4H, *H2,6b,9*), 3.54 (s, 4H, *H10*), 2.00, 1.97, 1.97, 1.86 (s, 3H, OCOCH_3).

2-(2-Aminoacetamido)-2-deoxy-1,3,4,6-tetra-*O*-acetyl-β-*D*-glucopyranose acetate salt (3)

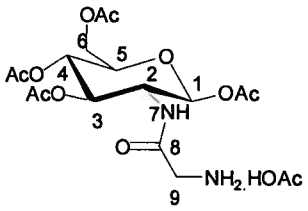

This was made by a similar, or improved method to that reported previously.[43] Larger scale reactions were done as outlined here, and smaller scale reactions could be done in much shorter reaction times (2 hr) under 200 psi of H_2 in a Parr hydrogenation bomb. Briefly, 2-((*N*, *N*-dibenzylamino)acetamido)-2-deoxy-*D*-glucopyranose (**2**) (2.36 g, 4.04 mmol) was dissolved in glacial acetic acid (30 mL); $Pd(OH)_2$ on carbon (20 %) (0.500 g, 0.714 mmol) was added, and the flask evacuated and filled with H_2. The reaction was stirred at room temperature under a positive H_2 pressure from a balloon for 12 – 20 hr. The reaction was monitored by TLC, and once the absence of both mono and dibenzylated materials was confirmed, the mixture was filtered through a celite plug, evacuated on a rotary evaporator to give a pale orange oil and analysed using ^{1}H NMR spectroscopy. The ^{1}H NMR spectrum was used in each case to quantify the amount of acetic acid associated with the product both for calculating yield and ensuring addition of sufficient base to neutralise all the acid in subsequent reactions. The crude reaction mixture was used as is in the next step (3.45 mmol, 85 % yield by ^{1}H NMR). ^{1}H NMR ($CDCl_3$, 400 MHz, δ): 6.00 (d, $^3J_{2,1}$ = 9.4 Hz, 1H, *H7*), 5.67 (d, $^3J_{1,2}$ = 8.8 Hz, 1H, *H1*), 5.15 (dd, $^3J_{3,2}$ = 10.4 Hz, $^3J_{3,4}$ = 9.6 Hz, 1H, *H3*), 5.07 (d, $^3J_{4,3}$ = 9.6 Hz, $^3J_{4,5}$ = 9.6 Hz, 1H, *H4*), 4.22 (m, 2H, *H2,6a*), 4.08 (dd, $^3J_{6b,5}$ = 2.1 Hz, $^3J_{6a,6b}$ = 12.5 Hz, 1H, *H6b*), 3.81 (dd, $^3J_{5,6a}$ = 4.6 Hz, $^3J_{5,6b}$ = 2.2 Hz, $^3J_{5,4}$ = 9.8 Hz, 1H, *H5*), 2.06 (s, 2H, *H9*), 2.03, 2.00, 1.99, 1.88 (s, 3H, OCOCH_3).

2-((*N*-(Pyridin-2-ylmethyl)amino)acetamido)- 2-deoxy-1,3,4,6-tetra-*O*-acetyl-β-*D*-glucopyranose (4)

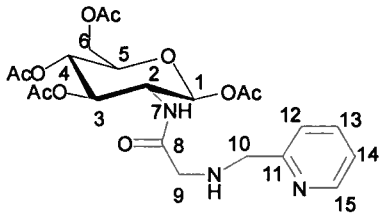

The synthesis of this compound was improved from that described previously.[43] 2-(2-Aminoacetamido)-2-deoxy-1,3,4,6-tetra-*O*-acetyl-β-*D*-glucopyranose acetate salt (**3**) (5.04 mmol) was dissolved in dry ethanol (30 mL), and an appropriate amount of sodium carbonate (to be in excess of the acetic acid present in the starting material) was added (3.73 g, 40.0 mmol). After stirring for

References begin on Pg 106

ten minutes to ensure all the acid was quenched, 2-pyridine-carboxaldehyde (478 μL, 5.00 mmol) was added to the reaction mixture. A very fast colour change to purple indicated a nearly instantaneous reaction, and within ten minutes the reaction was complete as verified by TLC. At this time, sodium borohydride (0.56 g, 15.0 mmol) was added and the reaction mixture stirred for ten minutes longer, as the purple colour faded. The reaction mixture was quenched with water, which also served to dissolve the excess sodium carbonate. The resulting mixture was extracted three times with dichloromethane; the organic fractions were combined and washed once with water, once with brine, then dried over magnesium sulfate before being filtered and reduced to a yellow oil on the rotary evaporator. This oil was purified using column chromatography (2 % methanol in dichloromethane) and the solvents removed *in vacuo* to give a white solid (1.31 g, 52 % yield). ^{1}H NMR (DMSO-d_6, 400 MHz, δ): 8.50 (d, $^3J_{7,2}$ = 4.3 Hz, 1H, *H7*), 8.09 (d, $^3J_{15,14}$ = 9.8 Hz, 1H, *H15*), 7.75 (ddd, $^3J_{13,12}$ = 7.5 Hz, $^3J_{13,14}$ = 7.6 Hz, $^4J_{13,15}$ = 1.8 Hz, 1H, *H13*), 7.38 (d, $^3J_{12,13}$ = 7.5 Hz, 1H, *H12*), 7.25 (m, 1H, *H14*), 5.88 (d, $^3J_{1,2}$ = 8.8 Hz, 1H, *H1*), 5.36 (dd, $^3J_{3,2}$ = 10.4 Hz, $^3J_{3,4}$ = 9.6 Hz, 1H, *H3*), 4.90 (dd, $^3J_{4,3}$ = 9.7 Hz, $^3J_{4,5}$ = 9.8 Hz, 1H, *H4*), 4.19 (dd, $^3J_{6a,5}$ = 4.8 Hz, $^3J_{6a,6b}$ = 12.9 Hz, 1H, *H6a*), 4.01 (m, 3H, *H2,5,6b*), 3.67 (s, 2H, *H10*), 3.11 (s, 2H, *H9*), 2.03, 2.01, 1.98, 1.92 (s, 3H, OCOCH_3).

2-((*N*-(Pyridin-2-ylmethyl)-*N*-(methoxyethanoic acid)amino)acetamido)-2-deoxy-1,3,4,6-tetra-*O*-acetyl-β-*D*-glucopyranose (5)

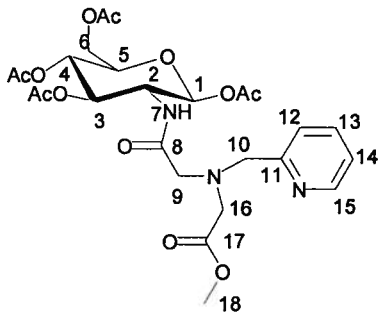

2-((*N*-(Pyridin-2-ylmethyl)amino)acetamido)-2-deoxy-1,3,4,6-tetra-*O*-acetyl-β-*D*-glucopyranose (**4**) (0.950 g, 1.92 mmol) was dissolved in dry dichloromethane (15 mL). Na_2CO_3 (0.406 g, 3.84 mmol) and methyl bromoacetate (0.241 mL, 2.88 mmol) were added. The flask was evacuated and filled with argon, and the reaction mixture stirred at room temperature for 48 hr. Water was added, the two layers were separated, and the organic layer was washed again with water, and once with brine, before being dried over $MgSO_4$. The drying agent was filtered off; the filtrate was evaporated on a rotary evaporator, and then purified by column chromatography on silica gel with 5 % methanol in dichloromethane as eluent. The solvents were removed *in vacuo* to give an off white solid (0.790 g, 72 % yield). ^{1}H NMR ($CDCl_3$, 400 MHz, δ): 8.98 (d, $^3J_{7,2}$ = 9.4 Hz, 1H, *H7*), 8.60 (d, $^3J_{15,14}$ = 4.5 Hz, 1H, *H15*), 7.67 (ddd, $^3J_{13,12}$ = 7.7 Hz, $^3J_{13,14}$ = 7.6 Hz, $^4J_{13,15}$ = 1.7 Hz, 1H, *H13*), 7.23 (m, 2H, *H12,14*), 5.84 (d, $^3J_{1,2}$ = 8.8 Hz, 1H, *H1*), 5.31 (dd, $^3J_{3,2}$

References begin on Pg 106

= 10.2 Hz, $^3J_{3,4}$ = 9.5 Hz, 1H, *H3*), 5.13 (dd, $^3J_{4,3}$ = 9.6 Hz, $^3J_{4,5}$ = 9.8 Hz, 1H, *H4*), 4.30 (m, 2H, *H2,6a*), 4.13 (dd, $^3J_{6b,5}$ = 2.0 Hz, $^3J_{6a,6b}$ = 12.4 Hz, 1H, *H6b*), 3.88 (m, 3H, *H5,10*), 3.71 (s, 3H, *H18*), 3.40 (d, $^3J_{16a,b}$ = 3.1 Hz, 2H, *H16*), 3.31 (s, 2H, *H9*), 2.09, 2.02, 1.99, 1.94 (s, 3H, OCOC*H*$_3$). ^{13}C NMR ($CDCl_3$, 100 MHz, δ): 171.90, 171.87, 170.89, 170.55, 169.59, 169.34 (O*C*OCH3, *C8,17*), 157.77 (*C11*), 149.87 (*C15*), 137.08 (*C13*), 123.34 (*C12*), 123.00 (*C14*), 92.62 (*C1*), 73.12 (*C3*), 72.93 (*C5*), 68.43 (*C4*), 61.91 (*C6*), 59.60 (*C10*), 58.64 (*C16*), 54.76 (*C9*), 52.76 (*C2*), 51.99 (*C18*), 20.96, 20.93, 20.80, 20.78 (OCO*C*H$_3$). IR ν_{max} (cm^{-1}): 3321 (w), 2958 (w), 1744 (s), 1663 (m), 1508 (m), 1390 (m), 1218 (s), 1038 (m). HR-MS (ES+ of MNa$^+$): m/z calcd for $C_{25}H_{33}N_3O_{12}Na$: 590.1962, found: 590.1948.

2-((*N*-(Pyridin-2-ylmethyl)-*N*-(ethanoic acid)amino)acetamido)-2-deoxy-*D*-glucopyranose (HL^1)

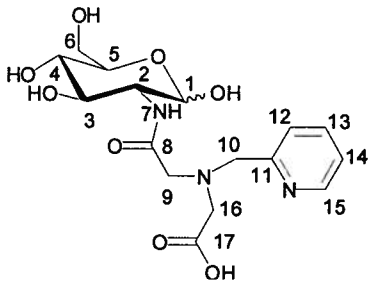

2-((*N*-(Pyridin-2-ylmethyl)-*N*-(methoxyethanoic acid) amino) acetamido)-1,3,4,6-tetraacetyl-2-deoxy-*D*-glucopyranose (**5**) (40 mg, 0.071 mmol) was suspended in 1 M NaOH (2 mL) and stirred vigorously. After about 5 min the solution became homogenous and slightly yellow. The reaction was complete according to ESI-MS after about 60 min. Amberlite CG-50 ion exchange resin was added and the resulting slurry stirred vigorously for 15 min, before the resin was filtered off. The aqueous filtrate was reduced to a yellow solid on the rotary evaporator before being taken up in a minimum amount of methanol and filtered to remove most of the NaOH. The methanolic solution was then purified by reverse phase HPLC, and the solvents removed *in vacuo* to give a pale orange oil (15 mg, 55 % yield). ^{1}H NMR (MeOH-d_4, 400 MHz, δ): 8.79 (s, 1H, *H15*), 8.41 (dd, $^3J_{13,12}$ = 7.4 Hz, $^3J_{13,14}$ = 7.0 Hz, 1H, *H13*), 7.93 (m, 1H, *H12*), 7.86 (m, 1H, *H14*), 5.10 (d, $^3J_{1,2}$ = 3.1 Hz, 0.75H, *H1α*), 4.66 (d, $^3J_{1,2}$ = 8.2 Hz, 0.25H, *H1β*), 4.41 (d, $^3J_{10a,10b}$ = 4.7 Hz, 2H, *H10*), 4.30, 4.02, 3.66 – 3.90, 3.50 – 3.64, 3.34 – 3.42 (*m, C2-6, 9,16α and β*). ^{13}C NMR (MeOH-d_4, 100 MHz, δ): 173.79, 172.72 (*C17*), 162.63, 162.29 (*C8*), 156.53 (*C11*), 145.78, 145.66 (*C13*), 143.35 (*C15*), 126.71 (*C12*), 126.22 (*C14*), 96.40, 94.27, 92.10 (*C1*), 77.58, 75.38, 73.16, 72.76, 72.26, 71.95, 71.71, 68.21 (*C3,4,5*), 62.28, 61.88, 58.31 (*C9,10,16*), 58.23, 55.48 (*C2*), 57.31, 57.17 (*C6*). IR ν_{max} (cm^{-1}): 3272 (s, br), 2918 (m), 1667 (s, br), 1538 (m), 1417 (w), 1188 (s), 1031 (s). HR-MS (ES+ of MNa$^+$): m/z calcd for $C_{16}H_{23}N_3O_8Na$: 408.1383, found: 408.1388.

References begin on Pg 106

(2-((*N*-(Pyridin-2-ylmethyl)-*N*-(ethanoic acid)amino)acetamido)-2-deoxy-*D*-glucopyranosyl)tricarbonylrhenium(I) (ReL^1)

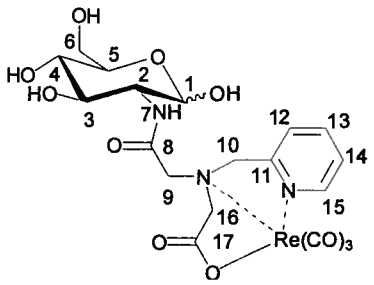

2-((*N*-(Pyridin-2-ylmethyl)-*N*-(ethanoic acid)amino)acetamido)-2-deoxy-*D*-glucopyranose (**HL^1**) (0.044 g, 0.11 mmol) and $[Re(H_2O)_3(CO)_3]Br$ (0.046 g, 0.11 mmol) were refluxed in methanol (5 mL) for 2 hr. After cooling to room temperature, the complex was purified by semi-preparative HPLC, and the solvents removed on a rotary evaporator to give a clear oil (0.049 g, 66 % yield). ^{1}H NMR (MeOH-d_4, 400 MHz, δ): 8.81 (d, $^3J_{15,14}$ = 5.4 Hz, 1H, *H15*), 8.09 (dd, $^3J_{13,14}$ = 7.8 Hz, $^3J_{13,12}$ = 7.8 Hz, 1H, *H13*), 7.73 (d, $^3J_{12,13}$ = 7.6 Hz, 1H, *H12*), 7.55 (dd, $^3J_{14,13}$ = 7.40 Hz, $^3J_{14,15}$ = 5.8 Hz, 1H, *H14*), 5.16 – 5.33, 4.34 – 4.70, 4.06 – 4.12, 3.65 – 3.91, 3.25 – 3.53 (*m, C1-6,8-10,16α and β*). ^{13}C NMR (MeOH-d_4, 100 MHz, δ): 197.8, 197.0, 196.4 (Re-*C*O), 183.6, 180.5 (*C8*), 168.4 (*C17*), 159.8, 159.6 (*C11*), 152.2 (*C15*), 140.4 (*C13*), 125.8 (*C12*), 123.9 (*C14*), 95.7, 93.7, 91.3 (*C1*), 76.9, 74.8, 72.1, 71.9, 71.3, 70.9 (*C3,4,5*), 69.4, 69.2, 69.1, 69.0, 68.8, 68.7 (*C9,10,16*) 61.5, 60.9 (*C6*), 57.1, 54.4 (*C2*). IR ν_{max} (cm^{-1}): 3292 (w, br), 2360 (m), 2341 (m), 2027 (m), 2015 (s), 1910 (s), 1863 (s), 1635 (m, br), 774 (m). HR-MS (ES+ of MNa^+): m/z calcd for $C_{19}H_{22}N_3O_{11}{}^{187}ReNa$: 678.0710, found: 678.0704.

2-((*N*-(1-Methylimidazol-2-ylmethyl)amino)acetamido)-2-deoxy-1,3,4,6-tetra-*O*-acetyl-β-*D*-glucopyranose (6)

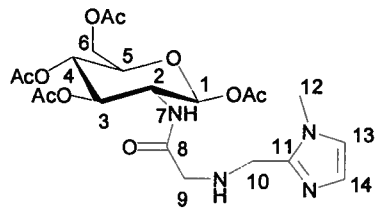

2-(2-Aminoacetamido)-2-deoxy-1,3,4,6-tetra-*O*-acetyl-β-*D*-glucopyranose (**3**) (6.52 mmol) was dissolved in dry ethanol (20 mL), and an appropriate amount of sodium carbonate was added to neutralise the associated acetic acid, as determined by ^{1}H NMR spectroscopy of starting material (4.60 g, 43.4 mmol). After stirring for ten minutes to ensure all the acid was quenched, 1-methylimidazole-2-carboxaldehyde (0.770 g, 6.99 mmol) was added to the reaction. A nearly immediate colour change to green was observed, and within ten minutes the reaction was complete, as tested by TLC. Sodium borohydride (0.780 g, 21.1 mmol) was added and the reaction mixture stirred for ten minutes longer, as the green colour faded. The reaction mixture was quenched with water (30 mL), which also dissolved the excess sodium carbonate. The solution was extracted three times with dichloromethane (3 x 30 mL), the organic fractions were

References begin on Pg 106

combined and washed once with water (30 mL), once with brine (30 mL), then dried over magnesium sulfate before being filtered and reduced to an oil on the rotary evaporator. This oil was purified using column chromatography (5 % methanol in dichloromethane) and the solvents evaporated *in vacuo* to give an off white solid (0.81 g, 25 % yield). ^{1}H NMR (MeOH-d_4, 400 MHz, δ): 7.67 (d, $^3J_{7,2}$ = 9.0 Hz, 1H, *H7*),6.95 (s, 2H, *H15*), 6.84 (s, 2H, *H14*), 5.80 (d, $^3J_{1,2}$ = 8.7 Hz, 1H, *H1*), 5.24 (dd, $^3J_{3,2}$ = 9.4 Hz, $^3J_{3,4}$ = 10.2 Hz, 1H, *H3*), 5.13 (dd, $^3J_{4,3}$ = 9.4 Hz, $^3J_{4,5}$ = 9.7 Hz, 1H, *H4*), 4.27 (m, 2H, *H2,6a*), 4.13 (dd, $^3J_{6b,5}$ = 2.2 Hz, $^3J_{6b,6a}$ = 12.4 Hz, 1H, *H6b*), 3.83 (ddd, $^3J_{5,4}$ = 9.8 Hz, $^3J_{5,6a}$ = 2.2 Hz, $^3J_{5,6b}$ = 4.7 Hz, 1H, *H5*), 3.77 (d, $^3J_{10a,10b}$ = 6.4 Hz, 2H, *H10*), 3.63 (s, 3H, *H13*), 3.29 (d, $^3J_{9a,9b}$ = 4.6 Hz, 2H, *H9*). ^{13}C NMR ($CDCl_3$, 100 MHz, δ): 171.76 (*C8*), 170.66, 169.32 (O*C*OCH$_3$), 144.21 (C*12*), 127.29 (*C14*), 121.31 (*C13*), 92.46 (*C1*), 72.81 (*C3*), 72.70 (*C5*), 67.89 (*C4*), 61.66 (*C6*), 52.73 (*C2*), 52.12 (*C9*), 44.98 (*C11*), 32.46 (*C15*), 20.90, 20.69, 20.56 (OCO*C*H$_3$). IR ν_{max} (cm^{-1}): 3324 (w), 2953 (w), 2360 (m), 2341 (m), 1743 (s), 1673 (m), 1519 (m), 1367 (m), 1214 (s), 1034 (s), 728 (m). HR-MS (ES+ of MNa$^+$): m/z calcd for $C_{21}H_{30}N_4O_{10}Na$: 521.1860, found: 521.1863.

2-((*N*-(1-Methylimidazol-2-ylmethyl)-*N*-(2-hydroxybenzyl)amino)acetamido)-2-deoxy-1,3,4,6-tetra-*O*-acetyl-β-*D*-glucopyranose (7)

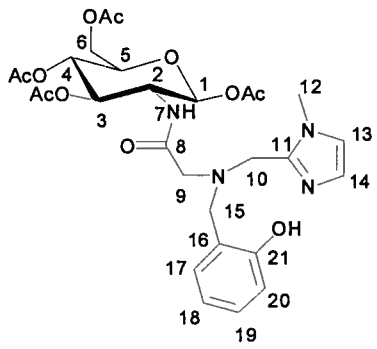

2-((*N*-(1-Methylimidazol-2-ylmethyl)amino)acetamido)-2-deoxy-*D*-glucopyranose (**6**) (0.800 g, 1.62 mmol) was dissolved in 1,2-dichloroethane (15 mL) and sodium carbonate (0.343 g, 3.24 mmol) was added. The reaction flask was purged for ten minutes with argon and salicylaldehyde (337 μL, 3.21 mmol) was added, and the reaction mixture stirred at room temperature for 30 min. Sodium triacetoxyborohydride (1.02 g, 4.83 mmol) was added and the reaction mixture stirred for 24 hr. Upon completion of the reaction, as determined by loss of starting materials by TLC, the solvent was removed by rotary evaporator and the off white solid partitioned between dichloromethane and water (20 mL each). The layers were separated and the aqueous layer washed twice with dichloromethane (20 mL), the two fractions of which were then combined. These were dried with brine (30 mL) then $MgSO_4$, filtered and reduced in volume on the rotary evaporator. The yellow solution was purified by column chromatography on silica gel using 4 % methanol in dichloromethane as an eluent, and the solvent was removed *in vacuo* to give an

References begin on Pg 106

off white solid (0.626 g, 64 % yield). ^{1}H NMR ($CDCl_3$, 400 MHz, δ): 7.97 (d, $^3J_{7,2}$ = 9.0 Hz, 1H, *H7*), 7.14 (ddd, $^3J_{19,18}$ = 7.2 Hz, $^3J_{19,20}$ = 8.2 Hz, $^4J_{19,17}$ = 1.5 Hz, 1H, *H19*), 7.07 (d, $^3J_{13,14}$ = 1.1 Hz, 1H, *H14*), 6.96 (dd, $^3J_{17,18}$ = 7.4 Hz, $^4J_{17,19}$ = 1.3 Hz, 1H, *H17*), 6.87 (s, 1H, *H13*), 6.85 (s, 1H, *H20*), 6.71 (dd, $^3J_{18,17}$ = 7.4 Hz, $^3J_{18,19}$ = 7.3 Hz, 1H, *H18*), 5.72 (d, $^3J_{1,2}$ = 8.4 Hz, 1H, *H1*), 5.10 (dd, $^3J_{3,2}$ = 9.6 Hz, $^3J_{3,4}$ = 9.9 Hz, 1H, *H3*), 5.00 (dd, $^3J_{4,3}$ = 9.8 Hz, $^3J_{4,5}$ = 9.4 Hz, 1H, *H4*), 4.23 (dd, $^3J_{6a,5}$ = 12.4 Hz, $^2J_{6a,6b}$ = 4.5 Hz, 1H, *H6a*), 4.02 (dd, $^3J_{6b,5}$ = 2.1 Hz, $^2J_{6a,6b}$ = 12.6 Hz, 1H, *H6b*), 3.96 (dd, $^3J_{2,3}$ = 9.4 Hz, $^3J_{2,7}$ = 9.6 Hz, 1H, *H2*), 3.84 (d, $^2J_{10a,10b}$ = 13.1 Hz, 1H, *H10*), 3.78 (ddd, $^3J_{5,6a}$ = 4.5 Hz, $^3J_{5,6b}$ = 2.0 Hz, $^3J_{5,4}$ = 9.9 Hz, 1H, *H5*), 3.67 (dd, $^2J_{15a,15b}$ = 15.6 Hz, $^2J_{15b,15a}$ = 14.1 Hz, 2H, *H15*), 3.62 (d, $^2J_{10b,10a}$ = 13.1 Hz, 1H, *H10*), 3.52 (s, 3H, *H12*), 3.18 (dd, $^2J_{9a,9b}$ = 16.7 Hz, $^2J_{9b,9a}$ = 10.6 Hz, 2H, *H9*), 2.03, 1.94, 1.85, 1.76 (s, 12H, OCO*CH*$_3$). ^{13}C NMR ($CDCl_3$, 100 MHz, δ): 171.71 (*C8*), 170.85, 170.26, 169.55, 169.04 (O*C*OCH$_3$), 157.42 (*C21*), 145.28 (*C11*), 131.14 (*C17*), 129.88 (*C19*), 125.93 (*C14*), 122.35 (*C16*), 121.82 (*C20*), 119.06 (*C18*), 117.85 (*C13*), 92.04 (*C1*), 72.84 (*C3*), 72.56 (*C5*), 68.27 (*C4*), 61.85 (*C6*), 56.57 (*C9*), 56.49 (*C10*), 53.24 (*C2*), 50.27 (*C15*), 32.70 (*C12*), 20.95, 20.87, 20.76, 20.68 (OCO*C*H$_3$). IR ν_{max} (cm^{-1}): 3274 (w), 1744 (s), 1674 (m), 1388 (m), 1211 (s), 1072 (m), 1035 (s), 760 (s). HR-MS (ES+ of MNa$^+$): m/z calcd for $C_{28}H_{36}N_4O_{11}Na$: 627.2278, found: 627.2288.

2-((*N*-(1-Methylimidazol-2-ylmethyl)-*N*-(2-hydroxybenzyl)amino)acetamido)-2-deoxy-*D*-glucopyranose (HL^2)

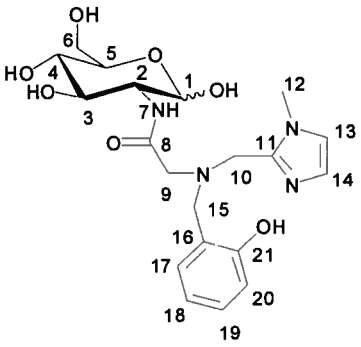

2-((*N*-(1-Methylimidazol-2-ylmethyl)-*N*-(2-hydroxybenzyl) amino) acetamido)-2-deoxy-1,3,4,6-tetraacetyl-*D*-glucopyranose (7) (0.225 g, 0.372 mmol) was dissolved in methanol (10 mL). An excess of NaOMe (0.110 g, 20.4 mmol) was added and the reaction mixture stirred at room temperature for two hours. Amberlite CG-50 ion exchange resin was added, and after ten min of rapid stirring, was removed by filtration. The filtrate was reduced in volume on a rotary evaporator, and the resulting yellow-orange oil purified by semi-prep HPLC. The solvents were removed *in vacuo* to give a pale yellow oil (0.040 g, 25 % yield). ^{1}H NMR (MeOD, 400 MHz, δ): 7.28 – 7.32 (m, 2H, *H20,14*), 7.18 – 7.20 (m, 1H, *H18*), 7.09 - 7.14 (m, 1H, *H17*), 6.76 – 6.82 (m, 2H, *H19,13*), 5.09 (d, $^3J_{1,2}$ = 3.4 Hz, 0.63H, *H1α*), 4.67 (d, $^3J_{1,2}$ = 8.3 Hz, 0.37H, *H1β*), 4.00 – 4.10 (m, 2H, *H10*), 3.79 – 3.95 (m, 4H, *α and β sugar protons*) 3.74 (s, 3H, *H12*), 3.72 (s, 2H, *H15*), 3.44 (s, 2H, *H9*)3.35 – 3.43 (m,

References begin on Pg 106

2H, *α and β sugar protons).* ^{13}C NMR (MeOD, 100 MHz, δ): 173.64, 173.24 (*C8*), 157.74, 157.59 (*C11*), 146.42 (*C21*), 133.31, 133.15 (*C18*), 131.20, 131.12 (*C17*), 125.48 (*C20*), 123.97 (*C16*), 121.25, 121.09 (*C19*), 119.65 (*C14*), 116.92 (*C13*), 97.23, 92.98 (*C1*), 78.49, 76.31, 73.54, 73.01, 72.93, 72.65 (*C3,4,5*), 63.20, 63.12 (*C6*), 59.96, 59.89 (*C9*), 58.88, 56.00 (*C2*), 57.61, 57.55 (*C15*), 49.50 (obscured by solvent peak – *C10*), 35.26, 35.18 (*C12*). IR ν_{max} (cm^{-1}): 3293 (s, br), 2942 (m, br), 1671 (s), 1609 (w), 1531 (m), 1459 (m), 1210 (s), 1133 (s), 757 (m). HR-MS (ES+ of MNa^+) *m/z* calcd for $C_{20}H_{28}N_4O_7Na$: 459.1856, found 459.1848.

(2-((*N*-(1-Methylimidazol-2-ylmethyl)-*N*-(2-hydroxybenzyl)amino)acetamido)-2-deoxy-*D*-glucopyranosyl)tricarbonylrhenium(I) (ReL^2)

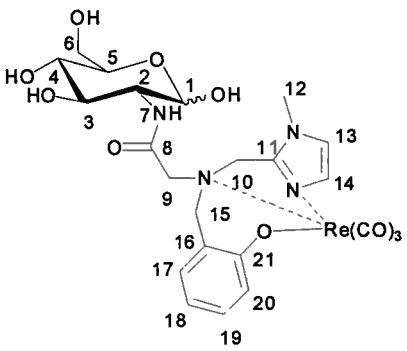

2-((*N*-(1-Methylimidazol-2-ylmethyl)-*N*-(2-hydroxybenzyl) amino)acetamido)-2-deoxy-*D*-glucopyranose (**HL_2**) (0.040 g, 0.92 mmol) was dissolved in methanol (5 mL), and $[Re(H_2O)_3(CO)_3]Br$ (0.036 g, 0.097 mmol) added. The reaction mixture was refluxed for 8 hr then the volume reduced on a rotary evaporoator before purification by semi-preparative HPLC, followed by removal of the solvents *in vacuo* to give a pale yellow oil (0.028 g, 43 % yield). ^{1}H NMR (MeOD, 400 MHz, δ): 7.53 (d, $^3J_{20,19}$ = 7.4 Hz, 1H, *H20*), 7.35 (dd, $^3J_{18,17}$ = 7.1 Hz, $^3J_{18,19}$ = 7.1 Hz, 1H, *H18*), 7.20 (d, $^3J_{17,18}$ = 5.8 Hz, 1H, *H17*), 7.14 (s, 1H, *H14*), 6.98 (m, 2H, *H13,19*), 5.10 (d, $^3J_{1,2}$ = 3.3 Hz, 0.45H, *H1α*), 4.40 (s, 0.55H, *H1β*), 4.66 – 4.95, 4.08 – 4.14, 3.64 – 3.81, 3.01 – 3.55, (m, 13H, *H2-6, 9,10,15α and β anomers*), 3.64 (s, 3H, *H12*). ^{13}C NMR (MeOD, 100 MHz, δ): 197.94, 197.44, 197.35, 196.55, 196.35 (*C*O), 181.29, 181.23 (*C8*), 158.24, 158.20 (*C11*), 152.17, 152.04 (*C16*), 135.03, 135.00 (*C20*), 133.00 (*C18*), 129.61 (*C14*), 125.88, 125.80 (*C17*), 121.49 (*C19*), 120.15, 120.01 (*C21*), 117.58 (*C13*), 96.19, 92.53, 91.99 (*C1*), 78.46, 75.69, 75.18, 73.51, 73.44, 72.36, 72.27, 72.13, 72.05 (*C3,4,5*), 68.18, 67.92 (*C15*), 65.29, 64.81, 64.43 (*C10*), 62.92, 62.74 (*C9*), 59.14, 58.95 (*C6*), 57.47, 57.42 (*C2*), 35.40, 35.28, 35.21 (*C12*). IR ν_{max} (cm^{-1}): 3232 (m, br), 2360 (w), 2028 (s), 1884 (s), 1672 (m), 1620 (s), 1198 (s), 1134 (s), 757 (m), 527 (s). HR-MS (ES+ of MH^+) *m/z* calcd for $C_{23}H_{28}N_4O_{10}{}^{187}Re$: 707.1363, found 707.1365.

References begin on Pg 106

3.2.3 ^{99m}Tc Complex Formation

$Na^{99m}TcO_4$ was obtained in saline solution from the UBC Hospital Department of Nuclear Medicine. It was added to an Isolink™ kit (Mallinckrodt) and the volume made up to 1 mL with 0.9 % saline solution. The resulting solution was heated at approx. 90 °C for 30 min. After cooling, the solution was neutralized with about 0.1 mL of 1 M HCl to pH 7 – 10 depending on the particular compound. Meanwhile, 10^{-4} M solutions of the ligands were prepared, and 0.5 mL of each was transferred to a reaction vial which was fitted with a septum and purged with N_2. Ligands containing a phenol as a chelating moiety were made up in ethanol and three equivalents of NaOEt were added to deprotonate the phenolate (0.15 mL of a 10^{-3} M solution in ethanol) prior to addition of $[^{99m}Tc(CO)_3(H_2O)_3]^+$. Ligands containing an acid chelating moiety were made up in aqueous PBS buffer (110 mM, pH 7.4, 0.9 % saline) and were used without the addition of base. Between 0.1 and 1 mL of the technetium Isolink™ reaction was added to each vial, and these were then heated between 70 – 80 °C for 30 min. The solutions were cooled then injected into the HPLC (with the corresponding cold standard rhenium complex) for analysis.

3.2.4 Cysteine and Histidine Challenges

The ^{99m}Tc complexes were synthesized as outlined above. Cysteine and histidine solutions were freshly made at 10^{-3} M in aqueous PBS buffer (110 mM, pH 7.4, 0.9 % saline). Cysteine or histidine solution (0.9 mL) was placed in a vial, and 0.1 mL of the technetium complex (in the reaction solution described above) was added to give a final volume of 1 mL with the concentration of competing amino acid one hundred times greater than that of the ligand used for making the technetium complex. The solution was incubated at 37 °C and aliquots removed at 1 hr, 4 hr and 24 hr for HPLC analysis. Each timepoint was done in triplicate from three separate incubation vials. The percentage of the initial complex remaining was examined, and the mean and standard deviation of three trials for each ligand with each of cysteine and histidine was calculated.

References begin on Pg 106

3.2.5 GLUT-1 Cell Uptake Studies

These experiments were conducted by me in the lab of Dr. Urs Häfeli in the UBC Faculty of Pharmaceutical Sciences. They were performed using LCC6-HER2 cells – a human breast cancer cell line chosen for its overexpression of the glucose transporter GLUT-1.[45] LCC6-HER2 cells were plated with Dulbecco's Modified Eagle Medium (D-MEM) (1X), liquid (high glucose) supplemented with 10 % Fetal Bovine Serum and 1 % Penicillin/Streptomycin. The cells were allowed to adhere at 37 °C in a humidified atmosphere containing 5 % CO_2. The plating was carried out in 75 cm^2 tissue culture flasks with 0.2 μm vented caps. The cultures were maintained in a humidified 5 % CO_2 atmosphere, with medium changes every alternate day. Subculturing was carried out every 3-4 days using Trypsin-EDTA (0.25 % Trypsin with Na_4EDTA) (1X) incubated for about 5 min at 37 °C for cell detachment. A hemacytometer was used for counting the cells to monitor cell proliferation.

On the experiment day, suspensions of cells with concentration $1x10^6$ cells/mL were prepared in 1 % PBS (pH 7.4). The suspension was aliquoted into 1.5 mL Eppendorf vials to get a final volume of 0.5 mL in each vial ($5x10^5$ cells). The compound to be tested was then added to the cells and the vial gently inverted. Each ^{99m}Tc complex (15 μCi) or ^{18}F-FDG (30 μCi) was used in 500 μL PBS solution. Each compound was added to the cells in glucose-free conditions, and in a final concentration of 5 mM D-glucose. The resulting suspensions were incubated at 37 °C for 30 min with shaking at 400 RPM. Following incubation, the vials were centrifuged at 1100 RPM for 5 min then 900 μL of the supernatant was removed. Cold PBS solution (900 μL) was added, and gentle mixing of the cells into the solution was achieved by gentle uptake and release of the solution from the pipette tip three times. This centrifuging and washing procedure was repeated four times in total to give the original supernatant and three washing supernatants. Finally the cells were vortexed in cold PBS (1 mL) to remove them from the vial wall and transferred to a tube for gamma counting. The activity in each cell sample was divided by the sum of all the supernatants for that sample to give a percentage of the original amount of activity that ended up associated with the cells. All experiments were carried out in quadruplicate. FDG was used as a positive control, and was repeated each day that these experiments were carried out to ensure experimental integrity.

References begin on Pg 106

3.2.6 Hexokinase Phosphorylation Studies

A 5 mM aqueous solution of test compound (100 μL) was added to a reaction vial such that a final concentration of 0.5 mM test compound, 10 U/mL hexokinase, 1 mM ATP, 4 mM $MgCl_2$ in a 30 mM TEOA (triethanolamine, pH = 6) buffer was achieved. The resulting solution was mixed gently by inverting each vial three times, and then incubated for 16 hr at 37 °C. Each solution (20 μL) was analysed by HPLC to determine whether any of the ATP had been converted to ADP, as would accompany the phosphorylation of a substrate. Using a Phenomenex Synergi 4 μm Hydro-RP 80 Å column (250 x 4.6 mm) and eluting with 30 mM KH_2PO_4, the retention time of ATP is 8.5 min, whereas that of ADP is 12.5 min.

3.3 Results and Discussion

3.3.1 Synthesis, Characterisation and Complex Stability

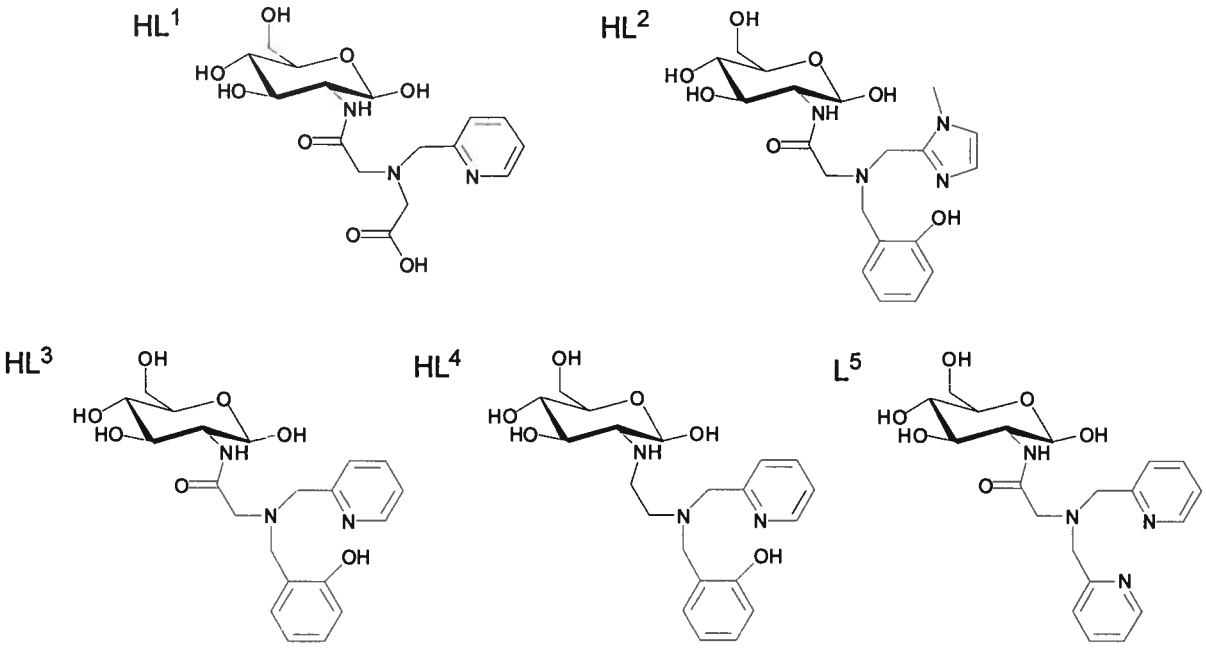

Figure 3.13 Compounds made and studied in this chapter. **HL**[3] and **HL**[4] were first made by Mr. Chuck Ewart,[43] and Dr. Neil Lim,[44] respectively, and both syntheses were subsequently improved and finalised by myself. **L**[5] was supplied by Dr. Tim Storr.[36]

References begin on Pg 106

The acetylated glucosamine starting material **1** was made in four steps from commercially available glucosamine, and could be obtained on a relatively large scale in moderate to good yields.[42] Dibenzylglycine was prepared from commercially available glycine in one step by an S_N2 reaction with benzylbromide in the presence of base, followed by precipitation.[41] The amide coupling of these two protected compounds to give **2** was initially performed by Chuck Ewart,[43] and subsequently investigated and optimized by myself (Scheme 3.2). A number of different coupling agents were tried and none were found to work better than EDC, so the main improvement made in this synthesis was the development of a precipitation protocol which provided very clean material without the need for column chromatography. The removal of the benzyl protecting groups from the primary amine[43] was improved in this work with the use of a Parr hydrogenation bomb. When working with up to ~ 0.5 g of starting material, 200 psi of H_2 pressure (which can easily be obtained in this apparatus) gave reaction times on the order of 1.5 – 2 hr, as opposed to 12 – 20 hr if a H_2 balloon was employed. Due to the volume constraints of the hydrogenation bomb, this improved deprotection was not always employed, but it did prove very useful and efficient for small to medium scale reactions.

The deprotected amine **3** was functionalized by addition of the metal binding groups in a stepwise manner (Scheme 3.2). The pyridyl arm had been utilized in compounds **HL**^{3}[43] and **HL**^{4} (Figure 3.13);[44] the major improvement to their method for addition of the first binding arm (via reductive amination to give **4**), was the use of $NaBH_4$ in place of $NaBH(OAc)_3$. The overall reaction time for the formation of the secondary amine was reduced from up to 2 days to 20 min. $NaBH(OAc)_3$ is a milder reducing agent than $NaBH_4$; it does not reduce aldehydes and as such works *in situ* so the two step reductive amination can be carried out in one pot. Reduction with $NaBH(OAc)_3$ lead to the formation of the tertiary amine, and was inconveniently slow, so the use of $NaBH_4$ was investigated. The change of solvent from 1,2-dichloroethane to ethanol, as necessitated by the solubilities of the particular reducing agents, resulted in the imine formation proceeding very rapidly, as evidenced by the nearly instantaneous colour change upon addition of aldehyde. TLC after 5 min was used to confirm the absence of any starting materials, and excess $NaBH_4$ was added. As $NaBH_4$ reduces aldehydes as well as imines, it was thought that the reduction of any excess aldehyde would prevent the formation of the tertiary amine, and this was found to be the case. As adequate yields were obtained via this method, it was not necessary to isolate the imine prior

References begin on Pg 106

to reduction. The whole reductive amination could be performed in one pot in a very short period of time. This methodolgy was applied to the synthesis of compound **6**, the methyl-imidazole analogue, and was found to work successfully in this case too.

The second chelating arm was installed by either a second reductive animation of salicylaldehyde to give compound **7**, or an alkylation to add a protected acetate arm to compound **5** (Scheme 3.2). As the reductive amination in this case was being used to make a tertiary amine from a secondary amine, there was no danger of overalkylation; $NaBH(OAc)_3$ was the reducing agent of choice as it could reduce the imminium ion formed *in situ*. The alkylation of the secondary amine via S_N^2 attack on methylbromoacetate proceeded as expected to give compound **5**.

The methyl protecting group on the acetate in compound **5** was chosen because it could be removed by NaOH, which would allow for concurrent deprotection of this group and the four acetyl groups on the sugar hydroxyls. This was found to be the case, and $\mathbf{HL^1}$ was prepared from **5** by vigorous stirring in 1 M NaOH. TLC and MS analysis showed that this reaction proceeded in very high yield. As the product of this reaction is very polar, reverse-phase HPLC (RP-HPLC) was needed to purify the resulting oil, and this dramatically lowered the overall isolated yield of the reaction.

To produce $\mathbf{HL^2}$ from **7** required only the deprotection of the glucosamine acetyl groups, which was achieved in good yield using NaOMe in MeOH. Although $\mathbf{HL^2}$ is not quite as hydrophillic as $\mathbf{HL^1}$, it still required purification by RP-HPLC, which again resulted in the isolated yield being much lower than the crude yield.

References begin on Pg 106

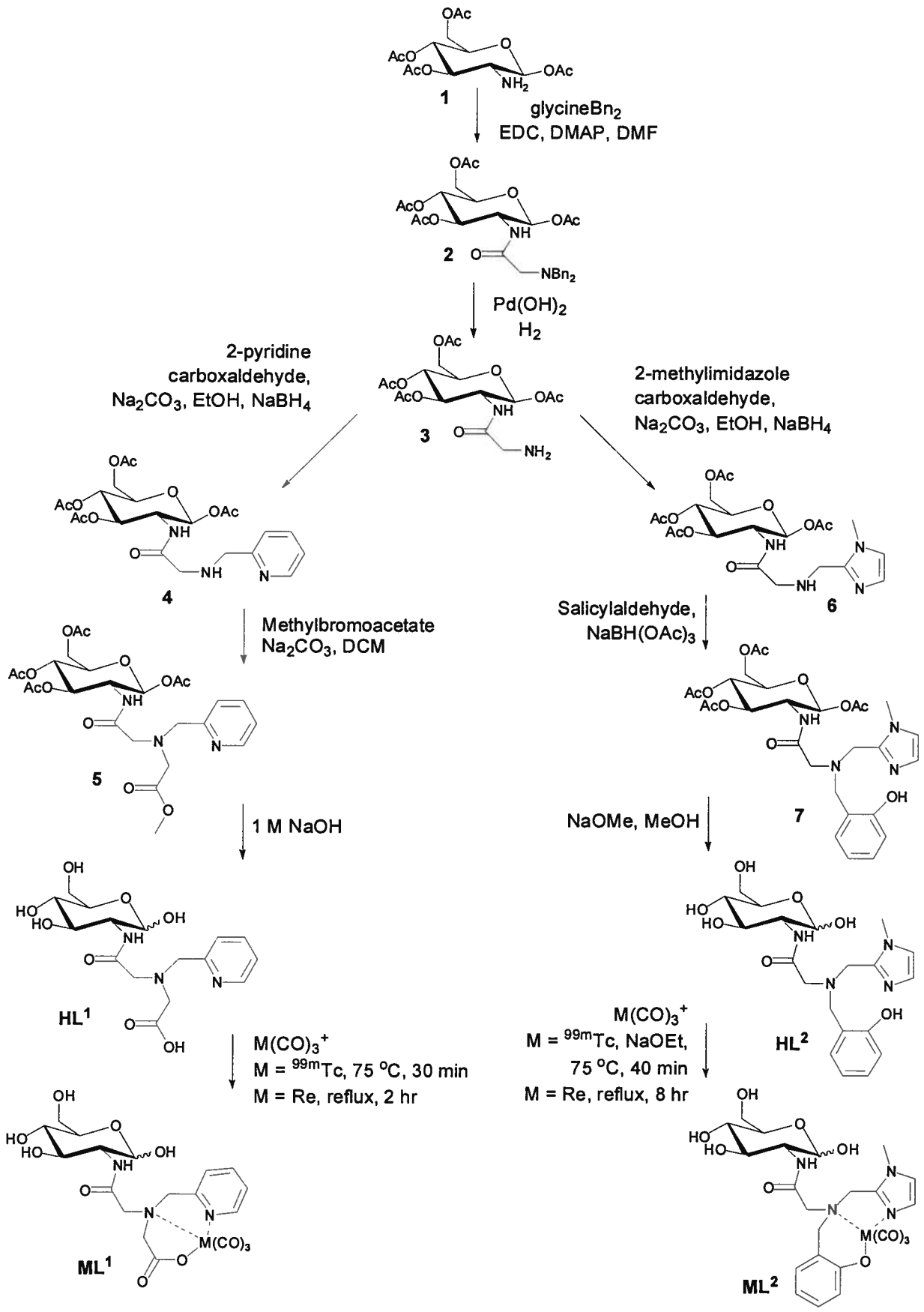

Scheme 3.2 The syntheses of HL^1, HL^2 and their metal complexes.

References begin on Pg 106

Complexation of either **HL**^{1} or **HL**^{2} to the rhenium tricarbonyl core proceeded in a straightforward manner by refluxing in methanol. The ligand containing the acid functionality bound to the metal core more quickly than the phenolate ligand **HL**^{2}, presumably due to the differing protonation states of the two ligands. These complexes were again purified by RP-HPLC, as the free glucose makes it very difficult to purify them on silica, by precipitation or by crystallization.

The ligands **HL**^{1} and **HL**^{2}, their rhenium complexes, and most chemical intermediates in the syntheses were characterized by HR-MS, IR, ^{1}H and ^{13}C NMR spectroscopy. A variety of 2-D NMR techniques such as COSY, HMQC, HMBC and TOCSY were used, as appropriate, for full assignment of ^{1}H and ^{13}C NMR signals.

HR-MS gave the expected peaks in each case for either $M+H^{+}$ and/or $M+Na^{+}$, verifying the presence of the target compound. The rhenium complexes exhibited the correct isotope pattern (^{185}Re = 37 % and ^{187}Re = 63 % natural abundance) to verify the presence of one rhenium. In a typical example, the HR-MS of compound **HL**^{1} shows peaks at 676.0610 (~55 % intensity) and 678.0704 (100 % intensity) corresponding to $C_{19}H_{22}N_3O_{11}{}^{185}ReNa^{+}$ and $C_{19}H_{22}N_3O_{11}{}^{187}ReNa^{+}$, respectively.

Infrared (IR) spectroscopy was used to verify the presence of the target compound by identification of key peaks corresponding to certain functional groups in that molecule. The deprotection of the acetyl groups on the sugars to reveal the proligands can be seen in the loss of the acetyl peak in the IR. The tetraacetyled proligand (**5**) had a strong peak at 1745 cm^{-1} (Figure 3.14), characteristic of ester groups which disappeared in the spectrum of **HL**^{1}, while strong broad peaks at 3272 cm^{-1} and 2918 cm^{-1} grew in, characteristic of the free hydroxyl groups revealed by the deacetylation (Figure 3.14). Deprotection of compound **7** to give **HL**^{2} caused the disappearance of a strong ester band at 1744 cm^{-1} accompanied by the appearance of bands corresponding to the –OH stretches of the acid and the hydroxyl groups at 3293 cm^{-1} and 2942 cm^{-1}.

References begin on Pg 106

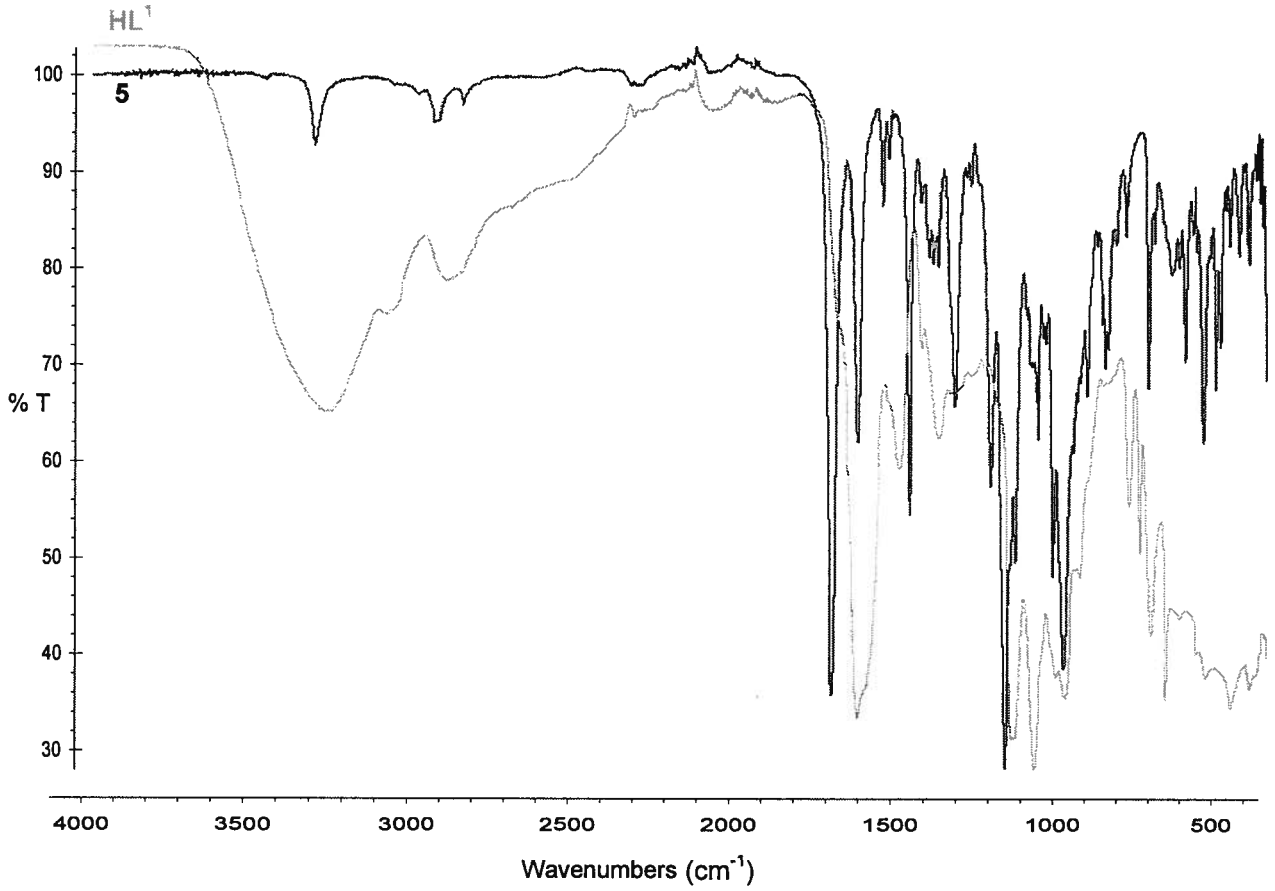

Figure 3.14 IR spectrophotometric traces of compound **5** (in black, starting at 98 % transmittance in the top left corner) and its deacetylated analogue **HL^1** (in gray, starting at 100 % transmittance in the top left corner).

IR spectrophotometry can also be very diagnostic of metal binding, so the spectra of the proligands and their metal complexes were compared. Figure 3.15 shows the overlaid spectra of **HL^2** and its rhenium tricarbonyl complex **ReL^2**. The decrease in relative intensity of the broad peaks at high wavenumber (around 3000 cm^{-1}) is due to the coordination of the acid functional group to rhenium, and the small peaks at similar wavenumber in the spectrum of **ReL^2** are due to the free –OH groups of the deprotected carbohydrate. The rhenium complex shows several more strong peaks than the corresponding ligand **HL^2**. The peaks at 2028 and 1884 cm^{-1} are due to the ReC≡O bonds. In $[Re(H_2O)_3(CO)_3]^+$ these peaks appear around 2000 and 1868 cm^{-1} respectively, and a shift to higher wavenumber as observed here is characteristic of metal binding in complexes of this type.[27] The carbonyl peak appears at 1671 cm^{-1} in the proligand **HL^2** and at 1672 cm^{-1} in the spectrum of the rhenium complex **ReL^2**. As this peak corresponds to the amide at *C*-2, it is not close enough to the metal coordinating portion of the molecule to be significantly affected by binding to the metal. This supports the metal binding of the desired coordination sphere and the pendant nature of the carbohydrate.

References begin on Pg 106

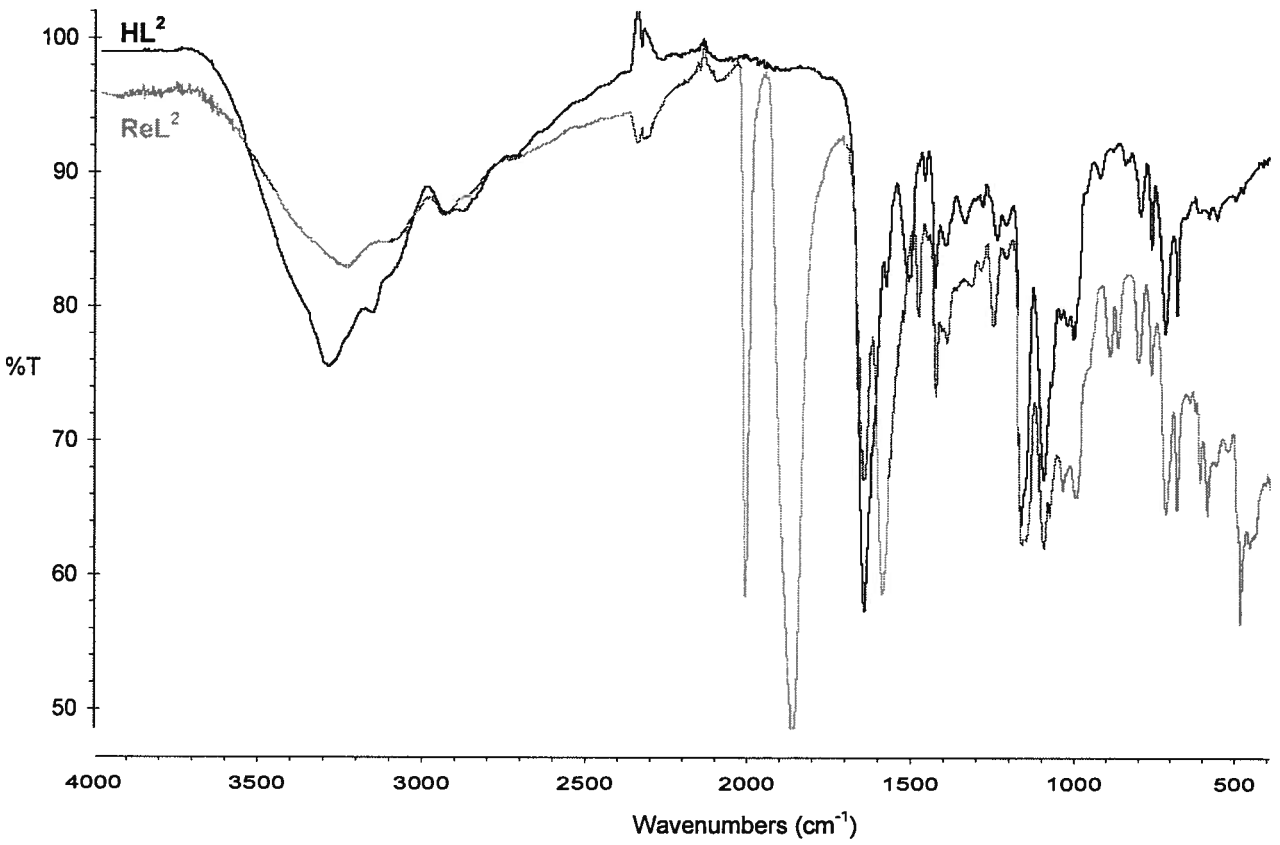

Figure 3.15 Overlaid IR spectra of $\mathbf{HL^2}$ (in black, beginning at 100 % transmittance at top left) and $\mathbf{ReL^2}$ (in gray, beginning at ~97 % transmittance at top left).

Similar observations can be made when comparing proligand $\mathbf{HL^1}$ with its rhenium complex, $\mathbf{ReL^1}$. Proligand peaks in the 2800 - 3300 cm^{-1} range decreased in relative intensity upon metal coordination as the acid f unctionaility became bound to the metal centre. Peaks corresponding to the ReC≡O bonds appeared at 2020 and 1910 cm^{-1}. The carbonyl peak shifted upon metal coordination; appearing at 1667 cm^{-1} in the proligand and 1635 cm^{-1} in the complex. This is because this peak corresponds to the acid moiety, which is very close to the metal, so would be expected to be affected by the coordination. This large shift supports the binding of the acid group to the metal.

^1H and ^{13}C NMR spectroscopy were used to further probe the identity of each compound made, as well as the coordination modes of the final complexes $\mathbf{ReL^1}$ and $\mathbf{ReL^2}$. The spectra of the chemical intermediates and the protected proligands **5** and **7** were unremarkable. All were rigorously assigned to ensure the identity of each compound. Deprotection of **5** and **7**

References begin on Pg 106

to give proligands **HL**^{1} and **HL**^{2}, respectively, led to more complicated NMR spectra. This is typical of sugar compounds where all the free hydroxyl groups lead the hydrogens on the pyranose ring all to be in similar chemical environments, especially those at *C*-3-*C*-5. These parts of both the ^{1}H and ^{13}C NMR spectra are difficult to fully assign and interpret, as can be seen in Figure 3.16, where 3.16a is the ^{1}H NMR spectrum of the protected **7**, and and 3.16b is that of **HL**^{2}. Comparing the two, it is easy to identify the large upfield shift and narrowing together of the sugar peaks. However, the aromatic peaks remain very diagnostic, and the anomeric protons at the *C*-1 position (5.1 and 4.7 ppm) confirm the presence of a non-protected glucopyranose ring. The same trends are observed when comparing the ^{1}H NMR spectra of protected **5** and **HL**^{1}, where the aromatic region remains essentially unchanged and the sugar peaks all undergo large shifts and narrowing with the *C*1 anomeric peaks being the only ones still clearly defined.

Figure 3.16c shows the ^{1}H NMR spectrum of **ReL**^{2}. Comparing this with Figure 3.16.b (**HL**^{2}) there are a number of changes that point toward the desired coordination mode. Firstly, the largest shifts seen are for the aromatic protons, which have collectively spread out and shifted downfield. These large shifts are indicative of metal binding occurring close to these hydrogen atoms. The peaks between 3 - 5 ppm have also shifted somewhat, though due to the overlapping it is difficult to tell exactly which peak has moved where. The only sugar peak that can be clearly seen is that of *C*-1α proton which appears at 5.1 ppm in both compounds. That it does not shift upon coordination means that its chemical environment has not changed significantly, and therefore that it is not close to the site of metal binding. The same trends are observed upon comparison of the ^{1}H NMR spectra of **HL**^{1} and **ReL**^{1}. The aromatic peaks spread and move downfield while the region between 3 - 5 ppm does not undergo such large changes, though again this is difficult to interpret in detail.

Again, the *C*1α peak is clearly seen and is found not to move significantly upon metal coordination.

References begin on Pg 106

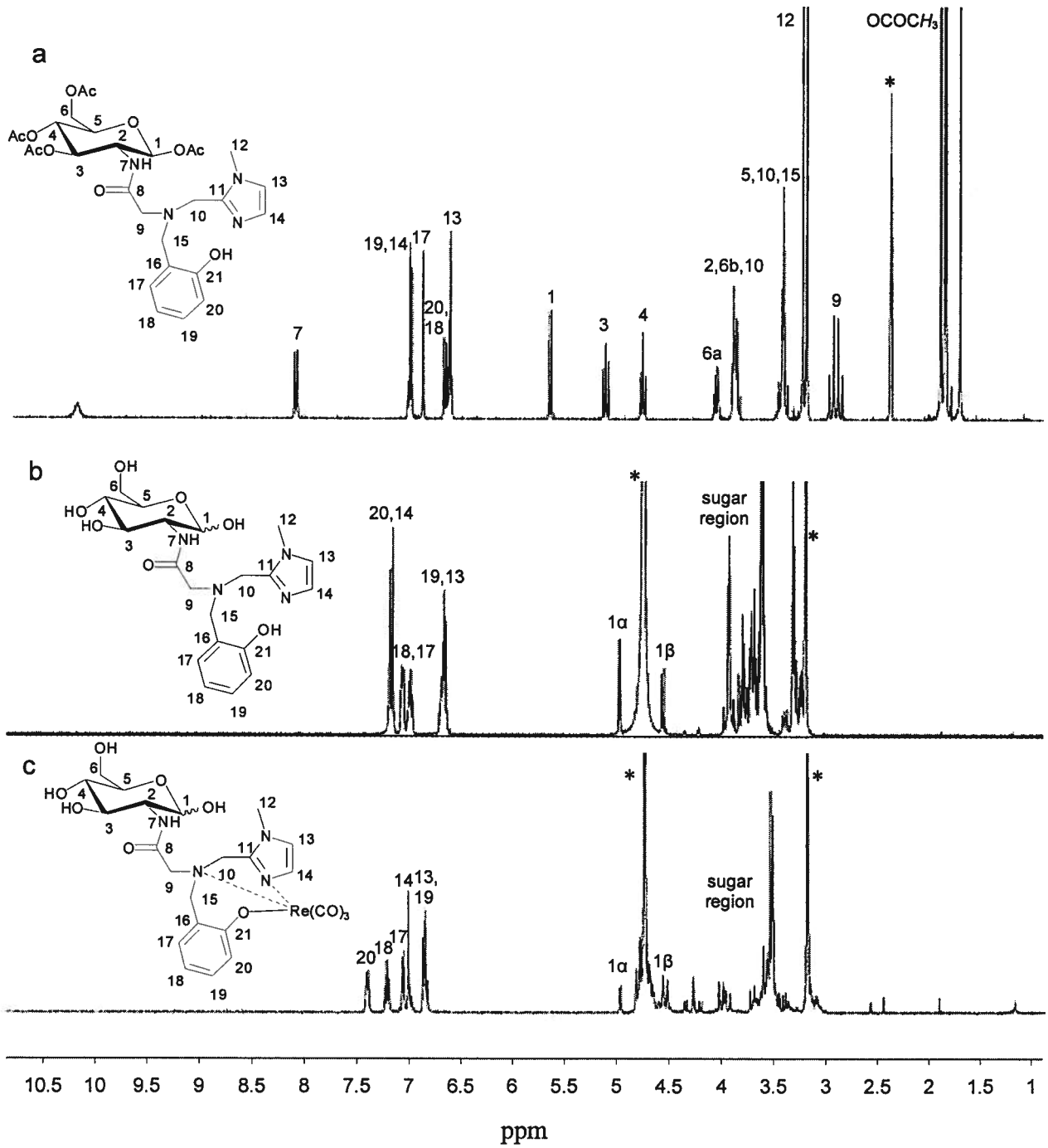

Figure 3.16 ^{1}H NMR spectra of a) **7** b) **HL^{2}** c) **ReL^{2}**, * shows the residual solvent peaks.

^{13}C NMR spectroscopy reinforces the conclusions drawn from analysis of the ^{1}H NMR data. Addition of the binding arms to build up **HL^{1}** and **HL^{2}** in a stepwise manner showed production of the correct number of new peaks in the expected δ range. Deprotection of **5** and **7** to reveal the proligands **HL^{1}** and **HL^{2}** led to several changes in the ^{13}C NMR spectra. These are illustrated by representative traces in Figure 3.17a and b, the ^{13}C APT spectra of **7**

and **HL**^{2} respectively. These spectra were recorded in different solvents for solubility reasons, so the exact chemical chifts are not comparable, although the trends still exist. One major change upon deprotection is the disappearance of the acetyl peaks in the regions around 170 ppm and 20 ppm, and a downfield shift of the peaks corresponding to *C*-1-*C*-6 of the carbohydrate. Due to the production of two anomers, the spectrum becomes much more complicated, with two peaks visible for many carbon atoms. As the anomers differ in their stereochemistry only at the *C*-1 position, the closer an atom is to this centre the more likely it is to be split, and the larger the gap between the two peaks. For example, the two *C*-2 peaks in **HL**^{1} are 2.7 ppm apart, as they are adjacent to the epimeric centers, whereas the aromatic carbons *C*-12-*C*-15 in the same molecule each show up as only one distinguishable peak, as they are fairly well removed from the amomeric centre. These features are all well illustrated in the examples shown in Figure 3.17a and b.

Coordination of the proligands to $[Re(CO)_3]^+$ results in several coordination induced shifts (CIS). A major feature of the spectra of the metal complexes is the appearance of three peaks due to the carbon atoms on the CO ligands around 194 ppm (see Figure 3.17c), a normal chemical shift for compounds of this type.[27] Similar to what is seen in the ^{1}H NMR spectra of these complexes, the aromatic signals move significantly compared to the signals coming from the rest of the molecule. Some aromatic signals shift very little, and others up to about 10 ppm either upfield or downfield, depending on that carbon's position with respect to the ligating atom. These shifts can be observed by direct comparison of Figures 3.17b and c. It can also be observed that the sugar peaks do not shift significantly from those of the free ligand.

Taken together this characterization information is all consistent with the structures put forward and expected to form under the given reaction conditions.

References begin on Pg 106

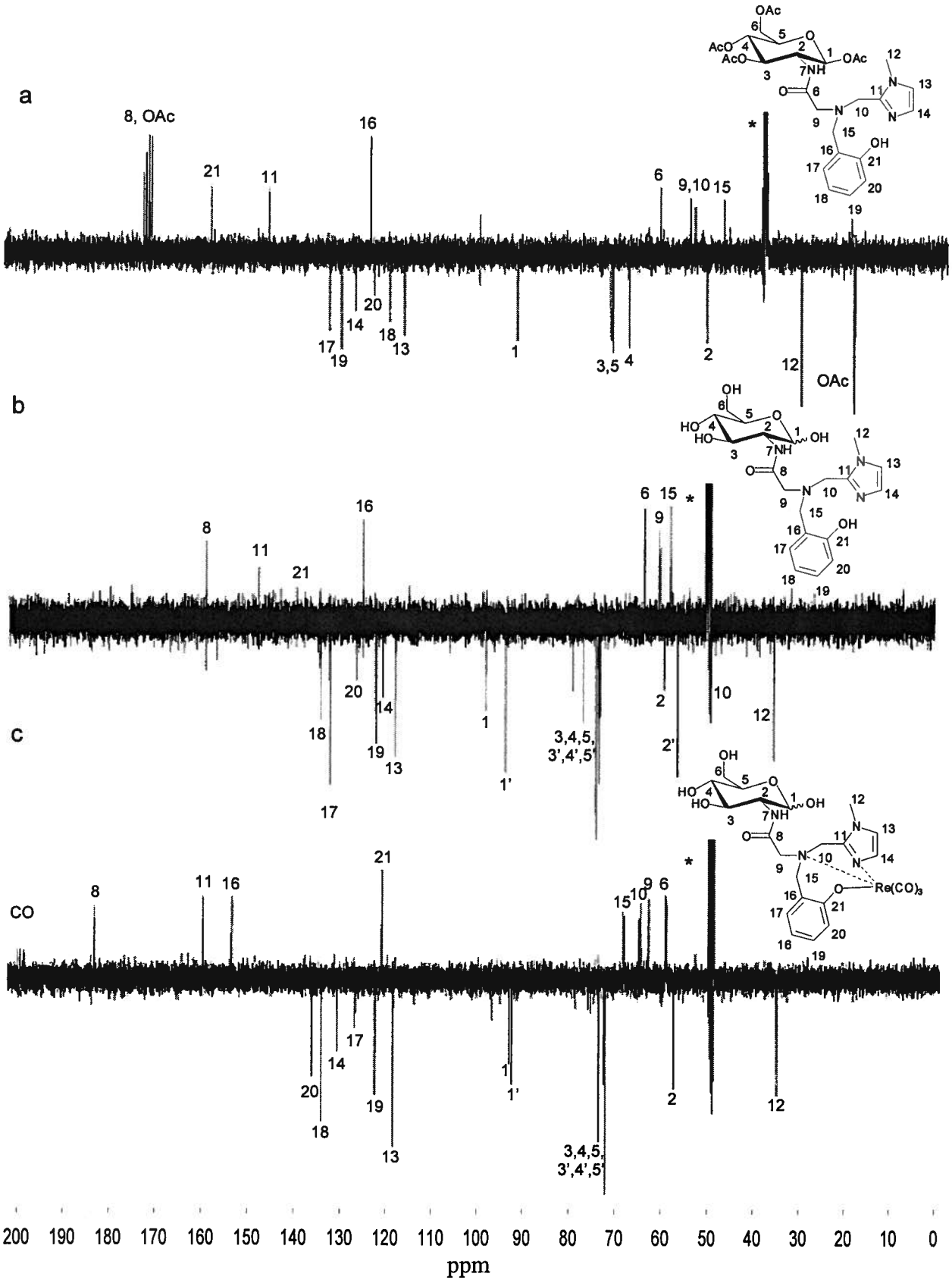

Figure 3.17 ^{13}C APT spectra of a) **7** b) **HL^2** c) **ReL^2**, * marks the residual solvent peaks.

As the rhenium complexes formed well, it was expected that formation of the ^{99m}Tc complexes would also proceed smoothly. This was found to be the case, and high radiochemical yields were achieved (Table 3.1). As was observed with rhenium complex formation, the acid-containing ligand **HL^1** gave faster coordination and higher yields. It also proceeded under milder conditions – an aqueous solution buffered to pH 7.4 gave excellent yields. At this pH all the acid groups are deprotonated and therefore ready to bind to the metal ion. The phenolate-based proligand **HL^2** was deprotonated with NaOEt prior to addition of the ^{99m}Tc precursor. This enabled good labelling yields in 30 – 40 min at 75 °C.

Table 3.1 Summary of labelling and stability results for the two novel ^{99m}Tc complexes made in this chapter.

Ligand	RT (Re compound)*	RT (^{99m}Tc compound)*	Radiochemical yield	Stability in cysteine – 24 hr	Stability in histidine – 24 hr
HL^1	12.9 min	13.2 min	94 %	94 ± 2 %	85 ± 3 %
HL^2	19.6 min	19.4 min	96 %	100 ± 4 %	94 ± 3 %

* HPLC conditions – 100 % H_2O (with 0.1 % TFA) linear gradient to 100 % ACN at 30 min.

The ^{99m}Tc complexes were analyzed using RP-HPLC. As discussed in Chapter 1.4, this is standard practice when performing radiochemistry as the radioactivity and very small amounts involved preclude the use of conventional chemistry characterization techniques. The thoroughly characterized rhenium complex was coinjected with the ^{99m}Tc complex and agreement of their retention times taken to mean that the technetium analogue is of the same chemical structure as the rhenium complex. There is normally a slight difference between the two retention times because 1) the UV (rhenium) and radiation (^{99m}Tc) detectors are in series, and 2) technetium and rhenium are not exactly the same, so their small differences may be enough to affect their relative retention times. Percentage radiochemical yield is calculated by integration of all the peaks that appear in the radiation trace. An example of a radioactive HPLC trace of **^{99m}TcL^1** is shown in Figure 3.18.

All ^{99m}Tc complexes were tested for stability in excess amounts of cysteine and histidine for

24 hr at 37 °C. The results are shown in Table 3.1. Cysteine and histidine are strong ligands for the tricarbonyl core, and are found ubiquitously *in vivo*. This method of measuring complex stability is routinely used in radiochemistry as an indicator of *in vivo* applicability of the given chelating system. The compounds shown here both exhibit satisfactory stability to allow for their further investigation as molecular imaging agents.

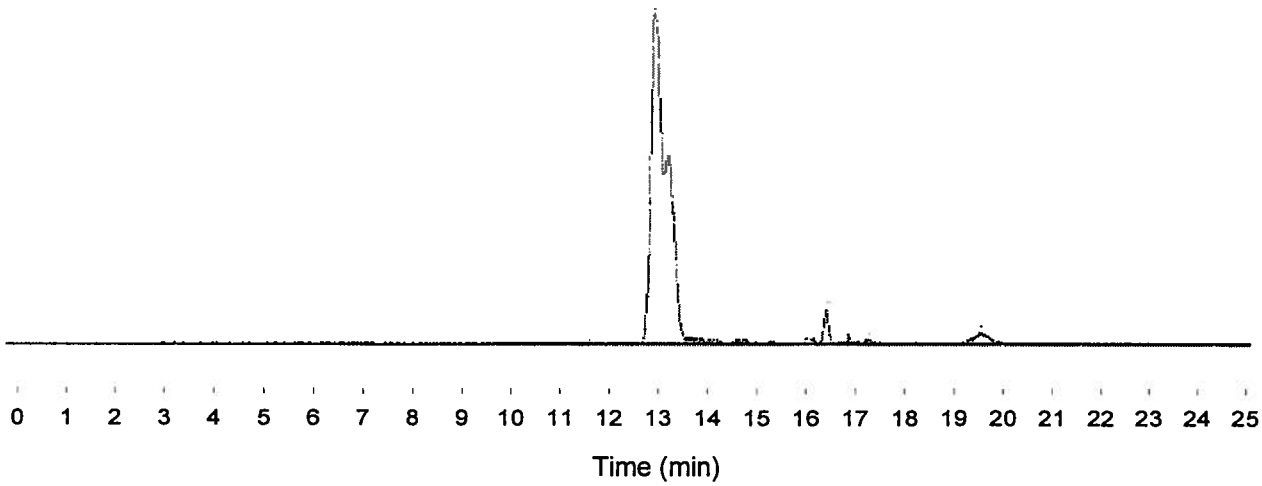

Figure 3.18 Radiation trace from HPLC of ^{99m}**TcL**^{1}. Retention time is around 13 min, with the small peak at 16 min due to unreacted starting material. The x-axis is arbitrary units corresponding to amount of radiation detected.

3.3.2 Cell Uptake Studies

Cell uptake of several ^{99m}Tc complexes was examined in LCC6-HER2 cells – a human breast cancer cell line with high concentrations of GLUT-1 glucose transporters on its surface.[45] The uptake was studied in the presence and absence of glucose to help elucidate the mechanism of any cell uptake observed – if uptake was found to be inhibited by the presence of high concentrations of glucose it would mean that the test compound and glucose were sharing the same cell uptake pathways. Figure 3.19 shows the results of this assay. It is clear from this graph that the cell uptake of each of the ^{99m}Tc compounds examined is independent of glucose. This means that the uptake seen is not due to the compounds being transported along the GLUT-1 transporters. It can also be seen that the actual percentage uptake for each of the compounds is quite low. For comparison, FDG, the positive control, showed uptake of around 3.4 % of the total activity when in a glucose free environment, and only 0.1 % when 10 mM glucose was present (results not shown for graphical clarity). This

References begin on Pg 106

illustrates both the amount of uptake that can be achieved by utilizing the GLUT-1 transporters, and the strong effect that 10 mM glucose will exhibit on a compound transported by such a mechanism.

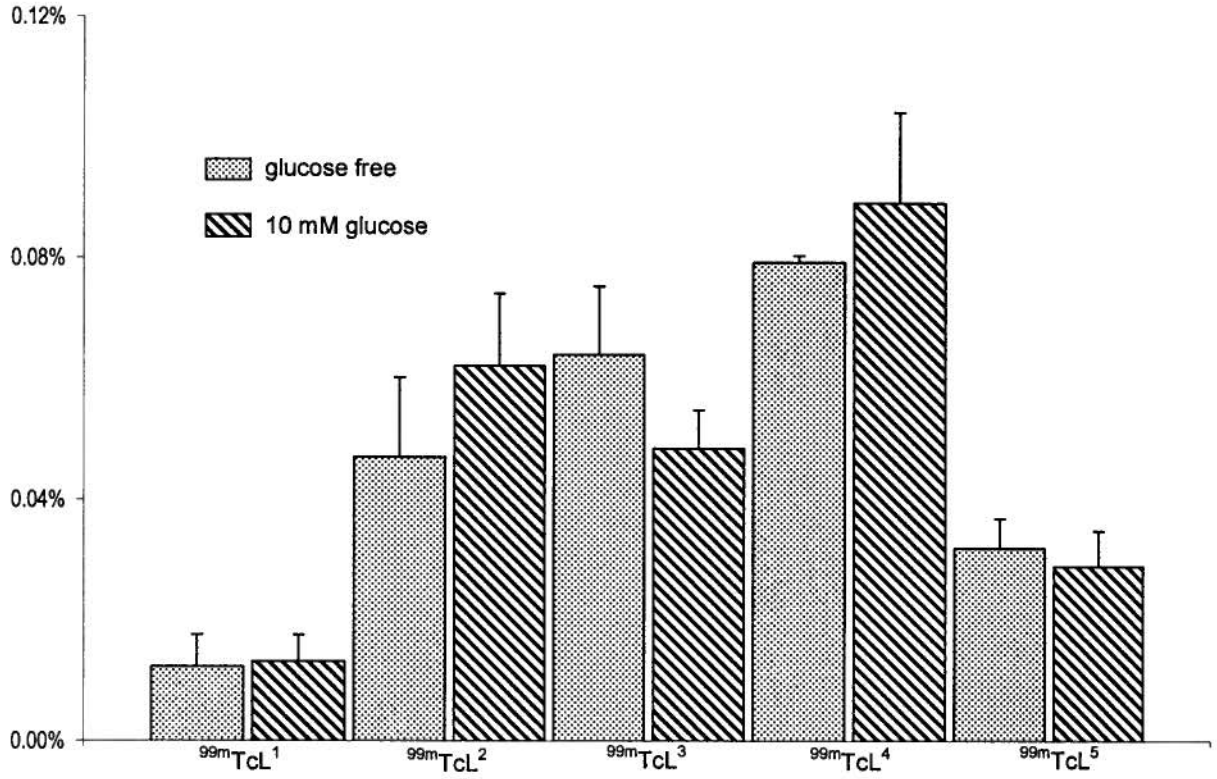

Figure 3.19 Results of cell uptake studies. Each compounds' uptake was examined in a glucose free environment and in 10 mM glucose solution. Average % of total activity in the cells after a 30 min incubation for four independent experiments are shown - error bars are standard deviations of the four.

Five technetium compounds (Figure 3.13) were tested in this assay. There were four neutral compounds ^{99m}**TcL**$^{1-4}$, and the cationic compound ^{99m}**TcL**^{5}. Given that less than 0.1 % of each of these compounds was taken up into cells after 30 min, it can be concluded that none of these compounds have any significant cellular uptake via GLUT-1 or any other mechanism. The overall trend is that lipophilic compounds have higher uptake, though again given the small percentages involved this is not a particularly robust conclusion. The cationic compound did exhibit an uptake lower than some of the neutral complexes, but had higher uptake than the neutral ^{99m}**TcL**^{1}. In a practical sense the exact mechanism of interaction is not of great importance, as the size of the uptakes observed mean that compounds of this type will not be of use as molecular imaging agents, as they will not be

References begin on Pg 106

able to enter cells in useful amounts.

3.3.3 Hexokinase Phosphorylation Studies

As discussed in Chapter 1.3, hexokinase phosphorylates glucose in the *C*-6 position, and is also known to phosphorylate certain glucose analogues. It was of interest to see if these compounds would be phosphorylated by hexokinase. This is an important property to be assessed when looking for a glucose based imaging agent, as without phosphorylation to make the compound negatively charged, it can diffuse out of a cell just as quickly as it diffused in. This would mean there would be no significant enhancement of signal in cells that overexpress hexokinase, regardless of GLUT expression and cell uptake.

Unfortunately none of the compounds tested were found to be phosphorylated by hexokinase. This may be because the metal-binding portions of the molecules are too large and bulky to allow the cleft in hexokinase to narrow as is required for phosphorylation to occur. Trying to circumvent this likely cause of the activity loss led to the idea of making long-chain glucosamine conjugates. The idea behind these is that the metal-binding portion of the molecule is held at a large enough distance from the active site that the closing of the cleft can occur without being blocked by the metal ion and chelate. This is the reasoning behind the long-chain compounds discussed in Chapters 4 and 5 of this thesis.

3.4 Conclusion

The phenolate ligand system is one that has been developed by the Orvig group relatively recently,[17, 27] and to our knowledge we are the only group to utilize this functionality as a ligand for the tricarbonyl core. This group was investigated as an alternative anionic binding group to provide a neutral complex when bound to the monocationic tricarbonyl core. The functional group normally used for this purpose in $[^{99m}Tc(CO)_3]^+$ chemistry is the carboxylic acid. We were interested in exploring different possibilities for binding groups and widening the cordination chemistry knowledge of this important radiochemistry core. It has been determined[27] that the phenolate group is indeed a suitable donor for the tricarbonyl core, as it binds to both the technetium and rhenium centres within a radiochemistry-appropriate timeframe and gives complexes stable to cysteine and histidine challenges. As the pKa of

References begin on Pg 106

the phenol is around 10, the reaction mixture needs to be made basic to enable sufficient ligand deprotonation for complex formation in a timely manner. In our systems this proceeded well and with no sign of degradation products, but these conditions may limit its general applicability. This potential drawback may be outweighed, however, by the increased lipophilicity of a phenol compared to an acid group, which in certain cases may be able to improve the biodistribution and solubilities of the resulting compound. As these biological properties can be very sensitive to small changes, this is a very useful addition to the expanding knowledge on the coordination chemistry of technetium.

The practical application of the compounds made in this chapter, whether based on phenolates or other ligand types, is not as we had initially hoped. To be a contender as a molecular imaging agent, a compound has to be taken up by and trapped in cells that overexpress the enzymes of interest. In the case of carbohydrate based imaging agents those enzymes are hexokinase and the GLUT family. The *in vitro* assays performed on the compounds in this chapter show no substrate activity either in terms of cell uptake via GLUT-1 or phosphorylation by hexokinase. The reason for these results is that these compounds are too different from glucose for the very specific enzymes to recognize and process the compounds as they would their native substrates. Figure 3.1 shows glucose and FDG, where the similarities between the two are very apparent. When trying to utilize a metallic radionuclide, it is not possible to make such small changes, as a metal binding group must always be added. But in this case at least, that perturbation is too large to allow for a functional imaging agent to be formed.

References begin on Pg 106

3.5 References

1. Kubota, K., *Ann. Nucl. Med.* **2001,** *15*, 471-486.

2. Herholz, K.; Salmon, E.; Perani, D.; Baron, J.-C.; Holthoff, V.; Frolich, L.; Schonknecht, P.; Ito, K.; Mielke, R.; Kalbe, E.; Zundorf, G.; Delbeuck, X.; Pelati, O.; Anchisi, D.; Fazio, F.; Kerrouche, N.; Desgranges, B.; Eustache, F.; Beuthien-Baumann, B.; Menzel, C.; Schroder, J.; Kato, T.; Arahata, Y.; Henze, M.; Heiss, W.-D., *NeuroImage* **2002,** *17*, 302 - 316.

3. Adam, M. J., *J. Label. Compd. Radiopharm.* **2002,** *45*, 167 - 180.

4. Adam, M. J.; Wilbur, D. S., *Chem. Soc. Rev.* **2005,** *34*, 153 - 163.

5. Risch, V. R.; Honda, T.; Heindel, N. D.; Emrich, J. L.; Brady, L. W., *Radiology* **1977,** *124*, 837 - 838.

6. Caner, B. E.; Ercan, M. T.; Bekdik, C. F.; Varoglu, E.; Muezzinoglu, S.; Duman, Y.; Erbengi, G. F., *NuklearMedizin* **1991,** *30*, 132 - 136.

7. Ozker, K.; Collier, B. D.; Lindner, D. J.; Kabasakal, L.; Liu, Y.; Krasnow, A. Z.; Hellman, R. S.; Edwards, S. D.; Bourque, C. R.; Crane, P. D., *Nucl. Med. Commun.* **1999,** *20*, 1055 - 1058.

8. Oh, S. J.; Ryu, J.-S.; Yoon, E.-J.; Bae, M. S.; Choi, S. J.; Park, K. B.; Moon, D. H., *Appl. Radiat. Isot.* **2006,** *64*, 207 - 215.

9. Yang, D. J.; Kim, C.-G.; Schechter, N. R.; Azhdarinia, A.; Yu, D.-F.; Oh, C.-S.; Bryant, J. L.; Won, J.-J.; Kim, E. E.; Podoloff, D. A., *Radiology* **2003,** *226*, 465 - 473.

10. Chen, Y.; Huang, Z. W.; He, L.; Zheng, S. L.; Li, J. L.; Qin, D. L., *Appl. Radiat. Isot.* **2006,** *64*, 342 - 347.

11. Yang, D. J.; Yukihiro, M.; Yu, D. F.; Ito, M.; Oh, C.-S.; Kohanim, S.; Azhdarinia, A.; Kim, C.-G.; Bryant, J. L.; Kim, E. E.; Podoloff, D. A., *Cancer Biother. Radio.* **2004,** *19*, 443 - 456.

12. Zuckier, L. S.; Dohan, O.; Li, Y.; Chang, C. J.; Carrasco, N.; Dadachova, E., *J. Nucl. Med.* **2004,** *45*, 500 - 507.

13. Chen, Y.; Xiong, Q.; Yang, X.; Huang, Z.; Zhao, Y.; He, L., *Cancer Biother. Radio.* **2007,** *22*, 403 - 405.

14. Chen, Y.; Xiong, Q.; Yang, X.; Huang, Z.; He, L., *Cancer Biother. Radio.* **2007,** *22*, 400 - 402.

15. Chen, X.; Li, L.; Liu, F.; Liu, B., *Bioorg. Med. Chem. Lett.* **2006,** *16*, 5503 - 5506.

16. Alberto, R.; Schibli, R.; Elgi, A.; Schubiger, P. A., *J. Am. Chem. Soc.* **1998,** *120*, 7987 - 7988.

17. Bayly, S. R.; Fisher, C. L.; Storr, T.; Adam, M. J.; Orvig, C., *Bioconjugate Chem.* **2004,** *15*, 923 - 926.

18. Ferreira, C. L.; Bayly, S. R.; Green, D. E.; Storr, T.; Barta, C. A.; Steele, J.; Adam,

M. J.; Orvig, C., *Bioconjugate Chem.* **2006,** *17*, 1321 - 1329.

19. Storr, T.; Obata, M.; Fisher, C. L.; Bayly, S. R.; Green, D. E.; Brudzinska, I.; Mikata, Y.; Patrick, B. O.; Adam, M. J.; Yano, S.; Orvig, C., *Chem. - Eur. J.* **2005,** *11*, 195 - 203.

20. Mikata, Y.; Shinohara, Y.; Yoneda, K.; Nakamura, Y.; Esaki, K.; Tanahashi, M.; Brudzinska, I.; Hirohara, S.; Yokotama, M.; Mogami, K.; Tanase, T.; Kitayama, T.; Takashiba, K.; Nabeshima, K.; Takagi, R.; Takatani, M.; Okamoto, T.; Kinoshita, I.; Doe, M.; Hamazawa, A.; Morita, M.; Nishida, F.; Sakakibara, T.; Orvig, C.; Yano, S., *J. Org. Chem.* **2001,** *66*, 3783 - 3789.

21. Pak, J. K.; Benny, P.; Spingler, B.; Ortner, K.; Alberto, R., *Chem. - Eur. J.* **2003,** *9*, 2053 - 2061.

22. Gottschaldt, M.; Koth, D.; Muller, D.; Klettte, I.; Rau, S.; Gorls, H.; Baum, R. P.; Yano, S., *Chem. - Eur. J.* **2007,** *13*, 10273 - 10280.

23. Schibli, R.; La Bella, R.; Alberto, R.; Garcia-Garayoa, E.; Ortner, K.; Abram, U.; Schubiger, P. A., *Bioconjugate Chem.* **2000,** *11*, 345 - 351.

24. Alberto, R.; Pak, J. K.; van Staveren, D.; Mundwiler, S.; Benny, P., *Biopolymers* **2004,** *76*, 324 - 333.

25. Lipowska, M.; Cini, R.; Tamasi, G.; Xu, X.; Taylor, A. T.; Marzilli, L. G., *Inorg. Chem.* **2004,** *43*, 7774 - 7783.

26. Safi, B.; Mertens, J.; De Proft, F.; Geerlings, P., *J. Phys. Chem. A* **2006,** *110*, 9240 - 9246.

27. Lim, N. C.; Ewart, C. B.; Bowen, M. L.; Ferreira, C. L.; Barta, C. A.; Adam, M. J.; Orvig, C., *Inorg. Chem.* **2008,** *47*, 1337 - 1345.

28. Chiotellis, A.; Tsoukalas, C.; Pelecanou, M.; Raptopoulou, C.; Terzis, A.; Papadopoulos, M.; Papadopoulou-Daifoti, Z.; Pirmettis, I., *Inorg. Chem.* **2008,** *47*, 2601 - 2607.

29. Petrig, J.; Schibli, R.; Dumas, C.; Alberto, R.; Schubiger, P. A., *Chem. - Eur. J.* **2001,** *7*, 1868 - 1873.

30. Dumas, C.; Petrig, J.; Frei, L.; Spingler, B.; Schibli, R., *Bioconjugate Chem.* **2005,** *16*, 421 - 428.

31. Schibli, R.; Dumas, C.; Petrig, J.; Spadola, L.; Scapozza, L.; Garcia-Garayoa, E.; Schubiger, P. A., *Bioconjugate Chem.* **2005,** *16*, 105 - 112.

32. Dumas, C.; Schibli, R.; Schubiger, P. A., *J. Org. Chem.* **2003,** *68*, 512 - 518.

33. Yang, Q.; Lundahl, P., *Biochemistry* **1995,** *34*, 7289 - 7294.

34. Mikata, Y.; Sugai, Y.; Yano, S., *Inorg. Chem.* **2004,** *43*, 4778 - 4780.

35. Storr, T.; Sugai, Y.; Barta, C. A.; Mikata, Y.; Adam, M. J.; Yano, S.; Orvig, C., *Inorg. Chem.* **2005,** *44*, 2698 - 2705.

36. Storr, T.; Fisher, C. L.; Mikata, Y.; Yano, S.; Adam, M. J.; Orvig, C., *Dalton Trans.* **2005**, 654 - 655.

37. Ferreira, C. L.; Marques, F.; Okamoto, M. R. Y.; Otake, A. H.; Sugai, Y.; Mikata, Y.; Storr, T.; Bowen, M. L.; Yano, S.; Adam, M. J.; Chammas, R.; Orvig, C., submitted for publication.

38. Banerjee, S. R.; Babich, J. W.; Zubieta, J., *Inorg. Chim. Acta* **2006,** *359*, 1603 - 1612.

39. Mindt, T. L.; Struthers, H.; Brans, L.; Anguelov, T.; Schweinsberg, C.; Maes, V.; Tourwe, D.; Schibli, R., *J. Am. Chem. Soc.* **2006,** *128*, 15096 - 15097.

40. Banerjee, S. R.; Levadala, M. K.; Lazarova, N.; Wei, L.; Valliant, J. F.; Stephenson, K. A.; Babich, J. W.; Maresca, K. P.; Zubieta, J., *Inorg. Chem.* **2002,** *41*, 6417 - 6425.

41. Breitenmoser, R. A.; Heimgartner, H., *Helv. Chim. Acta* **2001,** *84*, 786 - 796.

42. Silva, D. J.; Wang, H.; Allanson, N. M.; Jain, R. K.; Sofia, M. J., *J. Org. Chem.* **1999,** *64*, 5926 - 5929.

43. Ewart, C. B. M.Sc. Thesis. University of British Columbia, Vancouver, 2006.

44. Lim, N. C.; Adam, M. J.; Orvig, C., unpublished results.

45. Dragowska, W. H.; Ruth, T. J.; Adam, M. J.; Kozlowski, P.; Skov, K.; Bally, M. B.; Yapp, D. T. T. In *Studies of Tumor Microenvironment and Metabolic Activity in HER-2/neu Overexpressing Breast Cancer Xenografts by MicroPET and MRI*, American Association for Cancer Research, **2005**, p 900.

CHAPTER 4

^{99m}Tc-Labelling and *In Vitro* Assays of Long Chain Glucosamine-based Tridentate Ligands*

4.1 Introduction

4.1.1 Long Chain Bioconjugates of $[^{99m}Tc(CO)_3]^+$

The effect of linker length on phosphorylation of a substrate has been observed in non-sugar systems.[1] Thymidine kinases are proteins responsible for the phosphorylation of thymidine (Figure 4.1a), forming a nucleotide from the nucleoside by addition of a phosphate in the 5' position.[1] As these kinases are overexpressed in some types of cancer, they are of interest in molecular imaging in oncology. A series of compounds have been synthesized with a carbon chain between the tridentate technetium binding sphere and the thymidine moiety being varied in length between two and ten carbons.[1] Rates of phosphorylation of these compounds by thymidine kinase were tested relative to the native substrate thymidine, and rates were found to increase with increasing chain length.[1] The compound with a C_{10} linker shown in Figure 4.1 has a rate of phosphorylation of 71.5 (± 4.7) % that of thymidine, the native substrate. This is a very significant percentage given the large change in molecular structure between the two compounds, as illustrated in Figure 4.1a and b. The thymidine conjugates synthesized were also examined for their cell internalization properties.[1] The authors were curious as to whether there would be any nucleoside transporter mediated cell uptake. This was found not to be the case; there was a strong correlation between lipophilicity and cell uptake, indicating passive diffusion as the likely mechanism of transportation.[1]

An amino acid-conjugate (Figure 4.1d) was synthesized and examined for cell uptake via the LAT-1 amino acid transporter.[2] LAT-1 transports lipophilic amino acids and their analogues, and is found in high concentrations at the blood brain barrier (BBB).[3] Brain delivery of drugs and imaging agents is a large problem in medicine as the BBB excludes most foreign materials.[4] Uptake studies were performed on a range of compounds, and though most analogues showed no

* A version of this chapter will be submitted for publication: Bowen, M. L., Chen, Z.-F., Roos, A., Adam, M. J. and Orvig, C. Synthesis and Characterization of Organometallic Rhenium and Technetium Glucose Complexes against Hexokinase.

References begin on Pg 127

or poor activity, the analogue in Figure 4.1d showed K_i = 308 μM.[2] This is the first time that a metal-labelled compound has shown transport activity with the LAT-1 transporter.[2] Although there is some substrate scope accepted by this enzyme, the activity quickly drops if certain small modifications are made.[2]

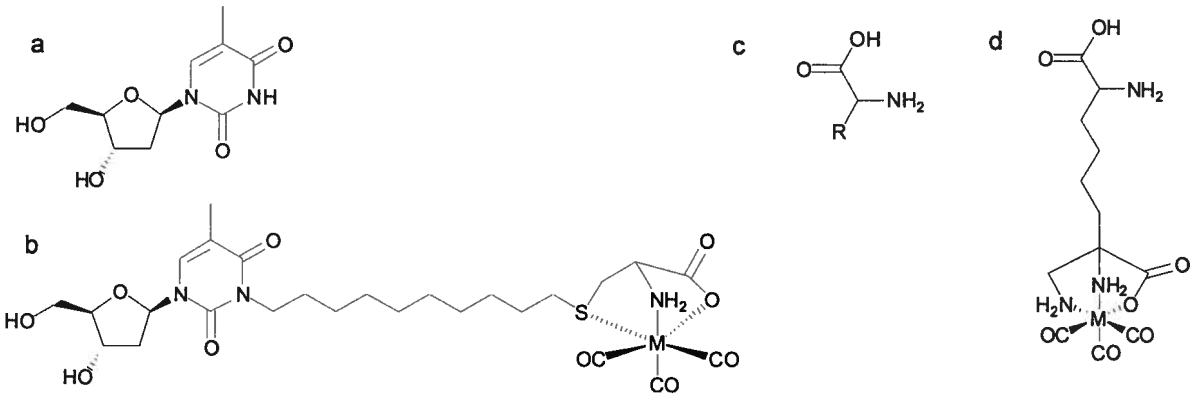

Figure 4.1 a) Thymidine b) a long chain (C_{10} linker) thymidine conjugate[1] c) a generic amino acid and d) long chain (C_5 linker) amino acid derivative;[2] these bioconjugates retain significant biological recognition of the parent compound in relevant assays, M = Re, ^{99m}Tc.

4.1.2 Long Chain Carbohydrate Conjugates of $[^{99m}Tc(CO)_3]^+$

There has only been one previous study, to our knowledge, investigating the potential merits of long chain carbohydrate conjugates as molecular imaging agents.[5] This included an investigation of phosphorylation by hexokinase and transport by GLUT-1 of the compounds synthesized,[5] and was discussed briefly in Chapter 1. The two long chain compounds in that work that are relevant to this Chapter will be examined in more detail here (Figure 4.2).[5]

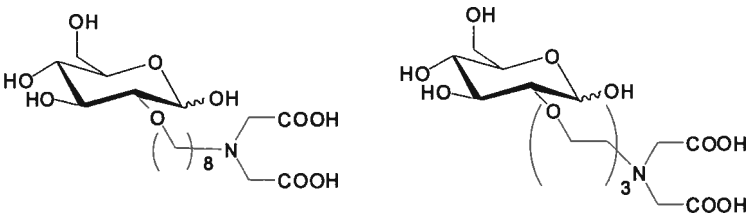

Figure 4.2 Two long chain glucose-based ligands for binding to the tricarbonyl core.[5]

The cellular uptake of the ^{99m}Tc labelled compounds (Figure 4.2) was found to parallel their lipophilicity.[5] The uptakes were also found to be independent of the concentration of both the

References begin on Pg 127

test compound and of cytochalasin B, a known inhibitor of GLUT-1.[5] This information points to the cellular uptake being due to unspecific passive diffusion rather than a GLUT-mediated uptake mechanism. The authors also modeled the interaction of these compounds with the active site of hexokinase.[5] Their rationale for synthesizing the long chain analogues was that this would allow for the carbohydrate to be in the active site of hexokinase, while the bulky metal tricarbonyl core with its tridentate chelate would be held far away from the active site. Because the active site of hexokinase is in a cleft which has to narrow in order for phosphorylation to occur,[6] having a bulky obstacle in the way may block the cleft from closing, and therefore the phosphate from transferring. *In silico* it appeared that the length of linker required to prevent this blocking was seven methylene units.[5] A hexokinase inhibition assay showed that two compounds, those with long alkyl chains (Figure 4.2), were strong inhibitors of hexokinase - K_i = 0.25 – 5.8 mM.[5] The shorter chain compounds did not exhibit any inhibitory character.[5] It was found that even the long chain compounds, which have nine atoms in their linker chains, were not themselves phosphorylated by hexokinase.[5]

The Orvig group has always been interested in glucosamine derivatives of these types of compounds due to the higher tolerances in structural variation of glucosamine analogues compared to glucose analogues exhibited by hexokinase and GLUTs.[7, 8] The extracellular binding of substrate to GLUT-1 is known to depend on interactions with the hydroxyl groups at *C*-1, *C*-2 and *C*-3.[9] When the hydroxyl group at *C*-2 of glucose is substituted, it loses its ability to hydrogen bond as the *O* no longer has a *H* attached. In contrast, when the *N* at the *C*-2 of glucosamine is monosubstituted, there is still one hydrogen attached to the nitrogen, so it is still able to hydrogen bond. For example, 2-NBDG (Figure 1.4c), with a dye appended directly to the secondary nitrogen at the *C-2* of glucosamine is found to be phosphorylated by hexokinase.[10] The same compound exhibits cell uptake properties characteristic of transport via GLUTs - the uptake is inhibited by both glucose and cytochalasin B.[10]

The work in this chapter exploits these properties of functionalized glucosamines and explores their abilities to accommodate long chain ^{99m}Tc labelled moieties and still retain certain enzyme activities. This chapter examines the effect of chain length on the *in vitro* properties of rhenium and technetium tricarbonyl complexes, while keeping the metal-binding and carbohydrate portions of the molecules constant.

References begin on Pg 127

4.2 Experimental

4.2.1 Instruments and Materials

All solvents and chemicals were reagent grade and were used as received unless stated otherwise. Solvents were HPLC grade, and were purchased from Fisher Scientific. Isolink™ kits were provided by Mallinckrodt Inc. (now Covidien). $Na^{99m}TcO_4$ was provided by the Nuclear Medicine Department at the University of British Columbia Hospital. The C6, C8, and C11 ligands and their Re complexes (Figure 4.3) were first made by Dr. Zhen-Feng Chen under my guidance.[11] The MTT cell toxicity assay and hexokinase inhibition studies of the C6 and C8 compounds were performed by an undergraduate summer student, Adrienne Roos, under my supervision.

The analytical TLC plates, which were aluminum backed ultra pure silica gel 60, 250 μm, and the flash column silica gel (standard grade, 60 Å, 32-63 mm) used were provided by Silicycle. HPLC analyzis of non-radioactive compounds was done on a Phenomenex Synergi 4 μm Hydro-RP 80 Å column (250 x 4.6 mm) in a Waters WE 600 HPLC system equipped with a 2478 dual wavelength absorbance UV detector run controlled by Empower software package. HPLC analyzes of radiolabelled complexes were performed on a Knauer Wellchrom K-1001 HPLC equipped with a K-2501 absorption detector and a Capintec radiometric well counter using a Phenomenex Synergi 4 μm Hydro-RP 80 Å column (250 x 4.6 mm).

4.2.2 ^{99m}Technetium Complex Formation

$Na^{99m}TcO_4$ (200 MBq) was obtained as a saline solution from the University of British Columbia Hospital, Department of Nuclear Medicine. It was added to an Isolink™ kit (Mallinckrodt) and the volume made up to 1 mL with 0.9 % saline solution. The resulting solution was heated at ~ 90 °C for 30 min. After cooling, the solution was neutralized with 1 M HCl (0.12 mL) to pH 7 as tested with pH paper. Meanwhile, 10^{-4} M ethanolic solutions of the ligands were prepared, and 0.5 mL of each was transferred to a reaction vial with three equivalents of NaOEt (0.15 mL of a 10^{-3} M solution in ethanol). The vial was purged with nitrogen for 10 min to provide an inert atmosphere and to ensure time for deprotonation of the phenolates. Between 0.1 and 1 mL of $[^{99m}Tc(CO)_3(H_2O)_3]^+$ was added to each vial, and the vial heated at 80 °C for 40 min. After

References begin on Pg 127

cooling, the solutions were injected into the HPLC (with the analogous cold standard rhenium complex) for analyzis.

4.2.3 Cysteine and Histidine Challenges

These experiments were performed as detailed in Chapter 3.2.4.

4.2.4 GLUT-1 Cell Uptake Assay

This was performed as detailed in Chapter 2.2.4.

4.2.5 Hexokinase Inhibition Assay

Hexokinase kits made up to contain 1 U/mL hexokinase, 1 U/mL glucose-6-phosphate dehydrogenase, 1 mM ATP and 1.5 mM NAD^+ were used in this assay. An aliquot (500 μL) of this solution was heated to 25 °C for 7 – 8 min and then transferred to a 1 cm pathlength cuvette for each trial. Rates were determined by adding one of four amounts of glucose: 10, 25, 50 or 75 μL of a standard solution (1.0 mg/mL glucose) to the cuvette, and the volume made up to 1250 μL with distilled water. The cuvette was gently inverted three times before being placed in a UV-vis spectrometer fitted with a water jacket equilibrated to 25 °C. The absorbance at 340 nm was recorded every 30 sec for at least five min. For each test compound five different concentrations were examined with each of the four glucose concentrations used above. The inhibitors were tested by adding either 25, 75, 100, 125 or 250 μL of a 5 mM stock solution of the compound to the assay mixture described above (final concentration of 0.1 – 0.5 mM) prior to addition of glucose. The same volume of hexokinase kit was used each time, with the total volume in the cuvette always being made up to 1250 μL with distilled water. As these factors were kept constant, changes in the rate of phosphorylation of glucose in the presence of a test compound were attributed to inhibition of the process by that test compound.

4.2.6 Hexokinase Substrate Assay

This was performed as detailed in Chapter 3.2.5.

References begin on Pg 127

4.2.7 MTT Cytotoxicity Assay

3-(4,5-Dimethylthiazol-2-yl)-2,5-diphenyltetrazolium bromide (MTT) is a dye commonly used in a colorimetric assay for studying the toxicity of compounds in a given cell line.[12] Human hepatocytes were used in this study, and the cells were cultured and maintained by Jessie Chen in the UBC Biological Services facility. On day 1 of the study, the cells were trypsinized to remove them from the flask wall to which they had adhered, then rinsed and counted on a hemocytometer. They were then diluted with media to a final concentration of $1x10^5$ cells/mL, and 100 μL of this solution was added to each well of a 96 well plate. The plates were incubated at 37 °C in a 5 % CO_2 atmosphere overnight. On day 2, test solutions were made up by dissolving varying amounts of the test compounds in media and 10 % fetal bovine serum. Test compound (100 μL of various concentration) was added to each well to bring the final well volume to 200 μL. Control wells were made up to 200 μL by addition of media containing 10 % fetal bovine serum. The plates were incubated at 37 °C in 5 % CO_2 for 72 hr. On day 5, a 2.5 mg/mL solution of 3-(4,5-dimethylthiazol-2-yl)-2,5-diphenyltetrazolium bromide (MTT) in PBS was prepared and added to each well (50 μL), and the plates were then incubated for a further 3 hr at 37 °C. The solution was removed, leaving the cells adhered to the sides of the wells, and dimethylsulfoxide (150 μL) was added to each well. The plates were gently shaken to solubilize the purple formazan crystals that had formed. The formazan was quantified using a plate reader to measure absorbance at 570 nm. At least four concentrations of each compound were tested, and all were done in quadruplicate.

Data were analyzed by setting the average absorbance of the control wells of each plate to 100 % cell viability. The average absorbance of each concentration of each compound was divided by the average absorbance of the control wells on that plate, and reported as an average percentage cell viability. Cisplatin was used as a positive control for cytotoxicity, and was found to have an IC_{50} value of 2.6 ± 0.3 μM, which is consistent with the literature.[13]

References begin on Pg 127

4.3 Results and Discussion

4.3.1 ^{99m}Tc Labelling and Cysteine/Histidine Challenges

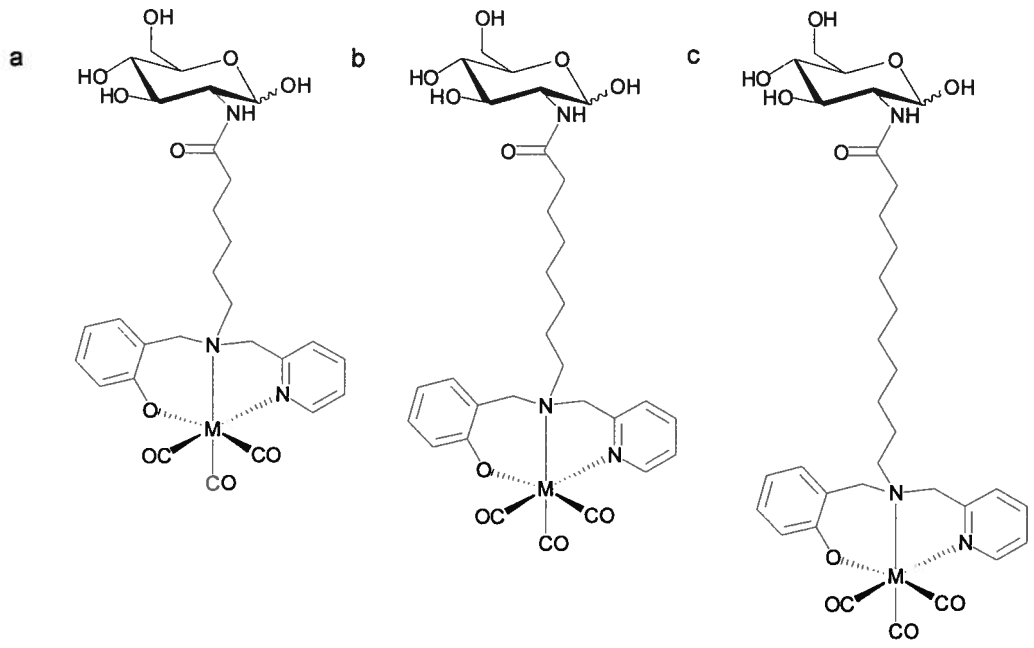

Figure 4.3 Long chain glucosamine conjugates studied in various assays in this Chapter: a) C6, b) C8 and c) C11, where the number refers to the number of carbons between *N* of the glucosamine and the *N* of the metal binding sphere; M = Re, ^{99m}Tc.

Although the original synthesis of the ligands and rhenium complexes (Figure 4.3 ligands, M = Re) were developed by myself and Dr. Z.-F. Chen, they were repeated several times and in some cases optimized by myself.[11] Once the sugars were deprotected to form the final proligands, the compounds decomposed over the course of days to weeks, and were repurified or synthesized just prior to use.

As these three ligands all possessed the same tridentate binding sphere, it was expected that their labelling would proceed in a similar manner. This was found to be the case, and the labelling yields were largely independent of chain length (Table 4.1).

References begin on Pg 127

Table 4.1 Results of ^{99m}Tc labelling and stability studies of three long chain glucosamine-based ligands.

Compound	RT (Re compound)*	RT (^{99m}Tc compound)*	Radiochemical yield	Stability in cysteine – 24 hr	Stability in histidine – 24 hr
C6	18.8 min	17.9 min	87 %	99 ± 2 %	95 ± 4 %
C8	20.8 min	21.7 min	93 %	100 ± 3 %	99 ± 3 %
C11	22.0 min	22.2 min	93 %	100 ± 3 %	93 ± 3 %

* HPLC conditions – 100 % H_2O (with 0.1 % TFA) linear gradient to 100 % ACN at 30 min.

As these ligands utilize a phenolate donor in the coordination sphere, a base was required for the labelling reactions to proceed quickly. The rhenium complexes could be formed without base by refluxing each ligand with the rhenium tricarbonyl precursor in methanol overnight. This is not practical when dealing with technetium and its six hour half life, so when radiolabelling, a base was used. Although labelling in aqueous media is desirable, there was concern over the lability of the amide bond when heated in the presence of hydroxide ions. The use of saline solution with addition of sodium hydroxide to pH 10 was explored, but was found to be unreliable. The method outlined in the Experimental section above had worked for similar compounds,[14] so was applied here, with good results. The proligand was dissolved in ethanol and three equivalents of NaOEt were added. This mixture was purged with nitrogen for 10 - 15 min, ensuring plenty of time for both ligand deprotonation and oxygen removal before addition of $[^{99m}Tc(CO)_3(H_2O)_3]^+$. The reaction mixture was heated at 80 – 90 °C for about 40 – 50 min, and gave consistently good radiochemical yields regardless of slight variations in time or temperature.

As expected, the retention times (RTs) increased with the length of the linker between the glucosamine and the metal binding sphere (Table 4.1). The C_{18} column used was non-polar and the eluent was 100 % H_2O (with 0.5 % TFA) to 100 % ACN over 30 min, from very polar to less polar. Thus polar compounds would be eluted earlier, as was observed. There are small discrepancies between the retention times of analogous technetium and rhenium complexes. As discussed in Chapter 3.3, the detectors for the two compounds (radiation and UV-vis detectors respectively) are connected in series, which means that their retention times would be expected

References begin on Pg 127

to be different. Also the two compounds are not identical, as they contain different metal ions and are present in very different concentrations, so it is normal that their retention times will differ slightly. A representative radiation trace from the HPLC is shown in Figure 4.4.

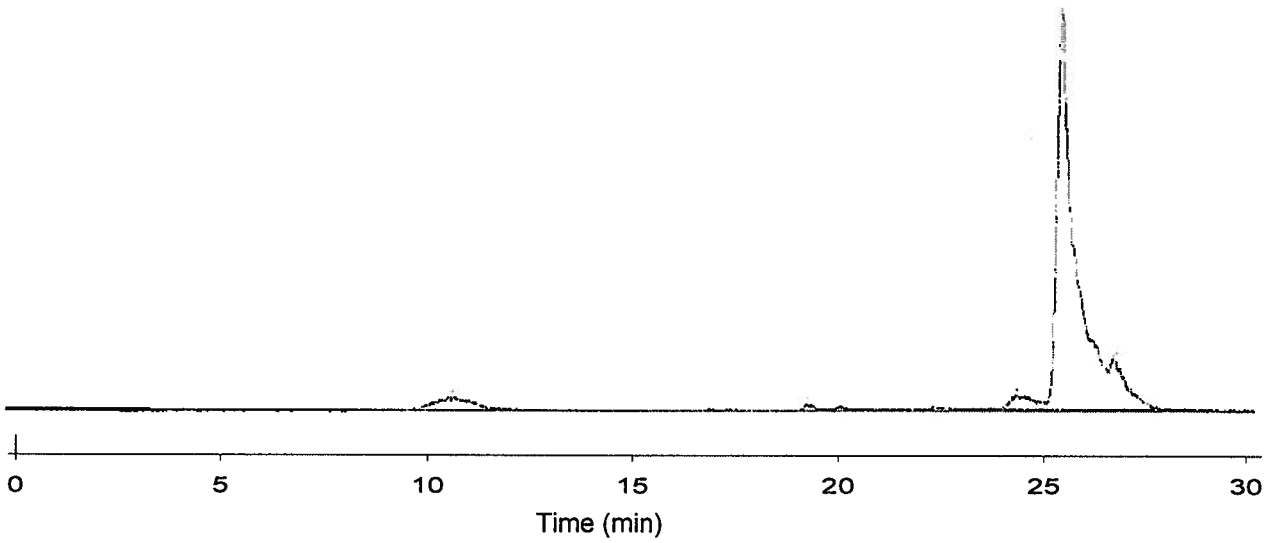

Figure 4.4 A representative radio-HPLC trace, for **C11^{99m}Tc**: the peak corresponding to this species appears at 26.6 min and represents a 91 % radiochemical yield. The small peak at 10- 11 min corresponds to unreacted starting material. The y-axis represents amount of radioactivity detected at a given time (arbitrary units).

These compounds share the same tridentate binding moiety and their stabilities when challenged with high concentrations of cysteine and histidine should be very similar. This was indeed true, with all three ligands binding tightly to ^{99m}Tc for 24 hr in the presence of large excesses of competing amino acids (Table 4.1). The cysteine and histidine challenges represent a simple model of an *in vivo* system where the synthesized ^{99m}Tc complex would be present in very small concentrations compared to a wide range of other potential donor molecules. It is very important to know that the ligand is not easily replaced by an endogenous competing ligand, as this would alter the biodistribution of the radiation. The complexes were essentially unchanged after 24 hr, a very good indication that they would be stable enough for *in vivo* applications.

4.3.2 Cell Uptake Assay

The compounds tested here showed modest cellular uptakes, which were not affected by the presence of glucose, suggesting that the cellular uptake observed is not due to the same mechanisms that are used to transport glucose. As can be seen in Figure 4.5, the uptake of the

References begin on Pg 127

compounds parallel their lipophilicity, with the C11 compound exhibiting the highest uptake and the C6 compound the lowest. The C2 compound with the analogous binding sphere ($^{99m}TcL^3$ discussed in Chapter 3) is shown here for context, and verifies trends in lipophilicity, as it has a lower cellular uptake than the longer chain compounds. Figure 4.5 also shows that addition of a large excess of glucose does not significantly affect the cellular uptake of any of the test compounds. These data together suggest that the observed uptake is due to passive diffusion through the lipid bilayer, where more lipophilic compounds can diffuse more easily.

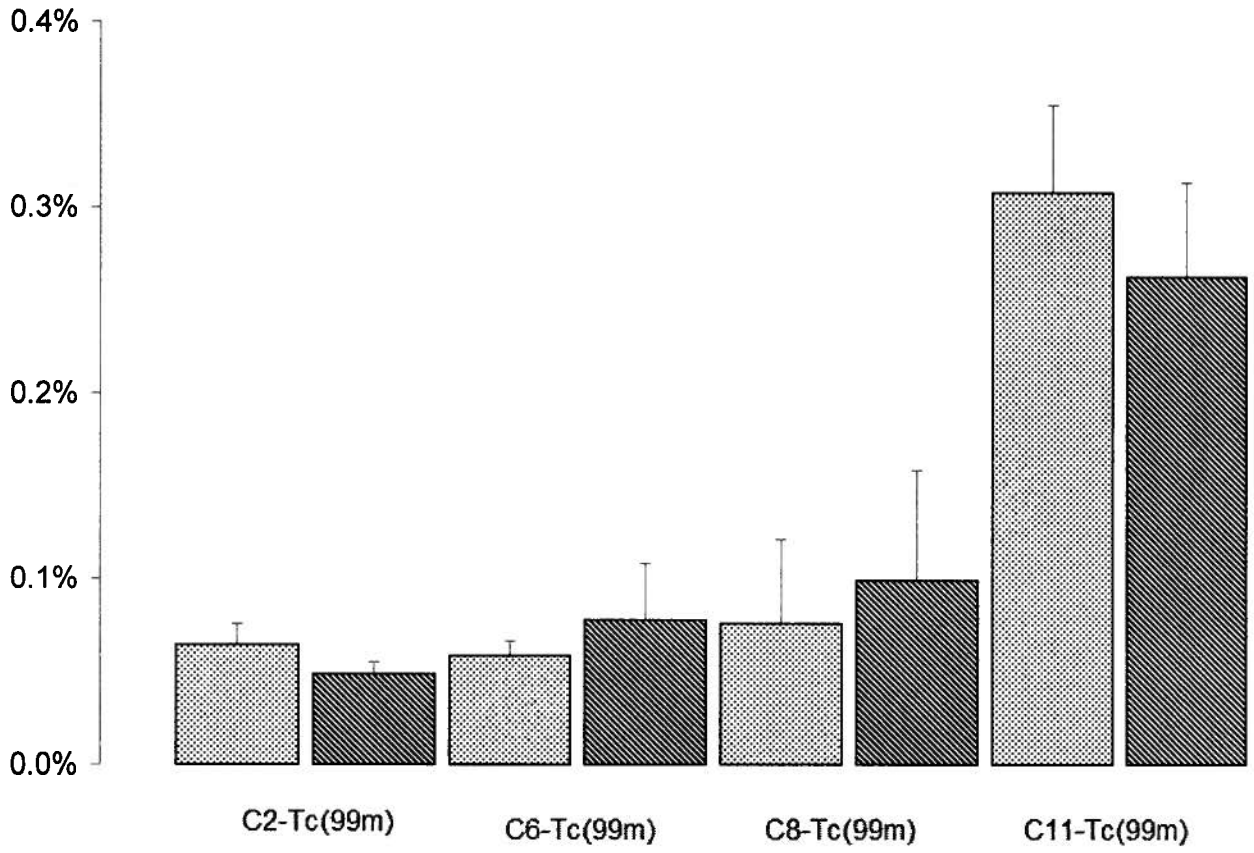

Figure 4.5 Percentage of activity taken up into LCC6-HER2 cells during a 30 min incubation. For each compound the results shown are the average of four separate experiments with error bars indicating the standard deviation. Each compound was tested in glucose free media (dotted bars) and in 10 mM glucose (striped bars).

A limitation of this assay is that it is not able to distinguish between cell uptake and membrane association. Further studies could be performed to distinguish between these two possibilities, but given the low level of activity associated with the cells, this is not really worthwhile, as the level at which they are being taken up (if at all) is too low to be useful in the context of a

References begin on Pg 127

molecular imaging agent. The mechanism by which they are being taken up (if at all) is not the same as that used for glucose, meaning the uptake will not increase in cells overexpressing glucose transporters. This is a necessary requirement for a cancer-targeting molecular imaging agent so as to get selective enhancement of uptake in the area to be imaged.

These same uptake tests were performed by Schibli and coworkers on the long-chain glucose based compounds (Figure 4.2) discussed in Chapter 4.1.[5] Their experiments were performed in HT29 cells, a human colon cancer cell line also known to overexpress GLUT-1.[5] As these experiments were performed in different cells in a different place, there may be some variation between the data sets. The uptake percentage values obtained for all the long chain compounds are quite similar, with the two glucose analogues found to have cell uptakes of 0.1 – 0.2 % of the activity to which they were exposed.[5] These uptake values did not vary significantly with the presence of glucose, the concentration of test compound, or the presence of a GLUT-1 inhibitor, meaning that the uptake observed is not due to GLUT-1 mediated transport. It seems unlikely that there is a significant difference between GLUT-1 interactions of the glucose and glucosamine substituted bioconjugates of this type.

4.3.3 Hexokinase Inhibition Studies

Hexokinase is the first enzyme in the oxidative phosphorylation chain, and is responsible for transferring a phosphate group from ATP to the *C*-6 position of a hexose. The details of this were discussed in Chapter 1.3, and the reaction scheme is shown in Scheme 4.1. A convenient way to quantitate this process is to couple this phosphorylation to the next step in the oxidative phosphorylation chain where glucose-6-phosphate dehydrogenase dehydrates glucose-6-phosphate and, in the process, converts NAD^+ into NADH. NADH absorbs strongly at 340 nm, and this can be used to monitor the rate of the two reactions. Although the increase in absorbance observed at this wavelength is due to the production of NADH, the phosphorylation catalysed by hexokinase is the rate limiting step in this scheme and the production of NADH effectively reports the hexokinase reaction rate.

This assay examined the test compounds to see if they were able to perturb the hexokinase catalysed phosphorylation of glucose. Absorbance at 340 nm was monitored at 30 sec intervals to determine the reaction rate at a range of substrate (glucose) concentrations. This

References begin on Pg 127

was done in the absence and presence of various concentrations of test compound. The initial rates were taken from the linear portion of the A_{340} *vs.* time graphs (normally the first 210 – 240 sec), and these rates were plotted *vs.* glucose (substrate) concentration. This was done for all combinations of glucose and test compound concentrations. A Lineweaver-Burk plot[15] (1/[glucose] vs. $1/V_i$) was generated for each test compound and least squares fitting used to determine the trend line for each concentration of test compound (Figure 4.6a). The position at which the lines for each concentration of test compound cross gives information on the mechanism of inhibition. Lines intersecting at the y-axis indicate competitive inhibition, those at the x-axis indicate non-competitive inhibition, and lines that meet between the two show mixed inhibition.[16] To determine the inhibition constant, K_i, for each test compound a plot of [inhibitor] *vs.* [glucose]/V_i was prepared (Figure 4.6b), and a least squares line fitted to this data. The intercept of this line with the x axis is equal to the $-K_i$ value of the test compound.

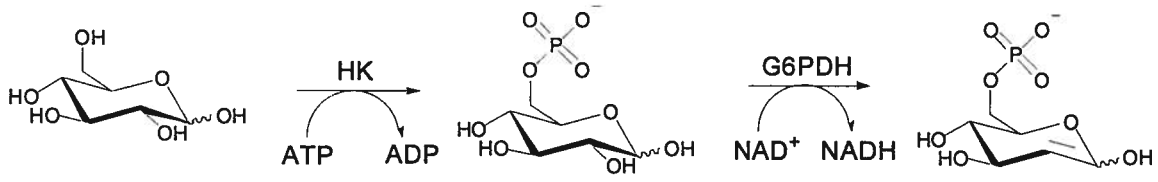

Scheme 4.1 Reaction scheme for phosphorylation of glucose by hexokinase (HK) and subsequent dehydration of the product by glucose-6-phosphate dehydrogenase (G6PDH).

The compounds tested in this work had Lineweaver Burk line intersection points close to the y axis, as can be seen for **C6L** in Figure 4.6a. This indicates either competitive inhibition or mixed inhibition with a large amount of competitive character is taking place. This means that the inhibitors must be able to bind to the active site of hexokinase. This is an excellent first step for these compounds, as if they are to be phosphorylated by hexokinase, they must be able to fit into the active site.

References begin on Pg 127

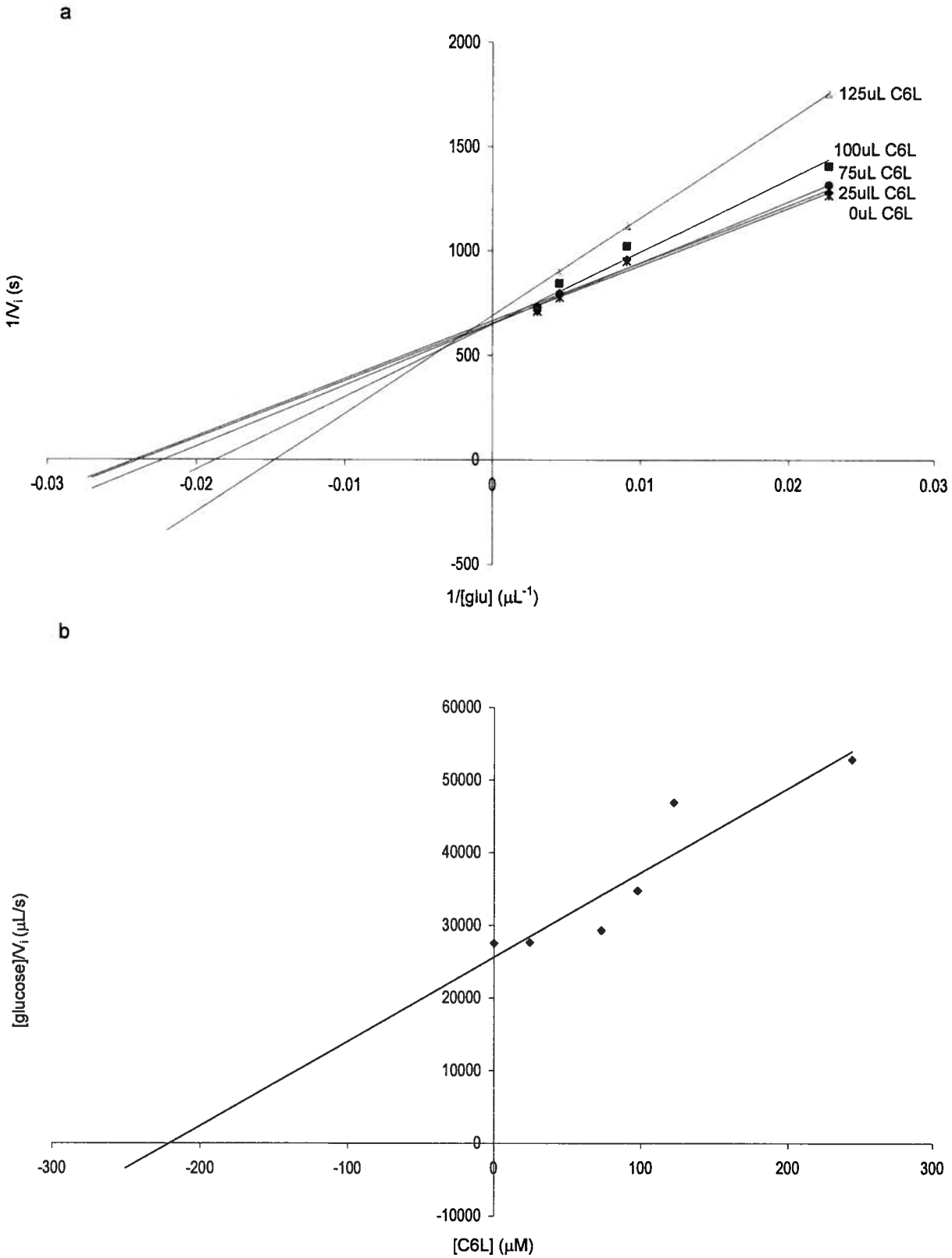

Figure 4.6 Plots showing data manipulation to determine K_i values: a) Lineweaver-Burk plot for **C6L**, b) K_i plot for **C6L**.

References begin on Pg 127

The C11 compounds were not tested in this assay due to solubility constraints. The C6 and C8 ligands and complexes that were tested all showed interaction with hexokinase: **C6L** $K_i = 220 \pm 30$ μM, **C6Re** $K_i = 500 \pm 60$ μM, **C8L** $K_i = 210 \pm 40$ μM, **C8Re** $K_i = 70 \pm 20$ μM. The two free ligands **C6L** and **C8L** have the same K_i values as each other, **C8Re** has a stronger interaction and **C6Re** a weaker interaction with hexokinase. We do not fully understand why this is the case. One possible reason **C8Re** exhibits a stronger interaction with hexokinase than **C8L** is that by coordinating the metal ion the chelating portion of the ligand becomes more ordered. The chelating arms no longer have the ability to rotate freely as they do in the ligand, so the metal complex may end up taking up less space. The reverse is seen for the C6 compounds where the ligand displays a stronger interaction with the enzyme than does the metal complex. Perhaps in this case the extra bulk added by the metal ion makes the compound too big to fit into the cleft. In the C6 compounds the metal binding moiety is closer to the active site than in the equivalent C8 compound, so making the complex bulkier would have a greater effect. It may also be that one of the compounds has a functional group in place to specifically interact with a residue on hexokinase, either in a favourable or an unfavourable manner.

This is a positive outcome for these compounds. Despite some minor differences between the test compounds, they all displayed μM inhibition constants with hexokinase. For comparison, FDG has an inhibition constant for hexokinase of 1060 μM.[17] The K_i values suggest that these compounds interact strongly enough with hexokinase to make it possible that they will be phosphorylated themselves.

Schibli and coworkers investigated the hexokinase inhibition properties of their glucose-based long chain conjugates and found results similar to what were found in this study.[5] They tested a range of compounds in their assay (see Figures 1.8, 1.9 and 1.10), the majority of which had short chains. The two long chain analogues (Figure 4.2) were the only ones that exhibited any appreciable inhibition of hexokinase. The PEGylated compound had $K_i = 250$ μM and the C8 compound $K_i = 5800$ μM.[5] The addition of two oxygen atoms in the alkyl linker chain changes the affinity for hexokinase by more than an order of magnitude.

The affinities of the long chain glucose and glucosamine analogues for hexokinase are very similar. Although the protocols for the two sets of experiments were the same, potential differences in equipment and experimental technique make it difficult to know how comparable

References begin on Pg 127

the data are. The glucosamine compounds seem to interact more strongly with the active site of hexokinase. Comparing the K_i values of the non-PEGylated glucose rhenium complex with that of **C8Re**, the glucosamine analogue has an interaction with hexokinase that is nearly two orders of magnitude stronger than the glucose compound (K_i = 70 *vs.* 5800 μM). As the PEGylated glucose compound has a much stronger interaction than its all carbon counterpart, this suggests that PEGylated glucosamine compounds could be worth investigating further.

4.3.4 Hexokinase Substrate Studies

Four compounds were tested in this assay: **C6L**, **C8L** and their respective [$Re(CO)_3$] complexes. Unfortunately none of them showed any significant phosphorylation by hexokinase. The assay solutions were examined using ESI-MS to search for any trace of phosphorylated species not detected by the HPLC assay. Although the concentrations involved were extremely low, the rhenium isotope pattern is a good handle to identify the metal complexes. Unfortunately no evidence of any phosphorylated products were seen. In combination with the HPLC results which show no significant ADP production above the hydrolysis levels of the control samples, these results suggest that no appreciable phosphorylation is occurring.

As discussed in Chapters 4.1 and 1.3, when hexokinase phosphorylates a substrate the two domains of the enzyme rotate together around the active site, narrowing the cleft in the middle. For a compound to be a competitive inhibitor of glucose phosphorylation it only has to bind to the open conformation of hexokinase; the cleft does not have to close. For a compound to be a substrate of hexokinase, the cleft needs to be able to close around the molecule in the active site in order for the phosphate group to be transferred. This could explain why the compounds examined in this Chapter can inhibit hexokinase in a manner that suggests they interact with its active site, but cannot themselves be phosphorylated.

4.3.5 MTT Assay

3-(4,5-Dimethylthiazol-2-yl)-2,5-diphenyltetrazolium bromide (MTT) is a yellow compound that is metabolized by mitochondrial reductase in living cells to purple formazan (Figure 4.7a). The purple colour is quantified by measuring absorbance at 570 nm (A_{570}). MTT metabolism is used to indicate the number of viable cells, as the more living cells there are, the more dye is

References begin on Pg 127

metabolized and the darker the purple colour produced. A_{570} is compared between control wells with no test compound and wells with varying concentrations of test compound. The control wells are taken to have 100 % cell viability, and the relative percentage of viable cells in test wells on the same plate are calculated with respect to this.

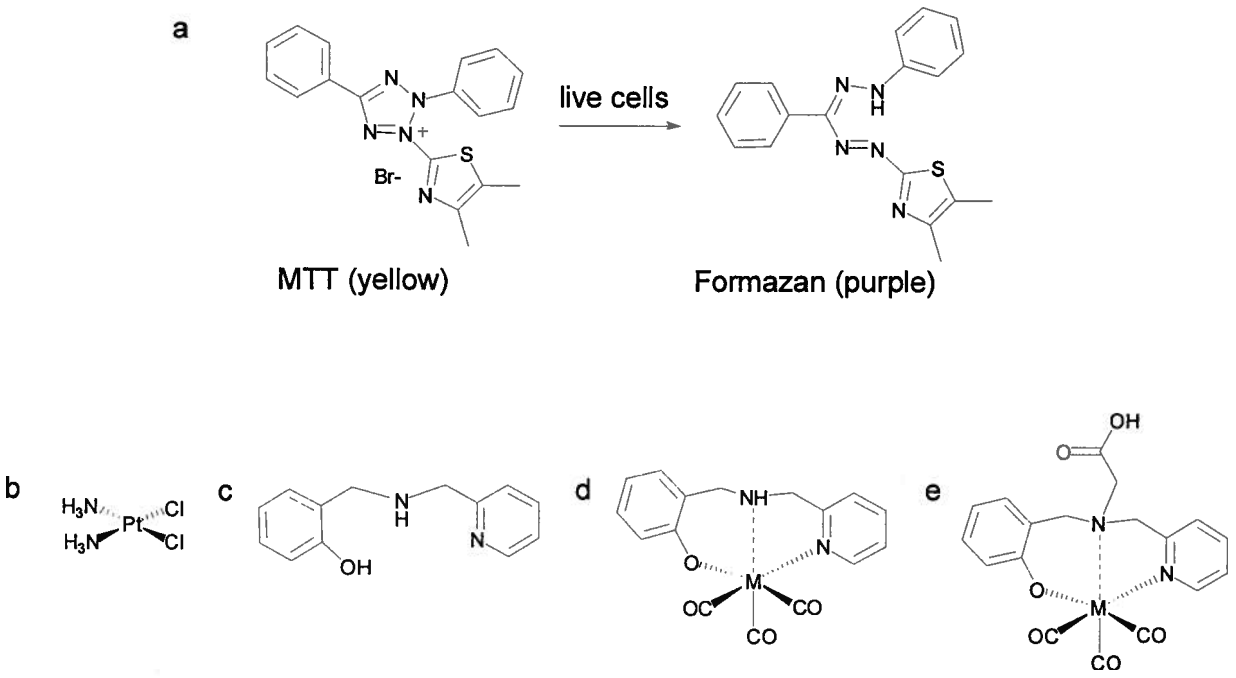

Figure 4.7 a) MTT dye, and its purple metabolic product formazan; b – e) compounds tested for toxicity in an MTT assay but not shown in Figure 4.3 above: b) cisplatin c - e) possible fragments of the compounds in Figure 4.3.

Due to solubility problems, the C11 compound was not tested. The C6 and C8 ligands and rhenium complexes were tested, along with selected ligand fragments (Figure 4.7c-e). Toxicity is normally less important in radiopharmaceutical compounds than in other drugs. The concentrations administered are very low and diagnostics of this type need only be administered once or a few times, not chronically like most therapeutics. Understanding toxicity adds to our knowledge of how these compounds may behave *in vivo*, and as such, the more information that can be gathered the better.

None of the ligands or rhenium complexes tested were found to exhibit any toxicity up to the maximum concentrations tested. **C6L, C8L** and **C6Re** were tested to a concentration of 1 mM, and (due to solubility constraints) **C8Re** was tested up to 100 μM. The tridentate binding unit alone (Figure 4.7c) showed some toxicity, with an IC_{50} value of 158 mM. Although this binding

References begin on Pg 127

unit does show significant toxicity, it is two orders of magnitude less toxic than cisplatin (used as positive control, IC_{50} = 2.6 mM). Two analogues of this compound (Figure 4.7d and e) were tested and found not to be toxic. This tridentate ligand bound to $[Re(CO)_3]^+$ (Figure 4.8d) was found to be non-toxic to 200 μM, its solubility limit in aqueous solution. The same tridentate core but with ethanoic acid appended to the aliphatic nitrogen (Figure 4.7e) was found to be non-toxic to 1 mM. It is highly unlikely that the binding group that exhibited the measureable toxicity (Figure 4.7c) would ever form *in vivo*. The compound would be administered bound to $[^{99m}Tc(CO)_3]^+$, meaning formation of this group would require the decomplexation of the metal tricarbonyl core and the breaking of a C-N bond. Cysteine/histidine challenge experiments show that decomplexation of this tridentate ligand happens at a negligible rate, while the spontaneous breakage of such a C-N bond would be unprecedented. If degradation were to occur, it would likely be at the amide bond resulting in a pendant acid group, where this type of compound was found not to be toxic. The typical amount of a ^{99m}Tc complex injected into a patient is 800 MBq, ~ 45 pmol.[18] As this is distributed throughout the whole body, the concentration found in any one place, even sites of preferential accumulation, would be so low that chemical toxicity is not of great concern.

4.4 Conclusion

This chapter details the formation and *in vitro* assays of long chain glucosamine-based tridentate ligands. Unfortunately these compounds are not transported or phosphorylated as carbohydrate analogues. In synthesising these metal chelates, the sugar has been modified to such an extent that it is no longer enzymatically recognized as such. It is not known how much change is too much, but work like that shown here aims to determine, and take advantage of, these acceptable limits. These compounds are much bigger than a monosaccharide, as shown in Figure 4.8. Comparing the molecular weights, glucosamine is 179 $g.mol^{-1}$, **C6^{99m}Tc** (the lightest metal conjugate made in this work) is 683 $g.mol^{-1}$, and **C11Re** (the heaviest metal complex made in this work) is 829 $g.mol^{-1}$. Glucosamine consists of one six membered ring; these metal complexes comprise three six membered rings with a heavy metal atom and a long carbon linker. As the linker length is required for the hexokinase activity, it may be advantageous to decrease the size of the metal chelating portion.

References begin on Pg 127

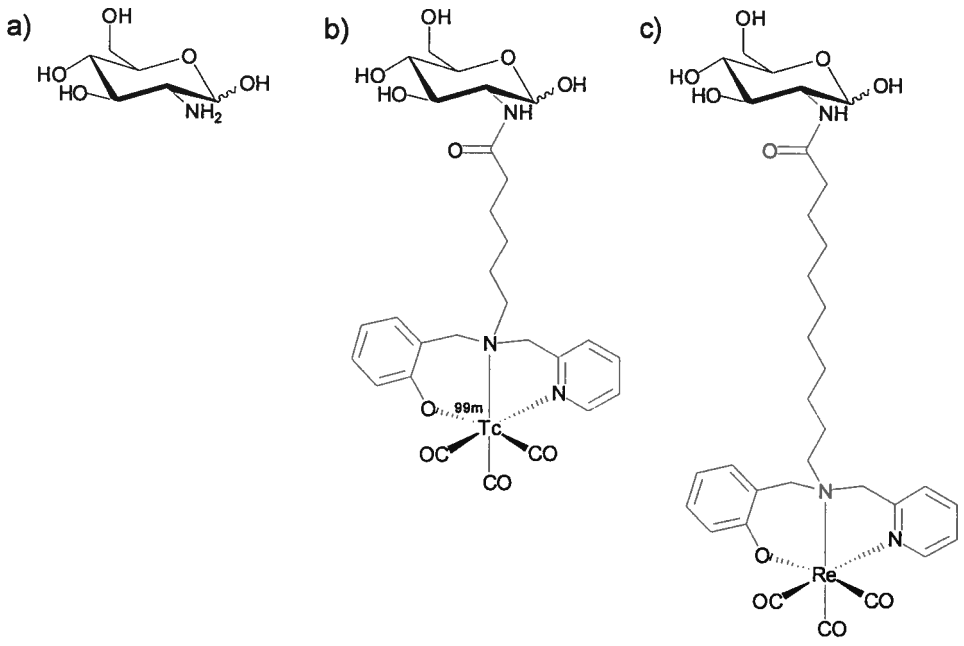

Figure 4.8 Size comparison of a) glucosamine, MW 179 g.mol^{-1} b) **C6^{99m}Tc**, MW 683 g.mol^{-1} and c) **C11Re**, MW 829 g.mol^{-1}.

Strong metal binding can be achieved with smaller chelating arms provided a tridentate binding sphere is maintained.[19] The thymidine kinase and amino acid long chain conjugates (Figure 4.1) discussed in the Introduction to this Chapter both have small tridentate binding spheres and retain at least some of the biological recognition of the parent compounds.[1, 2] The stability of these compounds was found to be adequate, with the thymidine kinase mimics remaining at least 95 % intact after incubation for 24 hr in PBS buffer,[1] and the amino acid analogue being stable for 24 hr in serum.[2]

Both these bioconjugates (in Figure 4.1) have a carbon chain of a significant size with respect to the overall size of the molecule as a spacer between the recognition part of the molecule and the metal chelate. The distance between the two portions of the molecule is proposed to allow the biologically active part to be recognized as a substrate, while the labelled part is far enough away not to interfere with this process. Although the recognition and catalytic mechanisms of each enzyme are different, these findings reinforce the merit in our approach to the long chain glucosamine conjugates.

References begin on Pg 127

4.5 References

1. Desbouis, D.; Struthers, H.; Spiwok, V.; Kuster, T.; Schibli, R., *J. Med. Chem.* **2008,** *51*, 6689 - 6698.

2. Liu, Y.; Pak, J. K.; Schmutz, P.; Bauwens, M.; Mertens, J.; Knight, H.; Alberto, R., *J. Am. Chem. Soc.* **2006,** *128*, 15996 - 15997.

3. Killian, D. M.; Chikhale, P. J., *Neurosci. Lett.* **2001,** *306*, 1 - 4.

4. Pardridge, W. M.; Oldendorf, W. H.; Cancilla, P.; Frank, H. J. L., *Ann. Intern. Med* **1986,** *105*, 82-95.

5. Schibli, R.; Dumas, C.; Petrig, J.; Spadola, L.; Scapozza, L.; Garcia-Garayoa, E.; Schubiger, P. A., *Bioconjugate Chem.* **2005,** *16*, 105 - 112.

6. Steitz, T. A.; Anderson, W. F.; Fletterick, R. J.; Anderson, C. M., *J. Biol. Chem.* **1977,** *252*, 4494 - 4500.

7. Speizer, L.; Haugland, R.; Kutchai, H., *Biochim. Biophys. Acta - Biomembranes* **1985,** *815*, 75-84.

8. Yoshioka, K.; Saito, M.; Oh, K.-B.; Nemoto, Y.; Matsuoka, H.; Natsume, M.; Abe, H., *Biosci. Biotech. Biochem.* **1996,** *60*, 1899 - 1901.

9. Kahlenbe, A.; Dolansky, D., *Can. J. Biochem.* **1972,** *50*, 638 - 643.

10. Speizer, L.; Richard, H.; Howard, K., *Biochim. Biophys. Acta* **1985,** *815*, 75 - 84.

11. Bowen, M. L.; Chen, Z.-F.; Roos, A.; Adam, M. J.; Orvig, C., manuscript in preparation.

12. Mosmann, T., *J. Immunol. Methods* **1983,** *65*, 55-63.

13. Wu, A.; Kennedy, D. C.; Patrick, B. O.; James, B. R., *Inorg. Chem.* **2003,** *42*, 7579-7586.

14. Lim, N. C.; Ewart, C. B.; Bowen, M. L.; Ferreira, C. L.; Barta, C. A.; Adam, M. J.; Orvig, C., *Inorg. Chem.* **2008,** *47*, 1337 - 1345.

15. Lineweaver, H.; Burk, D., *J. Am. Chem. Soc.* **1934,** *56*, 658 - 666.

16. Suzuki, Y.; Nakabayashi, Y.; Nakata, K.; Reed, J. C.; Takahashi, R., *J. Biol. Chem.* **2001,** *276*, 27058 - 27063.

17. Ferreira, C. L.; Ewart, C. B.; Bayly, S. R.; Patrick, B. O.; Steele, J.; Adam, M. J.; Orvig, C., *Inorg. Chem.* **2006,** *45*, 6979 - 6987.

18. Sampson, C. B., *Text Book of Radiopharmacy: Theory and Practice*. Taylor and Francis: Oxford, 1994; p 17.

19. Schibli, R.; La Bella, R.; Alberto, R.; Garcia-Garayoa, E.; Ortner, K.; Abram, U.; Schubiger, P. A., *Bioconjugate Chem.* **2000,** *11*, 345 - 351.

CHAPTER 5

Long Chain Glucosamine Cyclopentadienyl Ligands for the $[M(CO)_3]^+$ Core (M = Re, ^{99m}Tc)*

5.1 Introduction

Cyclopentadienyl (Cp^-) ligands have been shown to bind well to the $[M(CO)_3]^+$ (M = ^{99m}Tc, Re) core *via* a η^5 coordination mode to give 18-electron organometallic complexes.[1] These complexes are referred to as "piano stool" because of their shape, a flat Cp ring on top with three CO "legs" beneath. Cp ligands are monoanionic so the complexes they form with the monocationic metal tricarbonyl cores are neutral. These ligands are also attractive for their small size and lipophilicity, as well as the stability of the resulting complexes. The stability comes from the fact that these inert Tc(I) compounds have a low spin d^6 electronic configuration. The small size and lipophilicity can be exploited in the ability of complexes to fit into active sites of enzymes or for enhancing passive diffusion across membranes such as the blood brain barrier (BBB). For example, a long-chain fatty acid conjugate (Figure 5.1) has been labelled with $Cp^{99m}Tc(CO)_3$,[2] and was found to undergo beta-oxidation in the heart. Beta-oxidation is the process by which fatty acids are metabolized. They are broken down two carbon atoms at a time to produce acetyl-CoA, NADH and $FADH_2$.[3] The enzymes involved in beta-oxidation were able to utilize this bioconjugate as a substrate because the CpTc portion of the molecule was small enough not to significantly detract from the biological recognition and activity of the fatty acid portion.[2]

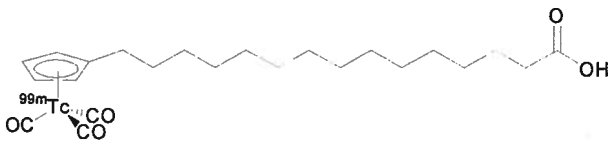

Figure 5.1 A $Cp^{99m}Tc$ conjugate that is metabolized by beta-oxidation in the heart.[2]

* A version of this chapter will be submitted for publication: Bowen, M. L., Adam, M. J., Orvig, C. Investigation of Long Chain Glucosamine-$[CpM(CO)_3]$ Complexes (M = Re, ^{99m}Tc) for Use in Molecular Imaging.

References begin on Pg 161

5.1.1 Synthesis of [CpM(CO)$_3$] Compounds

Cp^- is a widely used ligand known to bind to a range of metal ions with several different hapticities (normally 1, 3 or 5).[4] Its coordination to rhenium tricarbonyl has been known since the 1970's,[5] but very harsh reaction conditions were needed to make compounds of this type until relatively recently.[6] The introduction of a simple synthesis of $[^{99m}Tc(CO)_3(H_2O)_3]^+$ by Alberto and coworkers[7] has renewed interest in molecules of this type, and Cp complexes of this core are now an active field of investigation due to the favourable physical properties outlined above. Studies involve the functionalization of [CpM(CO)$_3$] complexes in a bid to affect their *in vivo* behaviour. There are two ways to functionalize a Cp-metal complex: either by functionalizing the Cp and then binding it to the metal, or by forming the metal-Cp complex and then adding functionality to that core. Within this framework there are many different methodologies that have been developed,[8] and the key ones are outlined below with a focus on the development of reaction types that are used in the syntheses carried out in this chapter.

The practical synthesis of $Cp^{99m}Tc$ complexes was pioneered in 1992 by Wenzel.[9, 10] A double ligand transfer (DLT) reaction was used (see Scheme 5.1a) to form ^{99m}Tc complexes from pertechnetate, a derivatized ferrocene and $Mn(CO)_5Br$ (as a carbonyl donor) at 150 °C in 30 – 90 % yield. The DLT is named as such because both the ligand types on the Re(I) in the reaction product were attached to different metal ions in the reactant species – both were transfered during the DLT reaction. Others have since remade these compounds for examination of their biodistribution,[11] and found that after heating at 150 °C for one hour and purifying the reaction mixtures by preparative TLC, only 20 – 25 % yield is reliably recoverable. Analysis of an aqueous solution 24 hr after synthesis, and the biodistribution of the compounds both strongly suggest the compounds are stable on the timescale relevant to imaging, both in aqueous solution and *in vivo*.

References begin on Pg 161

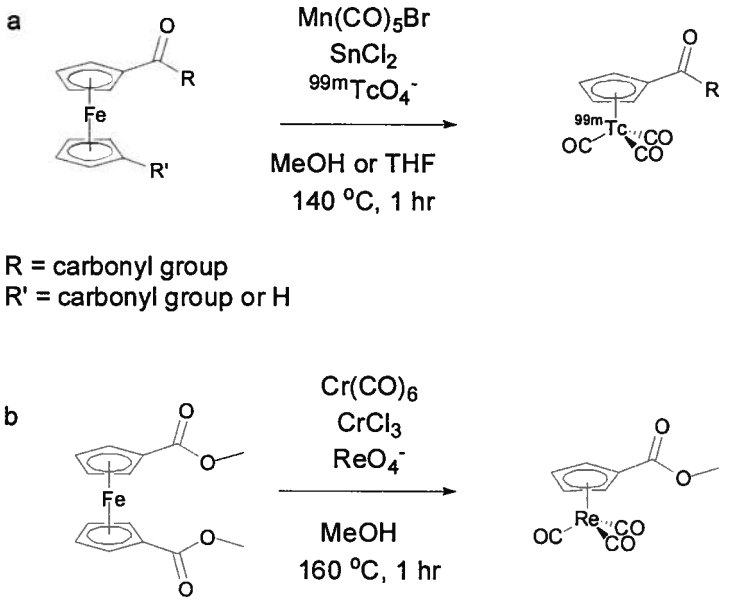

Scheme 5.1 Double Ligand Transfer (DLT) reaction: a) as pioneered by Wenzel[9] and b) as improved upon by Spradau and Katzenellenbogen.[12]

This DLT was improved upon and extended to rhenium by Spradau and Katzenellenbogen (Scheme 5.1b).[12] A major flaw in Wenzel's system that Katzenellenbogen addressed was that the Cp substituted Mn compound was also formed in the reaction, and was virtually impossible to separate from the desired ^{99m}Tc product, thus reducing the specific activity of the ^{99m}Tc compound. The modifications made by Katzenellenbogen included the use of $Cr(CO)_6$ as a CO source, and extensive optimization of solvents, temperatures, Cp substitution patterns and other additives.[12] Although this system works well for the synthesis of simple Re precursors like the one shown in Scheme 5.1a, which can then be coupled to other molecules of interest (as we have done in this work), the harsh experimental conditions preclude its widespread application. The reaction only produces useful yields when performed in methanol, meaning it cannot currently be used for radiochemistry where aqueous conditions are the norm. Another requirement that limits its usefulness is the need for the Cp ring that is transfered in the reaction to have an electron withdrawing group attached. The importance of this electron withdrawing group can be understood by examination of the proposed reaction mechanism (Scheme 5.2). The ring that is transfered in the course of the reaction has to bridge the two metals involved, and transfer from the iron of ferrocene to the rhenium carbonyl centre. The electron withdrawing group is proposed to stabilize intermediate **A** (in Scheme 5.2) where the Cp is bridging the two metal centres.[12]

References begin on Pg 161

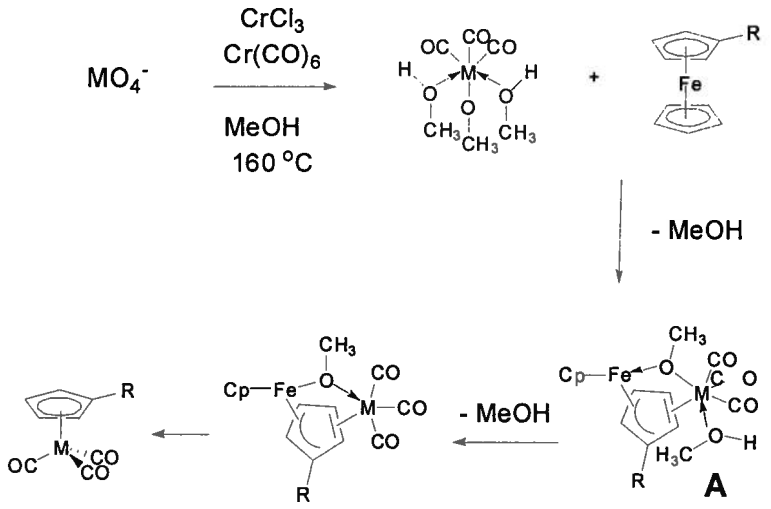

Scheme 5.2 Proposed mechanism of ring transfer in the DLT reaction.[12] The first step involves reduction of the metal centre and transfer of the CO ligands. This is followed by a multistep transmetallation sequence that tranfers the substituted Cp ring from the ferrocene to the other metal centre,[12] M = ^{99m}Tc, Re.

An alternative to the DLT is the single ligand transfer reaction (SLT), where the carbonyl ligands are already attached to the metal ion of interest, and only the Cp ligand transfers during the reaction. When an SLT reaction between $[Re(CO)_6]^+$ and acetylferrocene was performed in water alone no desired product was observed, but in a 1:1 mixture of DMSO and water, 60 % yield was obtained (Scheme 5.3a).[13] The DLT does not have this range of solvent availability due to the CO transfer step requiring donation from the bulk solvent, meaning it is limited to MeOH, and is therefore not readily transferable to the synthesis of radiopharmaceuticals.[12] The SLT with $[Re(CO)_6]^+$ is proposed to occur via two steps; the substitution of three carbonyl ligands with solvent molecules, followed by Cp exchange, as for the DLT mechanism shown above (Scheme 5.2). The observations in this work support the mechanism of ring exchange proposed above in the DLT reaction (see Scheme 5.2), where η^5 to η^3 ring slippage of the Cp gives it the ability to coordinate to the tricarbonyl metal centre and subsequent transmetallation results in the product.

References begin on Pg 161

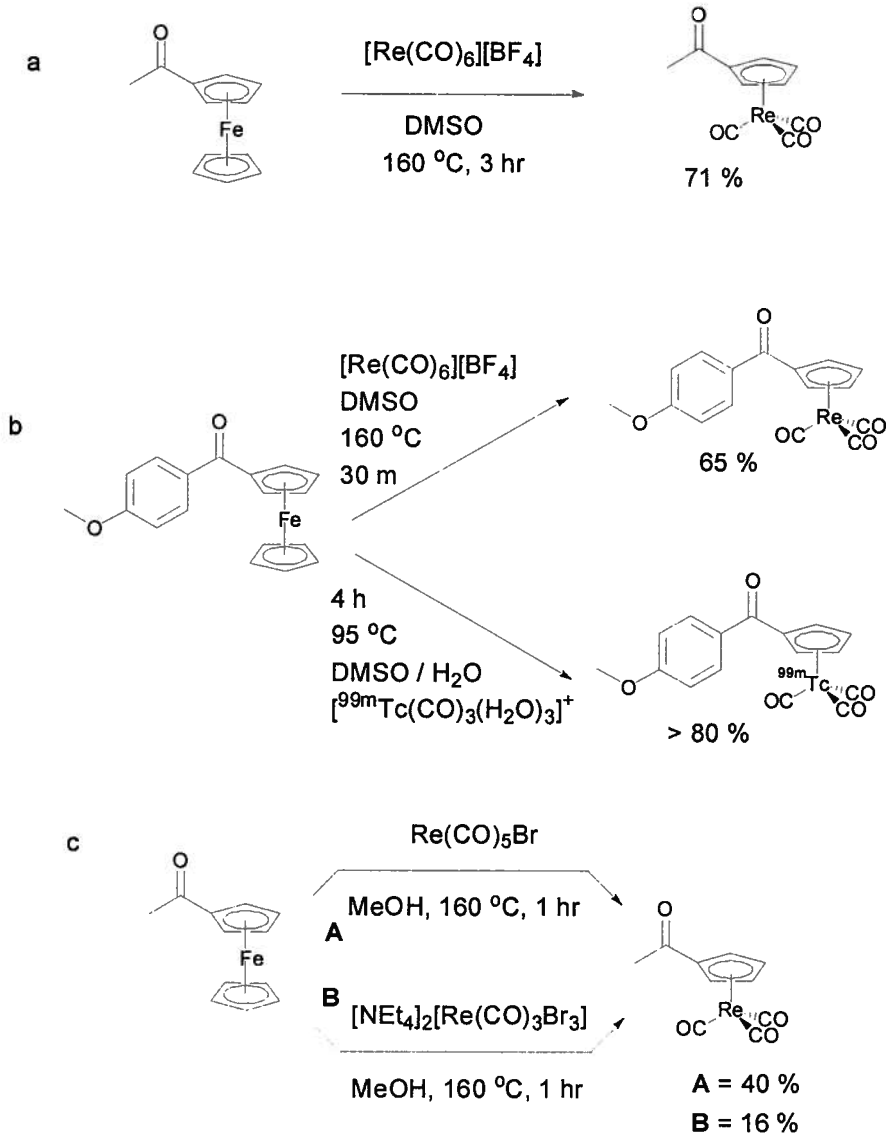

Scheme 5.3 Single Ligand Tranfer (SLT) reactions: a) using $[Re(CO)_6]^+$ starting materials[13] b) illustrating the difference in reaction conditions and yields between rhenium and technetium[14] c) lower yields result when using alternative rhenium starting materials.[15]

As this SLT reaction was proposed to go via a $[M(CO)_3(solvent)_3]^+$ intermediate, Jaouen, Alberto and coworkers attempted to extend it to the $[^{99m}Tc(CO)_3(H_2O)_3]^+$ core.[14] This would enable transfer of a substituted Cp ring from the iron centre of ferrocene directly to the $[M(CO)_3]^+$ core (Scheme 5.3b).[14] For the ^{99m}Tc reaction, the authors successfully used $[^{99m}Tc(CO)_3(H_2O)_3]^+$ as a precursor, and the reaction proceeded in the presence of water in good yield.[14] DMSO was needed to solubilize the ferrocene precursor so the reaction was performed in 1:1 DMSO:H_2O.[14] For the non-radioactive chemistry, the $[Re(CO)_6][BF_4]$ precursor was used and the reaction was carried out in DMSO due to the high temperature

References begin on Pg 161

requirements of the reaction.[14] No discussion is made of starting with the $[Re(CO)_3(H_2O)_3]^+$ precursor.[14]

The Orvig group[15] has also attempted to extend the scope of the SLT reaction to allow the use of commercially available ($[Re(CO)_5Br]$) or easily accessible ($[NEt_4]_2[Re(CO)_3Br_3]$)[16] starting materials. Although some success was achieved with these substrates in the SLT reaction (Scheme 5.3c), the yields produced were lower than those attained using $[Re(CO)_6]^+$ as a starting material.[15]

Alberto and coworkers pioneered the use of substituents to lower the pKa of the Cp ring.[17] This allowed for a significant amount of the Cp to be deprotonated at pH 7.4, so the labelling reaction could take place under ideal radiochemical conditions.[17] This was achieved *via* addition of an acetyl, an electron withdrawing group, to the Cp ring, which increased the amount of conjugation in the system and lowered the pKa to 8.6.[17] This meant ~5 % of the Cp rings were deprotonated at pH 7.4.[17] The substituted cyclopentadienyls were synthesized by reacting NaCp with the appropriately substituted ester (with loss of the alcohol portion of the ester) in yields of 50 - 60 % (Scheme 5.4a).[17] Once substituted, these Cp derivatives were found to be water soluble and relatively stable.[17] To form the metal complexes, the tricarbonyl precursor and the substituted NaCp were stirred in buffer (pH 7.4) at 85 °C for 2 hr.[17] The yields for the formation of the rhenium complexes were around 20 %, which the authors propose to be low due to competing metal cluster formation.[17] The analogous ^{99m}Tc reaction proceeds in 15 min at 90 °C to give a quantitative yield of the desired product (Scheme 5.4a).[17] These compounds were all found to be stable in solution for 24 hr at 37 °C.[17]

The three component procedure (Scheme 5.4b) was discovered by Minutolo and Katzenellenbogen, who found they could add three components together in one pot to obtain their desired products in good yields.[18] The Cp starting material for this reaction is a diaza substituted Cp, which upon reaction with a nucleophile in the presence of the metal tricarbonyl core produces the nucleophile-substituted Cp bound to the metal.[18] This reaction requires the use of relatively mild conditions: 85 °C for 45 min.[18] The yields vary depending on the nucleophile, ranging from 53 - 72 % isolated yield for the substituted rhenium complexes.[18] The drawbacks to this approach are the reactivity of the diaza starting material

References begin on Pg 161

and the requirement of exchanging the Br^- counterion of the rhenium starting metal to prevent bromination of the Cp ring (unless that is the desired product).[8]

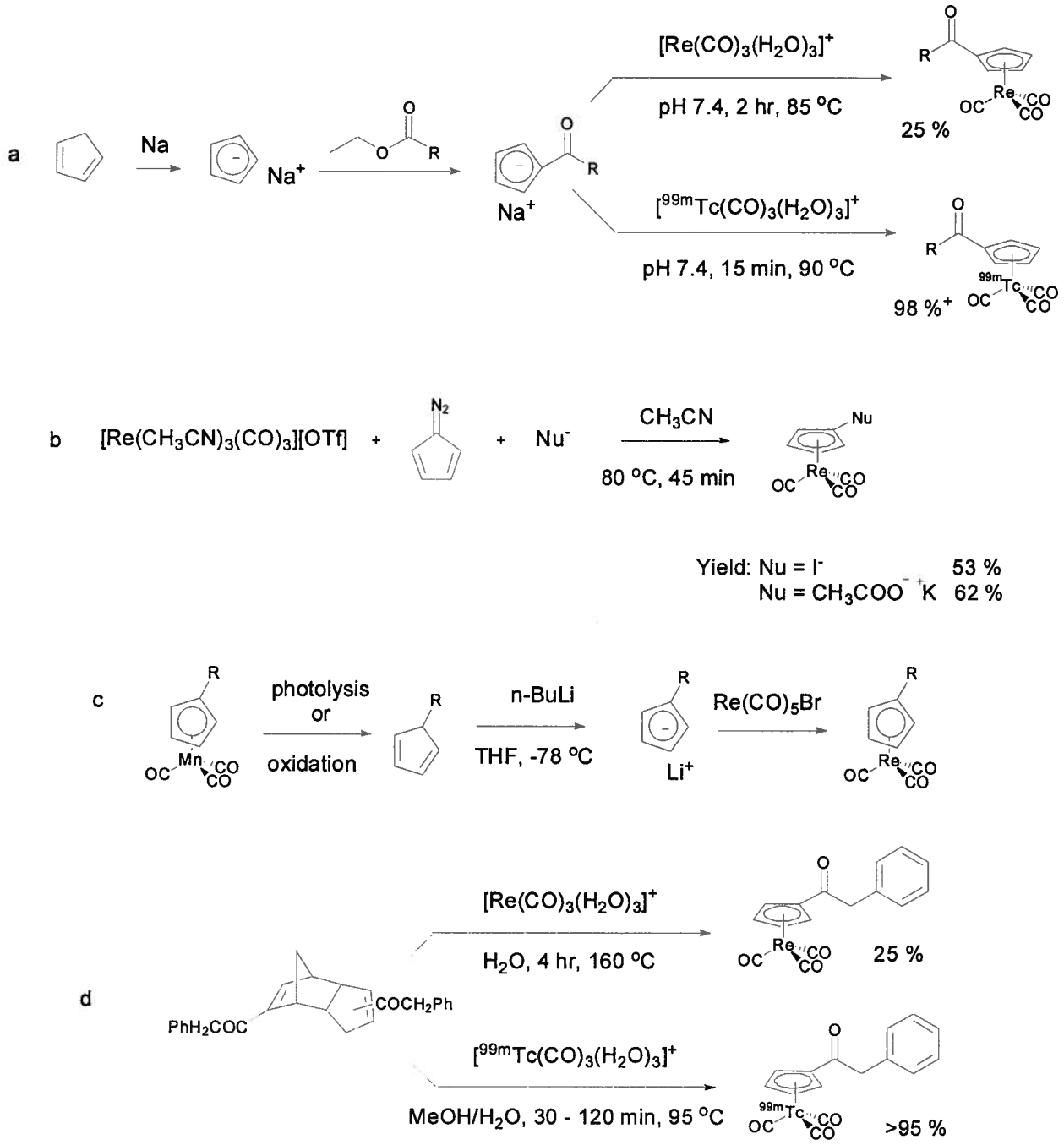

Scheme 5.4 Four alternative methods for forming $[CpM(CO)_3]$ complexes: a) deprotonation of a substituted Cp b) the three component system c) a decomplexation/recomplexation method and d) via a retro Diels-Alder reaction.

References begin on Pg 161

Jaouen and coworkers have utilized a method of decomplexation and recomplexation to make [CpRe(CO)$_3$] compounds (Scheme 5.4c).[19] They began with their functionalized Cp ligand bound to a metal ion (normally Mn) to stabilize it and allow for long-term storage.[19] The ligand is decomplexed *in situ* using light or oxidation, and following the addition of base and another metal ion, recomplexation occurs.[19, 20] This was applied to the synthesis of Re complexes to give ~ 45 % yield.[20] As well as the photolysis or oxidation inducer being necessary, this reaction also requires the use of *n*-BuLi at -78 °C,[20] which may preclude its widespread applicability. To our knowledge, details of the application of this method to radiochemistry with ^{99m}Tc have not been discussed.

Recently Alberto and coworkers have discovered a synthesis of [CpM(CO)$_3$] (M = Re, ^{99m}Tc) using a retro Diels-Alder (DA) reaction catalyzed by the metal ion which becomes substituted (Scheme 5.4d).[21] The synthesis of the [^{99m}Tc(CO)$_3$(H$_2$O)$_3$]$^+$ precursor can be performed *in situ* from [TcO$_4$]$^-$ and a reducing agent rather than requiring a two step reaction to make the precursor prior to addition of the proligand.[21] The authors have found that for the reaction to proceed, both the former diene and dienophile must be substituted with a weak metal binder like a carboxylate.[21] They observed a complete lack of free retro DA product (not metal coordinated).[21] These findings led the authors to conclude the mechanism of reaction first involves weak coordination of the dimerized ligand to the metal, followed by a metal-mediated retro DA reaction and η^5-Cp coordination.[21] The starting materials for this reaction can be made by either conjugating biomolecules to the acids on the DA dimerized product of (HCp-COOH)$_2$ (Thiele's acid), or by reacting NaCp with an ester of the desired targeting molecule and then dimerizing the resulting Cp.[21] By reacting the water sensitive NaCp to make a dimeric complex stable to both heat and water, the complexation reaction can take place in aqueous solution, as required for use in ^{99m}Tc labelling reactions (Scheme 5.4d).[21] The full scope of this reaction is yet to be explored, but work is continuing on labelling biomolecules and making polymer supported starting material to provide complexes with very high specific activities.[21]

There are some significant differences in the reactions of Cp with the tricarbonyl cores of rhenium compared to technetium (Scheme 5.3b and 5.4a,d). The difference between these two metals is much more noticeable in this area of chemistry than in the simple tridentate coordination chemistry seen in Chapters 3 and 4 of this thesis, where the two metals behaved

References begin on Pg 161

very similarly. The reasons for the differences in the Cp chemistry of the two metals seem to be a manifestation of their slightly different physical properties being exaggerated by the harsh reaction conditions required. The small differences in size and reactivity of rhenium and technetium combined with concentration differences in the tracer *vs.* macroscopic scales and solubility constraints of some starting materials lead to analogous compounds of the two congeners behaving quite differently. Details of this phenomenon, as applied to Cp chemistry, have not been thoroughly investigated to our knowledge.

5.1.2 Functionalization and Biological Studies of [CpM(CO)$_3$] Complexes

Jaouen and coworkers were pioneers in the field of protein labelling with the organometallic [CpM(CO)$_3$] core, reporting on the first such rhenium complex in 1993.[22] A Cp was substituted with an *N*-hydroxysuccinimide ester and was then bound to the metal centre, before reaction of the activated ester with free amines on the lysine sidechains of the protein.[22] Monoclonal antibody JOSS2-2 was found to retain satisfactory receptor recognition upon being labelled at 15 % of its available sites in this fashion.[22] The authors did not report any radioactive complexes, and the reaction times (15 hr)[22] do not lend themselves to radiochemistry. This was an important first step, and a key finding was the stability of the resulting compounds – no degradation was observed after incubation at 37 °C for 24 hr.[22]

The same researchers have applied the decomplexation/recomplexation method (Figure 5.5c) to the synthesis of rhenium-Cp tamoxifen derivatives (Figure 5.2a).[19, 20] They have gone on to make several derivatives and tested the rhenium compounds for their binding affinities to the estrogen receptors overexpressed in certain types of breast cancers.[23] The compound shown in Figure 5.2a showed the highest affinity of the compounds tested, with a relative binding affinity (compared to that of tamoxifen) of 31 ± 3 %.[23] Using computer modeling of the ligand binding sites of the receptors the researchers observed that the slightly larger size of the [CpRe(CO)$_3$] core compared to the phenyl group of tamoxifen is the cause of the decreased binding affinity.[23] The authors claim the need to find improved labelling reactions before being able to apply this work towards radioactive imaging agents.[23]

1-(2-Methoxyphenyl)-piperazine has been linked to a Cp ring, and the resulting ligand bound

to the tricarbonyl core (Figure 5.2b) via a deprotonation reaction (Scheme 5.3a).[24] A series of chain lengths were examined and were found to have a large effect on the recognition of the compounds.[24] The [CpRe(CO)$_3$] complex with a C_5 linker (Figure 5.2b) has a very high affinity *in vitro* (IC_{50} = 6 nM) for the 5-HT_{1A} serotonergic receptor.[24] This is of interest in imaging brain function as it has been linked to mental conditions such as anxiety and depression.[25] An analogous complex, but with the metal bound via a bidentate *N,N*-chelate rather than a Cp was also investigated, and was found to have an IC_{50} value of 5 ± 2 nM for the 5-HT_{1A} receptor *in vitro*.[26] Affinities of the two compounds are essentially the same, so in this case the use of Cp does not seem to confer any real advantages to the metal complex, though *in vivo* testing would be required to compare properties like BBB permeability.

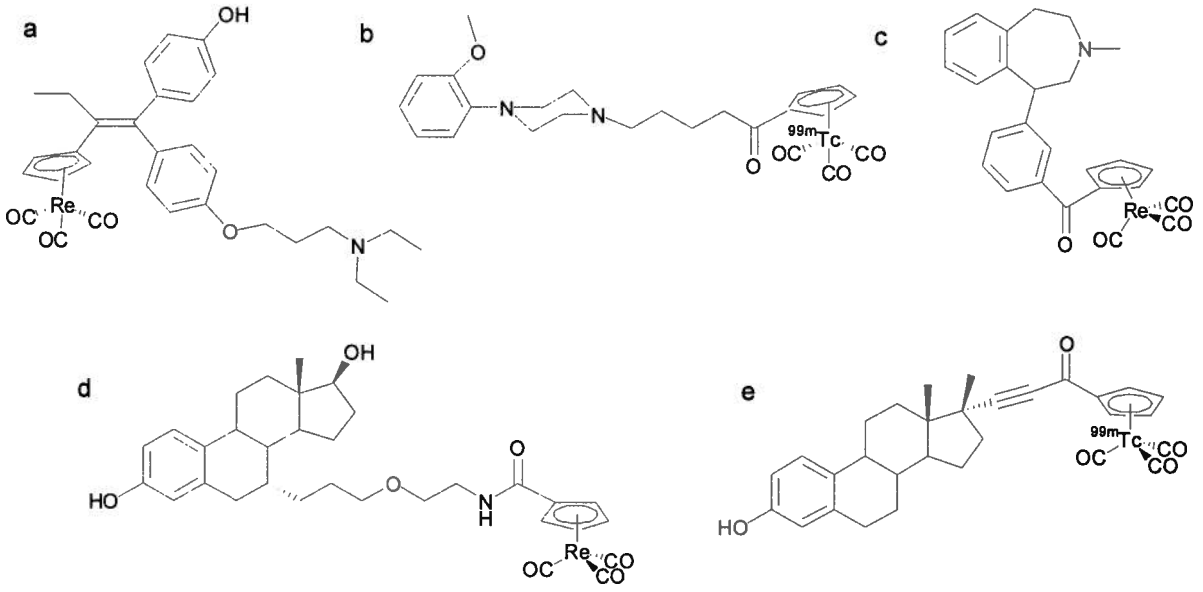

Figure 5.2 Some bioconjugates of the [CpM(CO)$_3$] core: a) a tamoxifen derivative made via a decomplexation/recomplexation reaction[20] b) a 1-(2-methoxyphenyl)-piperazine conjugate – a 5-HT_{1A} receptor ligand[24] c) a D_1 dopamine receptor ligand analogue[27] d) an estradiol analogue made via an amide coupling to the rhenium precursor[28] e) an alternatively linked ethynylestradiol analogue made via a SLT reaction.[14]

Known dopamine D_1 receptor ligands have been labelled with the [CpRe(CO)$_3$] core (Figure 5.2c).[27] The addition of the –$COC_5H_4Re(CO)_3$ group to the native ligand reduced the receptor affinity by half, but increased its selectivity for D_1 over other similar receptor types, showing promise as a target for ^{99m}Tc based imaging.[27] The authors claim this is a model for the ^{99m}Tc complex, but this extension has not, to our knowledge, been published. As the rhenium compound is made via an indirect and somewhat circuitous route, this synthesis is

References begin on Pg 161

not readily applicable to radiolabelling, and the ^{99m}Tc reaction may not have been developed. Steroid derivatives have been of interest in the field of molecular imaging for quite some time, and the Cp analogues of various steroids have been made.[1] Estradiol is of particular interest in imaging estrogen receptors overexpressed in many types of breast cancer.[14] A series of estradiol derivatives bound to various chemical forms of rhenium have been studied.[28] The Cp-Re analogues of interest here were synthesized via an indirect route, where the rhenium-Cp complex was made and then coupled to the functionalized steroid to give the bioconjugate.[28] The position of substitution on the estradiol and the type and length of the linker to the metal ion are both very important.[28] A 35 % binding affinity relative to estradiol (normalized to 100 %) could be achieved with a 7α substituion and a medium sized linker (Figure 5.2d).[28, 29] The analogous ligand with a thioether *S,S*-bidentate binding moiety was also synthesized, and was found to have inferior biological properties compared with its Cp counterpart.[29] The bidentate complex showed a relative binding affinity of 12 % compared to the analogous Cp compound (with no *O* in the linker compared to the one shown in Figure 5.2d) with an affinity of 29 %.[29] The authors do not speculate as to why such large differences are observed between the compounds. Others have suggested several factors that could contribute to this difference;[1] coordination of the bidentate thiol gives diastereomeric complexes which will have different biological properties to each other, and the coordination of Br^- to fill out the octahedral binding sphere increases the bulk at the metal centre.[1] Preliminary biodistributions of these very non-polar compounds showed high non-specific binding, proposed to be due to their high lipophilicities.[28] This study illustrates the large changes in *in vitro* properties that can be brought about by relatively small adjustments such as the substitution of a Cp ring for a bidentate chelate.

A different set of estradiol derivatives was made via a SLT reaction from the appropriately substituted ferrocene and either $[^{99m}Tc(CO)_3(H_2O)_3]^+$ or $[Re(CO)_6][BF_4]$ (Figure 5.2e).[14] The rhenium reaction occurred in moderate yield in DMSO at 130 °C after 1 hr, whereas the ^{99m}Tc reaction took place at lower temperatures – a nearly quantitative yield was achieved after 3.5 hr at 95 °C in 1:1 H_2O: DMSO.[14] The estradiol-substituted Cp ring transfered in better yield than the acetylferrocene that was used in the test rection,[14] suggesting steric bulk is well tolerated in this reaction. Also of note is that the SLT to the rhenium required protecting groups on the hydroxyl functionality of the steroid, whereas for the technetium reaction an excellent yield was obtained without the need for such protection.[14] These

References begin on Pg 161

reaction conditions were adapted for the ^{99m}Tc-glucosamine conjugates in this chapter.

Two glucosamine appended Cp ligands (Figure 5.3) and their Re and ^{99m}Tc tricarbonyl complexes were made previously in the Orvig group.[15] Their ability to inhibit the phosphorylation of glucose by hexokinase was examined, and they were found to be competitive inhibitors of this process, with the most efficacious (Figure 5.3, R = H, M = Re) having K_i = 330 ± 70 μM. This suggests that the small size of the Cp ligand may indeed be beneficial in helping to retain some activity of the carbohydrate *in vivo*. The compounds were assayed to determine whether they could themselves be phosphorylated by hexokinase, but unfortunately they were found not to be substrates.

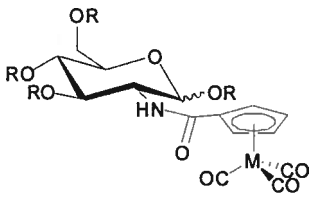

Figure 5.3 Cyclopentadienyl ligands functionalized with glucosamine ligands (R = H, Ac), and bound to the tricarbonyl core (M = Re, ^{99m}Tc).[15]

The current project builds on the promising results of this initial study and further probes the usefulness of compounds with a long alkyl linker between the carbohydrate and the metal chelate. As detailed in Chapters 1.3 and 4.1, the distance between the relatively bulky metal chelate and the carbohydrate (the part expected to interact with key enzymes) is crucial to retaining hexokinase's recognition of the modified compounds. Thus the purpose of this work was to combine the long chain linkers used in Chapter 4 with a significantly smaller metal binding sphere (Cp), with the aim of retaining key biological activities.

5.2 Experimental

5.2.1 Instruments and Materials

All solvents and chemicals were reagent grade and were used as received unless stated otherwise. Reagents were purchased from Acros unless otherwise stated. Solvents were HPLC

grade, and were purchased from Fisher Scientific. Dichloromethane was dried in a solvent purification tower, and was used as dispensed. Hydrogen and argon were purchased from Praxair. Isolink™ kits were provided by Mallinckrodt Inc. (now Covidien). $Na^{99m}TcO_4$ was provided by the Nuclear Medicine Department at the University of British Columbia Hospital.

Tricarbonyl(cyclopentadienylcarboxylic acid)rhenium was made in three steps from 1,1'-ferrocenedicarboxylic acid, according to literature procedures.[12, 30] 8-((*N,N*-Dibenzylamino)octylamido)-1,3,4,6-tetraacetyl-2-deoxy-*D*-glucopyranose and 6-((*N,N*-dibenzylamino)hexylamido)-1,3,4,6-tetraacetyl-2-deoxy-*D*-glucopyranose were first synthesized by Dr. Z.-F. Chen under my supervision.[31]

The analytical TLC plates, which were aluminum backed ultra pure silica gel 60, 250 μm, and the flash column silica gel (standard grade, 60 Å, 32 - 63 mm) used were provided by Silicycle. ^1H and ^{13}C APT, 2D COSY, HMQC and HMBC spectra were recorded on a Bruker DRX400 instrument at ambient temperature. The NMR spectra are expressed on the δ scale and were referenced to the residual peaks of the deuterated solvent. Infrared spectra were recorded on a Nicolet 6700 FT-IR spectrophotometer in transmission mode between 400 and 4000 cm^{-1} at a resolution of ± 0.09 cm^{-1}. ESI mass spectra were recorded on a Micromass LCT instrument. High resolution mass spectra (Micromass LCT TOF-MS) were provided by the Analytical Services Facility, Department of Chemistry, University of British Columbia. HPLC analysis of cold compounds was done on a Phenomenex Synergi 4 μm Hydro-RP 80 Å column (250 x 4.6 mm) in a Waters WE 600 HPLC system equipped with a 2478 dual wavelength absorbance UV detector run using the Empower software package. HPLC analyses of radiolabelled complexes were performed on a Knauer Wellchrom K-1001 HPLC equipped with a K-2501 absorption detector and a Capintec radiometric well counter. A Phenomenex Synergi 4 μm Hydro-RP 80 Å column (250 x 4.6 mm) was used.

5.2.2 Synthesis

6-Amino-hexylamido-1,3,4,6-tetra-*O*-acetyl-2-deoxy-β-*D*-glucopyranose (1)

6-((*N,N*-Dibenzylamino)hexylamido)-1,3,4,6-tetra-*O*-acetyl-2-deoxy-*D*-β-glucopyranose (0.50 g, 0.78 mmol) was dissolved in glacial acetic acid (5 mL), and $Pd(OH)_2$ (0.30 g, 0.43 mmol) was added. The black suspension was stirred vigorously in a Parr hydrogenation bomb. The system

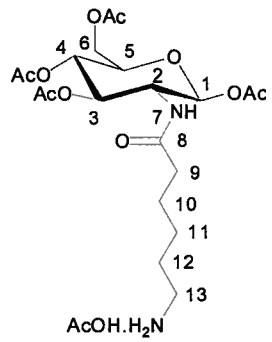

was filled with H_2 and purged three times, before being filled to 200 psi with H_2 and stirred at room temperature for four days. TLC and MS were used to confirm the absence of any benzylated materials, and then the mixture was filtered through celite and evacuated on a rotary evaporator. ^{1}H NMR spectroscopy showed that the material was pure enough to be used in the next step, and was also used to quantify the amount of acetic acid associated with the product to ensure enough base was added to neutralize this. A typical batch was a pale orange oil with two acetic acid molecules per product molecule (0.40 g, 89 % yield by ^{1}H NMR spectroscopy, used without further purification).

8-Amino-octylamido-1,3,4,6-tetra-*O*-acetyl-2-deoxy-*D*-β-glucopyranose (2)

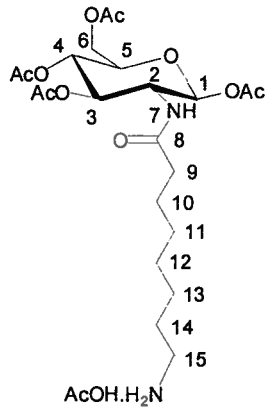

8-((*N,N*-Dibenzylamino)octylamido)-1,3,4,6-tetra-O-acetyl-2-deoxy-*D*-β-glucopyranose (0.29 g, 0.43 mmol) was hydrogenated over $Pd(OH)_2$ (0.30 g, 0.43 mmol) under 200 psi of H_2 in a manner similar to that used above. After five days the reaction mixture was filtered through celite, and the volume reduced on a rotary evaporator and used without further purification. ^{1}H NMR spectroscopy showed that the material was pure enough to be used in the next step, and quantified the amount of acetic acid present (normally around 2 equivalents per product molecule) to ensure enough base was added to neutralize this (0.37 mmol, 85 % crude yield by ^{1}H NMR spectroscopy).

Tricarbonyl{6-amino-hexylamido-*N*-(1,3,4,6-tetra-O-acetyl-2-amino-2-deoxy-β-D-glucopyranose)cyclopentadienyl carboxamide} rhenium (I) ($C6(Ac)_4Re$)

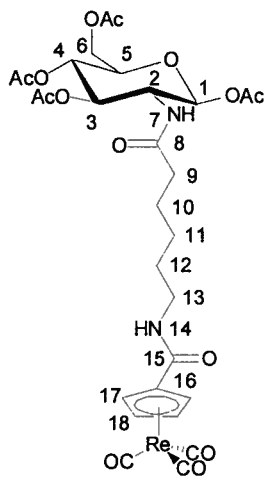

Tricarbonyl(cyclopentadienyl carboxylic acid)rhenium (0.058 g, 0.15 mmol) and 1-ethyl-3-(3-dimethylaminopropyl)carbodiimide hydrochloride (EDC) (0.044 g, 0.23 mmol) were dissolved in dry dichloromethane (5 mL). The flask was purged with argon for ten minutes and the resulting solution stirred at room temperature for three hours. 6-Amino-hexylamino-1,3,4,6-tetra-*O*-acetyl-2-deoxy-*D*-β-glucopyranose (**1**) (0.070 g, 0.090 mmol) in dry dichloromethane (3 mL) was added to the reaction mixture, followed by diisopropylethylamine (0.18 mL, 1.0 mmol). The resulting solution was stirred under inert atmosphere at room temperature for 24 hr.

References begin on Pg 161

The reaction mixture was washed twice with water (10 mL), once with brine (10 mL), and dried over $MgSO_4$. The drying agent was filtered out and the solution volume reduced on the rotary evaporator before purification by column chromatography on silica gel with 2 % methanol in dichloromethane as eluent. The solvent was removed *in vacuo* to give a colourless oil (17 mg, 14 % yield). ^{1}H NMR (DMSO-d_6, 400 MHz, δ): 8.17 (dd, $^3J_{14,13a}$ = 5.6 Hz, $^3J_{14.13b}$ = 5.6 Hz, 1H, *H14*), 7.92 (d, $^3J_{7,2}$ = 9.2 Hz, 1H, *H7*), 6.25 (dd, $^3J_{17,18a}$ = 2.4 Hz, $^3J_{17,18b}$ = 2.0 Hz, 2H, *H17*), 5.73 (d, $^3J_{1,2}$ = 7.2 Hz, 1H, *H1*), 5.70 (dd, $^3J_{18,17a}$ = 2.4 Hz, $^3J_{18,17b}$ = 1.6 Hz, 2H, *H18*), 5.18 (dd, $^3J_{3,2}$ = 10.0 Hz, $^3J_{3,4}$ = 10.0 Hz, 1H, *H3*), 4.88 (dd, $^3J_{4,3}$ = 10.0 Hz, $^3J_{4,5}$ = 10.0 Hz, 1H, *H4*), 4.19 (dd, $^3J_{6a,6b}$ = 12.8 Hz, $^3J_{6a,5}$ = 4.8 Hz, 1H, *H6a*), 3.96 (m, 3H, *H2,5,6b*), 3.09 (m, 2H, *H13*), 2.03, 2.00, 1.97, 1.94 (s, 3H, OCOC*H*$_3$, and 2H, *H9* overlapped), 1.42, (m, 4H, *H10,12*), 1.23 (m, 2H, *H11*). ^{13}C NMR (DMSO-d_6, 400 MHz, δ): 194.06 (Re-*C*O), 172.32 (*C8*), 169.96, 169.45, 169.20, 168.75 (O*C*OCH$_3$), 161.11 (*C15*), 96.15 (*C6*), 91.71 (*C1*), 87.05 (*C17*), 86.14 (*C18*), 72.13 (*C3*), 71.50 (*C5*), 68.10 (*C4*), 61.46 (*C6*), 51.77 (*C2*), 38.51 (*C13*), 35.39 (*C9*), 28.66 (*C12*), 25.69 (*C11*), 24.95 (*C10*), 20.43, 20.35, 20.26 (OCO*C*H$_3$). IR ν_{max} (cm^{-1}): 3305 (w, br), 2936 (w), 2359 (w), 2023 (s), 1916 (s), 1747 (s), 1643 (m), 1544 (m), 1388 (m), 1213 (s), 1034 (s), 737 (m), 596 (m), 511 (m). HR-MS (ES+ of MNa$^+$): m/z calcd for $C_{29}H_{35}N_2O_{14}{}^{187}$ReNa: 845.1544, found: 845.1567.

Tricarbonyl{8-amino-octylamido-*N*-(1,3,4,6-tetra-O-acetyl-2-amino-2-deoxy-β-D-glucopyranose)cyclopentadienyl carboxamide} rhenium (I) (C8(Ac)$_4$Re)

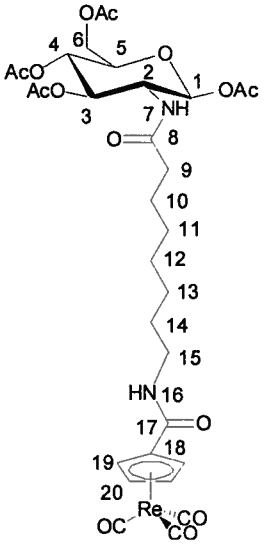

Tricarbonyl(cyclopentadienyl carboxylic acid)rhenium (0.024 g, 0.063 mmol) and 1-ethyl-3-(3-dimethylaminopropyl)carbodiimide hydrochloride (EDC) (0.015 g, 0.076 mmol) were dissolved in dry dichloromethane (5 mL). The flask was purged with argon and the resulting solution stirred at room temperature for four hours. 8-Amino-octylamido-1,3,4,6-tetra-*O*-acetyl-2-deoxy-*D*-β-glucopyranose (**2**) (0.070 g, 0.090 mmol) and diisopropylethylamine (0.18 mL, 1.0 mmol) were stirred in dry dichloromethane (2 mL) for 10 min, and then added to the activated acid solution. The resulting solution was stirred under inert atmosphere at room temperature overnight. Once TLC had confirmed the consumption of starting material, the solution was washed twice with water (7 mL), once with brine (10 mL), and dried over $MgSO_4$. The drying agent was filtered out and the solution reduced on the rotary evaporator before purification by column chromatography on silica gel with 1.5 % methanol in

References begin on Pg 161

dichloromethane as eluent. The solvent was removed *in vacuo* to give the product as a colourless oil (2 mg, 5 % yield). ^{1}H NMR (MeOH-d_4, 400 MHz, δ): 6.16 (dd, $^3J_{19,20a}$ = 2.3 Hz, $^3J_{19,20b}$ = 2.0 Hz, 2H, *H19*), 5.78 (d, $^3J_{1,2}$ = 8.6 Hz, 1H, *H1*), 5.57 (dd, $^3J_{20,19a}$ = 2.4 Hz, $^3J_{20,19b}$ = 2.4 Hz, 2H, *H20*), 5.28 (dd, $^3J_{3,2}$ = 10.6 Hz, $^3J_{3,4}$ = 9.4 Hz, 1H, *H3*), 5.02 (dd, $^3J_{4,3}$ = 9.4 Hz, $^3J_{4,5}$ = 10.2 Hz, 1H, *H4*), 4.28 (dd, $^3J_{6a,6b}$ = 12.5 Hz, $^3J_{6a,5}$ = 4.7 Hz, 1H, *H6a*), 4.10 (dd, $^3J_{6b,6a}$ = 12.5 Hz, $^3J_{6b,5}$ = 2.4 Hz, 1H, *H6b*), 4.06 (d, $^3J_{2,1}$ = 9.0 Hz, 1H, *H2*), 3.91 (ddd, $^3J_{5,6a}$ = 4.7 Hz, $^3J_{5,6b}$ = 2.3 Hz, $^3J_{5,4}$ = 10.2 Hz, 1H, *H5*), 3.26 (dd, $^3J_{15,14a}$ = 6.6 Hz, $^3J_{15,14b}$ = 6.6 Hz, 2H, *H15*), 2.13 (dd, $^3J_{9,8a}$ = 7.3 Hz, $^3J_{9,8b}$ = 7.3 Hz, 2H, *H9*), 2.07, 2.05, 2.01, 1.98 (s, 3H, OCOC*H*$_3$), 1.55, (m, 4H, *H10,14*), 1.29 (m, 6H, *H11,12,13*). ^{13}C NMR (MeOH-d_4, 100 MHz, δ): 194.34 (Re-*C*O), 176.65 (*C8*), 172.45, 171.82, 171.37, 170.74 (O*C*OCH$_3$), 164.86 (*C17*), 96.23 (*C18*), 93.51 (*C1*), 87.94, 87.91 (*C19*), 86.62, 86.59 (*C20*), 73.97 (*C5*), 73.91 (*C3*), 69.94 (*C4*), 63.10 (*C6*), 54.19 (*C2*), 40.64 (*C15*), 37.26 (*C9*), 30.51 (*C11*), 30.13 (*C13*), 30.12 (*C14*), 27.85 (*C12*), 26.90 (*C10*), 20.82, 20.79, 20.70 (OCO*C*H$_3$). IR ν_{max} (cm^{-1}): 3308 (w, br), 2931 (m), 2360 (s), 2341 (s), 2023 (s), 1920 (s), 1750 (s), 1646 (m), 1545 (m), 1218 (s), 1038 (m). HR-MS (ES+ of MNa$^+$): m/z calcd for $C_{31}H_{39}N_2O_{14}{}^{187}ReNa$: 873.1857, found: 873.1875.

6-Amino-hexylamino-*N*-(2-deoxy-β-*D*-glucopyranose) (3)

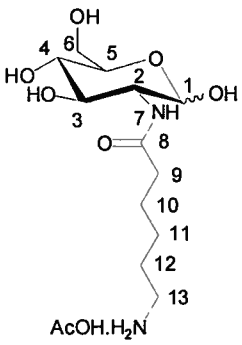

6-((*N,N*-Dibenzylamino)hexylamido)-1,3,4,6-tetra-*O*-acetyl-2-deoxy-*D*-β-glucopyranose (0.717 g, 1.12 mmol) was dissolved in methanol (15 mL). NaOMe (0.907 g, 16.8 mmol) was added, and the reaction mixture stirred at room temperature for 2 hr. Amberlite resin was added and the heterogeneous mixture stirred for 15 min before being filtered. The crude reaction mixture was purified by semi-preparative HPLC to give a pale brown oil (0.18 g, 32 % yield). The material obtained from the HPLC was dissolved in glacial acetic acid (5 mL) and added to a hydrogenation bomb with Pd(OH)$_2$ (0.18 g, 0.26 mmol). The bomb was sealed and purged with H_2 three times before being filled with H_2 to a pressure of 200 psi and the reaction mixture in the bomb stirred at room temperature for five days. The mixture was filtered through celite, washed with glacial acetic acid (10 mL) and evacuated on a rotary evaporator before being purified by semi-preparative HPLC. MS and ^{1}H NMR were used to confirm the nature of the oily product that resulted. The amount was estimated based on a comparison of the integration of the anomeric hydrogens with the CH_3 hydrogens of acetic acid.

References begin on Pg 161

8-Amino-octylamino-*N*-(2-deoxy-*D*-β-glucopyranose) (4)

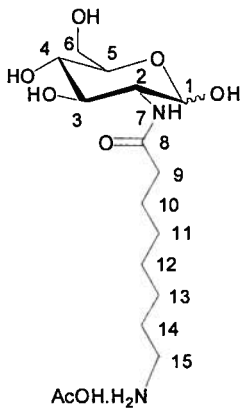

8-((*N,N*-Dibenzylamino)octylamido)-1,3,4,6-tetra-O-acetyl-2-deoxy-*D*-β-glucopyranose (0.256 g, 0.383 mmol) was dissolved in methanol (10 mL). NaOMe (0.207 g, 3.83 mmol) was added, and the reaction mixture stirred at room temperature for 4 hr. The reaction was quenched by stirring with Amberlite ion exchange resin for 10 min, filtered and purified by semi-preparative HPLC (0.090 g, 47 % yield). This product was transfered to a hydrogenation bomb with glacial acetic acid (5 mL) and $Pd(OH)_2$ (0.18 g, 0.26 mmol). The system was sealed and purged three times with hydrogen before being filled to a pressure of 200 psi and then stirred at room temperature for five days. The mixture was filtered through celite, washed with glacial acetic acid (10 mL) and evacuated on a rotary evaporator. MS and ^{1}H NMR spectroscopy were used to confirm the nature of the oily product that resulted. The amount was estimated based on a comparison of the integration of the anomeric hydrogens with the hydrogens of acetic acid.

Tricarbonyl{6-amino-hexylamido-*N*-(2-amino-2-deoxy-D-glucopyranose)cyclopentadienyl carboxamide} rhenium (I) (C6Re)

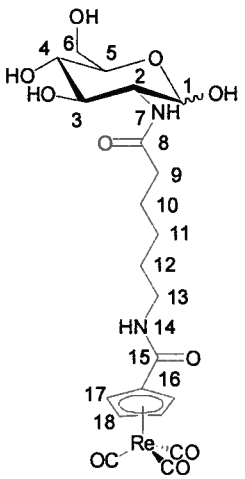

Tricarbonyl(cyclopentadienyl carboxylic acid)rhenium (0.074 g, 0.20 mmol) and N,N'-dicyclohexylcarbodiimide (DCC) (0.041 g, 0.20 mmol) were dissolved in dry dichloromethane (10 mL). Activated 4 Å molecular sieves were added, the flask was purged with argon and then stirred at room temperature for four hours. 6-Amino-hexylamino-*N*-(2-deoxy-β-*D*-glucopyranose) (**3**) (~0.009 g, 0.030 mmol, used as a crude oil from debenzylation reaction above) and diisopropylethylamine (1.0 mL, 5.7 mmol) were stirred in dimethylformamide (6 mL) for 10 min, before addition to the activated rhenium precursor solution. The resulting solution was stirred under inert atmosphere at room temperature for 40 hr. The reaction mixture was filtered, washed with dimethylformamide (5 mL), reduced on a rotary evaporator, taken up in dimethylsulfoxide (7 mL) and the resulting precipitate filtered off. The solution was purified by semi-preparative HPLC, and the solvent removed *in vacuo* to give a pale brown oil (0.0080 g, 41 % yield). ^{1}H NMR (MeOH-d_4, 400 MHz, δ): 6.16 (dd, $^3J_{17,18a}$ = 2.3 Hz, $^3J_{17,18b}$ = 2.2 Hz, 2H, *H17*), 5.57 (dd, $^3J_{18,17a}$ = 2.4 Hz, $^3J_{18,17b}$ = 2.2 Hz, 2H, *H18*), 5.10 (d, $^3J_{1,2}$ = 3.6 Hz, 0.8 H, *H1β*), 4.59 (d, $^3J_{1,2}$ = 8.4 Hz, 0.2 H, *H1α*), 3.82, 3.70, 3.31, 3.17 (m, 8H, *H2-6, α and β,H13*), 2.27 (t,

References begin on Pg 161

$^3J_{9,10a}$ = 7.6 Hz, $^3J_{9,10b}$ = 7.6 Hz, 2H, *H9*), 1.57, 1.35 (m, 8H, *H10-12*). ^{13}C NMR (MeOH-d_4, 100 MHz, δ): 194.36 (Re-*C*O), 175.24 (*C8*), 166.38 (*C15*), 97.22, 92.76 (*C1*), 93.92 (*C16*), 87.89 (*C17*), 86.63 (*C18*), 78.20, 78.05, 73.25, 72.75, 70.84 (*C3,4,5*), 63.01 (*C6*), 58.86, 55.99 (*C2*), 40.63, 40.60 (*C13*), 37.03 (*C9*), 32.11, 30.24, 27.62, 27.18, 26.73 (*C10,11,12*). IR ν_{max} (cm^{-1}): 3305 (m, br), 2931 (w), 2360 (m), 2341 (m), 2024 (s), 1921 (s), 1675 (m), 1639 (m), 1553 (m), 1203 (m), 1136 (m). HR-MS (ES+ of MNa^+): m/z calcd for $C_{21}H_{27}N_2O_{10}{}^{185}ReNa$: 675.1093, found: 675.1086.

Tricarbonyl{8-amino-octylamido-*N*-(2-amino-2-deoxy-D-glucopyranose)cyclopentadienyl carboxamide} rhenium (I) (C8Re)

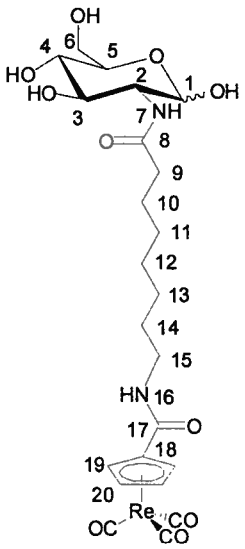

Tricarbonyl(cyclopentadienyl carboxylic acid)rhenium (0.085 g, 0.22 mmol) and dicyclohexylcarbodiimide (DCC) (0.052 g, 0.25 mmol) were dissolved in dry dichloromethane (5 mL). The flask was purged with argon and the resulting solution stirred at room temperature for 2.5 hr. 8-Amino-octylamino-*N*-(2-deoxy-*D*-β-glucopyranose) (**4**) (0.25 g, 0.23 mmol, as estimated from crude ^{1}H NMR studies of debenzylation reaction shown above) and diisopropylethylamine (0.74 mL, 4.5 mmol) were stirred in dimethylformamide (5 mL) for 10 min, before addition to the activated rhenium precursor. The resulting reaction mixture was stirred under inert atmosphere at room temperature for 40 hr, then the volume reduced on a rotary evaporator and the compound purified by semi-preparative HPLC. The solvent was removed *in vacuo* to give a pale brown oil (0.076 g, 50 % yield). ^{1}H NMR (MeOH-d_4, 400 MHz, δ): 6.16 (s, 2H, *H19*), 5.57 (s, 2H, *H20*), 5.10 (d, $^3J_{1,2}$ = 3.2 Hz, 0.75 H, *H1β*), 4.59 (d, $^3J_{1,2}$ = 8.4 Hz, 0.25 H, *H1α*), 3.73, 3.24 (m, 8H, *H2-6, α and β, H15*), 2.25 (dd, $^3J_{9,10a}$ = 7.4 Hz, $^3J_{9,10b}$ = 7.4 Hz, 2H, *H9*), 1.84 (m, 4H, *H10,14*), 1.39 (m, 6H, *H11,12,13*). ^{13}C NMR (MeOH-d_4, 100 MHz, δ): 193.80 (Re-*C*O), 176.33 (*C8*), 164.33 (*C17*), 96.78, 92.20 (*C1*), 95.63 (*C18*), 87.39 (*C19*), 86.07 (*C20*), 77.60, 75.64, 72.68, 72.19, 72.16, 71.88 (*C3,4,5*), 62.43 (*C6*), 58.27, 55.41 (*C2*), 40.28, 40.15 (*C15*), 36.96, 36.60 (*C9*), 29.91, 29.71, 29.65, 29.62, 29.38, 27.35, 26.48 (*C10,11,12,13,14*). IR ν_{max} (cm^{-1}): 3037 (w, br), 2934 (w), 2360 (s), 2341 (s), 2024 (s), 1921 (s), 1672 (m), 1636 (m), 1557 (w), 1201 (w), 1134 (w). HR-MS (ES+ of MNa^+): m/z calcd for $C_{23}H_{31}N_2O_{10}{}^{187}Re$ Na : 705.1434, found: 705.1420.

References begin on Pg 161

2-*N*-(6-Amino-hexylamido-1,3,4,6-tetra-O-acetyl-2-amino-2-deoxy-D-glucopyranose)-carboxamide -1-ferrocene (C6Fc)

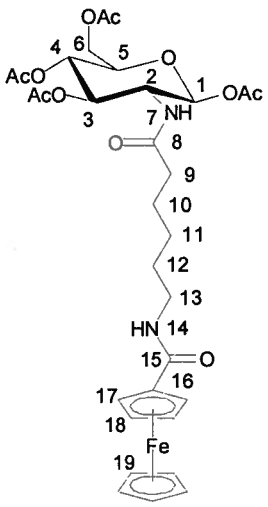

Ferrocenecarboxylic acid (0.359 g, 1.56 mmol) and 1-ethyl-3-(3-dimethylaminopropyl)carbodiimide hydrochloride (EDC) (0.329 g, 1.72 mmol) were dissolved in dry dichloromethane (10 mL). The flask was purged with argon and the resulting mixture stirred at room temperature for six hours. 6-Amino-hexylamido-1,3,4,6-tetra-*O*-acetyl-2-deoxy-*D*-β-glucopyranose (**1**) (amount of debenzylated product quantified by ^{1}H NMR, 1.40 mmol) and diisopropylethylamine (2.8 mL, 16 mmol) were stirred in dry dichloromethane (3 mL) for 10 min, before addition via syringe to the activated ferrocene. The resulting dark red-brown solution was stirred under inert atmosphere at room temperature for 40 hr. The solution was washed twice with water (2 x 10 mL), once with brine (15 mL), and dried over $MgSO_4$. The drying agent was filtered out and the solution reduced on the rotary evaporator before purification by column chromatography on silica gel with 1 % methanol in dichloromethane followed by 2.5 % methanol in dichloromethane as eluent. The solvent was removed *in vacuo* to give an orange oil (0.124 g, 12 % yield). ^{1}H NMR ($CDCl_3$, 400 MHz, δ): 6.05 (s, 1H, *H14*), 5.93 (d, $^3J_{7,2}$ = 9.0 Hz, 1H, *H7*), 5.75 (d, $^3J_{1,2}$ = 9.0 Hz, 1H, *H1*), 5.21 (dd, $^3J_{3,2}$ = 9.4 Hz, $^3J_{3,4}$ = 9.4 Hz, 1H, *H3*), 5.14 (dd, $^3J_{4,3}$ = 9.4 Hz, $^3J_{4,5}$ = 9.0 Hz, 1H, *H4*), 4.70 (dd, $^3J_{17,18a}$ = 2.0 Hz, $^3J_{17,18b}$ = 2.0 Hz, 2H, *H17*), 4.35 (dd, $^3J_{18,17a}$ = 2.0 Hz, $^3J_{18,17b}$ = 2.0 Hz, 2H, *H18*), 4.28 (m, 2H, *H2,6a*), 4.22 (s, 5H, *Cp-H*), 4.13 (dd, $^3J_{6b,6a}$ = 1.9 Hz, $^3J_{6b,5}$ = 12.4 Hz, 1H, *H6b*), 3.80 (ddd, $^3J_{5,4}$ = 9.8 Hz, $^3J_{5,6a}$ = 4.8 Hz, $^3J_{5,6b}$ = 2.3 Hz, 1H, *H5*), 3.37 (dd, $^3J_{13,12}$ = 6.6 Hz, $^3J_{13,12'}$ = 6.2 Hz, 2H, *H13*), 2.17 (dd, $^3J_{9,10}$ = 7.4 Hz, $^3J_{9,10'}$ = 7.4 Hz, 2H, *H9*), 2.10, 2.10, 2.04, 2.03 (s, 3H, OCOC*H*$_3$), 1.61 (m, 4H, *H10,12*), 1.38 (m, 2H, *H11*). ^{13}C NMR ($CDCl_3$, 100 MHz, δ): 173.00 (*C8*), 170.93, 170.91 (O*C*OCH$_3$), 169.38 169.20 (*C15*), 99.91 (*C1*), 92.51 (*C1*), 76.63 (*C16*), 72.82 (*C18*), 72.76 (*C17*), 70.32 (*C4*), 69.95 (*C19*), 68.04 (*C3*), 67.85 (*C5*), 61.60 (*C6*), 52.82 (*C2*), 38.92 (*C13*), 36.10 (*C9*), 29.16 (*C11*), 25.91 (*C12*), 24.56 (*C10*), 20.84, 20.65, 20.51 (OCO*C*H$_3$). IR ν_{max} (cm^{-1}): 3295 (w), 2934 (w), 1740 (s), 1633 (s), 1538 (s), 1366 (m), 1222 (m), 1035 (s). HR-MS (ES+ of MNa$^+$): m/z calcd for $C_{31}H_{40}{}^{56}FeN_2O_{11}Na$: 695.1879, found: 695.1895.

References begin on Pg 161

2-*N*-(8-Amino-octylamido-1,3,4,6-tetra-O-acetyl-2-amino-2-deoxy-D-glucopyranose)-carboxamide -1-ferrocene (C8Fc)

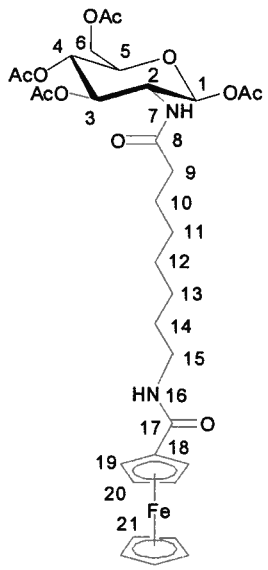

Ferrocenecarboxylic acid (0.050 g, 0.22 mmol) and 1-ethyl-3-(3-dimethylaminopropyl)carbodiimide hydrochloride (EDC) (0.046 g, 0.24 mmol) were dissolved in dry dichloromethane (8 mL). The flask was purged with argon and the resulting mixture stirred at room temperature for four hours. 8-Amino-octylamido-1,3,4,6-tetra-*O*-acetyl-2-deoxy-*D*-β-glucopyranose (**2**) (0.116 g, 0.240 mmol) and diisopropylethylamine (0.42 mL, 2.4 mmol) were stirred in dry dichloromethane (5 mL) for 10 min, before addition to the activated acid mixture. The resulting solution was stirred under inert atmosphere at room temperature overnight. Once TLC had confirmed the consumption of starting material the solution was washed twice with water (20 mL), once with brine (20 mL), and dried over $MgSO_4$. The drying agent was filtered out and the solution reduced on the rotary evaporator before purification by column chromatography on silica gel with 1.5 % methanol in dichloromethane as eluent. The solvent was removed *in vacuo* to give an orange oil (0.022 g, 15 % yield). ^{1}H NMR ($CDCl_3$, 400 MHz, δ): 5.94 (d, $^3J_{7,2}$ = 9.4 Hz, 1H, *H7*), 5.84 (dd, $^3J_{16,15a}$ = 8.6 Hz, $^3J_{16,15b}$ = 8.6 Hz, 1H, *H16*), 5.71 (d, $^3J_{1,2}$ = 8.6 Hz, 1H, *H1*), 5.19 (dd, $^3J_{3,2}$ = 9.4 Hz, $^3J_{3,4}$ = 9.4 Hz, 1H, *H3*), 5.12 (dd, $^3J_{4,3}$ = 9.4 Hz, $^3J_{4,5}$ = 9.4 Hz, 1H, *H4*), 4.68 (d, $^3J_{19,20}$ = 2.0 Hz, 2H, *H19*), 4.34 (d, $^3J_{20,19}$ = 2.0 Hz, 2H, *H20*), 4.26 (m, 2H, *H2,6a*), 4.20 (s, 5H, *Cp-H*), 4.11 (dd, $^3J_{6b,6a}$ = 2.4 Hz, $^3J_{6b,5}$ = 12.5 Hz, 1H, *H6b*), 3.77 (ddd, $^3J_{5,4}$ = 9.8 Hz, $^3J_{5,6a}$ = 4.7 Hz, $^3J_{5,6b}$ = 2.3 Hz, 1H, *H5*), 3.36 (dd, $^3J_{15,14}$ = 6.4 Hz, $^3J_{15,14'}$ = 7.0 Hz, 2H, *H15*), 2.13 overlapped (d, $^3J_{9,10}$ = 7.4 Hz, 7.4 Hz, 2H, *H9*), 2.10, 2.09, 2.03, 2.02 (s, 3H, OCOC*H*$_3$), 1.57 (m, 4H, *H10,14*), 1.32 (m, 6H, *H11,12,13*). ^{13}C NMR ($CDCl_3$, 100 MHz, δ): 173.39 (*C8*), 171.18, 170.88, 170.51 (O*C*OCH$_3$), 169.66 169.49 (*C17*), 92.84 (*C1*), 76.65 (*C18*), 73.05 (*C3*), 72.81 (*C5*), 70.56 (*C20*), 69.94 (*C21*), 68.29 (*C19*), 68.13 (*C4*), 61.90 (*C6*), 52.97 (*C2*), 39.50 (*C15*), 36.60 (*C9*), 29.96 (*C14*), 28.76 (*C12*), 28.61 (*C13*), 26.58 (*C11*), 25.46 (*C10*), 21.12, 20.93, 20.89 (OCO*C*H$_3$). IR ν_{max} (cm^{-1}): 3292 (w), 2939 (w), 2360 (s), 2341 (s), 1750 (s), 1630 (m), 1541 (m), 1218 (s), 1038 (m). HR-MS (ES+ of MNa$^+$): m/z calcd for $C_{33}H_{44}{}^{56}FeN_2O_{11}Na$: 723.2192, found: 723.2187.

References begin on Pg 161

5.2.3 ^{99m}Technetium Labelling via SLT

The appropriate ferrocene precursor was dissolved in dimethylsulfoxide to a final concentration of 1 mg/mL. This precursor solution (300 μL) was transfered to a 3 mL reaction vial which was sealed with a rubber septum and purged with nitrogen for 10 min. An aqueous solution of $[^{99m}Tc(CO)_3(H_2O)_3]^+$ (made using an Isolink™ kit as detailed in Chapter 3.2.3) adjusted to pH 7 (300 μL) was added through the septum, and the reaction mixture stirred at 80 °C for 120 min. Upon cooling, a sample was injected into the radioHPLC for analysis. For cell uptake studies the reaction mixture was purified by HPLC; the appropriate peaks were collected and used in the studies.

5.2.4 Hexokinase Substrate Assay

This was performed as detailed in Chapter 3.2.5.

5.2.5 GLUT-1 Cell Uptake Assay

This was performed as detailed in Chapter 2.2.4.

5.3 Results and Discussion

5.3.1 Synthesis and Characterisation

The single ligand transfer (SLT) refers to the transfer of a Cp ligand to the $[M(CO)_3]^+$ core from the iron of ferrocene. In the double ligand transfer (DLT) reaction, the metal of interest (in this case rhenium) begins in an oxidised state and over the course of the reaction is reduced, and accepts three carbonyl ligands and a Cp ligand from another metal species present in the reaction mixture. These reactions (detailed in Chapter 5.1.1) have both been shown to be selective for the transfer of Cp rings bearing electron-withdrawing substituents.[12]

These reactions are both employed in the syntheses in this Chapter. The SLT was utilized in the ^{99m}Tc chemistry; $[^{99m}Tc(CO)_3(H_2O)_3]^+$ is reacted with a substituted ferrocene which

References begin on Pg 161

transfers its functionalized ring to the technetium centre during the reaction. This reaction was not applied to the rhenium compounds because it has been found not to work for similar carbohydrate-based ligands.[15] The reaction conditions are likely too harsh, and the combination of high temperatures and solvent requirements produced only degradation products.[15] Instead, the DLT was used to synthesize the rhenium complexes via an indirect route of making [CpM(CO)$_3$] followed by coupling to the biomolecule of interest. The synthesis of rhenium compounds of this type via an indirect route where the Cp is bound to the Re and then functionalized further is not unique, and is commonly utilized when labelling proteins and other chemically sensitive biomolecules.[22, 27, 32]

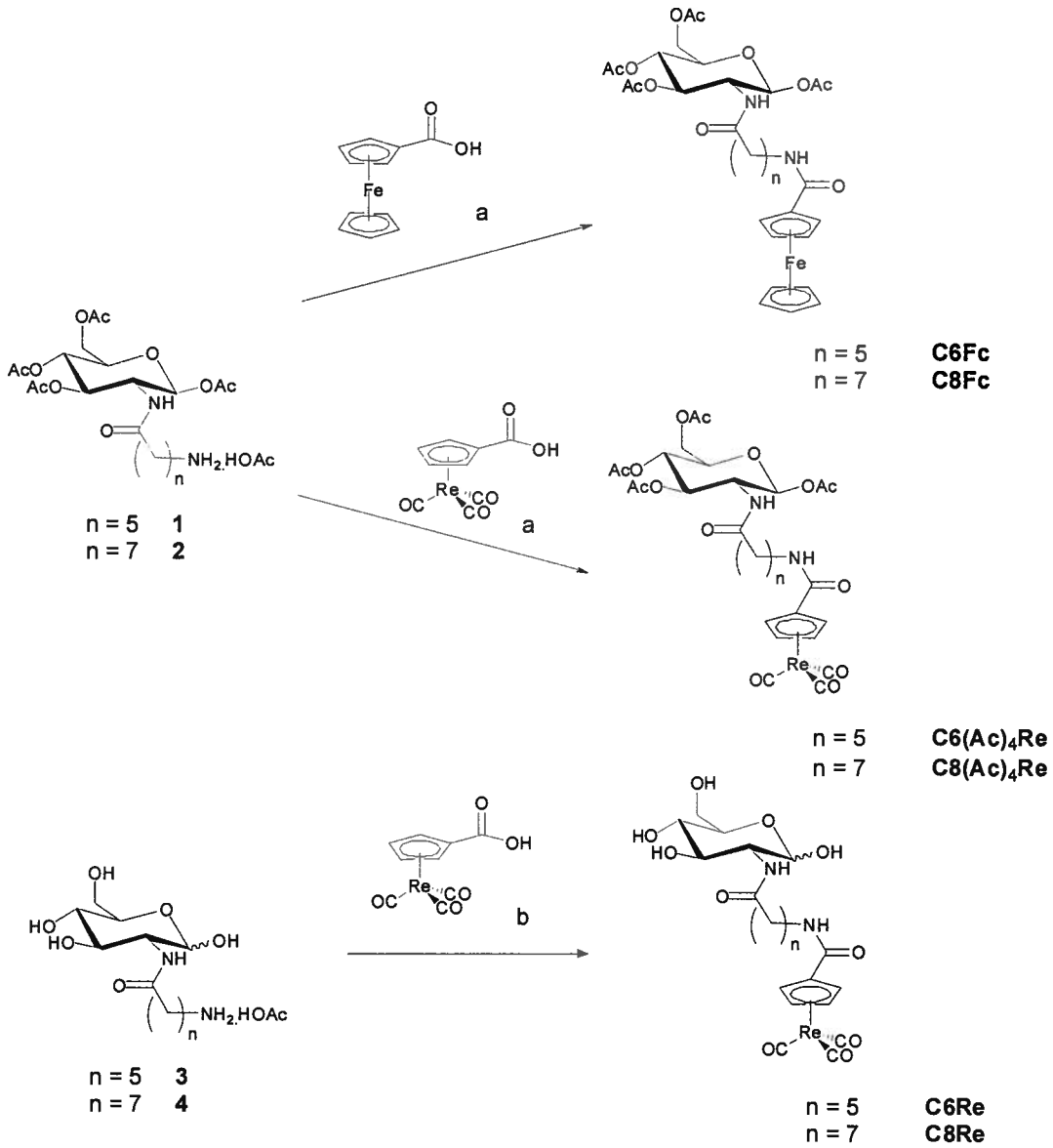

Scheme 5.5 Synthetic route to cold compounds used in this chapter: a) dry DCM, EDC, DIPEA b) dry DCM / DMSO, DCC, DIPEA.

References begin on Pg 161

As discussed in Chapter 5.1, there are several ways in which Cp compounds of this type can be synthesized. The aim of this work was to make long chain carbohydrate Cp complexes, and examine their *in vitro* properties relevant to molecular imaging. To this end, reactions that were thought to be most likely to work in systems of this kind were employed. If the resulting complexes were found to have promising properties, synthetic routes could be optimized by investigation of the wide variety of methods available.

The rhenium compounds were made via a two step process. The DLT was used to synthesize the rhenium starting material: $[HO_2CC_5H_4Re(CO)_3]$,[12] followed by an amide coupling to the appropriate sugar-linker compound to give the functionalized metal complex (Scheme 5.5). Once the protected sugar was bound to the $[CpRe(CO)_3]$ core, the removal of the acetyl protecting groups was attempted using NaOMe in methanol. This was not successful, and a large number of compounds were evidenced in both the MS and the TLC, including some without the rhenium isotope pattern. The use of NaOMe induced decomposition, as also occurred in the short-chain analogues of these Cp compounds.[33] Because of this the free-sugar complexes were made by deprotection of the sugar prior to coupling of the sugar-linker compound and the $[CpRe(CO)_3]$ core (Scheme 5.5). Sugar-substituted ferrocenes were prepared as substrates for the SLT reaction to access the $[Cp^{99m}Tc(CO)_3]$ complexes. These were made utilizing an amide coupling between the terminal *N* of the appropriate sugar-linker compound and the acid group of ferrocenecarboxylic acid (Scheme 5.5).

The ligands, their rhenium complexes, and ferrocene analogues used in the ^{99m}Tc labelling were all characterised by HR-MS, IR, ^1H and ^{13}C APT NMR spectroscopy. A variety of 2-D NMR spectroscopic techniques such as COSY, HMQC, HMBC and TOCSY were used as appropriate for full assignment of ^1H and ^{13}C NMR signals.

Deprotection of the long chain sugar starting materials was assessed using crude ^1H NMR spectroscopy. For the debenzylation reactions to make **1** and **2**, ^1H NMR spectra were used to confirm the absence of any aromatic resonances. As these reactions were performed in acetic acid, integrals of the acetic acid CH_3 peak compared to one of the product peaks gave the yield of product as well as the stoichiometry of acetic acid so sufficient base could be added in the next step to neutralize it completely. Compounds **3** and **4** were deacetylated prior to coupling to the metal centre, and ^1H NMR spectroscopy was used to ensure loss of both the acetyl and the

References begin on Pg 161

aromatic peaks. Once the acetyl groups were removed, the free hydroxyl groups complicate the ^{1}H NMR spectra to the point where they are not readily assignable, and their main use is to confirm the lack of acetyl peaks. These free sugar compounds were then debenzylated, and the ^{1}H NMR spectra became even more difficult to interpret. The spectra were used to confirm the lack of aromatic peaks as well as to quantify the acetic acid present by comparing the integrals of the *C*-1 anomeric peaks (the only quantifiable ones in the spectrum), with the acetic acid peak, as detailed above.

^{1}H and ^{13}C APT NMR spectroscopy were performed to confirm the identity of all final products. Figure 5.4 shows the ^{1}H NMR spectra of the three non-radioactive C6 metal complexes; the trends are exactly the same in the C8 compounds. The ferrocene complex **C6Fc** and the protected rhenium complex **C6(Ac)$_4$Re** (Figure 5.4a and b) both display clean spectra with the sugar peaks well defined and separated. The protons in the aliphatic linker chains are not well distinguished, but the chemical shifts and integrals match those of the expected products. Comparing the ^{1}H NMR spectra corresponding to these two compounds (Figure 5.4a and b), the large chemical shift changes affected by the different metal ions can be observed. The sugar peaks in the rhenium complex are spread further apart than those of the ferrocene. This is a very large effect, especially given the substantial distance between the atoms of the carbohydrate and the metal ions. The peaks corresponding to the Cp protons are shifted apart and substantially downfield in the rhenium compound compared to the analogous ferrocene. The fact that these protons exhibit the largest differences between the two molecules helps to confirm that the Cp rings are indeed the part of the ligand system bound to the metal ion.

The ^{1}H NMR spectra of the protected and deprotected rhenium complexes **C6(Ac)$_4$Re** and **C6Re** can be compared by looking at Figure 5.4b and c. Due to solubility constraints these two spectra were run in different solvents, meaning the chemical shifts are not directly comparable. The general trend can be observed, and the sugar protons seen to move upfield, narrow together and become very messy and difficult to interpret with deprotection of the acetyl groups. This is normal for deprotected sugars, and can also be observed in the ^{1}H NMR spectra shown in Chapters 2 and 3 of this thesis. These ^{1}H NMR spectra are not easy to interpret and therefore not as diagnostic as those of protected sugars, so ^{13}C and 2-D NMR spectroscopies are particularly useful in characterizing compounds containing free sugars.

References begin on Pg 161

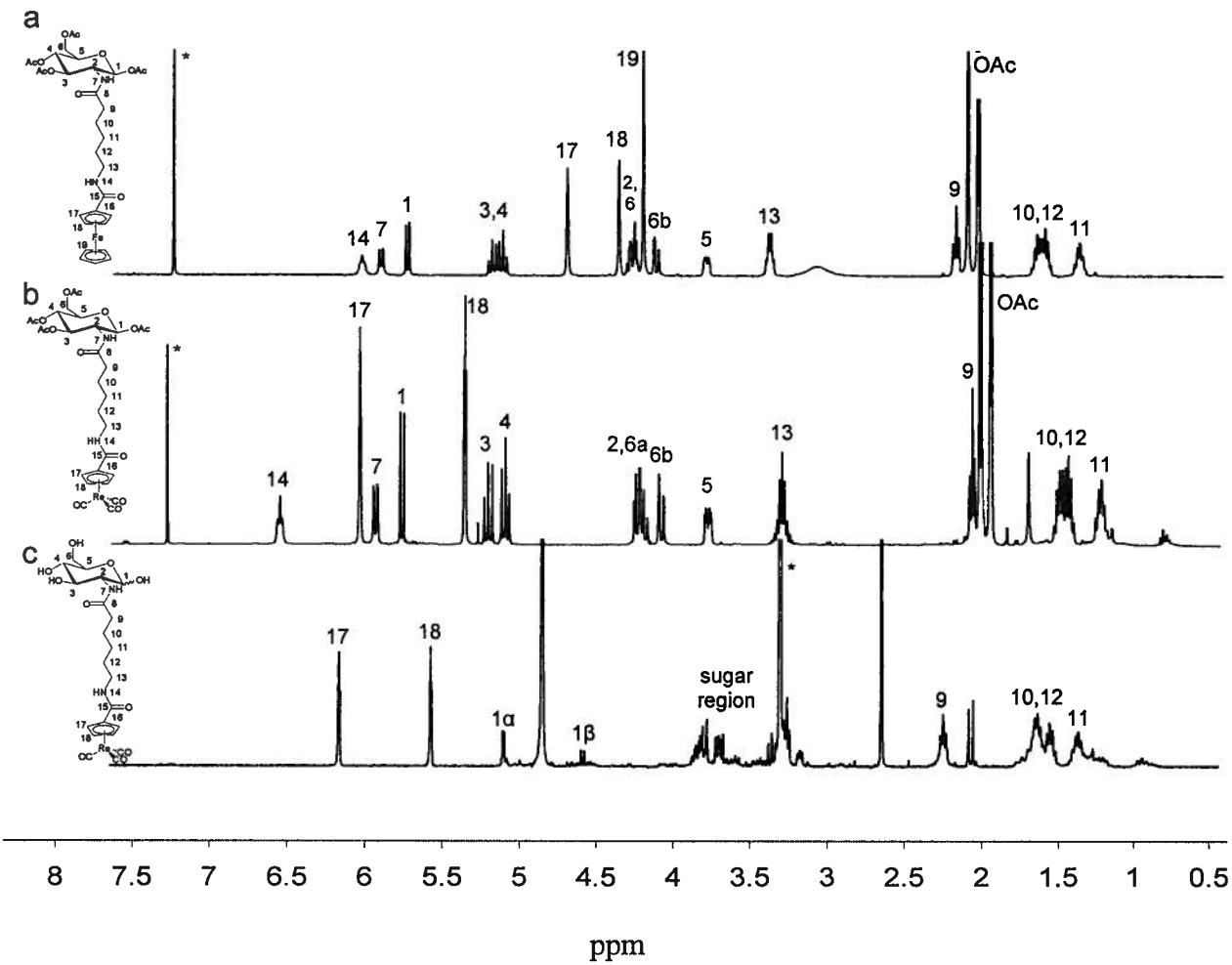

Figure 5.4 ^{1}H NMR spectra of: a) **C6Fc** b) **C6(Ac)$_4$Re** c) **C6Re**, * indicates solvent peak.

Figure 5.5 shows the ^{13}C APT spectra of the two C8 rhenium complexes made in this chapter. Figure 5.5a corresponds to the tetraacetylated compound **C8(Ac)$_4$Re**, and contains four peaks at each of 180 ppm and 20 ppm corresponding to the acetyl carbons which are absent in the spectrum of the deprotected analogue **C8Re** (Figure 5.5b). The other main difference between the two spectra is the number of peaks present. Upon deprotection of the sugar an anomeric centre is produced at *C*-1, meaning two diast ereomeric products are formed with different chemical shifts. As the two diastereomers are the same at all centres bar one, the signals of some atoms (particularly those further away from the anomeric centre) are the same for the two structures, meaning not all peaks are observed to double. For example, the CO peaks at ~193 ppm do not double as they are distant from *C*-1, but the proximal *C*-2 goes from being a single peak to two peaks separated by 2.9 ppm upon deprotection of the acetyl groups.

References begin on Pg 161

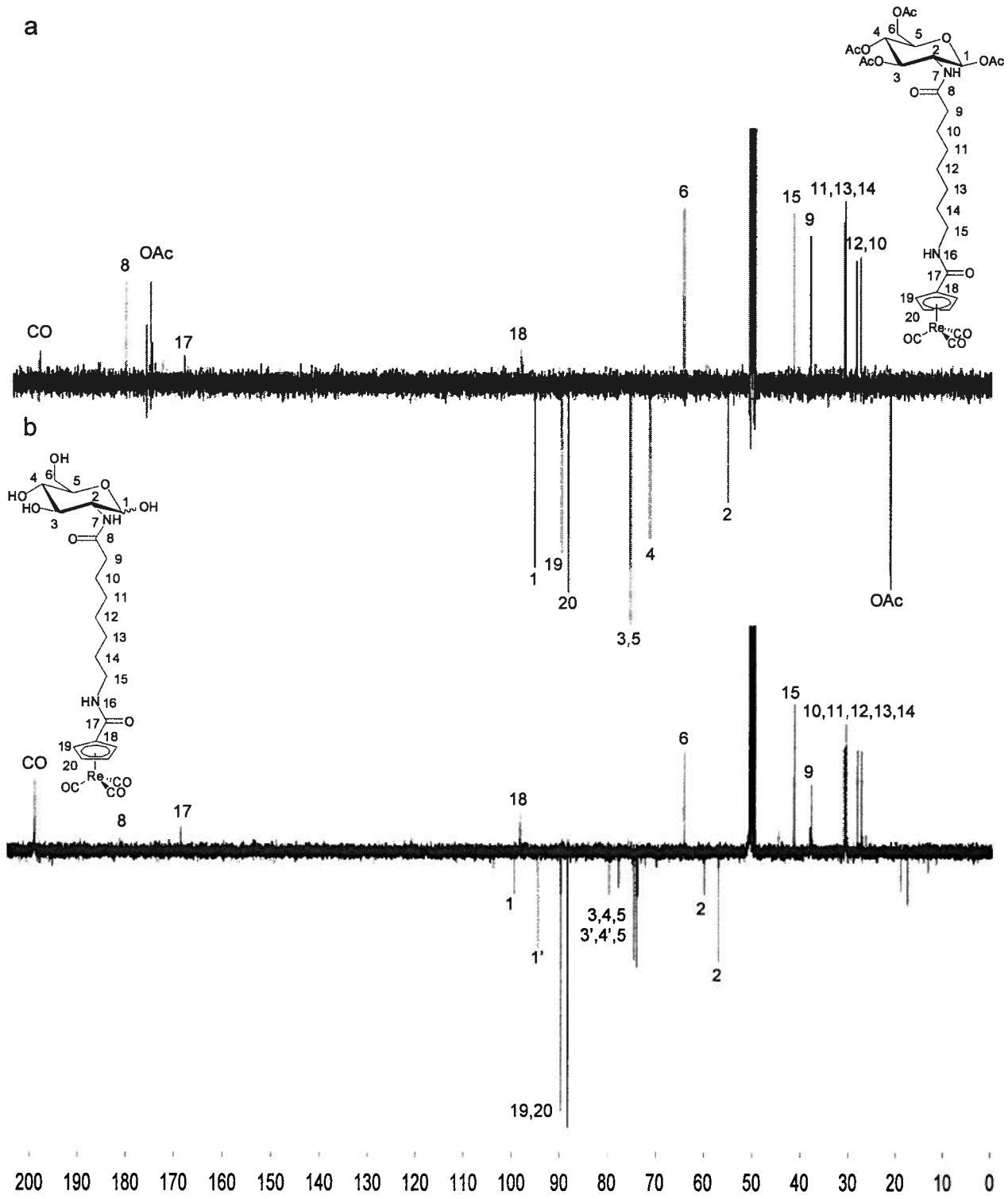

Figure 5.5 ^{13}C APT spectra of the two C8 rhenium complexes made in this chapter: a) **C8(Ac)$_4$Re** with acetylated sugars b) **C8Re** the deprotected sugar analogue, * indicates solvent peak.

The peak at ~ 193 ppm in the spectra of the rhenium complexes correspond to the three CO ligands, and there is only one of these peaks observed for each Cp compound. This is in contrast to the tridentate ligands discussed in Chapter 3 where the asymmetric coordination environment of the metal ion led to two or three CO peaks being present. The Cp ligand binds to the metal in a η^5 fashion in these compounds, and is free to rotate. This means only one peak is produced by the three CO ligands, as they all experience the same chemical environment on the NMR timescale.

The IR spectra of compounds can be used to identify the presence, absence or changes in the environment of major functional groups. As expected, the analogous protected and deprotected rhenium compounds showed very similar IR traces (Figure 5.6 shows representative C8 spectra). The key difference between the two is the presence of an ester carbonyl stretch at 1750 cm^{-1} in the protected compounds (e.g. **C8(Ac)$_4$Re**) that is not seen in the deprotected analogues (e.g. **C8Re**) which do not contain acetyl (ester) groups. The peak at 1218 cm^{-1} is assigned to the C-O stretch of the esters, and this peak also disappears following deprotection. Concurrent enhancement of the –OH peaks at ~ 3300 cm^{-1} confirms the presence of free hydroxyl groups.

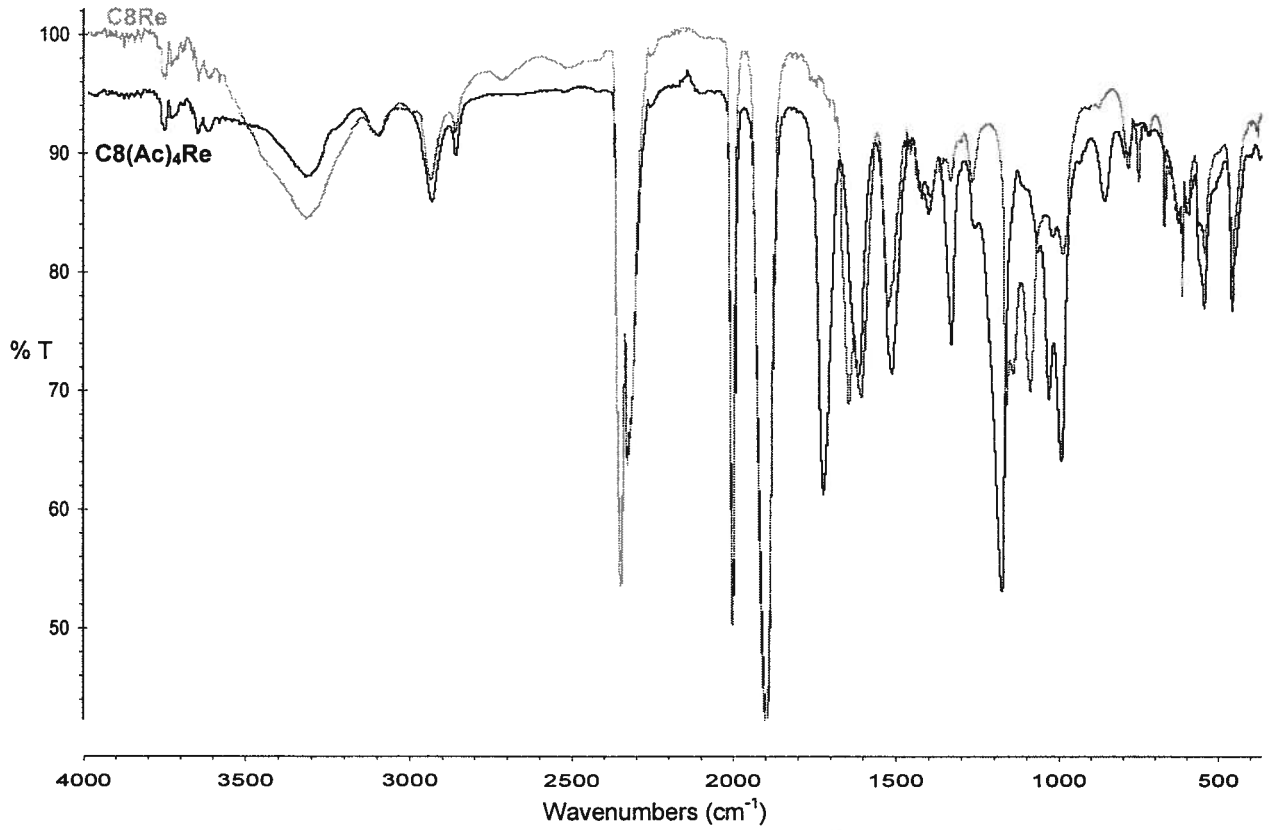

Figure 5.6 Overlaid IR spectra of **C8Re** (gray line, top left, 100 % transmittance) and **C8(Ac)$_4$Re** (black line, top left 95 % transmittance).

References begin on Pg 161

The IR spectra of the ferrocene and $(Ac)_4Re$ analo gues are also very similar. The major difference is the presence of the strong peaks around 2022 and 1918 cm^{-1} in the rhenium compounds, corresponding to the CO stretches of the carbonyl ligands. As the remainder of each of these two molecules is essentially the same and all other peaks are as expected, this is in line with the proposed structures. For example the peaks corresponding to the amide carbonyls appear at 1747 cm^{-1} in **C6(Ac)$_4$Re** and 1740 cm^{-1} in **C6Fc**, and the ester peaks at 1643 cm^{-1} in **C6(Ac)$_4$Re** and 1633 cm^{-1} in **C6Fc**.

HR-MS gave the expected peaks for $M+H^+$ and/or $M+Na^+$, with the rhenium complexes exhibiting their diagnostic isotope pattern (^{185}Re = 37 % and ^{187}Re = 63 % natural abundance). A diagnostic example is the HR-MS of **C6Re** with peaks at 675.1086 (~ 45 % intensity) and 677.1046 (100 % intensity) corresponding to $C_{18}H_{26}N_4O_{12}{}^{185}Re^+$ and $C_{18}H_{26}N_4O_{12}{}^{187}Re^+$, respectively.

The characterization data discussed above is all consistent with the proposed structures of the compounds synthesized.

Table 5.1 Retention times (RT) and yields of ^{99m}Tc labelling and HPLC analysis of two long chain glucosamine-based Cp ligands.

Ligand	RT * $C_n(Ac)_4Re$	RT * C_nRe	RT * $C_n{}^{99m}Tc$	Radiochemical yield
C6	23.2 min	17.0 min	16.8 min	25 %
C8	29.7 min	20.2 min	20.3 min	40 %

* HPLC conditions – 100 % H_2O (with 0.1 % TFA) linear gradient to 100 % ACN at 30 min.

The labelling reaction to make the $[Cp^{99m}Tc(CO)_3]$ complexes required slightly longer reaction times than those needed for the tridentate ligands discussed in Chapters 3 and 4; however, given the half life of ^{99m}Tc (6 hr), 2 hr is an acceptable reaction time. The aqueous solution of $[^{99m}Tc(CO)_3(H_2O)_3]^+$ was neutralized to pH 7 before being added to the ferrocene compound to begin the SLT reaction. It was, therefore, somewhat surprising to observe that the acetyl

References begin on Pg 161

protecting groups on the glucosamine were removed during the reaction (Scheme 5.6). This was evidenced by the HPLC retention time of a major component of the reaction mixture coinciding with that of the deprotected rhenium standard. There were no compounds with higher retention times to coincide with those of the protected rhenium compound (see Table 5.1). Further evidence of the deacetylation was seen in that reaction with NaOMe in MeOH did not change the HPLC trace of either the C6 or the C8 system, as it would if there were acetyl groups in the molecule. Upon further reflection, this *in situ* deprotection is probably to be expected, as the reaction involves elevated temperatures for two hours, and although the pH is neutral as tested by pH paper, there will be some OH^- ions in the reaction mixture, especially given that the Isolink™ kit used to make the ^{99m}Tc precursor is very basic.

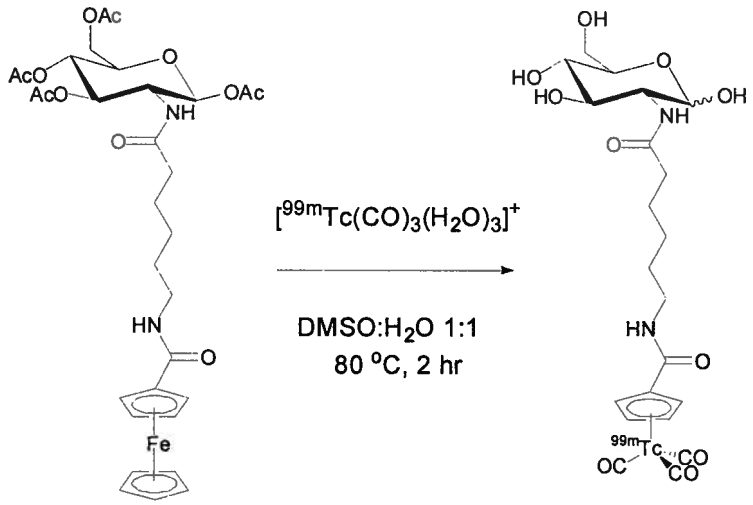

Scheme 5.6 Labelling scheme for **C6^{99m}Tc**. The same is used for the C8 analogue.

The radiation traces of these reaction mixtures (Figure 5.7) show unreacted starting material, product and small amounts of other compounds. As there is still ^{99m}Tc starting material present after 2 hr, it seems that it would be possible to increase the yield by simply reacting at higher temperature or for a longer time. This is not the case though, and longer reaction times lead to the appearance of more peaks and decreased yields of the desired product. It seems that by this time point the ferrocene precursor is no longer able to transfer a ring. One possible explanation for this is that the protecting groups are all removed by the 2 hr time point in the reaction. This would rationalize the observations that either increasing the reaction temperature or time does not increase the yield as it may be that only protected ligands will transfer. There would therefore be two competing reactions occurring – the glucosamine-bearing ring could either

References begin on Pg 161

transfer or be deprotected, and the relative time scales under these conditions may be such that the maximum yield is obtained within 2 hr. Other decomposition routes are also possible. It is worth noting that no reaction is observed after 3hr at 60 °C by radioHPLC. This does not rule out the possibility that the ferrocene precursor is decomposing at this temperature, but informs that the speciation of the ^{99m}Tc does not change under these conditions.

Others have also found the need for the protection of hydroxyl groups in reactions of this type.[14] When making rhenium estradiol derivatives via a SLT, it was found that the deprotected compound yielded only 12 % while protection of the two hydroxyl groups increased the yield to 41 % under the same reaction conditions.[14]

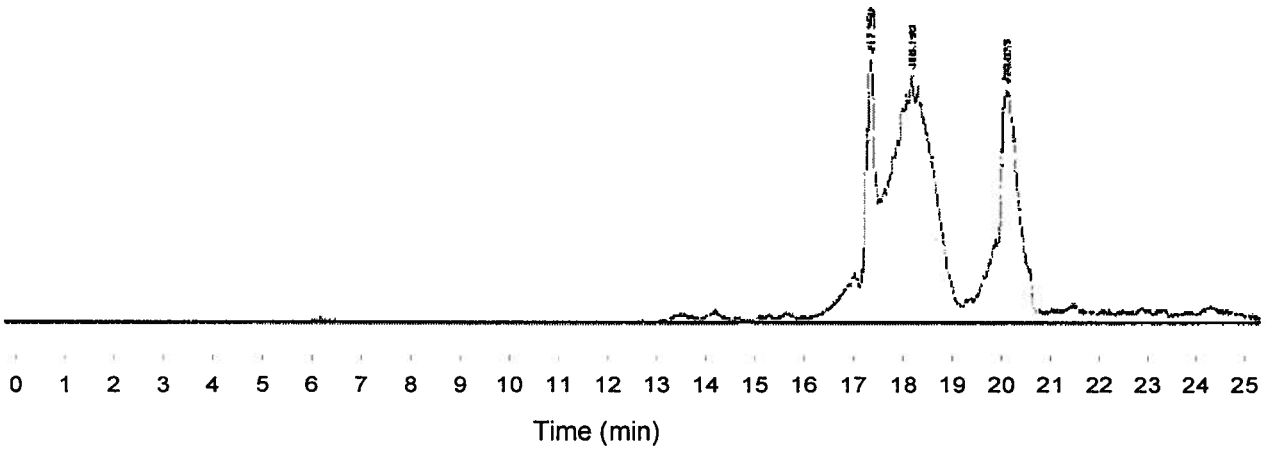

Figure 5.7 Radiation HPLC trace of **C8^{99m}Tc(CO)$_3$** after 2 hr reaction time. The peak at 20 min corresponds to the deprotected product, 18 min is tricarbonyl starting material and 17 min is an unidentified side product of the labelling reaction.

5.3.2 Hexokinase Substrate Assay

The rhenium complexes **C6Re** and **C8Re** were tested as substrates for the enzyme hexokinase. They were both found not to be substrates as they did not undergo a significant amount of phosphorylation under the conditions tested. As with the long-chain tridentate compounds in Chapter 4, the exact reasons for this have not been elucidated. It may be that the presence of the chain itself perturbs the carbohydrate too much for it to be recognized, or that the chain needs to be a little longer to place the metal binding sphere far enough away from the active site to allow hexokinase to fully close and perform the phosphorylation.

References begin on Pg 161

5.3.3 GLUT-1 Cell Uptake Studies

The two ^{99m}Tc compounds **C6^{99m}Tc** and **C8^{99m}Tc** were tested for their uptake in cells with high concentrations of GLUT-1 transporters on their surface (Figure 5.8). Both compounds showed non-negligible uptake; however, there was no significant decrease in their uptake in the presence of glucose, indicating that the compounds were not transported into the cells as carbohydrates. Comparing the magnitude of these cellular uptakes to those of the long-chain tridentate ligands discussed in Chapter 4 reveals no significant variation in uptake with binding sphere (Figure 5.8). The cell uptake is not significantly dependent on the size or lipophilicity of the metal binding portion in these compounds. It may be that the addition of a long alkyl linker attached to the glucosamine is enough of a perturbation that it prevents recognition and transport of the compounds as carbohydrates.

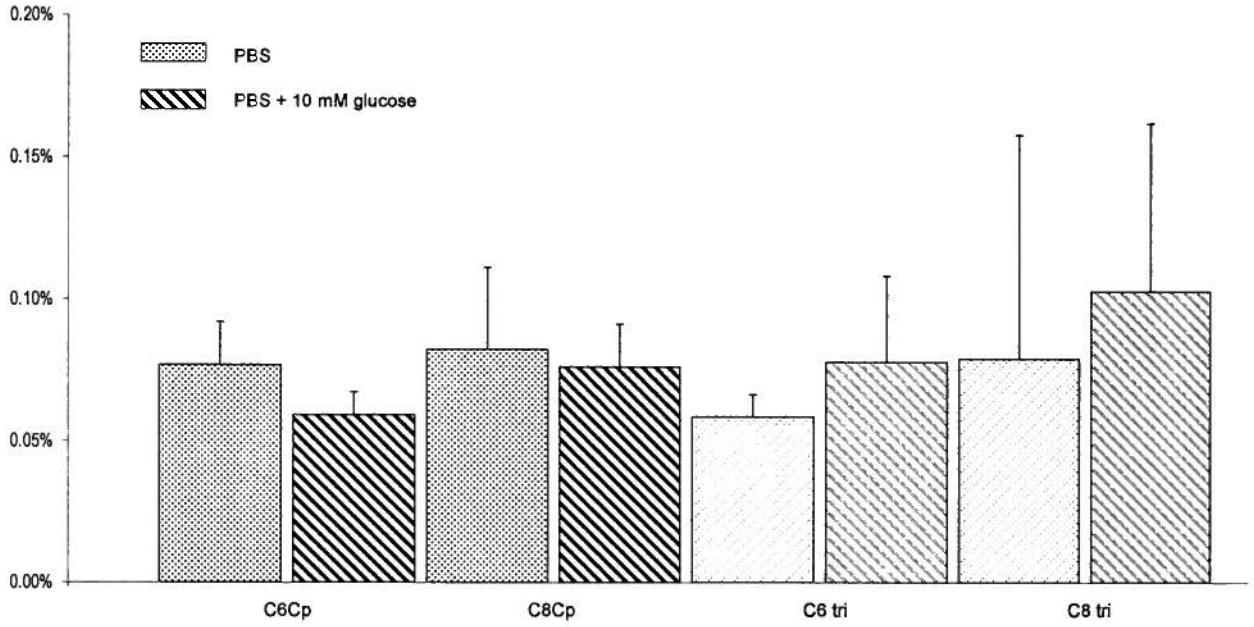

Figure 5.8 Comparison of cell uptake of **C6^{99m}Tc** and **C8^{99m}Tc** (black) with the equivalent chain length tridentate ^{99m}Tc complexes (blue) in the absence (spotted) and presence (striped) of glucose.

References begin on Pg 161

5.4 Conclusion

Synthesis of two long chain glucosamine based cyclopentadienyl complexes of both the technetium and rhenium tricarbonyl cores was successfully completed. The resulting compounds were not recognized or metabolized by either GLUT-1 or hexokinase, so will unfortunately not be useful as carbohydrate based molecular imaging agents. There are many methods known for the preparation of these types of substituted Cp complexes and further synthetic optimization could be carried out if more promising analogues were discovered.

References begin on Pg 161

5.5 References

1. Schibli, R.; Schubiger, P. A., *Eur. J. Nucl. Med.* **2002,** *29*, 1529 - 1542.

2. Uehara, T.; Uemara, T.; Hirabayashi, S.; Adachi, S.; Odaka, K.; Akizawa, H.; Magata, Y.; Irie, T.; Arano, Y., *J. Med. Chem.* **2007,** *50*, 543 - 549.

3. Schulz, H., *Biochim. Biophys. Acta Lipid Lipid Met.* **1991,** *1081*, 109 - 120.

4. Cotton, F. A.; Wilkinson, G., *Advanced Inorganic Chemistry*. John Wiley & Sons: New York, 1988; p 1171 - 1177.

5. Khotsyanova, T. L.; Kuznetsov, S. I.; Bryukhova, E. V.; Makarov, Y. V., *J. Organomet. Chem.* **1975,** *88*, 351 - 356.

6. Crocker, L. S.; Gould, G. L.; Heinekey, M., *J. Organomet. Chem.* **1988,** *342*, 243 - 244.

7. Alberto, R.; Schibli, R.; Elgi, A.; Schubiger, P. A., *J. Am. Chem. Soc.* **1998,** *120*, 7987 - 7988.

8. Le Bideau, F.; Salmain, M.; Top, S.; Jaouen, G., *Chem. - Eur. J.* **2001,** *7*, 2289 - 2294.

9. Wenzel, M., *J. Label. Compd. Radiopharm.* **1992,** *31*, 641 - 649.

10. Wenzel, M.; Saidi, M., *J. Label. Compd. Radiopharm.* **1993,** *33*, 77 - 80.

11. Saidi, M.; Kothari, K.; Pillai, M. R. A.; Hassan, A.; Sarma, H. D.; Chaudhari, P. R.; Unnikrashnan, T. P.; Korde, A.; Azzouz, Z., *J. Label. Compd. Radiopharm.* **2001,** *44*, 603 - 618.

12. Spradau, T. W.; Katzenellenbogen, J. A., *Organometallics* **1998,** *17*, 2009 - 2017.

13. Top, S.; Masi, S.; Jaouen, G., *Eur. J. Inorg. Chem.* **2002**, 1848 - 1853.

14. Masi, S.; Top, S.; Boubekeur, L.; Jaouen, G.; Mundwiler, S.; Spingler, B.; Alberto, R., *Eur. J. Inorg. Chem.* **2004**, 2013 - 2017.

15. Ferreira, C. L.; Ewart, C. B.; Bayly, S. R.; Patrick, B. O.; Steele, J.; Adam, M. J.; Orvig, C., *Inorg. Chem.* **2006,** *45*, 6979 - 6987.

16. Alberto, R.; Egli, A.; Abram, U.; Hegetschweiler, K.; Gramlich, V.; Schubiger, P. A., *J. Chem. Soc., Dalton Trans.* **1994**, 2815 - 2820.

17. Wald, J.; Alberto, R.; Ortner, K.; Candreia, L., *Angew. Chem. Int. Ed.* **2001,** *40*, 3062 - 3066.

18. Minutolo, F.; Katzenellenbogen, J. A., *J. Am. Chem. Soc.* **1998,** *120*, 4514 - 4515.

19. Top, S.; Kaloun, E. B.; Jaouen, G., *J. Am. Chem. Soc.* **2000,** *122*, 736 - 737.

20. Top, S.; Kaloun, E. B.; Toppi, S.; Herrbach, A.; McGlinchey, M. J.; Jaouen, G., *Organometallics* **2001,** *20*, 4554 - 4561.

21. Liu, Y.; Springler, B.; Schmutz, P.; Alberto, R., *J. Am. Chem. Soc.* **2008,** *130*, 1554 - 1555.

22. Salmain, M.; Gunn, M.; Gorfti, A.; Top, S.; Jaouen, G., *Bioconjugate Chem.* **1993,** *4*, 425 - 433.

23. Top, S.; Vessieres, A.; Pigeon, P.; Rager, M.-N.; Huche, M.; Salomon, E.; Cabestaing, C.; Vaissermann, J.; Jaouen, G., *ChemBioChem* **2004,** *5*, 1104 - 1113.

24. Bernard, J.; Ortner, K.; Spingler, B.; Pietzsch, H.-J.; Alberto, R., *Inorg. Chem.* **2003,** *42*, 1014 - 1022.

25. Graeff, F. G.; Guimaraes, F. S.; De Andrade, T. G.; Deakin, J. F., *Pharmacol. Biochem. Be.* **1996,** *54*, 129 - 141.

26. Alberto, R.; Schibli, R.; Schubiger, P. A.; Abram, U.; Pietzsch, H.-J.; Johannsen, B., *J. Am. Chem. Soc.* **1999,** *121*, 6076 - 6077.

27. Tamagnan, G.; Baldwin, R. M.; Kula, N. S.; Baldessarini, R. J.; Innis, R. B., *Bioorg. Med. Chem. Lett.* **2000,** *10*, 1113 - 1115.

28. Skaddan, M. B.; Wust, F.; Katzenellenbogen, J. A., *J. Org. Chem.* **1999,** *64*, 8108 - 8121.

29. Wust, F.; Skaddan, M. B.; Leibnitz, P.; Spies, H.; Katzenellenbogen, J. A.; Johannsen, B., *Bioorg. Med. Chem.* **1999,** *7*, 1827 - 1835.

30. Spradau, T. W.; Katzenellenbogen, J. A., *Bioconjugate Chem.* **1998,** *9*, 765 - 772.

31. Bowen, M. L.; Chen, Z.-F.; Roos, A.; Adam, M. J.; Orvig, C., manuscript in preparation.

32. Spradau, T. W.; Edwards, W. B.; Anderson, C. J.; Welch, M. J.; Katzenellenbogen, J. A., *Nucl. Med. Biol.* **1999,** *26*, 1 - 7.

33. Ferreira, C. L.; Orvig, C., unpublished results.

CHAPTER 6

Conclusions and Future Work

6.1 Multifunctional Metal Chelators as Potential Therapeutics for Alzheimer's Disease

6.1.1 3-Hydroxy-4-pyridinones

Chapter 2 of this thesis focused on the radioiodine labelling and subsequent study of two prototypical 3-hydroxy-4-pyridinones.[1] These two compounds were chosen as they represent the range of compounds synthesized as part of the Orvig group's Alzheimer's disease (AD) research programme. Iodine, specifically ^{125}I, was chosen as the radioactive isotope for this work because it was suited to our collaborators' experimental apparatus, was readily available through TRIUMF, and has well established labelling chemistry.[2, 3] Iododestannylation is a commonly used method for regioselective addition of a radioactive iodine. This methodology was taken advantage of in the labelling reactions in this thesis, and as it can only be applied to substrates with aromatic rings, this restricted the choice of which compounds to label. The substrate restriction comes from the fact that the Sn-alkyl bond is stronger than the Sn-aryl bond. As $Sn(alkyl)_3$ species are the leaving groups substituted by an iodine, the substrate to be labelled must be aromatic to ensure that that is the bond that breaks and the iodine will end up bound to the aryl ring, not an alkyl group. It may be that other, non-aromatic analogues will need to be radiolabelled and investigated as this project progresses, and in this case different labelling methodologies will need to be employed.

The *in vivo* experiments performed on the iodinated compounds showed that they are able to permeate the blood brain barrier (BBB) to enter into the brain.[1] The concentrations in which they access the brain are fairly modest, but may be sufficient to show some effects *in vivo*. These labelling experiments could be extended to elucidate more information on the mechanism of brain uptake as well as biodistribution and glycosidic cleavage of the compounds *in vivo*.

Further *in vivo* experiments with the same radiolabelled compounds could provide more mechanistic information. There are two experiments that would potentially give useful insight: comparing the brain uptake of glycosylated and non-glycosylated analogues (e.g. those in Figure

References begin on Pg 173

6.1) of a given pyridinone, or by performing uptake studies in the presence of compounds known to inhibit certain BBB transport proteins. Comparing the brain uptake of glycosylated and non-glycosylated analogues would give information on whether the glucose moiety was increasing or decreasing the BBB permeation. The non-glycosylated molecules are smaller, and less polar, and therefore would be expected to undergo passive diffusion across the BBB more rapidly.[4] If the GLUT transporters were being utilized by the glycosylated compounds then removal of the glucose group would decrease the amount of compound seen in the brain. This experiment would not give a definitive mechanism of uptake, but would add more valuable information to our overall knowledge. Some work toward this goal was carried out by synthesizing the non-glycosylated analogue of **pyrA** (Figure 6.1). This was not completed in time for the scheduled *in vivo* experiments, and given the relatively limited mechanistic information it would have provided it was decided not to carry out another round of experiments for this alone. The synthesis of this compound is fairly analogous to that performed in Chapter 2; an acetyl protecting groups is used, and cleaved following iodination, though there is no glycosylation step.

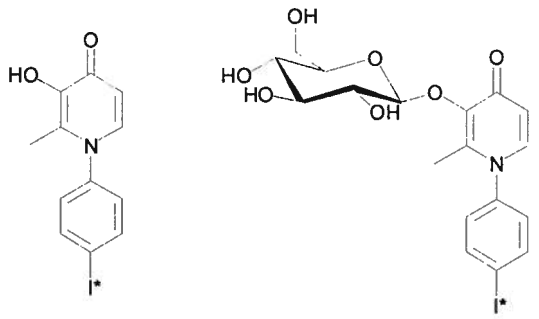

Figure 6.1 Non-glycosylated (left) and glycosylated (right) 3-hydroxy-4-pyridinone prototypes.

The addition of known inhibitors of BBB transport proteins to the perfusion experiments would give useful information on how our compounds access the brain. This would involve repeating the rat brain perfusion experiments, as before and in the presence of large amounts of compounds such as D-glucose and cytochalasin B, both of which are known to decrease the amount of a compound taken up via the GLUT transporters.[5] A decrease in the amount of test compound accessing the brain in the presence of such inhibitors would provide evidence for their uptake being via the GLUT route. If no such difference was seen between trials it would strongly suggest that the compounds were not taken up by the same route as glucose. There are

References begin on Pg 173

many different channels and proteins used for transport through cell membranes, and although having a glucose appended increases a compound's chance of being transported by a GLUT, it does not preclude its acceptance by other types of transport proteins. To test for receptor mediated uptake in general, an experiment could be done using increasing concentrations of test compound. If receptors were being utilized for transport, then above a certain concentration the receptors would become saturated, and uptake would no longer increase. If uptake was via passive diffusion then it would increase in a linear manner with increasing concentration of test compound. If this experiment showed our compounds to be transported via some kind of receptor, a battery of inhibitors of various channels could be tested. For example, the Na^+/K^+ATPase channel has been found to be the point of access for compounds such as cisplatin;[6] the known Na^+/K^+ATPase inhibitor ouabain[7] could be added to the assay and any affect this had on uptake would suggest an interaction of the test compound with Na^+/K^+ATPase.

Another very useful, but much more elaborate, *in vivo* experiment would be the monitoring of glycosyl bond cleavage and biodistribution by a double labelling procedure.[8] The two different labels would be chosen to emit radiation with significantly different energies, and each detector set to monitor just one of these energies. In this way the location of the two different atoms could be separately tracked. For the glycosylated pyridinones it would be most interesting to place one radioactive atom on the pyridinone portion of the molecule and the other on the carbohydrate. To minimize chemical changes to the carbohydrate a radioactive isotope of carbon or hydrogen would be preferable. ^{3}H (18.6 keV, $t_{1/2}$ = 12.3 yr) and ^{14}C (156 keV, $t_{1/2}$ = 5730 yr) could be used in combination with ^{123}I (159 keV) and ^{125}I (35 keV) respectively. Stability studies in plasma or a similar medium prior to *in vivo* experiments would be used to determine the relative stabilities of the different bonds in the molecule. It is expected that the glycosidic bond would be the weakest, and if the isotopic distributions were found to differ from each other *in vivo*, this would indicate cleavage of the glycosidic bond. The *in vivo* experimentation would be quite complex and the animals would need to be monitored over a significant length of time. Given the effort required for these experiments, it may be a better use of resources to use non-labelled compounds and have collaborators perform a general pharmacokinetic/pharmacodynamic study of the compounds. This could be done in normal mice to ensure the glycosidic bond cleaved and examine what portion of the administered compounds ended up in the brain. After these initial experiments it would be extremely interesting to see

References begin on Pg 173

how these compounds fared in a mouse model of AD, and to observe if there was any therapeutic effect, as we would hope.

Another complicating factor in this work is that the BBB is often compromised in AD patients.[9] This is thought to result in a decrease in concentration or activity of the GLUT transporters of the BBB.[10, 11] It has been suggested that a reason for this is the oxidative damage that occurs because of the Aβ–metal ion complexes.[12] This shows another potential advantage of our multifunctional approach to AD, but also complicates predictions of efficacy of compounds in different patients. Because of these complications it would be very useful to examine the BBB permeability of these glycosylated pyridinones in normal *vs.* AD human brain. It may be that a damaged BBB is more permeable to such compounds as the tight endothelial junctions that make up this barrier may be weakened such that brain access is increased. Experiments would need to be done to determine this.

Before such detailed studies would be carried out, basic efficacy must be proven by determining whether these compounds elicit any response in an animal model of AD. Any future work, be it biological testing or compound development and synthesis, will need to be based on the outcome of such studies.

6.1.2 *N,N,O,O*-Tetradentate Aminophenols

Another major class of compounds that have been studied in the Orvig group as potential AD treatments are the tetradentate N_2O_2 aminophenols.[13, 14] An example of a molecule of this class is shown in Figure 6.2. Like the pyridinones that were the focus of Chapter 2 of this thesis, some of these compounds were glycosyl protected to form prodrugs. Some work has been put into the radiolabelling of compounds of this type, such that they too could be tested for BBB permeability. Labelling was attempted, in an effort to synthesize the compound shown in Figure 6.2, using a simple electrophilic aromatic substitution reaction.[3] This particular substrate was chosen for its large degree of substitution on the aromatic rings, restricting the number of possible iodination products. The different substituents exert conflicting directing effects such that there is no clear preference of position for the iodination to occur. In addition, there are two rings present, so the possibility of one or both rings being iodinated adds further complications. As the amount of activity in the rat brain is what is being quantified, it is vital that each molecule

contains the same amount of activity, meaning these compounds would need to be separated before testing. It would be interesting to see the results of BBB permeation tests on compounds of this type, and if positive, to pursue the other *in vivo* experiments listed above in Chapter 6.1.1 with some prototypical aminophenols.

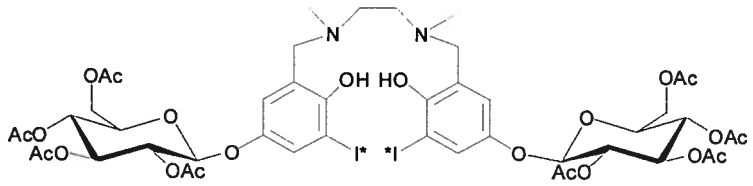

Figure 6.2 The aminophenol that has undergone some radioiodination attempts. The position of expected iodination is shown.

6.2 Carbohydrate Conjugates of ^{99m}Tc for Use in Molecular Imaging

The ultimate goal of the work in Chapters 3 - 5 of this thesis was to make a glucosamine-^{99m}Tc bioconjugate for use in molecular imaging. As discussed in Chapter 1 and the Introductions to subsequent Chapters, a successful carbohydrate-based imaging agent must be able to both enter cells and be phosphorylated in a manner similar to glucose. The end use of an imaging agent of this type would be as a marker of glucose metabolism, and as such the compound needs to behave similarly to glucose. As glucose metabolism is altered in heart disease, brain disorders, and cancer, this is where a compound of this type would be most useful. As detailed in Chapter 1.3, many cancer cells have increased energy requirements due to their rapid growth and inefficient metabolic pathways. For an imaging agent to be selective for cancerous tissue it must enter into and get trapped in those cells faster than in healthy tissue. The increased glucose needs of many cancer cells have led to them expressing higher concentrations of key glucose processing enzymes than normal cells. This is a key difference that we, and others, hope to take advantage of with carbohydrate-based radiopharmaceuticals. The two key enzymes to be targeted are the GLUTs and hexokinase. GLUTs are the major class of glucose transport enzymes, which, under ideal conditions, may be utilized to transport bioconjugates inside cells.[15-17] Hexokinase is the enzyme that catalyses the first step in glycolysis by addition of a phosphate group to the *C*-6 position of a carbohydrate. The resulting molecule is negatively charged, and as it is unable to diffuse back through the cell membrane, it is retained within the

References begin on Pg 173

cell. Thus the action of these two proteins working together results in molecules that are metabolized as carbohydrates entering (GLUT) and being trapped (hexokinase) selectively in cells that express high concentrations of both proteins.

The way in which the Orvig group has approached the problem of retaining GLUT transport is by choosing glucosamine as our sugar analog. Several functionalised glucosamine analogues have shown cell uptake by GLUT transporters. 2-NBDG (Figure 6.3a) is a compound with a relatively bulky group attached to the *N* of glucosamine that undergoes transport by GLUT-1 into human erythrocytes, as well as hexokinase phosphorylation.[15] Two other bulky glucosamine derivatives that are transported by the GLUT family are shown in Figure 1.4 in Chapter 1.3.[16, 17] We propose that the reason substituted glucosamines can be tolerated where substituted glucoses cannot is because of the ability of the *N-H* to participate in hydrogen bonding. An accepted mechanism of transport for compounds through the GLUT channels is by a rolling mechanism where each group around the carbohydrate must be able to form a hydrogen bond at various stages of the movement.[18] It is possible that investigation of other sugars for these bioconjugates would be advantageous, but given the evidence presented above it seems worth pursuing some of the other suggestions in this chapter before moving on to variations in sugar.

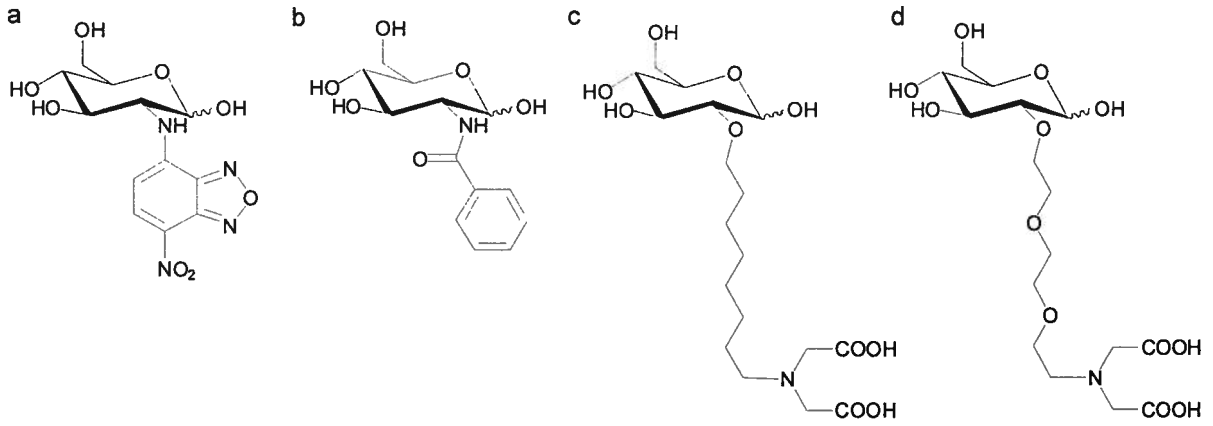

Figure 6.3 Carbohydrate based bioconjugates of interest for their interactions with key enzymes and/or investigation as molecular imaging agents, a) 2-NBDG[15] b) N-benzoyl glucosamine[19] c) a long alkyl chain glucose analogue investigated for use in molecular imaging[5] d) a glucose-based compound with a long polyethyleneglycol (PEG) chain investigated for use in molecular imaging.[5]

References begin on Pg 173

The Orvig group's approach to synthesizing compounds with hexokinase activity has been the use of long, alkyl linkers between the carbohydrate and the metal binding moiety. This approach is justified by the fact that the active site of hexokinase is in a narrow cleft that must close in order for phosphorylation to occur. If the bulky metal binding substituent is far enough from the carbohydrate in the active site it may be possible for this process to occur without the chelating arms getting in the way and blocking the subunits from closing together. The minimum distance required to allow for this to occur was calculated to be seven methylene units long.[5] This thesis has explored the *in vitro* properties of some compounds with linkers up to seven methylene units long, and these were all found not to be phosphorylated by hexokinase. It may be that the bulk of the metal binding groups used required the linker to be a little longer to move them slightly further away and allow the cleft to close completely. To that end it would be very interesting to make the C9 and/or C10 analogue of the compounds outlined in this thesis. The C9 compounds would likely have sufficient water solubility to allow for the appropriate assays to be performed, and certain analogues of the C10 chain compound may too.

Before making these new analogues, it may be worth investigating whether the C11 compound made in Chapter 4 is phosphorylated. This compound was not soluble enough to be tested as the shorter chain compounds were, but the solubility issues could be circumvented by examining the technetium complex instead of the rhenium. From the labelling and stability studies in Chapter 4, we know that the C11 ligand is soluble enough to form the ^{99m}Tc compound. Radio-HPLC could be utilized to determine the phosphorylation of the ^{99m}Tc complex directly. This would require the synthesis of the phosphorylated compounds as standards i.e. chemical synthesis of C11-Re-phosphate. This assay could be very informative as to the capacity of hexokinase to handle modified substrates, and has the added advantage of involving the exact species that would be the potential imaging agent, the technetium rather than the rhenium complex.

It may be possible to alter the longer chain compounds to increase their water solubility. One way in which this could be done is by converting the methylene chain to a polyethyleneglycol (PEG) chain. For example, in a paper by Schibli *et. al*, two long chain glucose compounds that were synthesized were found to exhibit an appreciable inhibition of hexokinase (Figure 6.3).[5] The PEGylated compound (Figure 6.3d) had K_i = 250 μM and the C8 compound (Figure 6.3c) K_i = 5800 μM.[5] This is a very significant difference; addition of two oxygen atoms down the alkyl chain improved the affinity twenty fold. This would be a very interesting adjustment to

References begin on Pg 173

investigate with our glucosamine compounds, as it could potentially have two benefits, increased water solubility and increased affinity for hexokinase (for example, Figure 6.4a).

N- Benzoyl glucosamine (Figure 6.3b) is a very high affinity competitive inhibitor of hexokinase with a K_i = 22 μM.[19] By comparison, *N*-acetyl glucosamine has K_i = 98 μM.[19] The compounds discussed in this work are similar to *N*-acetyl glucosamine in that they have a carbonyl group attached to the *C*-2 nitrogen, with an alkyl carbon in the alpha position. Although the alkyl "chain" of *N*-acetyl glucosamine ends after one carbon, whereas in our compounds it continues for quite some time before coming to a very bulky group at the end, in terms of what interacts with the actual active site, these compounds are very similar. The fact that adding an aromatic group to the carbon alpha to the carbonyl to give *N*-benzoyl glucosamine increases the affinity for the active site means this could be an avenue worth investigating with our compounds (for example, Figure 6.4c). One must be aware that these suggestions are only expected to have an effect on the compounds' interaction with hexokinase as a competitive inhibitor, not as a substrate. However, the two are not unrelated, and improving the way in which something fits into the active site can only be advantageous in the stepwise progression towards discovering a new substrate molecule.

The other part of the molecule that could be varied is the metal binding portion. Work towards this end was shown in Chapter 3, and from the *in vitro* studies reported therein it would seem that variations in the metal binding groups had no effect on the enzymatic recognition and processing of the molecules. For GLUT this is probably true, but for hexokinase the fact that these were short chain molecules means they are limited by factors other than their binding groups (their short chain length). Varying the binding groups may have an affect on hexokinase affinity, as well as on the overall solubility and biodistribution of these compounds.

One way in which the coordination chemistry of the tricarbonyl core could be expanded (that may be of use in building libraries of this type) is by the investigation of thiol binding groups. Thiols have been underutilized as ligands in this area of chemistry, especially as they have been calculated to be good donors for the tricarbonyl core.[20] There have been a few examples of thiols in this area of the literature,[21] but most work with sulfur uses thioethers, which have been found not to bind as well as thiols.[22, 23] Work in the Orvig lab has led to successful application of the phenolate group as a donor for the tricarbonyl core.[24] Although this group binds well, the

synthesis of the ^{99m}Tc complex requires use of a base, which may preclude its application in certain situations. A plausible alternative is the use of a thiophenol group (Figure 6.4b). The pH of the thiol proton is around 7, meaning it will be deprotonated at physiological pH so the labelling could likely proceed without the need for base. Work towards this goal has begun.

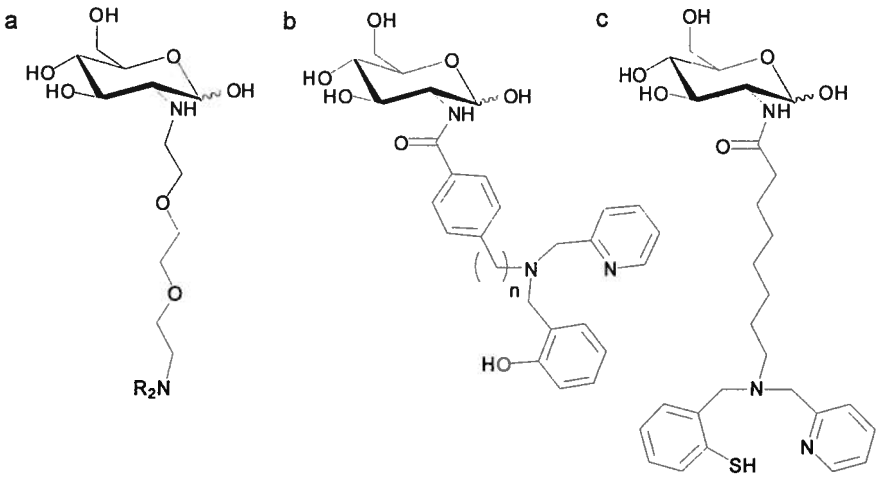

Figure 6.4 Compounds that could be explored as possible bifunctional ligands for the ^{99m}Tc core, a) a PEG chain analogue, R = any metal binding groups, a range should be investigated b) an analogue incorporating an aromatic ring into the linker c) a thioohenol ligand.

The key considerations when designing a binding group for the tricarbonyl core are affinity for the metal centre, size of the binding sphere, and overall charge and lipophilicity of the complex. In potential carbohydrate-based imaging agents, a neutral charge is desirable, which means that a monoanionic ligand set is needed. The ligand needs to have good affinity for the metal centre to ensure rapid complexation and that the complexes are stable once formed. This is best achieved by having at least one, and preferably multiple, nitrogen atoms as part of a tridentate binding sphere.[20, 25] Aromatic nitrogen atoms in particular are favoured, though their presence necessitates the presence of hydrophobic rings. Replacing one of these aromatic rings with a primary amino group would have an affect on the lipophilicity of the compound as well as the strength with which the ligand binds the metal ion. Lipophilicity and size are very important properties in determining the biodistribution of a compound, and require fine tuning for each molecule. These factors are all interrelated and need to be balanced with each other by synthesis and testing of a large range of compounds in a search for observable structure-activity relationships. The best chelate for each system will have to be investigated on a case by case

References begin on Pg 173

basis, as there is always a balance to be struck between the relative advantages of small size, strong metal binding, and lipophilicity.

The design of a ^{99m}Tc-carbohydrate conjugate for use in nuclear medicine is a difficult task. We believe it is a worthwhile goal because of the great benefits it would provide society if successful.

References begin on Pg 173

6.3 References

1. Schugar, H.; Green, D. E.; Bowen, M. L.; Scott, L. E.; Storr, T.; Bohmerle, K.; Thomas, F.; Allen, D. D.; Lockman, P. R.; Merkel, M.; Thompson, K.; Orvig, C., *Angew. Chem. Int. Ed.* **2007,** *46*, 1716 - 1718.

2. Adam, M. J.; Wilbur, D. S., *Chem. Soc. Rev.* **2005,** *34*, 153 - 163.

3. Seevers, R. H.; Counsell, R. E., *Chem. Rev.* **1982,** *82*, 575 - 590.

4. Levin, V. A., *J. Med. Chem.* **1980,** *23*, 682-684.

5. Schibli, R.; Dumas, C.; Petrig, J.; Spadola, L.; Scapozza, L.; Garcia-Garayoa, E.; Schubiger, P. A., *Bioconjugate Chem.* **2005,** *16*, 105 - 112.

6. Kishimoto, S.; Kawazoe, Y.; Ikeno, M.; Saitoh, M.; Nakano, Y.; Nishi, Y.; Fukushima, S.; Takeuchi, Y., *Cancer Chemoth. Pharm.* **2006,** *57*, 84 - 90.

7. McGowan, M. H.; Russell, P.; Carper, D. A.; Lichtstein, D., *J. Pharmacol. Exp. Ther.* **1999,** *289*, 1559 - 1563.

8. Salin, H.; Maitrejean, S.; Mallet, J.; Dumas, S., *J. Histochem. Cytochem.* **2000,** *48*, 1587 - 1592.

9. Kalaria, R. N., *Ann. N.Y. Acad. Sci.* **1999,** *893*, 113 - 125.

10. Mooradian, A. D.; Chung, H. C.; Shah, G. N., *Neurobiol. Aging* **1997,** *18*, 469 - 474.

11. Simpson, I. A.; Chundu, K. R.; Davies-Hill, T.; Honer, W.; Davies, P. D., *Ann. Neurol.* **1994,** *35*, 546 - 551.

12. Mark, R. J.; Pang, Z.; Geddes, J. W.; Uchida, K.; Mattson, M. P., *J. Neurosci.* **1997,** *17*, 1046 - 1054.

13. Storr, T.; Merkel, M.; Song-Zhao, G. X.; Scott, L. E.; Green, D. E.; Bowen, M. L.; Thompson, K. H.; Patrick, B. O.; Schugar, H. J.; Orvig, C., *J. Am. Chem. Soc.* **2007,** *129*, 7453 - 7463.

14. Storr, T.; Scott, L. E.; Bowen, M. L.; Green, D. E.; Thompson, K.; Schugar, H.; Orvig, C., Submitted for publication.

15. Speizer, L.; Haugland, R.; Kutchai, H., *Biochim. Biophys. Acta - Biomembranes* **1985,** *815*, 75-84.

16. Battaglia, G.; La Russa, M.; Bruno, V.; Arenare, L.; Ippolito, R.; Copani, A.; Bonina, F.; Nicoletti, F., *Brain Res.* **2000,** *860*, 149-156.

17. Zhang, M.; Zhang, Z.; Blessington, D.; Li, H.; Busch, T. M.; Madrak, V.; Miles, J.; Chance, B.; Glickson, J. D.; Zheng, G., *Bioconjugate Chem.* **2003,** *14*, 709 - 714.

18. Kahlenbe, A.; Dolansky, D., *Can. J. Biochem.* **1972,** *50*, 638 - 643.

19. Bertoni, J. M.; Weintraub, S. T., *J. Neurochem.* **1984,** *42*, 513 - 518.

20. Safi, B.; Mertens, J.; De Proft, F.; Geerlings, P., *J. Phys. Chem. A* **2006,** *110*, 9240 - 9246.

21. Lazarova, N.; Babich, J. W.; Valliant, J. F.; Schaffer, P.; James, S.; Zubieta, J., *Inorg. Chem.* **2005,** *44*, 6763 - 6770.

22. Gorshkov, N. I.; Lumpov, A. A.; Miroslavov, A. E.; Suglobov, D. N., *Radiochemistry* **2005,** *47*, 45 - 49.

23. Wust, F.; Skaddan, M. B.; Leibnitz, P.; Spies, H.; Katzenellenbogen, J. A.; Johannsen, B., *Bioorg. Med. Chem.* **1999,** *7*, 1827 - 1835.

24. Lim, N. C.; Ewart, C. B.; Bowen, M. L.; Ferreira, C. L.; Barta, C. A.; Adam, M. J.; Orvig, C., *Inorg. Chem.* **2008,** *47*, 1337 - 1345.

25. Schibli, R.; La Bella, R.; Alberto, R.; Garcia-Garayoa, E.; Ortner, K.; Abram, U.; Schubiger, P. A., *Bioconjugate Chem.* **2000,** *11*, 345 - 351.

APPENDIX 1

Rat Perfusion Experiments - as discussed in Chapter 2[1, 2]

These experiments took place in the laboratories of Dr. David Allen, Dr. Paul Lockman and Fancy Thomas at Texas Tech University Health Sciences Centre, Amarillo, TX. Male Fischer-344 rats (220-330 g; Charles River Labs, Kingston, N.Y.) were anesthetized with sodium pentobarbital (50 mg/kg). A PE-60 catheter filled with heparinized saline (100 units/mL) was placed into the left common carotid artery after ligation of the left external carotid, occipital and common carotid arteries (common carotid artery ligation is accomplished caudal to the catheter implantation site). The pterygopalatine artery was left open during the experiments. Rat rectal temperature was monitored and maintained at 37 °C by a heating pad connected to a feedback device (YSI Indicating Controller, Yellow Springs, Ohio). The catheter to the left common carotid artery was then connected to a syringe containing a physiologic perfusion fluid with 1.0 μCi/mL ^{3}H-choline, and **^{125}I-pyrA** or **^{125}I-pyrB** as described above. Perfusion fluid was filtered, warmed to 37 °C and gassed with 95 % air and 5 % CO_2. The perfusion fluid was infused into the left carotid artery with an infusion pump for 60 s at 10 mL/min (Harvard Apparatus, South Natick, MA). This perfusion rate maintained a carotid artery pressure of 120 mm Hg. Rats were then decapitated and cerebral samples obtained; the brains were removed from the skull, and the perfused cerebral hemisphere dissected on ice after removal of the arachnoid membrane and meningeal vessels. Brain regions were placed in scintillation vials and weighed. In addition, a 50 μL aliquot of the perfusion fluid was transferred to a scintillation vial and weighed. The brain and perfusion fluid samples were digested overnight at 50 °C in 1 mL of 1M piperidine. Fisher Chemical scintillation cocktail (10 mL) (Beckman, Fullerton, CA) was then added to each vial and the tracer contents assessed by dual-label liquid scintillation counting. Dual labeled scintillation counting of brain and perfusate samples was accomplished with correction for quench, background and efficiency. Brain vascular space was estimated from separate experiments and used to correct for radiotracer remaining within brain capillaries; apparent permeability surface-area coefficients (PA; BBB "permeability") were determined using the Crone-Renkin equation (Equation A.1):

$$PA = -F\, ln\, (1-K_{in}/F) \qquad \textbf{Equation A.1}$$

PA = permeability in mL/sec/g; F = flow rate through all capillaries of material being tested, normalised to radiotracer concentration in plasma; K_{in} = rate constant for the influx from blood-to-brain.[3]

References

1. Smith, Q. R.; Allen, D. D., *Meth. Mol. Med.* **2003,** *89*, 209 - 218.

2. Schugar, H.; Green, D. E.; Bowen, M. L.; Scott, L. E.; Storr, T.; Bohmerle, K.; Thomas, F.; Allen, D. D.; Lockman, P. R.; Merkel, M.; Thompson, K.; Orvig, C., *Angew. Chem. Int. Ed.* **2007,** *46*, 1716 - 1718.

3. Pardridge, W. M., *Introduction to the Blood-Brain Barrier*. Cambridge University Press: Cambridge, 1998; Pg 130.